NASA Contractor Report 3765

Experimental Study of Flow Reattachment in a Single-Sided Sudden Expansion

R. V. Westphal, J. P. Johnston,
and J. K. Eaton

GRANT NAG2-42
JANUARY 1984

NASA

NASA Contractor Report 3765

Experimental Study of Flow Reattachment in a Single-Sided Sudden Expansion

R. V. Westphal, J. P. Johnston, and J. K. Eaton
Stanford University
Stanford, California

Prepared for
Ames Research Center
under Grant NAG2-42

National Aeronautics
and Space Administration

Scientific and Technical
Information Office

1984

Acknowledgements

This research report covers work funded by two Federal Agencies: NASA Ames Research Center under Grant NAG 2-42 and the National Science Foundation under Grant CME-8017860. In addition, Dr. Westphal was partially supported for three years by a National Science Foundation Graduate Fellowship. Finally, the contributions of the companies that contribute to the Industrial Affiliates Program of the Thermosciences Division of the Mechanical Engineering Department of Stanford University are gratefully acknowledged.

Abstract

The reattachment of a fully turbulent, two-dimensional, separated shear layer downstream of a single-sided sudden expansion in a planar duct flow has been studied experimentally. The main objective of the research has been to study the process of reattachment, whereby a free shear layer becomes increasingly affected by the presence of a nearby solid surface. Complex structural changes occur in the reattachment region, including substantial pressure recovery, a peak and subsequent decay in turbulence stresses, and the beginnings of "recovery" of the reattached shear layer to the structure characteristic of wall-bounded turbulent shear flow. Even for high Reynolds numbers, the overall flow pattern (reattachment length) can be affected by slight changes in geometry and inlet conditions, which in turn alter the structure of the shear layer approaching reattachment. The specific objective of this study has been to examine the importance of changing the structure of the separated shear layer on the reattachment process itself.

Four series of experiments were designed to provide reattaching flows with slightly perturbed structure. For all cases, Reynolds number based on step height was greater than 20,000, the expansion ratio was 5/3, and the inlet boundary layer was less than one-half step height in thickness. From these, three main cases were selected for more detailed study. A crucially important phase of the work involved the development of a new "pulsed wall probe" for measurement of skin friction in the reattachment region, thus providing an unambiguous definition of the reattachment length. The detailed data obtained for two of the cases were used as a test case for turbulent flow computation by the recent 1980-1981 Stanford Conference on Complex Turbulent Flows.

Although the separating boundary layer was thin for all cases, a surprisingly strong dependence of reattachment length on the boundary layer thickness was found. The effects of Reynolds number, angle of the duct downstream of separation, and the addition of a regular array of embedded streamwise vortices into the separating boundary layer were also studied. Reattachment lengths in the range of seven to ten step heights were measured for the various cases. For each case, a thin, viscous region of strong backflow was identified adjacent to the surface substantially upstream of the reattachment point. It was possible to investigate this region in more detail than was previously possible using the pulsed wall probe developed for measuring skin friction in the reattachment region.

All seven reattaching flows studied were found to possess similar structure in spite of the variation in reattachment length among the cases. Quantitative features of reattachment--including the streamwise development of the mean and fluctuating velocity field, pressure rise, and skin friction--were found to be similar when distance was scaled by the reattachment length. A simple, functional definition of the reattachment zone as the region which extends roughly 40% of the reattachment distance about the reattachment location is proposed.

Table of Contents

List of Figures

List of Tables

Nomenclature

AR	Area ratio, W_2/W_1.
B	Maximum thickness of separation region.
C_f	Skin friction coefficient, $\tau_w/\frac{1}{2}\rho U_{ref}^2$.
C_p	Pressure coefficient, $(P - P_{ref})/\frac{1}{2}\rho U_{ref}^2$.
C_p^*	Reattachment pressure rise coefficient, $(C_p - C_{p,min})/(1 - C_{p,min})$.
h	Height of pulsed wall-probe wire array.
H	Step height.
ℓ_R	Extent of reattachment zone.
L	Body dimension.
P	Wall static pressure.
Re_H	Reynolds number based on step height, $U_{ref}H/\nu$.
Re_θ	Boundary layer momentum thickness Reynolds number, $U_e\theta/\nu$.
u	Fluctuating streamwise velocity component.
u'	rms value of u, $\sqrt{\overline{u^2}}$.
u_τ	Wall shear velocity, $\sqrt{\tau_w/\rho}$.
U	Streamwise velocity component, $\overline{U} + u$.
U^+	Inner velocity, $\overline{U}/u_\tau$.
U_e	Free-stream velocity.
W	Duct width.
W_1	Inlet duct width.
W_2	Exit duct width.
X	Streamwise coordinate.
X^*	Scaled streamwise position, $(X - X_R)/X_R$.
Y	Coordinate normal to step surface.
Y^*	Coordinate normal to opposite wall $(Y^* = W - Y)$.
Y^+	Inner coordinate, Yu_τ/ν.

Y_e Distance from wall surface to free stream.

Z Spanwise position coordinate.

Greek

ρ Fluid density.

ν Fluid kinematic viscosity.

τ Total shear stress.

τ_w Wall skin friction.

δ^* Boundary layer displacement thickness:

$$\delta^* \equiv \int_o^{Y_e} \left(1 - \frac{\overline{U}}{U_e}\right) dy$$

θ Boundary layer momentum thickness:

$$\theta \equiv \int_o^{Y_e} \frac{\overline{U}}{U_e} \left(1 - \frac{\overline{U}}{U_e}\right) dy$$

Π Coles' wake parameter.

γ Forward flow fraction.

α Downstream duct angle.

δ Boundary layer thickness.

Sub/Superscripts

$\overline{}$ Overbar, denotes time-average.

' Prime, denotes rms of a fluctuating value, e.g., $\sqrt{\overline{u'^2}} \equiv u'$.

ref Quantity measured at the reference location.

R Quantity measured at reattachment location, which is defined as the point of $\overline{C}_f = 0$.

Chapter 1

INTRODUCTION

1.1 Project Background

The single-sided sudden expansion provides a classic practical example of a two-dimemsional reattaching flow. In addition, it is a model case for study of the general characteristics of flows which exhibit regions of separation with reattachment. Reattachment--the process whereby a free shear layer becomes increasingly affected and finally dominated by the presence of an adjacent solid surface--occurs in a wide variety of engineering systems. A few examples of such systems are diffusers, airfoils at angle of attack, sudden area changes in pipes or ducts, and atmospheric flows over buildings, fences, hills, or bumps. Recent interest at Stanford in flow reattachment was motivated by studies of the performance of wide-angle planar diffusers, as explained by Kim et al. (1978).

Aside from providing direct physical insight which is useful in explaining flow phenomena in engineering systems, the single-sided sudden expansion configuration (also called the backward-facing step or "backstep") provides a particularly important case of a change in flow "species": from boundary layer before separation, to separated free shear layer, then back to a boundary layer. Reattachment is thus viewed as a zone of readjustment of the turbulence structure characteristic of the separated free shear layer to that of a flat-wall boundary layer. Because it lies near the boundary of current computational capabilities and involves several flow zones in one field, this type of flow was emphasized by the Organizing Committee of the 1980-1981 Stanford Conference on Complex Turbulent Flows as a particularly useful test case.

Our aim in the present study has been to provide a description of the process of two-dimensional, turbulent, incompressible reattachment which will be useful both to describe the important physical phenomena and to furnish data suitable for comparison and evaluation of numerical computations and models of this type of flow. To motivate the specific objectives of this study, the general features of the flow under study and relevant previous work will be reviewed below.

1.2 Flow Details--A Summary

In this section, some general features of the flow within a single-sided sudden expansion will be outlined. The picture presented here is necessarily drawn from the wealth of previous work in the field, which is reviewed in the next section. The intent of the following discussion is to give a groundwork in order to facilitate the more detailed review, and to establish necessary nomenclature.

1.2.1 Zones of Flow

The geometry and reference quantities needed to describe the case under study are given in Fig. 1-1. The flow field is separated into six zones; although these are not sharply defined, it will prove useful to discuss the flow field in terms of these zones. The zones are: I, the separated shear layer; II, corner eddy; III, backflow zone; IV, the reattachment region; V, redeveloping near-wall flow; and VI, the relaxing outer shear layer. The following description will be confined to the case of current interest: large step height ($\delta/H \leq O(1)$) and high Reynolds number ($Re_H \geq 10^4$). Zone numbers will not be assigned to the core region or opposite-wall boundary layer, since the structure of these is well known. Neither region is specifically discussed below.

Immediately downstream of separation, a free shear layer begins to grow (Zone I). In spite of the proximity of the lower bounding wall, this layer appears very similar to a plane mixing layer in both growth rate and turbulence structure. The features of this zone are sensitive to initial conditions such as the separating boundary layer characteristics and free-stream conditions, as is the case with other plane mixing layers. Zone I extends downstream for 3-5 step heights until the reattachment process begins.

Zone II--the corner eddy--is a complex region of reseparation, wherein velocities are very small--one to two orders of magnitude smaller than the free stream speed. This region is highly three-dimensional and extends for about one step height downstream; it is not of interest in the current study. Note that the reseparation is consistent with a small favorable pressure gradient which exists just downstream of the expansion.

To understand Zone III, the backflow zone, one needs to look at the reattachment zone first. The distinguishing feature of the reattachment zone, Zone III, is the very low mean velocity which exists therein. Hence, momentum changes are small and may be neglected, and conservation of streamwise momentum requires that the surface pressure gradient be balanced substantially by the stress gradient normal to the wall. Including the total time-averaged stress (including turbulent pseudo-stress) in τ,

$$dP/dx \approx d(\tau)/dy \quad . \tag{1-1}$$

The mean shearing stress at the surface vanishes at reattachment by definition (see below); stresses about one step height away from the surface are approximately those expected in a plane mixing layer. Equation (1-1) implies that a substantial adverse streamwise pressure gradient must exist in the reattachment region. This pressure rise, which actually begins upstream of the reattachment point itself, drives strong reversed flow into Zone III; this reversed flow supplies fluid required by entrainment of the separated shear layer. The negative velocities in Zone III reach a maximum of roughly 20% of the external flow velocity.

The reattachment region, Zone IV, is the area of central interest in the current study. As noted above, the region is characterized by very low mean velocity and strong adverse pressure gradient. Local turbulence intensities in this region are very large, and the flow is observed to reverse direction frequently. A tuft of yarn attached to the surface in this region will be observed to flop forward and backward; oil brushed onto the surface will be driven to form a visible line. The reattachment point (actually a spanwise line) is unambiguously defined for two-dimensional flow as the location of zero average wall skin friction. The distance from the step to the reattachment point is the reattachment length; this distance is the single most important length scale which describes the flow pattern, since the extent and location relative to the step of the different zones is specified by the reattachment point.

Downstream of reattachment, the attached layer recovers the structure of a flat-wall turbulent boundary layer. The recovery occurs in two stages: in Zone V, the near-wall flow quickly regains the structure of the zero-pressure-gradient boundary layer through the action of viscous and vigorous near-wall, small-scale, turbulent diffusion; the recovery of the outer layer (Zone VI) is, however, much slower. This is a very complicated flow in which the turbulence structure remaining after reattachment slowly regains the outer wake-like structure of a boundary layer. This change is effected by dissipation or "large eddies" and slow turbulent diffusion. The skin friction reaches approximately the asymptotic downstream value, and the near-wall velocity profile takes on the familiar law-of-the-wall shape approximately ten step heights downstream of reattachment. However, up to ten times (about 100 step heights) longer is required for the outer layer to achieve the shape factor and turbulent shear-stress distribution of a "normal" flat-wall turbulent boundary layer.

1.2.2 Governing Parameters

Even when attention is restricted to the case of high Reynolds number and large step height, the reattachment length, structure of individual zones, and the interaction between zones can be affected by geometry and initial conditions. Three main nondimensional parameters are thought to be most significant in describing the conditions for the simple expansion of Fig. 1:

i) Reynolds number based on step height: $Re_H = U_{ref}H/\nu$,

ii) Boundary layer thickness to step height: δ/H,

iii) Area ratio: $AR = W_2/W_1$.

Other potentially important factors include free-stream turbulence intensity and spectral character, step aspect ratio (ratio of step span to height), as well as the thickness of the boundary layer on the opposite wall.

It is simple to show (e.g., Leal and Acrivos, 1969) that the reattachment length must be directly proportional to Reynolds number for fully laminar reattachment. Interest in the current study is restricted to higher Reynolds numbers normally found in the kinds of applications which motivated this study; at $Re_H > 10^4$, the reattachment length is only very weakly dependent on Re_H.

Parameter (ii), boundary layer thickness, seems to have some effect on flow structure. δ/H would be expected to affect shear layer structure, and some combinations of Re_H and inlet boundary layer thickness could produce a laminar or transitional boundary layer at separation, depending on whether trips were used--even with fairly high Re_H. Parameter (iii), expansion ratio, provides a geometric constraint that would alter pressure distribution. Precisely what effect each parameter actually has not been well understood; hence, this question will receive more attention in the detailed literature review which follows.

1.2.3 Measurement Difficulties

Comparison of experiments and evaluation of the previous works on the subject are made more complicated by lack of reliable instrumentation suitable for use in the complex regions I-V. Many factors contribute to these difficulties. Streamline curvature and gradients of static pressure normal to the surface are expected to affect the turbulence structure. Extreme levels of turbulence intensity and fluctuating flow direction occur in the reattachment region, and the mean velocity profiles do not possess a simple similarity shape as in a boundary layer. Thus, extreme caution must be applied when considering results obtained by conventional methods that have sometimes been used in zones where their applicability is questionable (e.g., hot-wire anemometry used in the backflow or reattachment zones).

1.3 Previous Work

Separation with reattachment is the subject of intensive current study, as evidenced by the extensive body of literature which exists concerning flow reattachment in a wide variety of configurations. Comprehensive reviews of earlier works related to the turbulence structure of two-dimensional, incompressible, reattaching flows were undertaken by Mueller (1961) and by Bradshaw and Wong (1972). Recently, Eaton and Johnston (1980, 1981) conducted an extensive update of these works. They concentrated attention on the particular case of the incompressible backward-facing step. Eaton and Johnston evaluated 23 such studies and assessed the importance of experimental parameters and measurement techniques in comparing the results from different investigations. This review will not duplicate these recent reviews, but will concentrate specifically on those works which give insight into the details of the reattachment process.

Four areas will be covered by the review. First, even though this study is of incompressible flow, reattachment with supersonic free-stream velocity should be considered, as there must always be an essentially incompressible region about the reattachment location, where velocity is zero. Reattachment heat transfer provides an important means of describing gross features of flow reattachment, and local maxima in heat transfer have been observed in the reattachment region. Configurations other than the backward-facing step are included, because the approximate balance between streamwise pressure and normal stress gradient in these cases is the same as for the backstep. Listed roughly in order of increasing relevance to the study of incompressible reattachment in the single-sided sudden expansion, the areas reviewed are as follows:

- Reattachment with compressible external stream (Sect. 1.3.1).
- Surface heat transfer behavior by reattachment (Sect. 1.3.2).
- Incompressible studies which include turbulent reattachment in configurations other than the step (Sect. 1.3.3).
- Two-dimensional sudden expansion (including the symmetric expansion, Sect. 1.3.4).

Because of the large number of relevant references, the difficulties of measurement using older techniques and the general lack of understanding of both flow structure and the relative importance of governing parameters, it is not possible to provide a concise, distilled review in the following sections. Also, the deeply interested reader will probably need to study several of the underlying references to follow the review. Thus, the reader may wish to skip to Section 1.3.5, if only an overview of the present study is desired.

1.3.1 Reattachment with Compressibility

Early work on flow reattachment was motivated by the supersonic "base pressure problem"--i.e., the prediction of form drag of missiles and other projectiles. Kim et al. (1978) pointed out the substantial differences between the case of supersonic reattachment and the subsonic case; the supersonic flow contains shock and expansion waves within the separating shear layer and in the reattachment zone. Also, the Prandtl-Meyer relation can be used to relate turning angle and base pressure. The supersonic work of Reda and Page (1969) demonstrates these differences. They studied flow over a step at Mach 3.05 and, using color Schlieren and interferometer photography, showed the corner lip shock and flow turning at separation and reattachment. Previously, Korst (1956), Chapman et al. (1958), and Hastings (1963), for example, all studied various aspects of the supersonic base flow problem.

In spite of the important differences between the compressible and incompressible cases, some useful observations can be made. Chapman et al. (1958) proposed a theory for correlating the pressure rise by reattachment. Their work also emphasized the importance of Reynolds number in determining the laminar, transitional, or turbulent nature of reattachment. Depending on the type of reattachment, different behavior of the pressure rise was observed. Settles et al. (1980) conducted an experiment on a modified backstep at Mach 3 using an angled surface near reattachment to avoid the initial turning and lip shock near separation, so that the base pressure is quite near the free-stream value. Despite these studies, little information is available regarding the details of the reattachment process at high Mach number.

1.3.2 Heat Transfer at Reattachment

Heat transfer in regions of separation and reattachment with high free-stream Mach number has received substantial attention for applications such as the space shuttle and ICBM vehicles during re-entry. In their review of this field, Fletcher et al. (1974) listed over 100 experimental and theoretical studies in two-dimensional configurations and 85 for axisymmetric geometries. Naysmith (1958) and Seban et al. (1959) reported greatly reduced heat transfer coefficients in the separated region downstream of a step as compared to the upstream (attached) flow. A local maximum in heat transfer in the reattachment region was reported, followed by reduced heat transfer in the recovery zone. Chilcott (1967) and Reda and Page (1969) reviewed heat transfer phenomena in the reattachment zone of supersonic flows.

Several important studies regarding heat transfer in the reattachment zone of a subsonic flow downstream of an expansion or step have been reported. These include Filleti and Kays (1967), Seki et al. (1976a,b), Zemanick and Dougall (1970), Seban et al. (1959), and Seban (1964).

Filleti and Kays (1967) studied heat transfer on the isothermal surface downstream of a symmetric planar duct expansion. Air was the working fluid, and two expansion ratios were used with a high duct Reynolds number. In spite of the symmetric geometry, the flow downstream of the expansion was quite asymmetric; reattachment zones on the two sides of the expansion differed in length by about a factor of three. Comparing their heat transfer results to those of Abbott and Kline (1961), they concluded that the maximum heat transfer rates occurred in the reattachment region. The peak in heat transfer for longer stalls was lower and broader than that for the shorter stalls; for the expansion ratio of 3.1, the peak Nusselt number was about six times the far-downstream value, whereas for the long stall it was only about three times this same value. The peak Nusselt numbers are influenced by expansion ratio and Reynolds number.

In a similar study, Seki et al. (1976a,b) studied heat transfer using a constant heat-flux surface downstream of a symmetric channel expansion for a broad range of Reynolds number and expansion ratios. They also found asymmetric flow and proposed a simple correlation of maximum Nusselt number and stall length which takes account of the observed asymmetry and dependence of stall length on expansion ratio. Seki et al. found that Nusselt number depends on Reynolds number to the 2/3 power--about as proposed by Filleti and Kays (1967) and Zemanick and Dougall (1970) for a pipe expansion.

Zemanick and Dougall (1970) examined heat transfer on the constant heat flux surface in a pipe expansion using three expansion ratios and fully developed turbulent upstream flow. Reynolds number based on upstream diameter was in the range $0.4\text{–}9 \times 10^4$, depending on diameter ratio; the three values of the latter employed were 1.22, 1.85, and 2.33. Local maximum heat transfer rates always occurred 5–10 step heights from the expansion; these values were 3–5 times the fully developed downstream Nusselt number for the expansion ratios tested. About 25 downstream pipe diameters were required for the Nusselt number to recover the value for a fully developed downstream flow in the case of $Re = 5 \times 10^4$ and diameter ratio 1.85. A simple correlation was given to relate maximum Nusselt number (based on downstream diameter) to upstream Reynolds number; it seemed to correlate their results over the range of Re tested and all expansion ratios.

Seban et al. (1959) and Seban (1964) studied heat transfer in the reattaching air flow over a single backstep at high step Reynolds number. The earlier study utilized a blunt model with a surface step placed in a wind tunnel (two models were tested); the later work employed a single-sided expansion in a planar duct flow. In addition to measuring surface temperature along the constant heat flux test surface, surface pressure distribution and some anemometry data using Pitot probes and hot wires were reported. Seban (1964) extracted some rather tentative conclusions from these results. He showed that the Reynolds analogy between heat and momentum transport certainly does not hold near reattachment. He also showed that the negative skin friction in the backflow region does not seem to evolve as it would if a "reverse" turbulent boundary layer began growing at the reattachment point. The recovery of the reattached-layer velocity profile was also described in some detail.

1.3.3 Reattachment in Other Configurations

Turbulent reattachment occurs in other two-dimensional and axisymmetric geometries aside from the backward-facing step. All nomenclature for these examples is shown in Fig. 1.2. The configurations include: bluff bodies with downstream splitter plates; fences and ribs; airfoils at moderate angle of attack, hills, and humps; and pipe expansions. Less obviously relevant are the cases of planar and axisymmetric contractions (including the forward-facing step) where the separation and reattachment occur following the sharp edge; these latter will not be covered in the following review. Direct comparison of many of these flows with the sudden expansion is made difficult because these configurations generally produce more complex flows (with the possible exception of the sharp-edged fence). Several potentially interacting separated regions can exist. Often, the separation location is not fixed; the mean dividing streamline can leave the separation location at a substantial angle to the mean flow direction. However, many similarities in the features of reattachment persist, and these will be emphasized by citing recent representative experimental work below.

1.3.3.1 Bluff Bodies with Splitter Plates

Flow about bluff bodies with trailing splitter plates (Figs. 1-2a,b) has received considerable attention over the past 30 years, probably due to the early realization that the use of splitter plates could reduce base drag by about one-third in a certain range of body Reynolds numbers (cf. Arie and Rouse, 1956). This work, as well as studies by Roshko and Lau (1965), Bearman (1965), and Smits (1981) will be discussed below. Smits (1979) has prepared a critical review of this subject which goes into details not covered below.

The classic and oft-referenced study on reattachment to a splitter plate placed downstream of a normal plate model in a wind tunnel is that of Arie and Rouse (1956), who investigated turbulent reattachment on the splitter using a wind tunnel with its wall contoured to simulate an infinite stream. Hot-wire anemometry measurements of mean velocity were used to deduce the streamline pattern, from which the reattachment length appears to be $17H \pm 1.5H$. In spite of the fairly high Reynolds number used ($Re_H = 4 \times 10^4$), one expects the initial boundary layer to be very thin and laminar, due to the strong acceleration of the flow around the sharp corner just prior to separation. Maximum values of turbulence quantities found in this study occurred in the reattachment zone.

The streamline pattern reported by Arie and Rouse shows that the mean dividing streamline leaves the separation point at an appreciable angle to the mean-flow direction. The general shape of the reattachment region streamline pattern does, however, appear very similar to that which results from a step reattachment. Thus, for comparison to the step, take the effective step height to be the maximum distance between the mean dividing streamline and the surface (denoted B). Then the "aspect ratio" of the separation bubble is defined as X_R/B. For the results of Arie and Rouse, $B = 2.6H$, giving $X_R/B = 6.5$--an aspect ratio very much like that found for the separation produced downstream of a single-sided sudden expansion. The following discussion will show that the separated regions produced in many two-dimensional geometries have similar aspect ratios.

Roshko and Lau (1965) gave important insight on pressure rise by reattachment in their study of pressure recovery on a splitter plate placed downstream of several different-shaped forebodies. Shapes used were a square-nosed plate the same thickness as the splitter, normal plates (similar to those of Arie and Rouse), and three blunt-nosed models. The free-stream velocity was kept constant at 8.7 m/s for all cases; owing to the small sizes of models employed, the separating flow was certainly laminar for all cases. However, $Re_H = 0.15 - 1.5 \times 10^4$, and the authors reported that transition to turbulence occurred in the shear layer after separation, so that the reattaching flow was more or less turbulent. This study extended the theory of Chapman et al. (1958) to define a normalized reattachment pressure rise coefficient for subsonic flow, and this quantity was shown to collapse to a single curve for all cases considered when streamwise distance was normalized by the reattachment length. Reattachment length was determined by two methods--(i) using a surface oil flow, and (ii) placing a total pressure probe on the surface (presumably, reattachment was assumed to coincide with the location where the pressure reading of an upstream-facing probe equaled that of a downstream-facing one).

Bearman (1965) investigated the suppression of vortex shedding in a bluff body wake owing to the addition of splitter plates of varying length. He found that shedding was suppressed for splitters longer than 2.5 body heights (A), although reattachment (visualized using the surface oil-flow method) did not occur on the splitter unless it was at least 2.9 base heights long. The bluff body used was fairly long ($L_1/A = 6$, giving Re_x at separation of 2.5×10^5), and a trip was used. Therefore, the case with the longest splitter (8.53 step heights) is very much like a backstep configuration. The corresponding parameters are $Re_H = 4.2 \times 10^4$, $\delta/H = 1.1$, and expansion ratio = 1.03. The reattachment length in step heights was 6.2, and the reported base pressure coefficient for this case is -0.22. Some anemometry data from a single hot wire are reported.

Smits (1981) reported results of a study using "very long" splitter plates at high Reynolds numbers ($Re_H = 1 - 15 \times 10^4$). The scaling of Roshko and Lau (1965) for the surface pressure distribution was seen to collapse these data very well (note the higher Re_H used in this study). Compared to that of Roshko and Lau, some 25 cases were investigated which used different-sized plates set at angles from 30-90° to the splitter to produce separation. Reattachment length depended strongly on blockage ratio (analogous to expansion ratio for the backstep); reattachment length decreased from over 30H to about 14H as blockage increased from 1% to 10%. The decrease can be explained simply by considering the reduction in the maximum height of the mean dividing streamline caused by the velocity constraint of the nearby parallel solid surface; this height is about 2.5H for 1% blockage, but only 1.5H with 10% blockage. Reattachment length was obtained by using a small-diameter (1.06 mm) Preston tube to measure skin friction in the recovery region, then extrapolating the distribution back to find the location of $\overline{C}_f = 0$. Although the trends reported in this study should be reliable, the actual reattachment lengths may be affected by a reported spanwise nonuniformity in the reattachment line.

1.3.3.2 Fences, Ribs, and Wedges

Obstructions of rectangular or triangular cross-section mounted on a surface exhibit multiple regions of separation and may possibly have several reattachment points (see Figs. 1-2e,f,g). Of most interest here are cases with blocks that are high ($\delta/H \leq O(1)$) and not very long ($L_1/H \leq O(1)$), including fences (very thin, sharp-edge ribs and wedges). Studies by Plate and Lin (1965), Good and Joubert (1968), Ranga Raju and Garde (1970), Ranga Raju et al. (1976), Durst and Rastogi (1980), Castro and Fackrell (1978), and Castro (1981) illustrate the important features of this class of flows.

In attempting to simulate atmospheric forward-facing flow over hills, Plate and Lin (1965) studied air flow over a flat-faced, sharp-edged wedge. Two wedge heights and four free-stream velocities were used, giving $Re_H = 0.78 - 6.3 \times 10^4$. Two relatively large wind tunnels were used, resulting in thick boundary layers ($\delta/H = 1-10$) ahead of the wedge and small blockage ratios (1.4-2.8%). Surface pressure distributions, mean velocity (from a Pitot probe), and streamwise turbulence intensity (using a single hot wire) were reported. Reattachment length was determined using a specially built twin hot-wire probe and discriminator circuit. The reattachment location was defined as the point where the flow direction was downstream 50% of the time. Pressure distribution scaled approximately on wedge height, and the pressure coefficient varied little with Reynolds number. Reattachment length varied about 2.5 H when velocity was varied from about 6 to 17 m/s, when the test geometry was held constant ($L/H = 2$). The maximum streamwise turbulence intensity in the reattachment region was reported to be 22-24% for $Re_H = 3 - 6 \times 10^4$, δ/H about 2, and $L/H = 2$.

Good and Joubert (1968) examined flow of a moderately thick turbulent boundary layer ($0.43 \leq \delta/H \leq 12.5$) over a fence. For the thinnest oncoming boundary layer at $Re_H = 1.76 \times 10^5$ and with the fence providing about 10% blockage in the wind tunnel, they reported $X_R/H = 13.3$ and $B/H = 2.15$. Again, taking B as the effective step height, we find $X_R/B = 6.2$. Approximately 2/3 of the overall pressure rise is accomplished by the reported reattachment location, the latter having been inferred from streamline patterns generated from mean velocity measurements obtained using a Pitot probe.

Ranga Raju and Garde (1970) studied the form drag of inclined fences placed within a smooth-wall turbulent boundary layer. The experiments covered the range $0.195 \leq \delta/H \leq 4.35$ and $Re_H = 0.46 - 33 \times 10^4$; blockage varied from 1.2% to 43%. Base pressure decreased substantially with increasing blockage, and the effects of blockage and boundary layer thickness on drag coefficient were found to be independent. A later study by Ranga Raju et al. (1976) extended this work to cases in which the boundary layer developed on a rough surface.

Blockage of the wind tunnel created by the fence causes a substantial variation in reattachment length, as was recently shown by Durst and Rastogi (1980) in their investigation of reattachment downstream of fence/rib obstacles mounted on a flat wall. For the case of a fence using $Re_H = 2 \times 10^4$ and $\delta/H = 0.5$, reattachment length varied from 10.5 H for 50% blockage to about 17.5 H for approximately no blockage. In these cases, the reattachment location was determined using an oil and titanium mixture brushed onto the surface. The length of the recirculation was reduced if the fence was not sharp-edged and if it was made wider (i.e., a rib was substituted for the fence); the amount of the reduction (1-2 H) appeared to be largely independent of the blockage ratio. This last conclusion is supported by Castro and Fackrell (1978), who found that reattachment length downstream of a square-section block was decreased by about 2.5 H with $\delta/H = 9.3$ for 1% to 12% blockage.

The main intent of the investigation of Castro and Fackrell (1978) was to study the effect of blockage and boundary layer thickness on reattachment length and drag coefficient for flow over fences. Three different fence heights were used, giving $Re_H = 0.6\text{-}2.5 \times 10^4$ and $\delta/H = 0.29\text{-}9.3$. Using a differential twin pressure probe to define the reattachment location (reattachment was presumed to coincide with the location where the upstream-facing and downstream-facing pressure ports gave equal readings), they found reattachment length to be strongly affected by both blockage and boundary layer thickness. For example, at 5% blockage, reattachment length is decreased from about 16.5 H to 12 H for an increase in boundary layer thickness from 0.3 H to 9.3 H. Three values of δ/H from 0.3 to 1 all show about the same reattachment length over the range 1% to 12% blockage. Interestingly, the sensitivity of reattachment length to blockage is substantially less for thicker boundary layers, implying that these parameters do not act independently. This conclusion stands in contrast to the aforementioned work of Ranga Raju and Garde (1970), who found that the effect of these two parameters on drag coefficient could be considered independently.

Castro (1981) studied flow of a turbulent boundary layer over a rib of square cross-section ($L_1/H = 1$) mounted on a wall with $Re_H = 1.6 - 3.2 \times 10^4$; very thick as well as fairly thin boundary layers were used. Of relevance here is the study using δ/H of 0.34 to 0.8, which revealed some evidence of a shortening of the reattachment length with increasing boundary layer thickness. Unfortunately, no estimate of the magnitude of the reduction or even of the reattachment lengths was provided.

1.3.3.3 Airfoils, Hills, and Humps

Since separation occurs on a faired surface for this class of flows, they are somewhat less appealing as model configurations for the study of reattachment. One study, that of Tani (1974), which also reviews literature on airfoils with separation bubbles, will be discussed. Tani studied the laminar leading-edge separation which can occur in subsonic flow at moderate angle of attack. If the (displacement thickness) Reynolds number of the separating boundary layer is high enough, the separated flow undergoes transition to turbulence. Reattachment on the airfoil (with substantial pressure recovery) can then occur if the available pressure rise equals or exceeds that required by the external stream, i.e., if the angle of attack is not too great.

1.3.3.4 Pipe Expansion

Subsonic turbulent reattachment in an axisymmetric pipe expansion (Fig. 1-2d) has been extensively studied, due to the obvious direct applications in engineering systems. Teyssandier and Wilson (1974), Freeman (1978), Back and Roschke (1972), and Ha Minh and Chassaing (1979) presented representative studies of the problem. Teyssandier and Wilson (1974) performed an integral analysis of the flow using a simple mean-velocity profile family scaled by the velocity difference across the layer. Freeman (1978) used a laser-Doppler anemometer to measure velocity up to the reattachment region in a case with co-flowing hot and cold streams at the inlet to the expansion. Temperature profiles downstream were independent of Reynolds number for Re_D of 2×10^4 to 4×10^4. Reattachment length was inferred from velocity profiles as $X_R/H = 5$.

Back and Roschke (1972) studied water flow through a fairly large pipe expansion (diameter ratio 2.6) in the transitional Reynolds number range, $Re_D = 20\text{-}4200$; the separating boundary layer was very thin and undoubtedly laminar. Reattachment length (inferred from the motion of wall-injected dye) was determined for the range of Re_D, and the results are reproduced in Fig. 1-3(a). Note that $X_R/H = 9.5$ at the highest Re_D. The authors also report that the maximum backflow velocity (which occurs in the middle of the separated region) increases from about 6% to 21% of the free-stream velocity as Reynolds number is increased from 70 to 350.

Ha Minh and Chassaing (1979) studied the flow of air through an expansion with diameter ratio of 2 using $Re_D = 7.2 \times 10^4$ and $\delta/R = 0.3$ (case B of their study). Hot wires and Pitot tubes were used to measure mean velocity and construct streamline patterns from which a reattachment length of $x_R/H = 9$ was inferred. Maximum streamwise turbulence intensity relative to the centerline velocity was about 19%, with this peak coming in the reattachment region, followed by a rapid decay downstream. An interesting comparison can be made between their cases B and C; the latter uses an axisymmetric free jet. The effect of the wall as the shear layer approaches reattachment can be clearly seen--streamwise turbulence intensity increases rapidly just prior to reattachment, then drops rapidly downstream in the case of the pipe expansion. For the axisymmetric jet, the turbulence intensity increases with streamwise development to the value of the self-preserving flow far downstream.

1.3.4 Planar Sudden Expansion

Investigations of subsonic turbulent reattachment in single-sided and symmetric planar sudden expansions have been critically reviewed by Eaton and Johnston (1980,1981), who list 23 such studies in their summary table, reproduced here as Table 1-1. The intent of this review is to update their summary (see Table 1-2) and to highlight aspects of previous studies most relevant to the current study of reattachment. The evolution of instrumentation over the last 30 years has had a remarkable effect on the type and quality of information obtained in the reattachment zone. For this reason, the discussion below will divide the previous studies into three groups:

- Earlier studies--five older investigations which utilized traditional diagnostics (flow visualization, static pressure measurements, Pitot and hot-wire anemometry) seem to lay the groundwork for current research and are included here.
- Recent detailed investigations--these will include studies wherein mostly traditional measurement techniques were utilized. It must be noted that, while these did not in general provide much new physical insight into the problem, the results were much more reliable, since they could be benchmarked against

previous studies, and the hot-wire technique was greatly improved during the era in which they were carried out.

- Studies employing advanced measurement techniques--in the 1970s, advances in instrumentation provided the potential to overcome the inherent difficulties of traditional measurement techniques when used in separated and reattaching flows. A number of investigations, principally employing the pulsed-wire and laser-based anemometers, will be mentioned in this connection.

1.3.4.1 Earlier Studies

Five early investigations of subsonic, turbulent reattachment have laid the groundwork for physical understanding of flow within the sudden expansion downstream of single and double steps. The authors of these are Hsu (1950), Moore (1960), Tani et al. (1961), Abbott & Kline (1961), and Mueller (1961). Using surface pressure distributions, Pitot and hot-wire anemometry, and flow visualization, many important features of flow reattachment were discovered. These are listed below.

(i) Substantial pressure recovery accompanied reattachment (Hsu, Moore, Tani et al., Mueller).

(ii) Maximum streamwise turbulence intensities of 16-20% of the free-stream velocity occur near the reattachment zone (Hsu, Tani et al., Mueller). Abbott & Kline (the only study in water), using a hot film, found a maximum intensity of only 10%--this result has largely been attributed to measurement error.

(iii) Peak backflow velocities are 20-30% of the free-stream speed and occur halfway between the step and the reattachment location (Hsu, Abbott & Kline, Tani et al., Mueller).

(iv) The profiles of turbulent shear and normal stresses evolve similarly in the reattachment region.

(v) Reattachment length lies in the range 7 ± 1.5 step heights for all boundary layer thicknesses and expansion ratios tested, so long as the Reynolds number is reasonably high (Tani et al., Mueller, Hsu, Abbott & Kline). Step height was therefore used to normalize streamwise distance for comparing results.

(vi) Streamline patterns constructed from velocity profiles (Hsu, Tani et al., Mueller) or visual methods (Abbott & Kline, Moore) were used to provide an indication of reattachment length with typical quoted accuracy of about ± 1 step height.

Despite a successful description of the gross features of the backstep flow, nagging doubts remained as to the accuracy and completeness of the measurements, the range of parameters covered and their potential effects on flow structure, and the actual physics of the reattachment process--especially the possible importance of large-scale turbulent motions. Detailed studies (still utilizing mostly classical measurement techniques) were undertaken to address these questions.

1.3.4.2 Detailed Investigations

Chapman et al. (1958) showed the extreme sensitivity of the nature of reattachment (especially as to reattachment length and pressure recovery) at low to moderate Reynolds number. A number of studies have examined the low Reynolds number behavior of the flow, including those of Leal and Acrivos (1969), Goldstein et al. (1970), and Sinha et al. (1981). The last study showed the dependence of reattachment length on Reynolds number (obtained by varying step height and free-stream velocity); this result is shown in Fig. 1-3(b). The relevant conclusion for the current study is that reattachment length depends strongly on Reynolds number for $Re_H \leq 10^4$. However, the effects of inlet boundary layer state and thickness were not quantified. The comments of Chapman et al. (1958) point up the fact that the streamwise location of transition to turbulence is the important determining factor for flow structure.

Studies of backward-facing steps restricted to high Reynolds number were undertaken by Bradshaw and his students at Imperial College of Science and Technology in London, to ascertain more carefully details of sensitivity to aspect ratio and incoming boundary layer state (Brederode & Bradshaw, 1972), downstream recovery of the reattached layer (Bradshaw & Wong, 1972), and the turbulence structure of the flow near reattachment (Chandrsuda, 1975, and Chandrsuda & Bradshaw, 1981). Although hot-wire anemometry was used throughout to characterize the turbulence structure (casting some doubt on measurements in the regions of interest in the current study), many useful observations were made in the course of these investigations.

Brederode & Bradshaw (1972) studied the effects of finite tunnel span on nominally two-dimensional flow. They found that the effects of the side walls on reattachment length were opposite, depending on the laminar or turbulent state of the separating boundary layer. They also provided the oft-quoted criterion that the ratio of step height to tunnel span should be greater than about 10 to assure a reasonable region of two-dimensional flow near the centerline.

In their study of the recovery region, Bradshaw & Wong (1972) promulgated a "strength of perturbation" criterion for classifying flows with separation based on ratio of boundary layer thickness to step height. They asserted that the structure of the downstream flow can be independent of boundary layer thickness only for very thin separating boundary layers--this was in fact used as a design criterion for Chandrsuda's later study. The parameters of their study were $\delta/H = 0.12$, $Re_H = 4.3 \times 10^4$; the downstream wall was angled slightly in an attempt to simulate an infinite stream (the nominal expansion ratio was 1.25). The recovering flow displayed a non-monotonic return of its skin friction (measured with a Preston tube) to the value appropriate to the far-downstream flow. The intermittency profile of the recovering layer was seen to be a hybrid between that characteristic of a boundary layer and that of a shear layer. Recovery of the shape parameters of the reattached layer to those of a "normal" flat-wall boundary layer was still not completed at $X/H = 52$, the last measurement station for this experiment. Through rough estimates of typical turbulence length scales in the shear layer upstream of reattachment and in the recovering flow, the authors concluded that the large eddies were "split in two" at reattachment; hence reattachment was described as a region of shear layer bifurcation.

Chandrsuda & Bradshaw (1981, from Chandrsuda's thesis of 1975) studied the turbulence stresses and turbulence energy balance in the reattachment region. The idea of the experiment was to produce a reattaching flow that simulated free-stream conditions (using a sloped opposite wall) and a very thin separating boundary layer to attempt to negate the effects of boundary layer thickness on the flow structure in the reattachment region. The experimental parameters were $\delta/H = 0.04$ (laminar), $Re_H = 10.8 \times 10^4$; the opposite wall was sloped inward at a 1.5° angle (the nominal expansion ratio was 1.4). Reattachment length was determined to be 5.9 step heights, from surface oil-flow visualization; this was in good agreement with an extrapolation of the skin friction measured with Preston and Stanton probes downstream of reattachment. The Stanton tube was also used to measure skin friction in the reversed-flow region, and a negative skin friction of $C_f = -0.001$ was noted at $X/H = 3$. Through analysis of their single and crossed hot-wire data in the separated and reattaching flow, the authors contended that the shear layer upstream of reattachment is very similar to a plane mixing layer*. The alteration of the turbulence structure in the reattachment region itself is explained by the confinement of the large eddies by the adjacent surface.

Narayanan et al. (1974) studied pressure recovery in the backstep using variable step height but constant free-stream velocity and inlet boundary layer thickness at separation. To simulate free-stream conditions (i.e., to simulate an expansion ratio of 1), some experiments utilized a contoured opposite wall. The range of nondimensional parameters obtained (via changing only step height) was $Re_H = 0.36\text{-}6.0 \times 10^4$, $\delta/H = 0.2\text{-}3.33$; expansion ratio was 1.01-1.14 for the cases without "area compensation". Surface-pressure coefficient and reattachment length (obtained via surface-oil flow observation) were reported. Reattachment length varied between about 5.8-6.4 step heights for all the "uncompensated" (straight opposite wall) cases, and compensation decreased the reattachment length for all step heights tested by about 0.3 H. The authors proposed an arbitrary streamwise length scale and empirical pressure scale to obtain a better collapse of their data than was possible by using the coordinates of Roshko & Lau (1965).

---

*Hot-wire data in regions of flow reversal are not expected to be accurate (see comments of Ha Minh and Chassaing, 1979, below), but conclusions drawn do appear qualitatively valid.

The effects of system rotation on shear-layer behavior and reattachment distance was studied by Rothe & Johnston (1975) at Stanford. A water channel, with flow visualization as the predominant diagnostic method, was used. The expansion ratio was 2, the Reynolds number range was $Re_H = 0.3\text{-}2.8 \times 10^4$, and the inlet flow was nearly fully developed. Rotation (about a spanwise axis) can be either stabilizing or destabilizing to visually observable motions in the shear layer; the effects of both senses of rotation on reattachment distance was reported. The authors reported that their findings indicated that "...augmentation of three-dimensional turbulent mixing can reduce X_R/H (reattachment distance) in stationary systems..." For a highly destabilized shear layer, a reattachment distance of $X_R/H = 3$ was noted, whereas without rotation the reattachment length was 7.8 step heights. In this study, reattachment length was obtained using a tedious procedure of frame-by-frame analysis of motion picture records of dye and hydrogen bubble motions. Plots of percent forward flow at the surface versus distance along the wall in the reattachment region were then generated. By fitting a smooth curve through these data, the location of 50% forward flow (assumed to coincide with the reattachment position of $C_f = 0$) was located. The authors attributed an uncertainty of $\pm$ 0.4 H to reattachment length determined in this manner.

Bandyopadhyay (1977) reported some visualization of the turbulent motions near reattachment. He reported:

> "...the motions (of the shear layer) are highly three-dimensional...(the re)attachment point fluctuates widely and large and vigorous eddies proceed downstream...intermittency extending virtually through the layer..."

The visualization technique was accomplished using a laser light source to illuminate smoke introduced into the flow. Some high-speed motion pictures were taken, and fairly high velocities (up to 11 m/s) were employed.

The studies of Kim et al. (1978, 1980) have contributed tremendously to the expertise and understanding needed for the flurry of research activity in our group. These studies employed two different step heights; the free-stream velocity, thickness of the separating boundary layer, and upstream duct width were held constant. Using the nondimensionalization which has been followed throughout this review, the parameters for the experiment are summarized below.

H, cm	Re_H	δ/H	AR	Aspect Ratio
3.81	4.66×10^4	0.30	1.5	16
2.54	3.11×10^4	0.45	1.33	24

Conventional measurement techniques (except a special technique for intermittency measurement) were used to obtain surface pressure distributions, cross-stream static pressure variation, mean velocity and turbulence stresses, and intermittency profiles. Emphasis in these studies was placed on obtaining a complete mapping of the static pressure field and obtaining turbulence data to be used in modeling, especially for the near-field recovery region. The reattachment location (determined by surface oil flow and by observing the motion of wool tufts attached to the surface) was reported to be 7 ± 1 step heights for both step heights used. A new normalization of the pressure coefficient was proposed to account for the pressure recovery obtained when expansion ratios near the Borda-Carnot optimum of 2 are used. Cross-stream variation in static pressure was mostly caused by high values of the turbulent normal stress $(\rho v'^2)$, rather than by streamline curvature. The intermittency measurements of Kim et al. and conclusions regarding the evolution of turbulence quantities downstream of reattachment are in general agreement with the observations of Chandrsuda & Bradshaw (1981). A new correlation of the derived eddy viscosity profile with boundary layer parameters in the recovery region was proposed.

In a study of flows relevant to the simple pipe expansion, Ha Minh and Chassaing (1979) studied flow of a thin $(\delta/H = 0.05)$ boundary layer over a step at $Re_H = 10 \times 10^4$. The step was a bluff model placed in a wind tunnel of circular cross-section which created about 6% blockage in the facility, roughly equivalent to an expansion ratio of 1.06. Mean velocity and turbulence stresses measured with hot-wire and Pitot probes as far as $X/H = 12$ were (quite cautiously) reported by the authors, who warned that, "...in spite of the precautions that have been taken...the experimental results in such flow patterns still have large errors." The authors remind that, "...where the velocity vector locally reverses, the hot-wire anemometer measurements lose all significance, since the thermal dissipation depends only on some effective cooling velocity," and that the results "...obtained by a pitot tube, after detecting the direction of the local velocity, seem to be more accurate." The reported reattachment length (presumably deduced from velocity profiles) was 6.4 step heights. Other results from this study using a pipe expansion and an axisymmetric jet were mentioned in a previous section.

Kuehn (1980) presented a bit of new data and analysis of existing data to support the contention that reattachment length tends to increase with increasing expansion ratio. The new data presented give reattachment distance and some velocity profiles in the recovery region for two straight-step cases with AR = 1.14 and 1.33, $Re_H \geq 4 \times 10^4$, and δ/H approximately 1 and 0.5. The author asserts that differences in pressure gradient are responsible for the dependence of X_R/H on AR, and reports reattachment length obtained in a case of sloped upper surface (the surface was sloped to superpose a pressure gradient on the reattaching flow). This configuration was later studied in some detail by Driver & Seegmiller (1982).

1.3.4.3 Studies Using Advanced Measurement Techniques

Recent work on the backstep has been aided by advances in instrumentation for highly complex turbulent flows. Instruments for making time- and directionally-resolved velocity measurements that have become available include the flying hot-wire anemometer (e.g., Coles and Wadcock, 1978), the pulsed-wire anemometer (Bradbury & Castro, 1971), and laser-based optical anemometers. Only the last two have been employed in studies of the backstep to date, and these have never been checked against each other by the same investigator. Thus, although the potential for improved reliability in the results is great, one must approach existing results from these new techniques with some caution. Studies employing the pulsed-wire anemometer are those of Baker (1977) (also reported by Moss et al., 1979), Eaton & Johnston (1980), and Cheun et al. (1981). After these are discussed below, studies which employed laser anemometry will be reviewed.

Baker (1977) reported on the use of the pulsed-wire anemometer to study flow in three different step configurations: a backstep, a forward-facing step, and a rib. The backstep used $Re_H = 5 \times 10^4$, $\delta/H = 0.7$, and an expansion ratio of 1.1 and had a step aspect ratio of 18. The reported reattachment length (from surface-oil flow visualization) was 5.8 step heights. Extensive evaluation of the pulsed-wire technique, including calibration and comparison with a hot wire , was undertaken, and the author gives observations concerning practical aspects of the use of the probe. Generally good agreement was noted between the pulsed wire and hot wire in regions where both techniques should work. As anticipated, the hot wire seems to undermeasure turbulence intensity in the separated shear layer, the recirculation zone, and the reattachment zone. Several limitations of the pulsed wire were noted by Baker, including the tendency for calibration drift and the extreme fragility of the sensors. As with the other two studies to be discussed below, Baker used the pulsed wire only to measure the mean and fluctuating streamwise velocity component. Owing to the large probe size and orthogonal-wire geometry, near-wall ($Y/H < 1$) velocity measurements could not be obtained. The technique was limited to flows with a maximum velocity of about 15 m/s.

The study of Eaton & Johnston (1980) was performed with constant geometry and three different free-stream velocities, giving Re_H of about 1, 2.2, and 4×10^4; this variation in free-stream velocity with constant geometry caused a change in state of the separating boundary layer from laminar to transitional and finally to turbulent. At the highest Reynolds number used, $\delta/H = 0.2$, the boundary layer is tripped to make it fully turbulent at separation. The pulsed wire was used to measure mean and fluctuating streamwise velocity. These data were augmented by crossed hot-wire data in the outer part of the shear layer. Surface pressure distributions and anemometry data were presented for all three cases up to $X/H = 12$. The reported reattachment length at the highest Reynolds number is eight step heights.

This study also reported the development of a "thermal tuft" (see Eaton et al., 1979) for determination of near-wall instantaneous flow direction. This device was used to locate reattachment with the assumption that the reattachment location corresponds to the point where the flow direction is downstream 50% of the time. More accurate determination of the reattachment location was made possible with this device, and some investigations of the time-dependent aspects of reattachment were explored, including the possibility of "low-frequency" motions in the reattaching flow. The similarity of the separated flow structure to that of a plane mixing layer was confirmed by a separate experiment, in agreement with Chandrsuda's conclusion. Correlation length scales in the shear layer were not found to be much longer in the spanwise direction than in the normal direction. Some of the current investigation was undertaken concurrently with the end of Eaton's study and is reported by Eaton and Johnston (1980).

Very recently, Cheun et al. (1981) have made some use of the pulsed-wire anemometer in their study of the effect of free-stream turbulence and boundary layer thickness on reattachment. Two boundary layer thicknesses, $\delta/H = 0.14$ and 0.67, and two different free-stream turbulence intensities (0.5% and 3.5%) were tested with $Re_H = 5.45 \times 10^4$, and an expansion ratio of 1.12. Under these conditions, increasing free-stream turbulence had very little effect on flow structure. However, there was a tenuous indication that the thinner boundary layer caused a shorter reattachment length, but the magnitude of the decrease was not evaluated. Only a few pulsed-wire profiles were reported, and there were no pressure data or recovery information. Much of the anemometry from this preliminary report is from single hot wires.

Nearly all workers using lasers have realized the need to shift the frequency range by using either a rotating grating or Bragg cell so that the direction of the velocity vector can be ascertained. Some studies have employed two-color systems so that instantaneous determination of two velocity components was possible. Many schemes for identifying and eliminating "bias" errors have been proposed, but there seems to be no general agreement as to the sources or potential magnitude of possible measurement errors. Obvious limitations of the laser systems are the need for optical access, the necessity for seed in appropriate quantity and of the right size, and the limitations imposed by the fairly short focal distance used in most systems. As mentioned above, the workers have not yet compared their laser measurements in the recirculation and reattachment regions directly with either of the other methods (i.e., the flying hot wire or the pulsed wire) available for making directionally resolved velocity measurements.

Laser-Doppler anemometry has been used extensively at low Reynolds number in the sudden expansion--such studies include those of Durst et al. (1974), done in air with a tracker and oil-droplet seeding using a symmetric expansion, of Cherdron et al. (1978), who did some visualization to augment their investigation of the onset of instability, and of Restivo & Whitelaw (1978), who were interested in the turbulence field for Re_H less than 3000. These studies have no direct relevance to the current work, but do help to evaluate laser-anemometer performance in recirculating flow.

One group has reported the use of photon-correlation processing of a Doppler signal in the backstep--Grant et al. (1975) and Mullin et al. (1980). The former study concerns a backstep with only a moderate Reynolds number ($Re_H = 0.35 \times 10^4$) in air with an effective expansion ratio of 1.5. The latter report concerns the effects of free-stream unsteadiness and will not be discussed here; the same basic laser system was apparently used. The objective of the earlier study seems to have been to demonstrate the use of the photon correlation system in this flow. A few profiles of mean and fluctuating streamwise velocity for $0.5 \leq X/H \leq 4.5$ are provided and compared to results of Tani et al. (1961). The maximum measured turbulence intensity at $X/H = 4.5$ is 22%--significantly higher than Tani's, but in good agreement with other laser and pulsed-wire measurements. The maximum backflow velocity is about 25% of the free-stream speed at $X/H = 3$.

Using a single-component laser system with the beams rotated at ±45° to the through-flow direction, Etheridge & Kemp (1978) were able to deduce turbulent shear stress, as well as streamwise mean and fluctuating velocity. They used an open-channel water flow and reported on inlet-flow uniformity as well as velocity and turbulence data as far as 8.26 step heights downstream. The reattachment length for their configuration (deduced from streamline patterns) is reportedly 4.9 step heights--the lowest known reported value for a backward-facing step with turbulent reattachment. The streamwise evolution of u'/U_{ref}, which obtains a maximum value of about 22%, doesn't begin to decay rapidly until after $X/H = 6$. Previous investigations have been cited which overwhelmingly agree that the stress decay begins very near the reattachment location. Since the same trend is seen in reported $\overline{u'v'}$, one suspects that their reported reattachment length is in error—the actual reattachment location is probably much nearer to $X/H = 6$.

Four very recent and relevant studies, done at higher Re_H, will be discussed next. The first is that of Bremmer (1980), which used a single-sided expansion with area ratio of 2, $\delta/H = 0.3$, and $Re_H = 17 \times 10^4$. Unfortunately, the inlet duct used was square, so for an expansion ratio of 2 the step aspect ratio is only 1—hardly a configuration which could be expected to produce two-dimensional separated flow! However, this study does provide detailed information on the design and use of a laser system and a backstep in air at high velocity (see also Stevenson et al., 1979, for these details).

Smyth (1979) reported a study of plane symmetric expansion in a water flow with $Re_H = 0.75 \times 10^4$, a nominally fully developed turbulent inlet profile, and an expansion ratio of 1.5. Peak values of u'/U_{ref} were about 19%, and the downstream flow was quite symmetric.

Durst & Tropea (1981) used two water-channel facilities to study the dependence of reattachment length on Reynolds number and expansion ratio (see Fig. 1-3(c)). Reattachment length was determined by extrapolating the line of zero mean velocity (as located using a laser-Doppler anemometer) to the surface. Area ratios of 1.1 to 3 were employed, and the range of Reynolds number was about $Re_H = 0.3\text{-}4 \times 10^4$. The authors show a strong dependence of reattachment length on expansion ratio at constant Re_H; for expansion ratio about 2, $X_R/H = 8.5$, whereas at $AR = 1.1$, $X_R/H = 5.3$ (with $Re_H = 1.5 \times 10^4$). They also point out the similar shape of the plots of X_R/H vs. Reynolds number curves at constant area ratio. This observation suggests that the effect of area ratio on reattachment distance may be uncoupled from that of Reynolds number (and possibly boundary layer thickness).

Driver & Seegmiller (1982) used a two-component LDV in a wind tunnel with $Re_H = 3.8 \times 10^4$, $\delta/H = 1.5$, and expansion ratio of 1.13. The effect of sloping the opposite wall was studied; the intent was to superpose an adverse pressure gradient on the reattaching shear layer (see Kuehn, 1980). A novel technique for making directionally resolved average skin-friction measurements using a laser to measure the time-dependent thickness of an oil film was also employed. The authors report complete sets of data, including surface-pressure distribution, the laser anemometry, and the skin friction in the reattachment zone. Much more will be said about this study later, as it represents the most complete set of data for the backward-facing step obtained to date with advanced instrumentation.

1.3.5 Implications of Previous Work

The literature review revealed several remaining unanswered questions regarding the features of reattachment. Those of direct relevance to the current study are enumerated below.

1. The generally accepted definition of the reattachment point for two-dimensional flow is the location of zero time-averaged wall skin friction. A striking variety of methods has been used to locate the reattachment point, but it is not clear how some of the results can be related to the unambiguous quantitative measure of the reattachment position ($\overline{C}_f = 0$). When this study began, there were no reported time-dependent measurements of skin friction in a reattachment region.

2. There appears to be a large (but often unstated) uncertainty in reported reattachment lengths--this is due in part to the ambiguity in the definition of reattachment length mentioned above. For example, the uncertainty assigned to the visual measurements of reattachment length by Kim et al. (1978) was ± one step height (out of seven). This uncertainty could be critical, because the strong streamwise gradients of static pressure, turbulence stresses, and heat-transfer coefficient occur very near reattachment and over a distance less than the reattachment length.

3. Nearly all the currently available data for the backstep at high Reynolds number put reattachment length in the range $5.6 \leq X_R/H \leq 8.5$. However, reattachment length in the single-sided sudden expansion at high Reynolds number does appear to vary systematically in this range

with expansion ratio and separating boundary layer thickness. The precise nature of the variation is a subject of continuing research.

4. No specific study of the sensitivity of the reattaching flow to changes in shear layer structure has been performed. Shear layer curvature, streamwise pressure gradient, state and thickness of the detaching boundary layer, and free-stream turbulence are a few of the parameters which different investigators have thought to be important in determining the structure (e.g., rapid decay of turbulence stresses downstream of reattachment) of the reattaching flow. However, a complete list of such parameters does not seem to have been formulated.

5. In other cases (aside from the sudden expansion) where two-dimensional, turbulent reattachment occurs, complicating factors (multiple, possibly interacting, separation regions; stronger curvature of the mean dividing streamline; different streamwise pressure gradients experienced by the separated shear layer during its evolution) obscure direct comparison of the features of reattachment. However, many qualitatively similar characteristics were noted above for all of these cases of reattachment.

6. A physical description of the reattachment process does not exist. The role of coherent motions or "large eddies" in the reattachment process is unknown; very little information on the spectral nature and turbulence length scale in the reattachment region exists. Development of such a model is being slowed by the scarcity of reliable quantitative data (even regarding time-mean properties) near the reattachment point.

7. Most data sets for the single backstep suffer from insufficient documentation of flow conditions—in fact, in their evaluation of such studies for the 1980-1981 Stanford Conference on Complex Turbulent Flows, Eaton & Johnston (1980b) chose the investigation of Kim et al. (1980) as the most suitable for comparison with computations. Since this study did not utilize advanced measurement techniques, a large uncertainty must be attributed to results for the reattachment, recirculation, and separated shear layer regions.

1.4 Objectives of the Current Study

The overall objective of this work has been to provide a physical and quantitative description of two-dimensional turbulent flow reattachment in a single-sided expansion. Specific objectives listed below were motivated by the perception gained from the literature and from previous work at Stanford in the same research group (the Heat Transfer and Turbulence Mechanics laboratory at Stanford in the Thermosciences Division of the Mechanical Engineering Department). The four most relevant previous studies in our laboratory were those of Abbott & Kline (1961), Rothe & Johnston (1975), Kim et al. (1978,1980), and Eaton & Johnston (1980).

THe three major objectives of this work are:

1. Measure skin friction in the reattachment region

    a. Design and test a new concept for use of the pulsed-wire anemometer to measure skin friction (Eaton and Johnston, 1980, proposed the new concept and reported the early results for the work to be discussed here).

    b. Calibrate and qualify the device as extensively as possible to verify measurements and uncertainties.

    c. Use the device to measure skin friction in the reattachment region, thereby providing an unambiguous measure of the reattachment length.

2. Measure the sensitivity of the reattachment region structure to modifications in the structure of the separated shear layer upstream of reattachment. Changes in shear layer structure are to be effected by changes in structure of the separating boundary layer and augmentation of shear layer curvature.

    a. On the basis of preliminary tests, select two configurations (in addition to one "baseline" case) which produce substantial variation in the separated shear layer structure. It is supposed that such changes could be simply characterized by changes in the reattachment length.

    b. Quantify the similarities and differences in the three selected cases.

3. Document several cases well enough that these could be used as a basis for checking numerical computations of turbulent flows.
   a. Provide a simple, canonical inlet condition (i.e., a fairly thin, fully turbulent, separating boundary layer with a low free-stream turbulence level).

   b. Assure the spanwise uniformity of the inlet mean velocity profile.

   c. Cross-check measurements using different techniques, where possible.

   d. Check that two-dimensional conservation equations are satisfied for the resulting data set.

The next two chapters describe apparatus and procedures employed in the study. Note that Chapter 3 specifically covers development of the skin-friction probe (first objective). Results of the three main experiments are then presented and discussed in Chapters 4, 5, and 6.

Author(s)	B.L. Thickness at Separation δ/h	R_θ Separation	B. L. State at Separation	Re_h	Free-Stream Turbulence $\overline{u'}/U_o$	Aspect Ratio	Reattachment Length x_R/h	Turbulence Data	max $\overline{u'v'}/U_o^2$ x 100	max $\overline{u'}^2/U_o^2$ x 100	Configuration
Abbott & Kline [8]	.16-1.97	800-1600	Turb.	$2x10^4$ $-5x10^4$		2-15	7±1	Hot-film dubious results	—	—	Sudden expansion; double-sided
Baker [18]	.71	3500	Turb.	$5x10^4$	.15%	18	5.7-6.0	u' PWA u'v' x-wire	1.1	4.2	Small step in large tunnel y_1/y_o = 1.10
Bradshaw & Wong [2]	0.13	730	Lam.	$4.2x10^4$		30.5	6	--	—	—	Sudden expansion, shaped upper wall
Chandrsuda [6]	0.04	570	Lam.	$1.1x10^5$	0.07%	15	5.9	$\overline{u'}$ u-wire v', u'v' x-wire	1.1	2.7 4.0 w/ u-wire	Sudden expansion; top wall sloped down at 1.7°
Denham [20]	0.5	~150	Lam./ Turb.	$3x10^3$	--	20	6	u' laser	—	5	Sudden expansion 2:3
Eaton [10] & Johnston	0.23	890	Turb. trans.	$3.9x10^4$	0.3%	12	7.97	u' pulsed wire anem.	—	4.5	Sudden expansion 3:5
Eaton [10] & Johnston	0.23	510	Trans.	$2.3x10^4$	1.0%	12	8.2	u' pulsed wire anem.	--	3.4	Sudden expansion 3:5
Eaton [10] & Johnston	0.18	240	Lam.	$1.1x10^4$	0.3%	12	6.97	u' pulsed wire anem.	—	3.7	Sudden expansion 3:5
Etheridge & Kemp [19]	2.0	600	Trans.		2%		5.0	Frequency shifted LDV $\overline{u'}, \overline{v'}, \overline{u'v'}$	1.7	4.2	Free surface water channel; distance to surface = 14.5 h.
Grant [21]	--	--	Turb.	$3.4x10^3$	--	23	--	Laser u'	—	4.5	Small step in large tunnel
Haminh & Chaissing [15]	.05	—	Turb.	$1x10^5$	.1%	6	~6	--	—	--	Sudden expansion 5.5-6.6
Hsu [13]	.13	3300	Turb.	$2.5x10^5$	3.5%	4.5	>6.0 (6.3)	Hotwire u', $\overline{u'v'}$	50	3.6	Sudden expanpansion 2:3
Kim et al. [9]	.45	1400	Turb.	$3.0x10^4$	~.6%	24	7±1	$\overline{u'}, \overline{v'}, \overline{u'v'}$ x-wire	.95	2.47	Sudden expansion 3:4
Kim et al. [9]	.30	1400	Turb.	$4.5x10^4$	.6%	16	7±1	$\overline{u'}, \overline{v'}, \overline{u'v'}$ x-wire	1.00	2.84	Sudden expansion 3:4.5
Kuehn [24]	—	4950/ 12,000	Turb.	--	—	6	7	--	--	--	Sudden expansion 3°-4°
Kuehn [24]	--	4950/ 12,000	Turb.	—	--	12	6.74/ 6.51	--	--	--	Sudden expansion 3.5°-4°
Narayanan et al. [28]	3.33-.2	1800	Turb.	—	.03%	166-10	5.6-6	--	—	--	Small step in lg. wind tunnel
Rashed et al. [41]	—	—	—	$3.9x10^4$	.3%	10	6	u' hotwire	—	—	Sudden expansion 2.4:2.8
Roche [26] & Johnston	.5	<900	Trans. turb.	—	5.5%	15	7	—	—	—	—
Seki [16]	—	—	—	$3.3x10^4$	?	?	?	Hot-wire u'	.6	1.1	Sudden expansion, double sided
Smyth [11]	Fully devlpd.	—	Turb.	$7.0x10^3$	—	30	6	Laser $\overline{u'}$, $\overline{v'}$, $\overline{u'v'}$, $\overline{w'}$	1.1	2.8	Double-sided expansion 1:1.5
Tani [12]	.28	2100	Turb.	$6x10^4$	?	47.5	6.5-6.9	$\overline{u'}$ u-wire $\overline{u'v'}$ rotatable slant wire	1.3	3.5	Small step in large channel y_1/y_o = 1.07
Tropea & Durst [23]	2	1080	Trans. turb.	$5.5x10^3$	2%	—	15	Laser $\overline{u'}$, $\overline{v'}$, $\overline{u'v'}$	—	2.8	Free Surface water channel 7.5:1

Table 1-1 : Summary of previous experiments with backward-facing steps, from Eaton and Johnston (1981)

REFERENCE	ReH × 10^4	AR	δ/H	H cm	Uref m/s	u'/Uref %	B L (1)	W3/H (2)	Xr (3)	Anem. Meth.	Available Data (4)
Seban, Emery, Levy (1959) [air]	1.6 - 4.9	1.06	1.05 - 0.84	0.64	46 - 137	NA	T	24	6, c	NONE	Cp, Nu
	5.2 - 15.6	1.23	0.06 - 0.17	2.06	46 - 137	NA	L-R	7.4	5, c	NONE	Cp, Nu
Seban (1964) [air]	8.	1.29	0.25	2.54	46	NA	T	12	6, c	HW, TP	Cp, Nu, T, U
Bremmer (1980) [air]	17.1	2.0	0.3	10.16	25	2.0	T	1	6.9, a	LDV	Cp, U, u', v', u'v'
Durst and Tropea (1981) [water]	0.2 - 2.0	1.14, 1.25	(5)	4.0	.05 - 0.5	(6)	L-T	15	(6), a	LDV	U, u' (sparse)
	0.2 - 3.0	1.4 - 2.0	(5)	2.0	0.1 - 1.0	(6)	L-T	30	(6), a	LDV	U, u' (sparse)
	3.0	2.0	(5)	4.0	0.75	(6)	T	15	8.7, a	LDV	U, u' (sparse)
Sinha, Gupta, Oberai (1981) [air]	0.066	1.02	2.24	0.625	1.8	0.15	L	64.8	18, b	HW	Cp
	0.132	1.04	1.12	1.25	1.8	0.15	L	32.4	9.3, b	HW	Cp
	0.265	1.09	0.56	2.5	1.8	0.15	L	16.2	5.7, b	HW	Cp, U, u'
Chuen, Toy, Moss (1981) [air]	6.1	1.12	0.14, 0.67	9.0	9	0.5	L, T	15.2	NA	HW, PW	U, u', v'
Driver and Seegmiller (1982) [air]	3.78	1.13	1.47	1.27	44.2	NA	T	12	6, a	LDV	Cp, Cf, U, u'v', u'+v'

NA - Not available; not given by the authors or easily calculable from given data.

NOTES

1. State of separating boundary layer; L - laminar, R - transitional, T - turbulent
2. Aspect ratio - tunnel span divided by step height.
3. Reattachment length and technique for determinig it; a - velocity field or skin friction measurements; b - visual; c - from location of maximum surface heat transfer.
4. Type of data provided by authors (in addition to reattachment length, provided by all except Chuen et al., 1981)
5. Durst and Tropea (1981) used a fully-developed duct flow as the inlet condition.
6. Reattachment length varies with Reynolds number and expansion ratio.

Table 1-2 : Supplement to Table 1-1 : Backward-facing step experiments

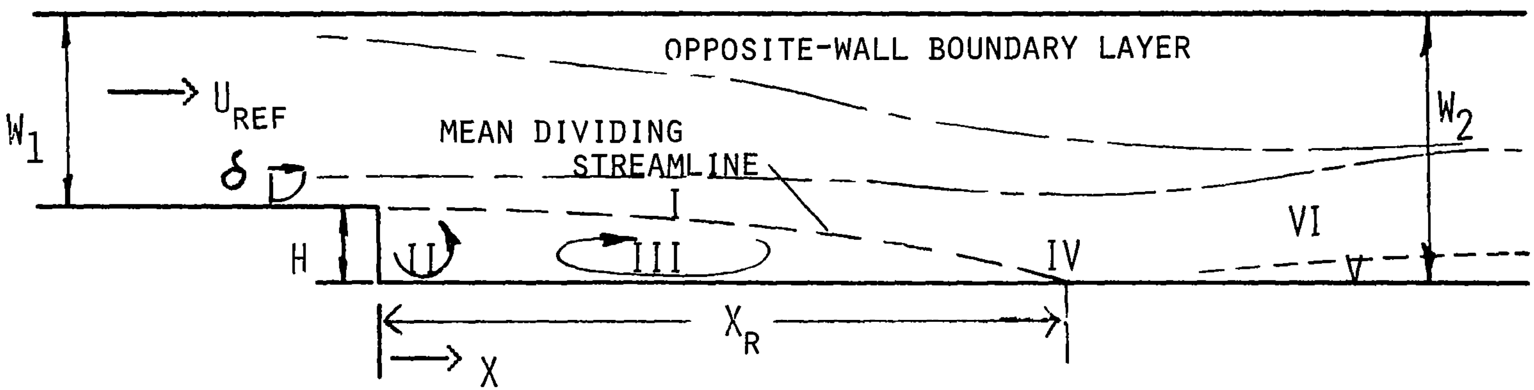

FLOW ZONES :

I SEPARATED SHEAR LAYER
II CORNER EDDY
III BACKFLOW ZONE
IV REATTACHMENT ZONE
V REDEVELOPING NEAR-WALL FLOW
VI RELAXING OUTER SHEAR LAYER

DEFINED QUANTITIES :

$AR = W_2 / W_1$

$RE_H = U_{REF} H / \nu$

Fig. 1-1. Geometry and flow zones for reattachment in the single-sided planar sudden expansion.

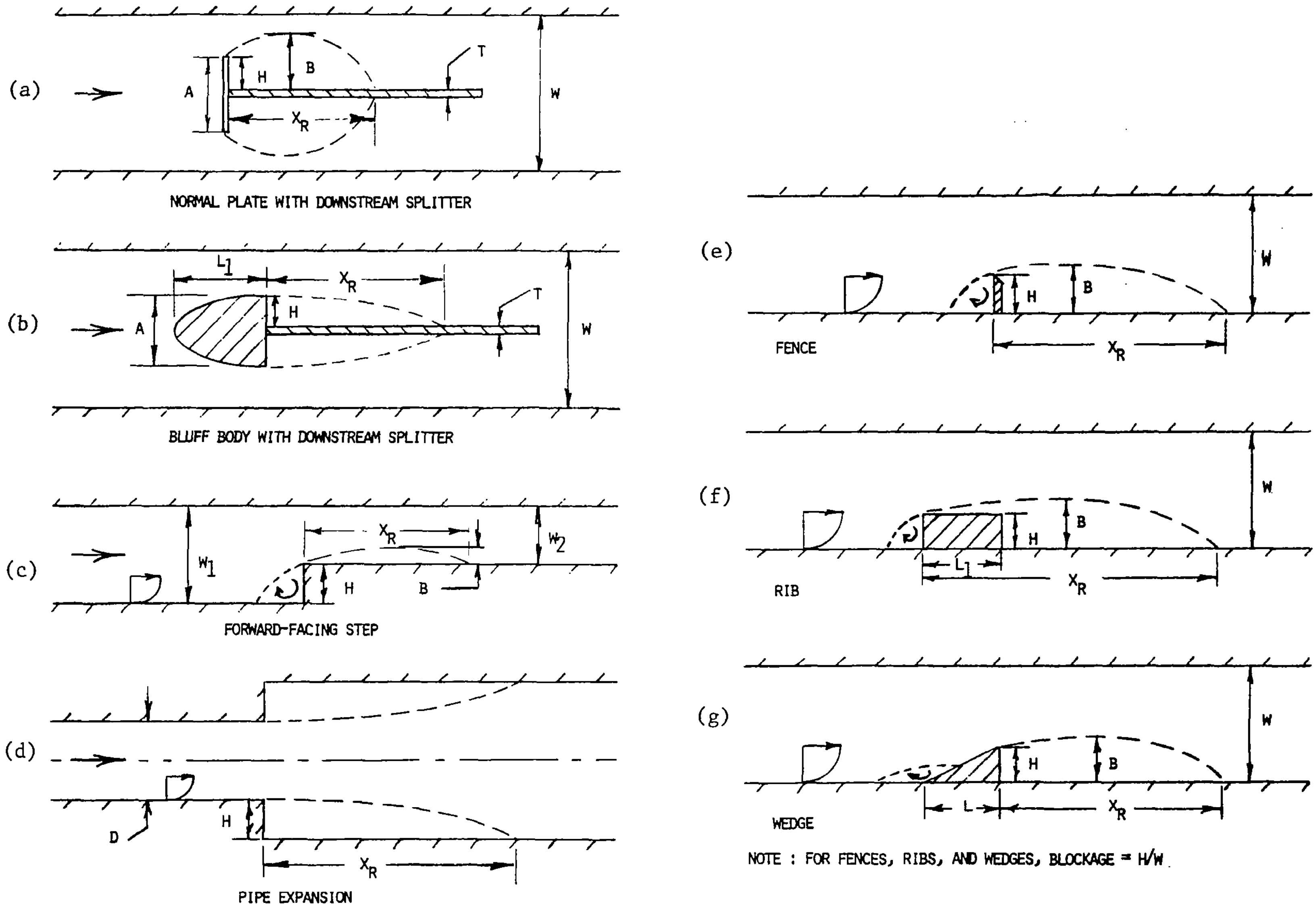

Fig. 1-2. Nomenclature for configurations other than the step which exhibit two-dimensional turbulent reattachment.

(a)

(b)

(c)

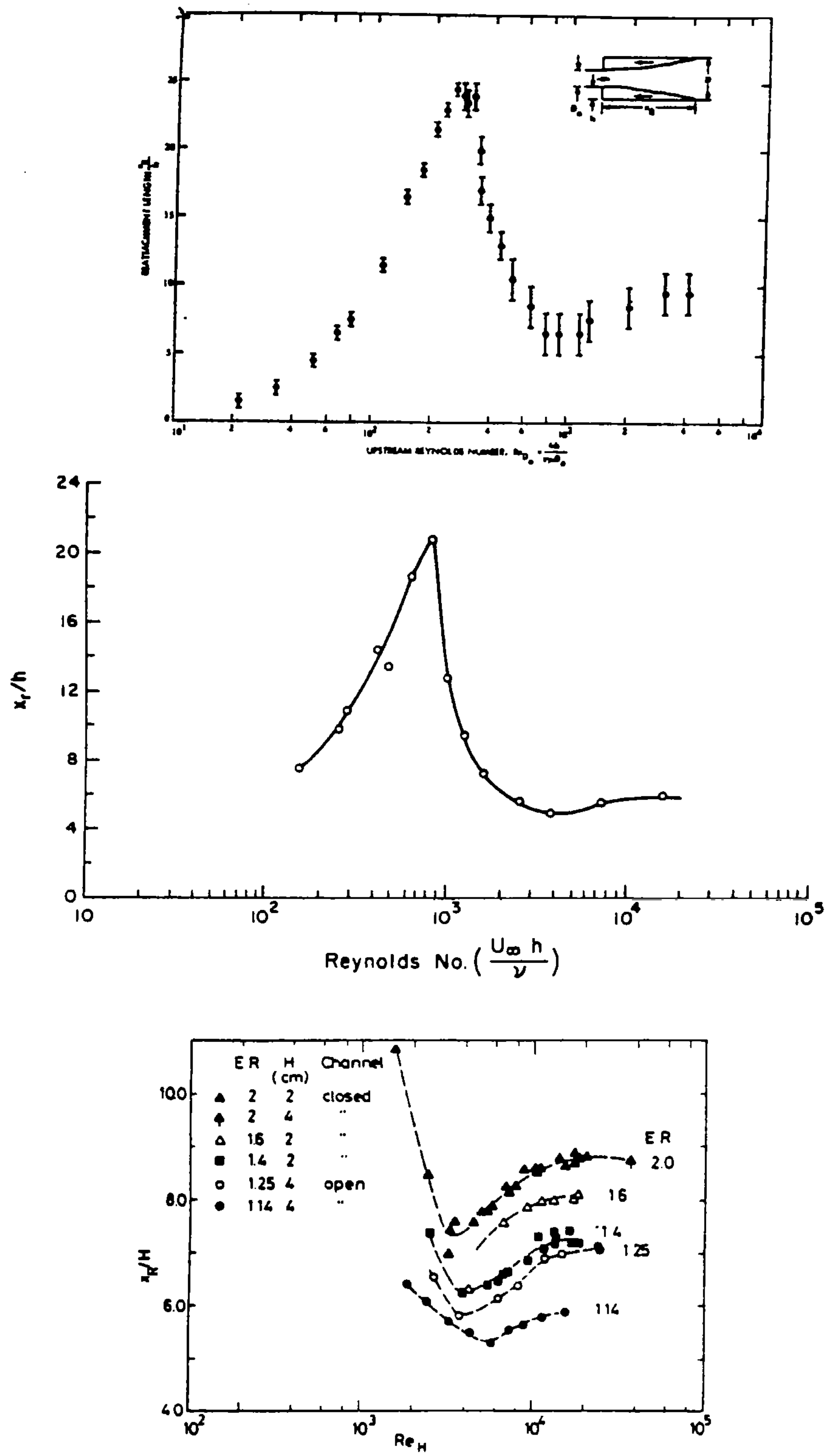

Fig. 1-3. Dependence of reattachment distance on Reynolds number shown by previous investigators. (a) Pipe expansion, from Back and Roschke (1972). (b) Backstep, from Sinha et al. (1981). (c) Backstep, with area ratio as a parameter, from Durst and Tropea (1981).

Chapter 2

APPARATUS AND PROCEDURES

In this chapter, the wind tunnel and specialized instrumentation used to obtain the results reported and discussed in the remainder of this report are described. Since the development of the pulsed-wall probe (for measuring skin friction in the reattachment region) required rather detailed design and qualification testing, it is treated separately in Chapter 3. The first section is a description of the wind tunnel. Modifications undertaken to improve flow uniformity and reduce turbulence intensity to the test section are briefly described--more detail is available in Appendix A. In the next section, the various specialized instruments (other than the pulsed-wall probe) are listed, and procedures for setup and use of the equipment are recorded.

Uncertainty estimates for the primary measurands are provided with the discussion on experimental procedures. An attempt has been made to identify the important known contributing factors to the quoted uncertainties. Since a main objective of the current work has been to provide data for comparison with numerical computations, all uncertainties are estimated at Nth order and to standard (20:1) odds (following Moffat, 1981). The method of Kline and McKlintock (1953) has been followed in propagating the uncertainties of the primary measurands through data-reduction equations. Where possible, the uncertainty estimates are checked by overlapping measurements of the same quantity with two different techniques.

A dedicated microcomputer was employed to facilitate many aspects of data acquisition, reduction, and plotting. Details for much of the software written in conjunction with this project can be found in reports which are held in the Internal Laboratory Report file of the Heat Transfer and Turbulence Mechanics Group, Mechanical Engineering Department, Stanford University.

2.1 Wind Tunnel

2.1.1 Blower and Upstream Flow Conditioning

A small blower-type open-return wind tunnel was used for all the experiments. At the outset of this project, the facility was precisely that used by Eaton and Johnston (1980) and described in their report. A three-phase synchronous electric motor is used to drive an eddy-current clutch, which in turn drives the airfoil-blade blower. This arrangement allows precise control of blower speed by varying the clutch voltage. Filtered air (nominal filter size 5 microns) is delivered through a diffuser to the settling chamber, where flow-conditioning devices are located. An 8:1 contraction precedes the test section (described in the next section).

Early in this work substantial nonuniformities in spanwise mean velocity upstream of the test section were discovered, using continuous spanwise traverses of total pressure taken approximately 2.5 cm upstream of the step edge. For these tests, the test-section step surface was removed to allow easy access for a spanwise traverse mechanism. A deficit in total pressure within the boundary layer along the step surface was found; the problem was most evident in the two traverses at $Y/W_1 < 0.5$, where a total pressure deficit of 10-20% existed. Of most concern was the observation that the nonuniformity was worst near the tunnel centerline--the location of most of the instrument ports used for access to obtain velocity profiles. The free-stream turbulence intensity measured in this facility was 0.5% at 12 m/s--this seemed higher than desirable.

Modification of the entire flow-conditioning arrangement was undertaken to improve spanwise uniformity and reduce free-stream turbulence intensity. A short settling chamber was added between the blower and the diffuser, in which grids were installed, followed by a honeycomb. This arrangement provided a better inlet flow to the diffuser downstream, making stall of that device less likely. The diffuser (a short, vaned design) was totally reworked as well. A small-mesh screen was installed at the inlet, and the vanes were removed. A constant-pressure design was selected, wherein coarse grids were employed to negate any pressure recovery and to enhance mixing (and thus flow uniformity). The settling chamber was shortened by removal of one segment of duct, which was replaced by a shorter segment for holding a set of three screens. Just upstream of the screen set, the existing long, large-celled honeycomb was replaced by an array of plastic soda straws, which served as a smaller, shorter honeycomb. The suction assembly was removed from the contraction, as it was thought to be unnecessary.

Results of the modifications were reflected in the spanwise total pressure profiles; spanwise uniformity in total pressure across the middle half-span was well within 2% for all values of Y/W_1 tested. The measured free-stream turbulence intensity was less than 0.25% at 15 cm upstream of the step, one half of the original level. In Appendix A, all the details of the facility modifications are provided.

2.1.2 Test Section

The wind tunnel test section was fitted into the nozzle exit downstream of the contraction. Several slightly different configurations were employed during the course of the study, but all used the same essential parts, with minor modifications. The test surfaces were made of Plexiglas sheet of thickness 1.27 cm (0.5 in.) and were 60.96 cm (24 in.) wide. The length of the wall upstream of the step could be varied by removing sections of wall so that L_1 = 0, 30.5, and 76.2 cm were possible. Two different arrangements of the supporting sidewalls were used--the first is the same as that used by Kim et al. (1978) and later Eaton & Johnston (1980). This arrangement was used here only for the angled-duct work (Series 2), and for Series 1b. For the other tests, a different supporting structure and sidewalls were used to provide more accurate positioning of the test walls and better access for flow visualization.

Static pressure taps were provided to allow surface pressure measurements. Instrument ports were machined in the test walls to allow access for probes and visualization equipment. The geometry of the static taps and standard instrument ports is shown in Fig. 2.1. Little machining of test surfaces was required for this study, as most of the test section parts were salvaged from the apparatus used by Kim et al. (1978) and later modified by Eaton & Johnston (1980).

2.2 Equipment

Specialized equipment was used to investigate flow characteristics, including pressure rise by reattachment, the velocity field, the reattachment distance, visual information, and skin friction. For hot-wire and total pressure profiles, an automated traverse was used. A microcomputer was purchased to facilitate data acquisition, reduction, and plotting. The computer system was mainly used for data acquisition in conjunction with anemometry and skin-friction measurements.

2.2.1 Lab Computer System

A microcomputer manufactured by Digital Equipment Corporation (DEC) was purchased and dedicated to the project. The computer, the LSI 11/2 version of the PDP 11-03 MINC (Modular Instrument Computer), was configured with 64 kB of memory and dual single-sided floppy disk drives (1 MB total storage capacity). Six interface boards were also purchased to allow communication with lab instruments for data acquisition and control. These interfaces included a real-time programmable clock, digital input and output modules (16 lines each), a digital-to-analog converter (D/A, four output channels), an analog-to-digital converter (A/D, 16 single-ended inputs), and a separate preamplifier for the A/D. The D/A and A/D both had 12 bits resolution. The preamplifier allowed the A/D to be used for current and resistance as well as voltage measurements and for true differential amplification of input voltages with gains of 0.5 to 500. Convenient interconnections between modules were provided by an extension to the DEC Q-bus.

Serial communication using standard IEEE-488 protocol was provided with the DEC MINC. This interface was used for connection to a dot-matrix printer (Integral Data Systems model 460), as well as to link the MINC to various other larger computers. The most frequently used computer was the Stanford campus facility (C.I.T.), which maintains an IBM 3033. Special software was written to permit the MINC to emulate a terminal and transfer data and programs to C.I.T. for storage on hard disk or tape. Some data processing was also performed at C.I.T., which maintains an extensive collection of numerical and statistical analysis subroutines. Figure 2-2 shows a schematic of the computerized data-acquisition system.

2.2.2 Pressure Measurement

Atmospheric pressure was measured daily using a mercury manometer located on the ground floor of Building 500. These readings (corrected for temperature) were used to compute air density. An uncertainty of ±0.2 cm of mercury is attributed to these measuremeents.

Total pressure and wall static pressure measurements were made using a Celesco model P7-D diaphragm-type pressure transducer (± 0.1 psid full-scale) with a Celesco model CD10B carrier demodulator whose voltage output varied linearly with pressure difference. This output was read directly by the MINC through the A/D or input to an HP-2401C integrating digital voltmeter. For measuring pressure distributions, no calibration of the transducer was necessary, as the linearity coefficient was found to be very stable for days at a time (± 0.25%). However, drift in the output voltage with no pressure difference (the zero level) was noted over an hour to be as much as a few millivolts, so the zero was rechecked every half-hour or so. When calibration of the transducer against a known pressure difference was necessary (as when using a Keil probe to calibrate a hot wire), a Combist micromanometer (1 inch of water full-scale) was used to measure a reference pressure. The uncertainty in pressure measurements done in the above way is estimated to be ± 0.001 inches of water.

2.2.3 Temperature Measurement

Flow temperature was monitored with an Omega violet-black thermistor (type P/N UUA-35J3, nominal resistance 5 kohms at 25°C), which was permanently installed at the wind tunnel exit. Diurnal variations in room air temperature of up to 5°C and seasonal variations of over 10°C are experienced in our rather large, open laboratory. The flow temperature could not be controlled at all, so that temperature variation had to be accounted for in all results. The temperature was used to compute air properties and monitored during use of the hot wires, as explained below. Temperature is related to thermistor resistance using a fit to the Omega calibration done by Simonich and Moffat (1982):

$$\frac{1}{T} = A + B \ln R + C(\ln R)^3 ,$$

with R in kohms and T in Kelvin,

$$A = 1.2858 \times 10^{-3}$$

$$B = 2.3599 \times 10^{-4}$$

$$C = 9.4329 \times 10^{-8}$$

The rms error of this fit over the range of 15-40°C is 0.01°C.

The uncertainty in determination of flow temperature using a thermistor is composed of contributions due to the resolution and accuracy of the MINC preamplifier used to read the resistance, the ability of the fitting function to represent the calibration, and the degree to which the standard factory calibration can be expected to apply to a particular thermistor. Based on observations from Arvizu and Moffat (1981), the absolute uncertainty in measured temperature is estimated to be ± 0.2C. Occasional comparison of measured values with a quartz thermometer indicated that this estimate was reasonable.

2.2.4 Wall-Flow Direction

The "thermal tuft" first described by Eaton et al. (1979) was used to measure the fraction of time that the flow was in a given direction near the wall in the reattachment region. This device, described in more detail by Eaton et al. (1981) consists of an array of three parallel wires. The center wire ("heater") of the array is continuously heated by a constant-current power supply. The thermal wake from this wire is detected by one of the flanking "sensor" wires, which are operated in a differential bridge configuration. A comparator is used, and the bridge output is either low (about 25 mV) or high (about 5 volts), depending on the sign of the imbalance. Although the device is nominally symmetric, up to 15% difference in calculated forward flow fraction can be noticed, depending on probe orientation. Not surprisingly, the largest differences in reading from the opposite orientations were found at locations where $\gamma = 0.5$. However, repeatable results were obtained if the two readings were averaged. Thus, each measurement actually consists of averaging two measurements obtained from using the probe in the two opposite orientations. The averaging time needed to obtain converged results is, of course, dependent on flow speed and length scales encountered in the turbulence motions. Sixty seconds were typically required in the backstep with inlet free-stream velocity of 12 m/s.

The thermal tuft probes, bridge, and power supply were precisely those built and used by Eaton & Johnston (1980). The sign of the bridge imbalance was averaged using an HP-2401C integrating digital voltmeter. The probe wire array was positioned about 0.5-1.0 mm from the surface; for this height, the results were not too sensitive to the precise position. A heater current of 1.5 amps was used. The uncertainty in forward flow fraction arising from sensitivity to orientation and resolution of the measuring equipment was estimated at 2%, which appears to agree with the repeatability of the measurements.

2.2.5 Probe-Traverse Mechanism

Profiles of mean and fluctuating streamwise velocity were measured at discrete locations where instrument ports were provided. These profiles were obtained by inserting the anemometer into a traverse mechanism, which consisted of a tube and flange which were bolted to the test-section wall. The end of the flange fit flush with the wind tunnel inner surface and had a hole through which the probe stem could slide. The stem was clamped to a piston, which slid in the inner bore of the tube. This piston, in turn, was attached to a threaded drive mechanism. For hot-wire and total pressure profiles, an automated drive was fitted onto the traverse, whereas a manual traverse using a micrometer was used for positioning the pulsed-wire probe. The manually operated traverse was graduated in increments of 0.025 mm.

The automated traverse used a threaded lead screw attached to a stepping motor driven by a translator manufactured by Superior Electric Company (SLO-SYN model ST-103). Two lines of the digital output module of the MINC were used to provide TTL pulses; the number of pulses determined the number of steps executed by the stepping motor, and the direction of motor rotation was determined by which line was pulsed. Each step was about 0.01 mm, and the positioning accuracy was independently verified to be better than 0.02 mm.

2.2.6 Total Pressure Probe Anemometry

A total pressure probe was used in conjunction with a wall static pressure tap to measure dynamic pressure in regions of low turbulence and no flow reversals. From these data, mean velocity was computed using the Bernoulli equation. The total pressure probe was made of a hypodermic needle (0.71 mm OD), which was hooked into a semicircular shape to avoid probe-stem interference effects. The small probe tip was soldered into stainless steel tubing (4.75 mm OD) which formed a stem. The stem was clamped to the motorized traverse described above, and the traverse was mounted in the wall opposite the surface with respect to which the wall was to be located (e.g., the opposite wall boundary layer was probed with the traverse mounted in the step wall). The wall location was found in one of two ways. If a port was available beneath the probe tip, a metal plug was inserted and an ohmeter attached to plug and probe stem. Otherwise, the wall was located by eye first, then this position refined by traversing the probe away from the wall until the pressure began to rise very rapidly. Either technique can be used to locate the surface to an accuracy of ± 0.05 mm, after some practice.

The pressure transducer described in Section 2.2.2 was calibrated for data acquisition; the thermistor temperature and atmospheric pressure were needed for data reduction. In some cases, no wall static pressure tap was available at the streamwise location of the probe; in these cases, the static pressure distribution was interpolated, and all readings were modified accordingly. The correction of Young and Maas (1936) for the effects of velocity gradient on the effective probe position was the only correction applied to the results. Since the upstream reference total pressure and temperature were continually rechecked during data acquisition, the slow drift in wind tunnel temperature and reference pressure should not affect the accuracy of the results. The main purpose of these results was to check the accuracy of hot-wire and pulsed-wire data in regions of overlapping applicability.

Uncertainty in velocity measured with a total pressure probe and the effective probe position in a turbulent, wall-bounded shear flow is influenced by several factors. These include the uncertainty in pressure measurement and the possible effects of turbulence, mean velocity gradient, and wall proximity on the measured dynamic pressure. By normalizing velocity on a simultaneously measured reference dynamic pressure, the uncertainty in determining air properties is removed from consideration. The following table summarizes uncertainty estimates for the range of conditions encountered in the present experiment. For these estimates, $U_{ref} = 12$ m/s, as is the case in all the experiment where total pressure measurements were performed.

Uncertainty in Velocity Measured with Total Pressure Probe
(expressed as a percent of the measured value of U/U_{ref})

U/U_{ref}	Best Case-- Uniform Flow	Worst Case-- $u'/U_{ref} = 0.15$
0.2	± 4.5%	± 5.0%
0.5	1.5	3.0
1.0	0.5	2.5
Uncertainty in effective probe position:		
Near the surface:	± 0.1 mm	
Away from surface:	0.05 mm	

2.2.7 Hot-Wire Anemometry

A single hot-wire anemometer was used to obtain mean and rms components of streamwise velocity in regions where no flow reversals were present, although some of the results taken for comparison with the pulsed-wire anemometer purposely violated this criterion. Commercial probe tips (DISA type 55P) were used; different tip geometries were necessary, depending on how close to the surface information was needed and whether the tip should protrude upstream of the stem. All probes had 5 micron platinum-plated tungsten sensor wires of length 1.25 mm oriented normal to the nominal flow direction and parallel to the duct surface. Appropriate DISA probe stems were mounted in the motorized traversing mechanism. The sensor was operated by a TSI, Inc. model 1050 constant-temperature bridge at nominal overheat ratio of 1.8. Frequency response was adjusted to be 3 dB down at 20 kHz, as determined by the Freymuth method recommended by TSI. The bridge output was low-pass filtered (DC pass) at 20 kHz cut-off, using either a Krohn-Hite model 3202 or Frequency Devices model 901F filter. The filtered output was read by the MINC A/D.

Use of the A/D presented a problem in resolving very low-intensity turbulent fluctuations. For the bridge and overheat ratio used, fluctuations of the order $u'/\overline{U} < 0.5\%$ could not be discerned from the noise inherent in the resolution of the 12-bit A/D converter. However, since the upstream flow is the only region where such low turbulence intensities are encountered, it was decided not to remedy the lack of resolution for low values of $u'/\overline{U}$–turbulence measurements with intensities greater than 1% are not significantly affected by this problem. When measuring the tunnel free-stream turbulence quoted in Section 2.1.1, the linearized form of the hot-wire response equation was used. For this measurement, a TSI model 1076 true rms meter was used to read the rms bridge output voltage.

Software was written on the MINC to automate calibration and profile acquisition. The procedure followed was first (before each profile was taken) to calibrate the hot wire in the free stream upstream of the expansion with a Keil probe used as reference. King's law was fit to a set of calibration data obtained by changing the blower speed in increments to yield a table of values of the filtered bridge output voltage versus velocity. For calibration over the range 5-15 m/s, an exponent of 0.45 was generally specified, resulting in a least-squares fit with rms error of less than 2%.

The probe and motorized traverse would then be positioned at the desired streamwise measurement port, and the wall would be located as described for the total pressure traverses above. A sampling rate of a thousand per second or less would be used to obtain several thousand samples, the required sampling period being as long as about 50 seconds for the data in the recovery region downstream of reattachment. The calibration was implemented by the software (no linearizers were used), so that only mean and rms velocity was stored for each point. A profile of 30 points could be obtained in less than 45 minutes, during which time variations in flow temperature were less than 0.5°C.

Uncertainty in the values of $\overline{U}$ and u' measured with a hot-wire anemometer has recently been treated by a committee of experts at the

1980-1981 conference of Complex Turbulent Flows recently held at Stanford. They provided guidelines for typical uncertainties if "good practice" is adhered to. Since the author attended these meetings, it was possible to determine what "good practice" would require, and the resulting equipment and procedures described above reflect the impressions gained. Consequently, the estimates below were derived from the aforementioned committee report (see Kline et al., 1981).

Uncertainty in Hot-Wire Velocity Measurements

$u'/\overline{U}$	Uncertainty Expressed as a Percent of the Measured Value $\overline{U}$	u'
< 0.3	± 2%	± 2-4%
> 0.3	Measurements at high local turbulence levels are provided for comparative purposes only and are not expected to be reliable.	

2.2.8 Pulsed-Wire Anemometry

A pulsed-wire anemometer of the type originally developed by Bradbury and Castro (1971) was used to measure streamwise velocity. Since this relatively new technique is currently in use in just a few laboratories around the world, operating details will be presented in some detail below. In Appendix D, pulsed-wire measurements of mean and fluctuating streamwise velocity are compared to results from a hot wire to further evaluate the accuracy of the measurements.

The pulsed-wire probe used for all experiments was the same probe used by Eaton & Johnston (1980), and very similar to the one which Baker (1977) used for his study of a backward-facing step. A cental "heater" wire of diameter 12 microns is flanked by two 5-micron sensors made of platinum-plated tungsten wire. These wires are soldered to supports which are fitted into a stem of about 7 mm OD. The nominal distance between the heater and sensors is about 3 mm, and the length of all wires is approximately 10 mm. Although the probe is nominally symmetric, the device actually used was not carefully aligned. This led to much different calibration constants for the two wires, as explained below.

Special electronics were needed to provide the voltage pulse to the heater wire and to discern the arrival and time-of-flight of the hot tracer created when the heater was pulsed. A Malvern Instruments, Ltd. type L.B.J. pulsed-wire anemometer was used for this purpose. The operating parameters of this device were very carefully optimized for the desired calibration range, so that "noise" created by the highly turbulent flow past the sensor wires would not trigger the time-of-flight counter. This constraint required selection of a fairly low sensor wire current with a high output gain and careful setting of the trigger detection level. The following settings of the Malvern adjustments were used.

Adjustment	Setting
Pulse amplitude:	40 volts
Trigger level:	3 (- wire), 2.5 (+ wire)
Sensor current:	4 milliamps
Output gain:	7 X

With the above settings and the probe used for this study, only a limited useful calibration range could be obtained. A characteristic of the pulsed-wire anemometer is that the signal amplitude is inversely related to velocity; this sets the limit for the highest velocity which can be used for a given setting of the trigger level. Signal amplitude is very high at low velocity (less than 5 m/s), so the lowest calibration velocity is determined by the accuracy with which the low velocity is known. Since a Keil probe was used to calibrate the pulsed wire, it was decided to extrapolate the calibration rather than to try to actually measure velocity and time-of-flight for velocities less than 1.5 m/s. Frequent calibration of the probe was thought to be necessary, based on the observations of other workers (e.g., Baker, 1977). However, calibration constants did not appear to vary as much or as systematically as Baker (1977) found. Nonetheless, automatic calibration was possible, so the probe could be calibrated in less than 15 minutes; therefore, the calibration procedure was repeated approximately every hour. Typical calibration range and constants are recorded below. Note that, due to the aforementioned geometric asymmetry of the probe, the range and constants for the two wires are much different. This means that the probe was always oriented with the "- wire" downstream relative to the tunnel main flow direction.

		Constants	
	Calibration Range	A	B
- wire	1.5-13 m/s	3.0×10^3	1.0×10^6
+ wire	1.5-8 m/s	1.5×10^3	1.2×10^6

The calibration relation recommended by Bradbury & Castro (1971) and found satisfactory by Baker (1977) was also used here:

$$U = \frac{A}{T} + \frac{B}{T^2}$$

with U the velocity in m/s and T the time-of-flight in microseconds. The rms error of the calibration function fit was generally less than 5%.

The MINC was used to actuate the Malvern electronics to acquire a velocity sample, read the time-of-flight, and implement the calibration function. Since the Malvern anemometer is equipped with an interface of antiquated design, some rather complicated strategies were necessary to make available MINC interface hardware work properly. The software evolved as more experience with the MINC exposed better ways to implement the interface. The software used is contained in Westphal (1982).

The usual operating procedure for obtaining pulsed-wire velocity profiles was first to calibrate the probe in both orientations against a reference velocity measured by a Keil probe placed in the uniform, low-turbulence free stream upstream of the step edge in the test section. The blower speed was automatically stepped in about a dozen increments to give a table of values of velocity versus time-of-flight. A least-squares fit to the calibration function described above would then yield the calibration constants and rms error. The entire calibration procedure took less than 15 minutes for both wires.

Following calibration, the probe and traverse were moved to the desired location and a velocity profile acquired. The position of the probe relative to the surface was calculated by measuring the probe position in the traverse; this measurement was verified by eye. The accuracy in locating the probe in this manner is about ± 0.5 mm. This was acceptable because of the large size of the probe, which prevents measurements closer to the wall than within about 6 mm. One or two thousand samples were taken at each location, from which mean and rms streamwise velocity was computed. A sampling rate of 3-15 per second was used, depending on which interface software was used to operate the electronics. Typically, twenty points were taken for each profile at even spacing (the near-wall region cannot be probed, due to the large probe size).

Accuracy of measurements of mean and fluctuating velocity measured by the pulsed-wire anemometer has been treated by Castro and Chuen (1982), who make a few observations of relevance to the current study. The pulsed-wire cannot be expected to yield reliable measurements of u' in flows of very low local turbulence intensity ($u'/\overline{U} < 10\%$) due to the inherent signal-to-noise ratio of the device. In flows of moderate local turbulence intensity ($10\% < u'/\overline{U} < 30\%$), the expected accuracy of u' measurements is comparable to that of hot-wire measurements (about 15% uncertainty in u'). Uncertainty in u' is not expected to increase for higher-intensity turbulent flows, where hot wires cannot be used. Uncertainty in $\overline{U}$ and u' arising from the finite size of the probe when used in a mean velocity gradient, as well as the signal-to-noise ratio, has been estimated by Eaton and Johnston (1980). Considering also the accuracy to which the calibration function fits the calibration data, the following guide to pulsed-wire measurement uncertainty obtains. Note that the uncertainties are expressed as a percent of U_{ref} in the table.

Uncertainty in Velocity Measured with the Pulsed-Wire Anemometer
(Estimates are for the particular case of $U_{ref} = 12$ m/s)

$\overline{U}$ m/s	$u'/\overline{U}$	Uncertainty Expressed as a Percent of U_{ref}	
		$\overline{U}/U_{ref}$	u'/U_{ref}
0-5	> 0.1	± 5%	± 2%
5-12	"	2	3
0-5	0.05-0.1	5	5
5-12	"	2	5
0-5	< 0.05	5	totally unreliable
5-12	"	2	"

2.2.9 Smoke-Wire Flow-Visualization Technique

The smoke-wire flow-visualization technique was used to examine the visually observable motions in the separated flow. A fine wire was coated with oil to form small, evenly spaced droplets through the action of surface tension. A DC voltage applied to the wire vaporizes the oil, which then condenses to form bright, white streaklines in the flow. A high-intensity strobe flash of very short duration was used to illuminate the smoke and effectively freeze the action so that a still photograph may be obtained. Alternatively, high-speed motion pictures could be taken, using intense, focused flood lighting. The smoke-wire technique has been used by many researchers—e.g., Corke et al. (1977) and Batill & Mueller (1981). The advice of Prof. Hassan Nagib and his students at Illinois Institute of Technology, who have extensive experience in using the smoke wire, has been valuable in performing the visualization for this study. Generally, the use of smoke-wire visualization is most prevalent in air flows of moderate speed (less than 10 m/s).

Control circuitry is needed to apply voltage to the smoke wire and synchronize the photographic equipment with the presence of the smoke. A complete commercial system, including a relay and timing box, was purchased from Flow Visualization Systems for this purpose. Although some high-speed motion pictures were taken, the length of time when smoke is present is so short (less than 0.25 sec) that less than a few hundred frames could be exposed at 600-800 frames per second. All of the results shown later were obtained using still photography with strobe illumination and a 35 mm SLR camera. Push-processing and contrast enhancement were used in developing and printing the photographs. In Appendix B, a more complete description of the experience gained in the various aspects of using the smoke-wire is provided.

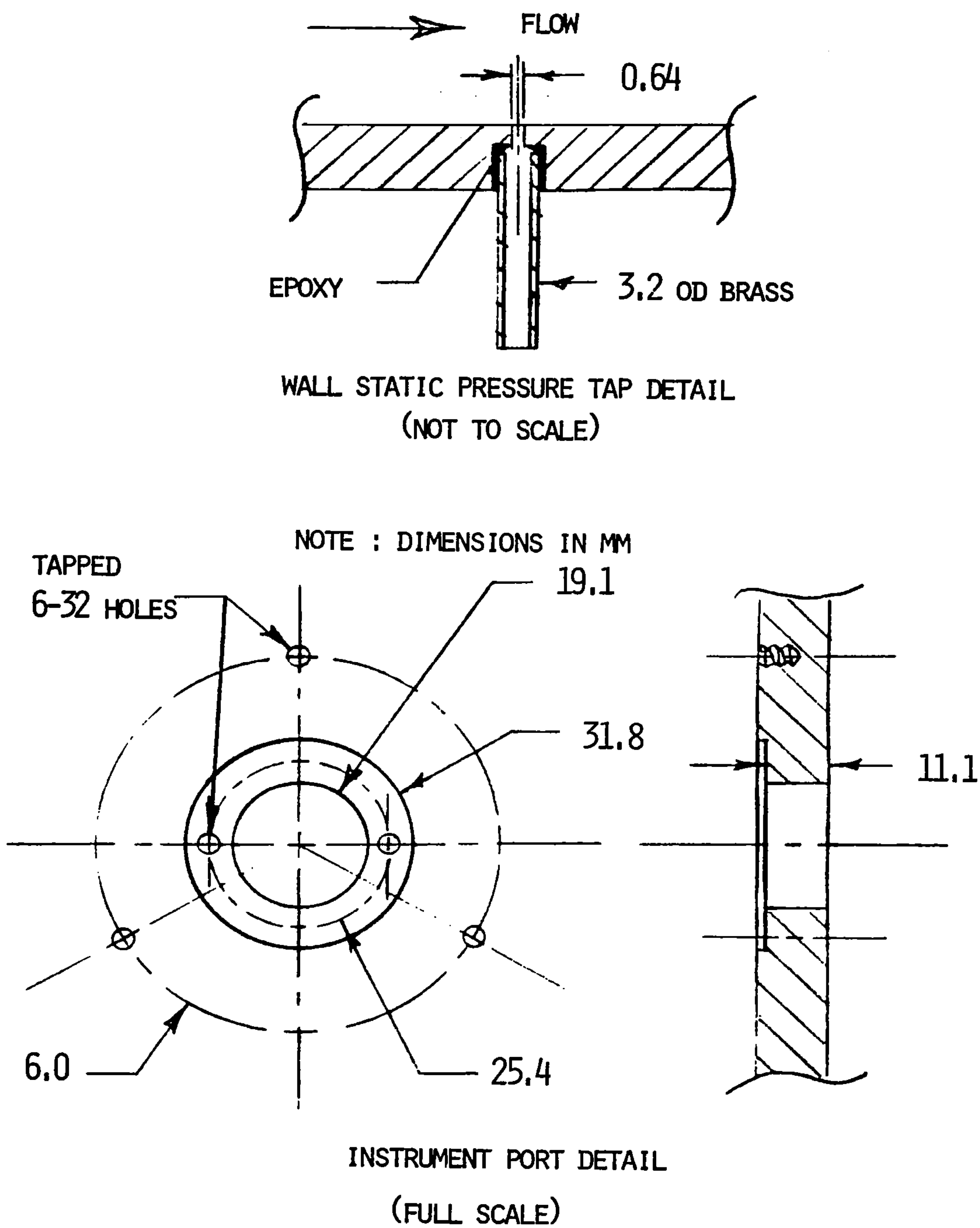

Fig. 2-1. Static pressure tap and instrument port details.

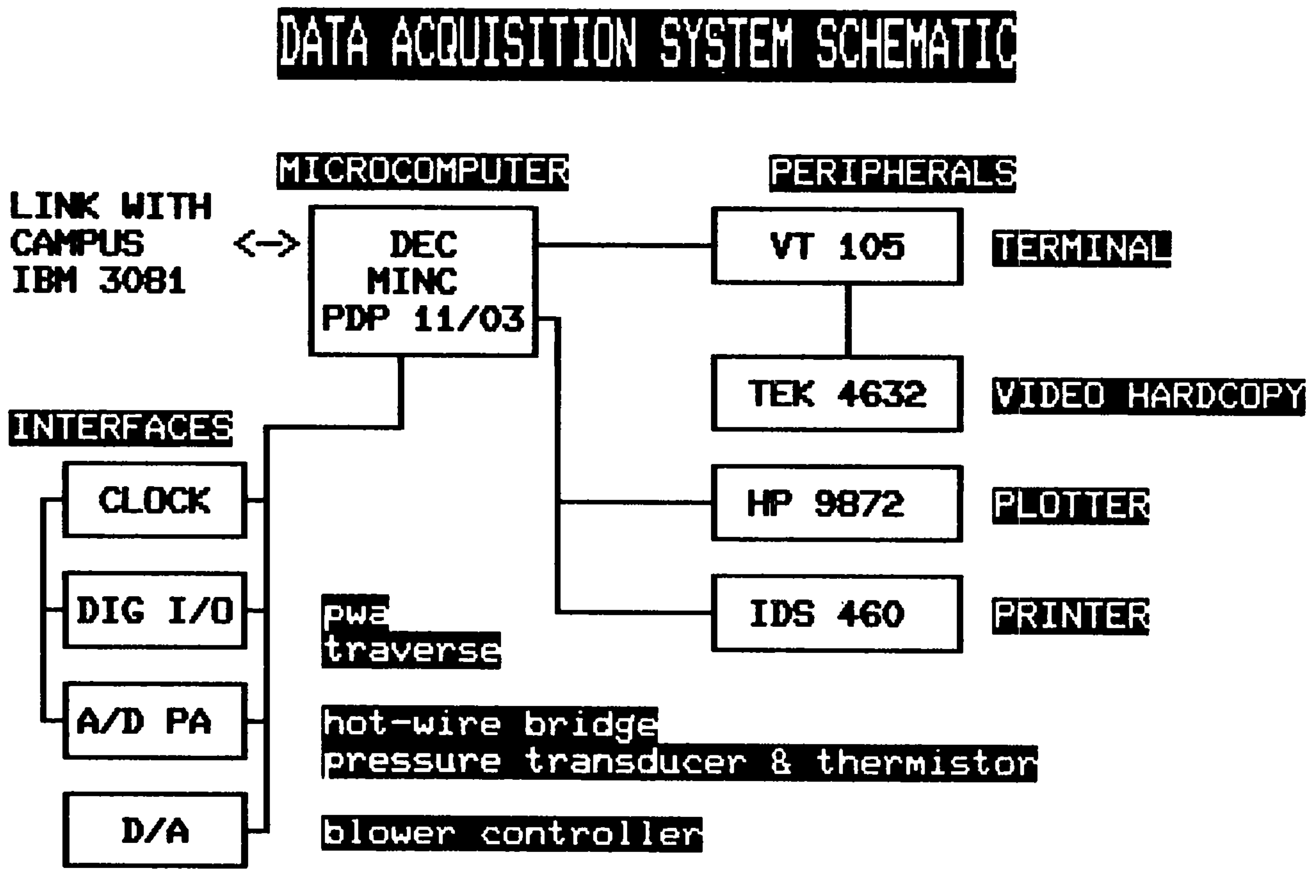

Fig. 2-2. Data-acquisition system schematic.

Chapter 3

PULSED WALL PROBE

A main objective of this study was to measure skin friction in the reattachment region, primarily as a means of unambiguously defining the reattachment length. Since no technique was available for measuring wall shearing stress in this highly turbulent flow, an idea promulgated by Eaton and Johnston (1980) was pursued in an attempt to develop a suitable instrument, the pulsed wall probe. Early results appear in their work, as well as in Westphal et al. (1981) and Eaton et al. (1981). The reader is referred to these references for more discussion of the technique. Below, a brief survey of methods of determining wall shear stress is presented. Then the design, development, calibration, and qualification of the pulsed wall probe are presented. Measurements of skin friction in the reattachment region of the backward-facing step are shown in Chapter 5, and methods of deducing the reattachment length are compared in App. C.

3.1 Skin-Friction Measurement Techniques

A wide variety of techniques exists for measuring skin friction in fluid flow over a solid surface; Winter (1977) provides an extensive review of the most common techniques. However, at the outset of this study, no method existed which was fully adequate for measuring skin friction in a low-speed, reattaching air flow. The following features are responsible for the difficulties encountered.

- Highly turbulent, reversing flow near the surface.
- Large local streamwise gradients (of pressure and skin friction).
- Very low magnitude of the time-mean stresses encountered at a two-dimensional reattachment (or detachment) point.
- Unknown structure of the near-wall flow (e.g., no near-wall similarity properties of the profile shape are known).

Following essentially the classification proposed by Winter (1977), Table 3-1 presents the techniques known to the author. Appendix F is a bibliography of works related to the various techniques, some of which are referred to below.

Only two direct methods (which actually measure a force or deflection) exist--the floating element and the viscosity-balance method. Floating elements are usually very sensitive to local pressure gradients and are normally used in higher-speed air flows, because of the difficulty in measuring very small forces or deflections. The viscosity-balance method (see particularly the work of Tanner and co-workers, 1976a, b and 1977a,b, as well as Monson and Higuchi, 1981) has only recently been applied to separated flows, with apparently successful results. Using the viscosity balance, Driver and Seegmiller (1982) very recently presented results in a backstep flow which will be discussed in Chapter 6.

Techniques which rely on the analogy between surface heat or mass transfer and skin friction have been highly developed for use in many turbulent flows. Mass transfer measurements require a rather specialized facility and have been exploited most notably by Hanratty and co-workers (see, e.g., Mitchell and Hanratty, 1966, and Sirkar and Hanratty, 1970a,b). Surface heat transfer measurements are commonly made using surface-mounted hot wires or films; early work in this area is adequately summarized by Bellhouse and Schultz (1966). More recent work has sought to improve substrate response (e.g., Ajagu et al., 1982), provide directional detection (e.g., McCroskey and Durbin, 1972, and Higuchi and Peake, 1978), and examine time-dependent skin friction (e.g., Sandborn, 1979). Notwithstanding these advances, the use of techniques based on a surface transport analogy in the presence of reversals in flow direction is not recommended, since the analogy itself is not known to be applicable under these conditions.

The most popular and simple methods for ascertaining skin friction in low-speed air flows assume some sort of similarity in the shape of the mean velocity profile near the wall. Methods based on this idea include those which use a "crossplot" of velocity profile data (e.g., the familiar fitting methods of Clauser and Coles), as well as the Preston or Stanton probe (see, e.g., Patel, 1965). The so-called "sublayer fence" (Vagt and Fernholz, 1973, Pontikos and Bradshaw, 1981) is the technique in this classification which seems least restrictive in that similarity is required only in the very near-wall region. Similarity laws have not been formulated for separated flows; this would seem to preclude the use of any "crossplot"-style methods. The high turbulence levels and instantaneous reversals of flow direction require that any similarity-based method have directional resolution and time-dependent response. This is precisely the idea behind the pulsed wall probe.

The pulsed wall probe provides a means of measuring velocity very near a wall using an adaptation of the pulsed-wire anemometer of Bradbury and Castro (1971). The measured instantaneous velocity very close to the surface is assumed to be related to the instantaneous wall shear--i.e., similarity of the instantaneous velocity profile near the surface is assumed. Ginder and Bradbury (1973) have attempted to implement this idea in a film gauge (Peclet number = 0)*, and met with severe difficulties. It was thought that the film gauge had too little sensitivity and also suffered from difficulties associated with substrate response. Both problems are overcome by the probe design described below.

3.2 Probe Design and Operating Procedures

3.2.1 Principles of Operation

A schematic of the pulsed wall probe and a cross-sectional view of the device are shown in Fig. 3-1. A tracer of heated air is generated by the center wire of an array of three parallel wires. Height of the wire array from the surface may be varied in the current design from 0.1 mm to 10 mm. The tracer is convected toward one of the flanking sensors by the flow; the arrival of the tracer is detected as a rise in temperature of one of the sensors. The convection time is related to the velocity through a calibration function. Since practical devices for use near reattachment _must_ operate at low Peclet numbers, this calibration is not a simple proportionality. Further complications arise at low

*Peclet number ($= dU/\alpha$, where d is the spacing between wires, U is the local velocity, and α is the thermal diffusivity) is a measure of the relative amount of thermal diffusion of the heated tracer during the convection time.

Peclet number, due to the effects of a mean velocity gradient on thermal diffusion of the hot tracer. Thus, the probe must be calibrated in conditions of local velocity and local gradient which are identical to the expected measurement conditions. This requirement may be relaxed if conditions of only relatively high Peclet number are to be encountered (as in a turbulent boundary layer). The actual performance of the device used here is evaluated below.

3.2.2 Electronics Setup

Control electronics built by Malvern Instruments are used to supply the pulsing, tracer detection, and timing capability. Figure 3-2 shows a block diagram of the control scheme. The same unit used for operating the pulsed-wire anemometer (described in Chapter 2) was used to operate the wall probe. Because of the parallel-wire configuration, signal amplitude and signal-to-noise ratio (SNR) both increase with increasing velocity (in contrast to the pulsed-wire anemometer, for which signal amplitude and SNR decrease with increasing velocity). This feature, coupled with the different heater and sensor wire lengths employed, necessitates the use of different optimal settings of the electronics.

Pulse amplitude:	20 volts
Trigger level:	2 (both wires)
Sensor current:	3 milliamps
Output gain:	4 X

The essentially digital nature of the pulsed wire makes it necessary to use a computer to process the time-of-flight data. The MINC was used for this purpose, with the same interface software as developed for the pulsed-wire anemometer (see Westphal, 1982).

3.2.3 Calibration

To provide a flow with an analytically known velocity distribution, a laminar flow channel facility was built for which the skin friction can be quickly and acccurately determined from the streamwise pressure gradient. Figure 3-3 shows a schematic of the facility, which consists of parallel plates spaced 3.175 mm apart. The channel dimensions are designed to provide a two-dimensional laminar channel flow with at least a 30 cm length of fully developed flow. The walls were made from aluminum tool plate which was Blanchard ground and hand-polished to obtain very smooth and flat walls. The spacers were made from ground tool steel precisely 3.175 mm thick, and latex rubber tubing seals were installed in slots milled into the test plates to assure that no leakage of air into the channel would occur. Plenums were equipped with flow conditioning and a nozzle upstream to provide minimum disturbance. By monitoring the signal from a hot wire in the flow, it was found that laminar flow was achieved up to a Reynolds number based on channel spacing of about 2500.

The effective range over which the facility can be used gives skin-friction values in the range 0.06–0.44 N/m^2. By way of comparison, the skin friction in the boundary layer upstream of separation with U_{ref} = 12 m/s in the backstep flow is about 0.34 N/m^2, with average wall shear-stress values in the recovering boundary layer being about 0.15 N/m^2. Of course, fluctuations of skin friction about the mean levels occur, so that the range of the calibration must extend beyond the range of expected mean values.

The facility was first used to evaluate the effect of Peclet number on the calibration function. A non-dimensionalization of the functional dependence of time-of-flight on velocity appropriate to this evaluation is given below.

$$\frac{UT}{d} = f\ \frac{dU}{\alpha},\ \frac{dG}{U} \tag{3-1}$$

where d is wire spacing, U is local velocity, G is local velocity gradient, and α is thermal diffusivity. These parameters can be viewed as the ratios of physically meaningful times. They are, respectively, the ratio of time-of-flight to nominal convection time,* the ratio of diffusion to convective time (Peclet number), and the ratio of convection time to characteristic time of diffusion in a velocity gradient. For a given position of the pulsed-probe wire array in the laminar

*Obviously, $UT/d = 1$ for an ideal device.

channel, a fixed value of dG/U results as the channel Reynolds number is changed, because the profile shape is parabolic, independent of Reynolds number. In this way, dG/U could be held constant to examine the effects of Peclet number on the calibration independently. Figure 3-4(a) shows the results. At low Peclet number, the curve tails up as the tracer is more diffuse when it arrives at the sensor wire--this indicates the aforementioned degradation of SNR at lower velocities. Furthermore, the curve shows that at lower Peclet numbers the calibration relation is significantly affected by velocity gradient.

The conclusion from this test was that the probe must be calibrated directly for the effects of thermal diffusion and local gradients if it is to be used very near a solid surface, as we propose. Specifically, it is intended to use the probe to measure skin friction through the assumption of local instantaneous similarity between the measured velocity at a distance h from the surface and the wall shear stress. For very small h, U is small so that the Peclet number would be very small, resulting in a loss of sensitivity like that experienced by Ginder and Bradbury (1973) for the pulsed film gauge. However, it is expected that the validity of the similarity assumption becomes less certain at higher h. As a compromise between loss of sensitivity at small h and lesser reliability of the operating assumption of similarity for larger h, it was decided to operate the array at approximately 0.18 mm from the surface. This would put the wire array at $Y^+ = 7$ in a typical turbulent boundary layer with $U_e = 12$ M/s and $\delta = 2$ cm, and yields $dG/U = 10$ (assuming a linear velocity profile near the wall). Thus, the probe must be calibrated at fixed h for measurements near reattachment, where a significant percentage of the samples will have low Peclet number.

The parabolic velocity profile for fully developed laminar channel flow was verified at one Reynolds number by calibrating the probe on the channel centerline and traversing across the flow--see Fig. 3-4(b). The agreement between the parabolic curve and the measured data is excellent except near the wall, where significant effects of the velocity gradient make the centerline calibration inappropriate, as would be expected from the above discussion.

As was noted above, it was decided to calibrate the probe at the fixed value of $h = 0.18$ cm in the laminar channel over the range 0.6–0.44 N/m^2. Both wires were calibrated independently, due to slight geometric asymmetry of the probe. Similarity between the local instantaneous velocity and the wall shear is assumed, i.e.,

$$\tau_w = f(U(h)) \tag{3-2}$$

The functional relation was simply selected to be that found in the laminar channel—a parabolic profile shape. The channel dimensions and value of h used give

$$\tau_w/\mu = 0.94 \frac{U}{h} \tag{3-3}$$

This is the calibration used for all data presented in the following chapters.

In practice, the calibration procedure simplifies when the above assumptions are made. It was found to be satisfactory to use the same functional form for the dependence of velocity of time-of-flight as for the pulsed-wire anemometer. Also, the air temperature in the calibration flow is the same as in the test flow, so the calibration is formulated directly as

$$\tau_w = \frac{A}{T} + \frac{B}{T^2} \tag{3-4}$$

A table of a dozen or so values of wall shear stress versus time-of-flight was obtained by varying the channel Reynolds number in each orientation of the probe. Calibration constants A and B were then found by least-squares fitting to the calibration data. The rms error of this fit is typically less than 2% over the range 0.06–0.44 N/m^2.

3.2.4 Uncertainty in Skin-Friction Measurements

Probable sources of uncertainty in skin-friction measurements were assessed. The following mechanisms were considered: (1) random errors in tracer detection, (2) signal dropout at very low velocity, (3) effects of temperature variation, (4) noise produced by the turbulent flow over the sensor wires, (5) prong interference, and (6) goodness of fit of the calibration function. Good practice elminates the importance of points 3-6. Temperature effects are minimized by calibrating at the temperature of the flow in which measurements are to be made. Noise will not cause triggering of the detection electronics if a careful setup of the settings is performed to give noise immunity. Prong interference effects are probably negligible in our wind tunnels, judging by the excellent results obtained in measuring the velocity profile in the laminar channel, which is of much smaller cross-section (0.32 × 15 cm) than is the wind tunnel (8-12 × 60 cm). The rms error in the calibration fit was found to be only 2%. This leaves only points 1 and 2 for more careful consideration.

Random errors in detection of the tracer arrival were evaluated in the steady laminar flow, where a 2% standard deviation in time-of-flight is measured, although the flow is nominally steady. This has negligible effects on measurement of average skin friction, since a very large number of samples (2000 samples per point) are used to form the averaged quantities. In turbulent boundary layer flows, fluctuation intensities of 20-30% are common, so the accuracy of the measurement of rms fluctuation intensity is not expected to be affected by the random error in detection of the tracer arrival.

At low values of skin friction (less than $0.04 \ N/m^2$), the signal amplitude falls below the detectable level. The result is a "hole" in the calibration for skin friction in the range $-0.04 < \tau_w < 0.04 \ N/m^2$. If skin friction in this range occurs, it is very likely to be interpreted as a zero reading. However, not much loss in accuracy of measurements reported herein occurs, because vigorous fluctuations in skin friction always occur in the reattachment region, even when the average skin friction is zero. This means that many samples will be detectable, and a reasonably accurate measure (compared to the full-scale value) of average skin friction is still possible—even with as many as 50% of the tracers in the "hole" region.

An overall estimate of the uncertainty in measurement of average wall shear stress of 5% of full-scale was made from the above considerations. This is equivalent to a constant uncertainty of about $0.02 \ N/m^2$ for the results reported herein. This translates to an uncertainty of approximately 15% of the local values of skin friction in the recovery region of the step flows, and an uncertainty of approximately 5% in the values of skin friction measured in the boundary layer upstream of separation. This uncertainty estimate can be verified in cases in which other methods can be used. Note that this estimate does not consider possible error which may arise if the assumption of instantaneous similarity is not valid. At present, there is no information upon which to evaluate this critical assumption. What can be said is that, in cases where other methods have been checked against the measurements with the pulsed wall probe, agreement has been within the quoted uncertainty.*

3.3 Qualification Tests

Several tests were performed to qualify the pulsed wall probe as a valid technique for measurement of time-dependent wall shear stress. The fully developed channel-flow facility of Hussain and Reynolds (1975) was available for use in these tests. It is an excellent facility for these purposes, because it provides a turbulent flow for which the average wall skin friction can be accurately deduced from the streamwise pressure gradient along the channel. In Fig. 3-5, the probability density function (PDF) measured in the channel flow is compared with that reported by Sandborn (1979) for the similar case of a fully developed turbulent flow in an open water channel. Both PDFs display the positive skewness characteristic of near-wall turbulent flow, and about the same fluctuation level relative to the mean. Over the range $0.1 < \tau_w < 0.3$ N/m^2, the pulsed wall probe gave 2-4% lower values of average skin friction than that deduced from measurement of the channel pressure gradient. This is within the estimated uncertainty; however, the repeatability of the sign of the disagreement suggests that the similarity assumption may be the cause of the difference.

The fluctuating component of skin friction is not obtained by any of the usual methods used to obtain average skin friction. However, due to the time-dependent measurement capability of the pulsed wall probe, these data are also obtained here. For the channel, the intensity of

---

*Qualification tests are discussed in the next section, as well as in Westphal et al. (1981) and Eaton et al. (1981).

skin-friction fluctuations can be estimated from Hussain and Reynolds' (1975) reported near-wall hot-wire data:

$$\frac{C_f'}{\overline{C}_f} = \lim_{y \to 0} \frac{u'}{\overline{U}} \tag{3-5}$$

For channel Reynolds number based on centerline velocity and half-width in the range 1.8×10^4 to 2.7×10^4, the fluctuation intensity measured by the pulsed wall probe was found to be constant, and velocity profiles available from Hussain and Reynolds (1975) at Reynolds numbers of 2.3×10^4 and 3.2×10^4 both gave about the same estimate of fluctuation intensity.

$C_f'/\overline{C}_f$ in Fully Developed Turbulent Channel Flow

Source	Re $\times 10^{-4}$	$C_f'/\overline{C}_f$
Pulsed wall probe	1.8-2.7	0.24 ± 0.02
Hussain and Reynolds (1975), using Eq. (3-5) and hot-wire data	2.3-3.2	0.28 ± 0.04

Although the estimate from Hussain's data is quite uncertain, this does provide some assurance that the pulsed wall probe is giving a reasonable measurement of C_f'.

Further comparisons of the skin friction measured in the upstream boundary layer and for the boundary layer along the opposite wall of the step flow are made in Chapter 5. Generally good agreement with the values of skin friction estimated from fitting boundary layer profiles to the log-law of the wall is demonstrated for these cases, providing further qualification of the technique.

The pulsed wall probe has been successfully tested for making time-dependent measurements of skin friction in two-dimensional turbulent air flows of low speed, where skin-friction levels are quite low (less than 0.5 N/m^2). Uncertainty in the results has been estimated at about 5% of the full-scale value of 0.5 N/m^2. A better evaluation of the assumption of wall similarity, which is critical to a complete assessment of the technique, awaits better understanding of the structural details of near-wall turbulence.

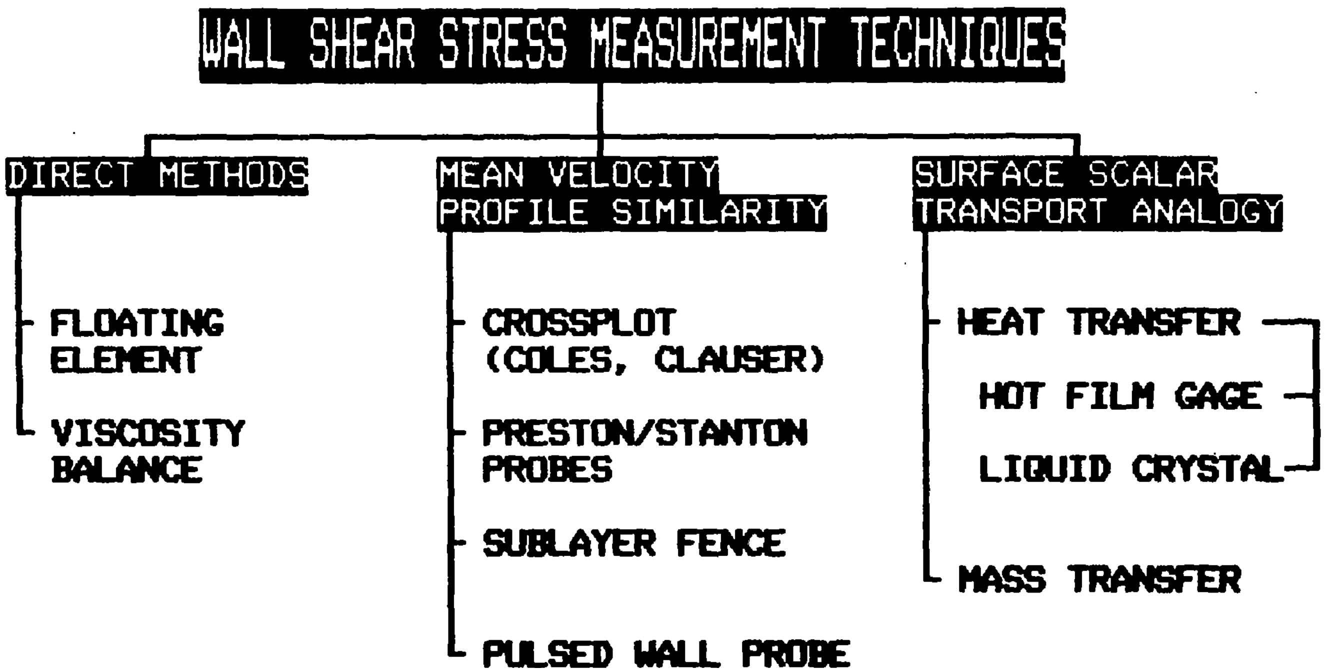

Table 3-1 : Classification of techniques for measurement of wall shear stress

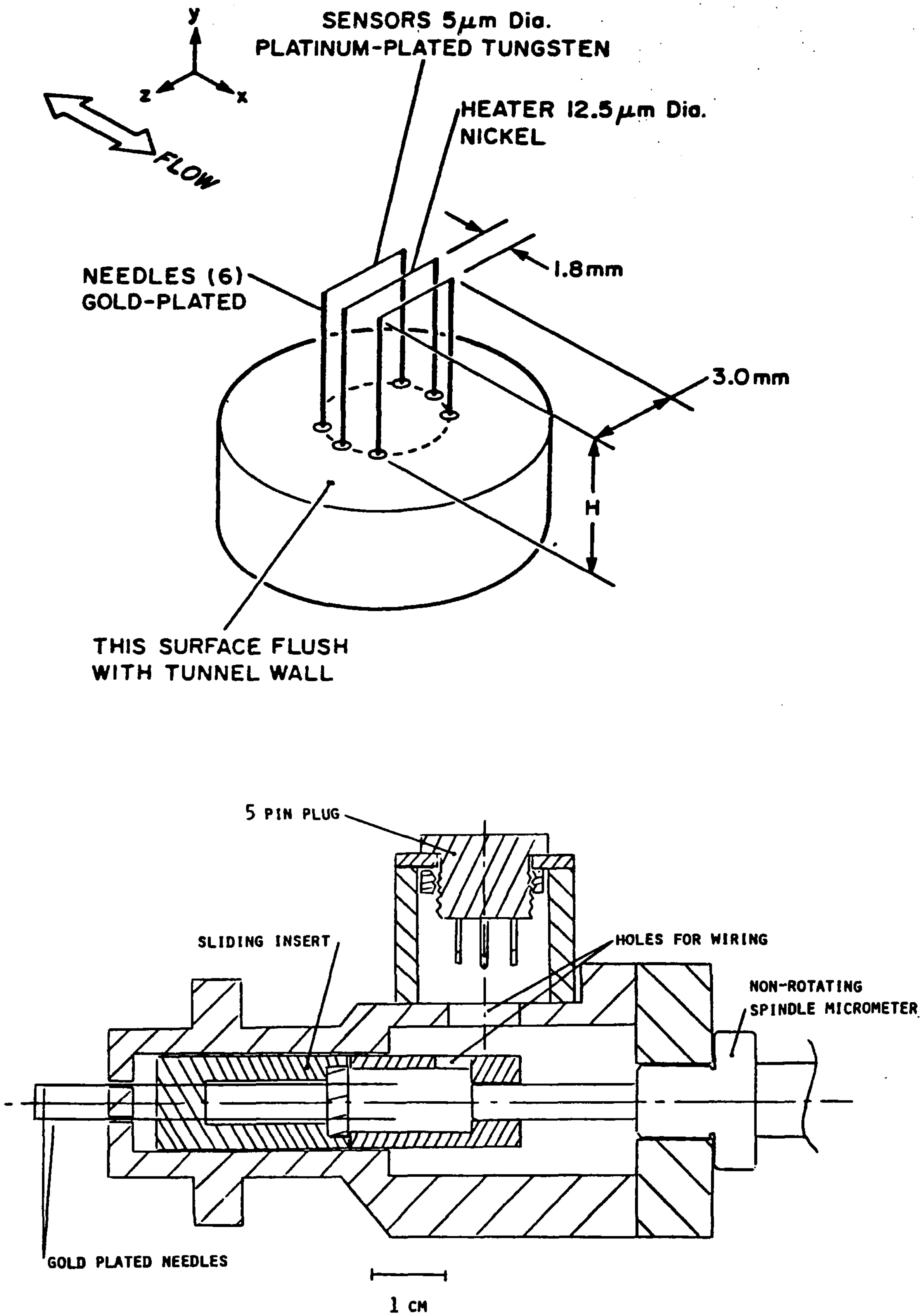

Fig. 3-1. Pulsed wall probe schematic and construction details.

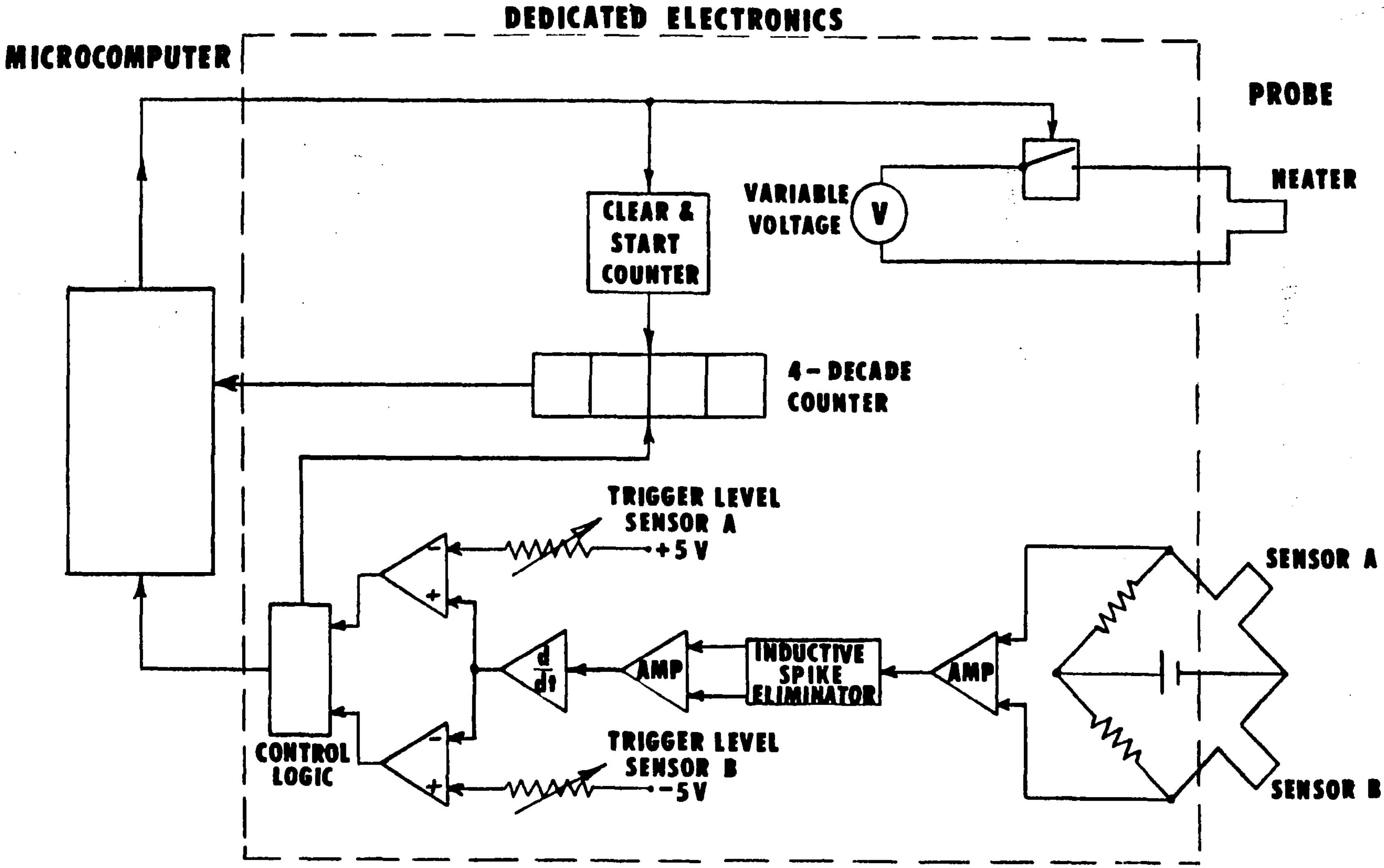

Fig. 3-2. Block diagram of pulsed wall probe control electronics.

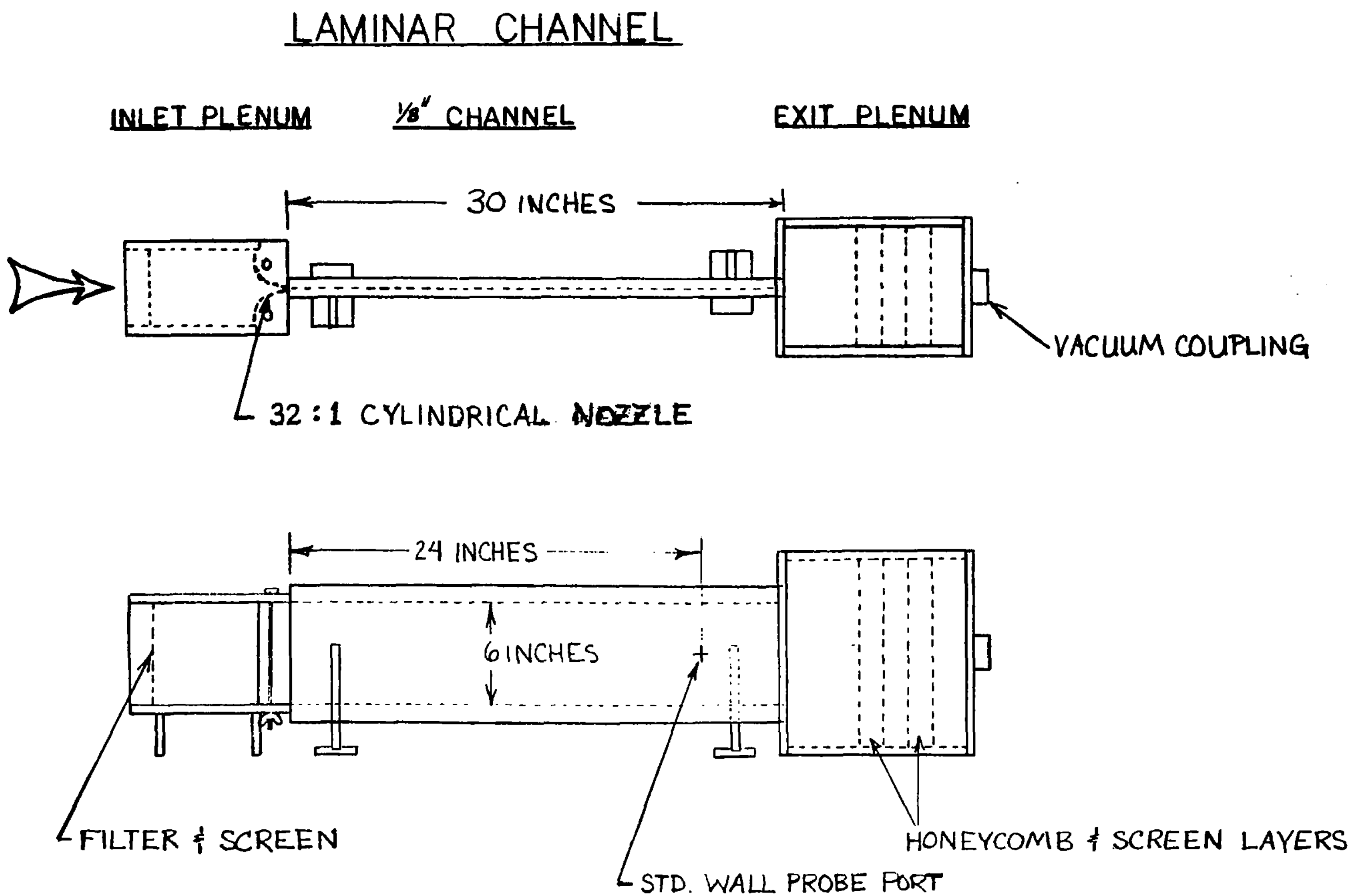

Fig. 3-3. Laminar channel calibration facility schematic.

(a) Effect of thermal diffusion and velocity gradient on pulsed wall probe calibration relation.

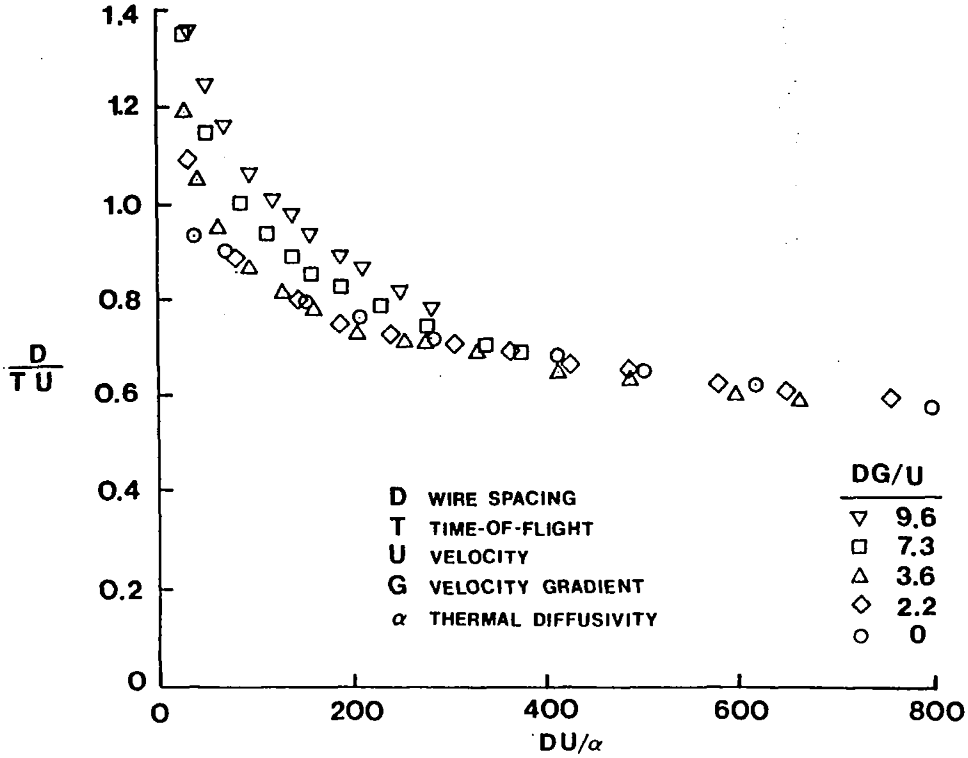

(b) Measured velocity profile in the laminar channel compared to the theoretical parabolic profile.

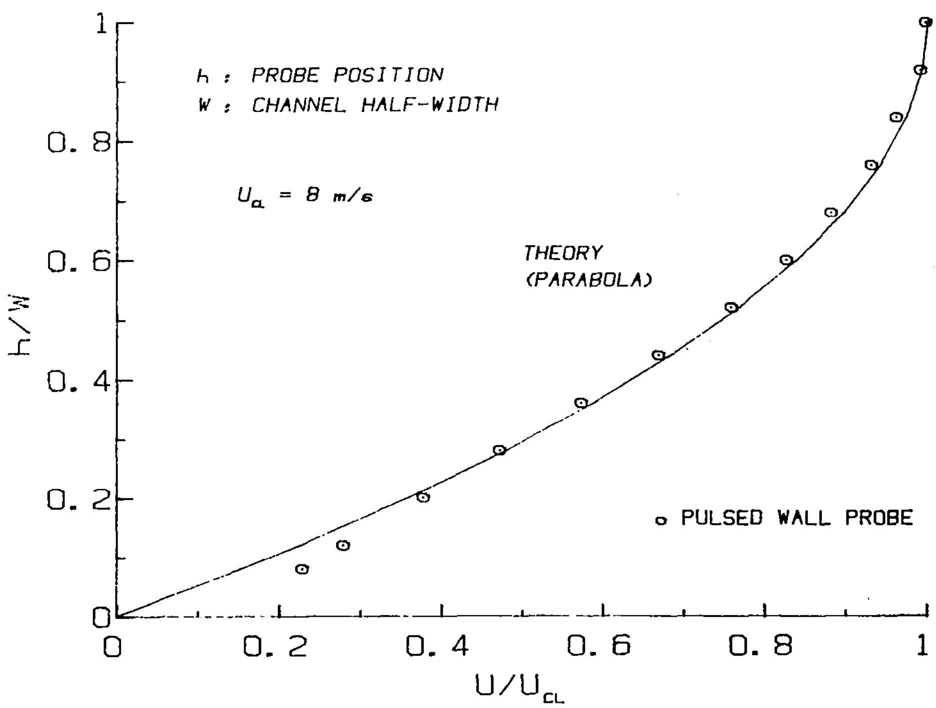

Fig. 3-4. Laminar channel flow results.

(a)

(b)

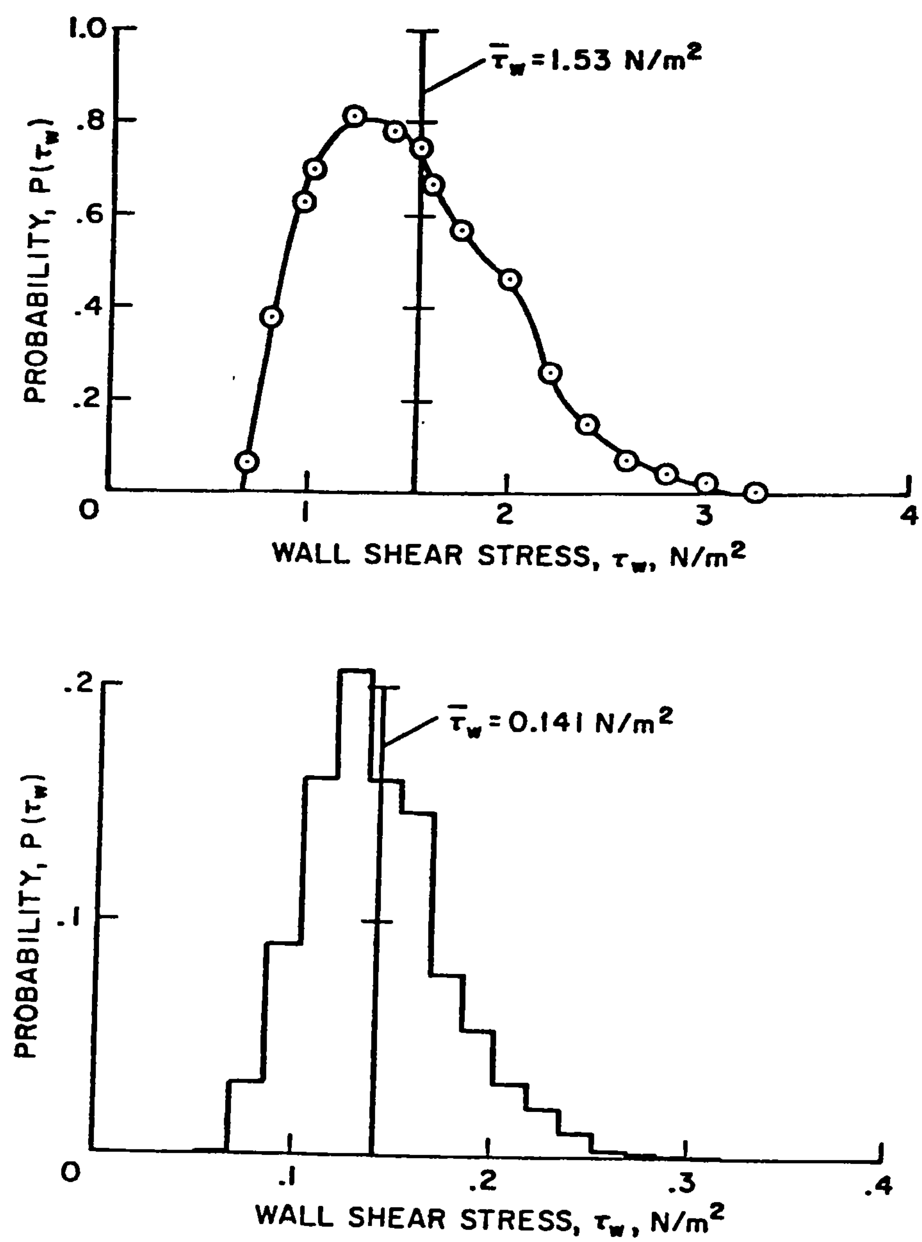

Fig. 3-5. Probability density functions for fully developed turbulent flow. (a) Film gauge, open-channel water flow, from Sandborn (1979). (b) Pulsed wall probe, two-dimensional air flow.

Chapter 4

PRELIMINARY EXPERIMENTS

In keeping with the objectives outlined in Chapter 1, a series of preliminary experiments was performed. From these, a baseline experimental configuration was chosen, and two additional configurations were then selected so that detailed comparison of three cases of reattachment could be undertaken. In this chapter, results of four series of preliminary experiments are reported and the selection of the three main cases is explained. Results from the three main experiments are then presented in Chapter 5. All results are discussed in Chapter 6.

Essential differences in quantity and quality of the data obtained in preliminary experiments (Section 4.1, below), as compared to the three main "record" experiments (Chapter 5) should be noted. For the preliminary series, effects of changing parameters were characterized chiefly through measurement of reattachment length. No anemometry data were taken, and the guidelines suggested in the objectives given in Chapter 1, point 3, were not adhered to. The three record experiments are much more fully documented and were more carefully executed. Only the record experiments were performed with the intention of providing results of quality suitable for comparison with computations.

4.1 Results of Preliminary Experiments

Several preliminary experiments were performed to examine the sensitivity of the reattaching flow to changes in shear layer structure. Three parameters were varied: ratio of boundary layer thickness to step height (δ/H), the angle of the downstream duct (α), and Reynolds number based on step height (Re_H). Some speculation regarding the effects of boundary layer thickness and Reynolds number has been provided by the discussion of Chapter 1. The angled duct was intended to augment the curvature of the separated shear layer upstream of reattachment--thus directly addressing the possibility that the stabilizing or destabilizing effects of curvature of the free shear layer is important in determining the reattaching flow structure (see, e.g., Castro and Bradshaw, 1976). A separate series of tests was performed using two types of vortex generators in the separating boundary layer. Thus, results from a total of four test series will be discussed. Table 4-1 summarizes the preliminary tests and establishes nomenclature used to refer to each below.

Obviously, the specific selection of experimental configurations was heavily influenced by the capabilities of the apparatus. Early in the work, it was decided to hold the step height constant at $H = 5.08$ cm for all the studies. Since the inlet duct width was not adjustable, this implied a constant area ratio of $AR = 1.67$ and an aspect ratio of 12 (greater than the value of 10 recommended by Brederode & Bradshaw, 1972). A larger step height would have compromised the step aspect ratio, and a smaller one would have reduced the resolution attainable with available probes and instrument ports, as well as reducing the step height Reynolds number. It was desired to maintain as high a Reynolds number as practicable, to provide a more canonical set of results (recall the discussion of the effect of Re_H on reattachment length in Chapter 1). A further constraint was placed on experiments in which detailed anemometry data were to be obtained, since the pulsed-wire anemometer used had a maximum usable velocity of about 13 m/s (a nominal maximum upstream velocity of 12.2 m/s was thus selected). The step height of 5.08 cm and upstream speed of 12.2 m/s yield a value of $Re_H = 4.2 \times 10^4$. This seemed high enough to ensure little dependence of reattachment length on Reynolds number.

4.1.1 Series 1: Effect of Boundary Layer Thickness and State

Three values of boundary layer thickness could be obtained with the different lengths of the flat wall upstream of the step. The three configurations are shown in Fig. 4-1. The thinnest boundary layer (series 1a) is produced by removing all upstream test walls so that the nozzle exits directly into the expansion. This gives an estimated boundary layer thickness of 0.06 H*, which is laminar for a free-stream velocity

---

*The upstream boundary conditions were not measured for this case, since no instrument ports existed in the nozzle. The quoted values are estimates based on standard boundary layer formulae and an assumed effective origin (the effective flat-wall length was assumed to be 30.5 cm). The uncertainty in the quoted δ/H value is estimated to be $\pm$ 0.02 H.

of 12 m/s. The medium thickness case (series 1b) was precisely that of Eaton & Johnston (1980); their exact configuration (before facility modifications described in Chapter 2) was used. The boundary layer thickness for this case is about 0.2 H; it is turbulent with $Re_\theta = 850$. The longest upstream surface produces a turbulent boundary layer of thickness 0.4 H and $Re_\theta = 1500$ (series 1c). All these tests were performed with a free-stream velocity of $U_{ref} = 12.2$ m/s, a step height of $H = 5.08$ cm, and an area ratio of $AR = 1.67$.

For series 1a, the thin laminar boundary layer, distributions of wall static pressure and forward-flow fraction were obtained. Static pressure along the step wall is presented in Fig. 4-2 using the conventional normalization on the free-stream dynamic pressure, and the reference pressure is taken at $X/H = -1.25$ on the opposite wall (this is the only configuration for which a reference pressure location other than $X/H = -3$ was used). Streamwise distance is normalized on step height; again note that no information upstream of the step was obtained in this configuration, due to lack of instrument ports and pressure taps in this region. Forward flow fraction (obtained with the thermal tuft) is shown in Fig. 4-3, using the same normalization for streamwise distance.

Distributions of wall static pressure and forward-flow fraction for series 1b and 1c are also shown in Figs. 4-2 and 4-3, respectively. The reference static pressure location for these two cases was $X/H = -3$. The location of 50% forward flow $(\gamma = 0.5)$ for each case is extracted by interpolation of Fig. 4-2, and the results are given below. The correspondence between the 50% forward-flow location and the reattachment point was discussed in Chapter 3.

Series 1: Location of $\gamma = 0.5$

		X/H
1a.	Thin laminar boundary layer, $\delta/H = 0.06$:	7.0
1b.	Turbulent boundary layer: $\delta/H = 0.2$:	8.0
1c.	Turbulent boundary layer: $\delta/H = 0.4$:	8.6

4.1.2 Series 2: Effect of Angled Downstream Duct

Several modifications to the test section were made to allow the duct downstream of the step to be set at an angle of 0° to 15° to the centerline of the inlet duct. A schematic of the test section and relevant nomenclature are shown in Fig. 4-4. Surface static pressure and forward-flow fraction distributions are given for four cases--$\alpha = 0°$, 5°, 10°, and 15°--in Figs. 4-5 and 4-6, respectively. The first case, 2a, is nominally equivalent to 1c; these were performed with slightly different test-section configurations. As such, these series may be compared to demonstrate the repeatability and uncertainty in results*. The location of $\gamma = 0.5$, obtained by interpolation of the results of Fig. 4-5, are listed below.

Series 2: Location of $\gamma = 0.5$

		X/H
2a.	$\alpha = 0°$	8.7
2b.	$\alpha = 5°$	9.1
2c.	$\alpha = 10°$	9.5
2d.	$\alpha = 15°$	9.7

4.1.3 Series 3: Effect of Varying Free-stream Velocity

The effect of varying the free-stream velocity (and thereby Re_H) was studied using the configurations of series 1a and 2c; these are designated as series 3a and 3b, respectively. For series 3a, the free-stream velocity was varied in the range $6 < U_{ref} < 26$ m/s. For series 3b, $9 < U_{ref} < 21$ m/s. It must be emphasized that varying free-stream velocity with constant geometry does <u>not</u> strictly vary only Re_H; one would expect the inlet boundary layer thickness to vary as well (roughly as $U_{ref}^{-0.2}$ for a turbulent separating boundary layer, and as $U_{ref}^{-0.5}$ for a laminar inlet boundary layer). Partial distributions of γ were obtained, sufficient to allow determination of the location of $\gamma = 0.5$ recorded below and shown in Fig. 4-7.

---

*The location of $\gamma = 0.5$ for the two cases differs by about 0.1H, well within the uncertainty of the thermal tuft measurements and the accuracy in setting up the test section geometries.

Series 3: Location of $\gamma = 0.5$

	U_{ref}, m/s	X/H
3a.	9.2	9.5
	12.2	9.5
	16.5	9.2
	20.4	9.1
3b.	5.9	7.2
	8.7	7.0
	12.6	7.0
	16.0	6.9
	21.5	6.4
	25.8	6.2

4.1.4 Series 4: Effect of Imbedded Inlet Vorticity

Two different designs of vortex generators were tested using the configuration of series 1c (straight step with $\delta/H = 0.4$, $AR = 1.67$, and $Re_H = 4.2 \times 10^4$) as the basis for the tests. Particulars of the generator configurations used are shown in Fig. 4-8. Again, sufficient partial γ distributions were obtained to allow determination of the location where $\gamma = 0.5$.

Series 4: Location of $\gamma = 0.5$

		X/H
4.a.	Large triangular generator	6.8
4.b.	Small triangular generator	7.2

There was considerable concern that the reattachment produced in these cases might not be very two-dimensional, especially with the larger generators. Figure 4-9 shows spanwise surveys of γ at a few streamwise locations in the reattachment region. The reattachment line appears much more two-dimensional in the second case, 4b, with the smaller generators.

4.2 Selection of the Main Experiments

Three cases were selected which were investigated in detail. The baseline case (hereafter referred to as case A) selected was 1c, which provided a thick, well-developed turbulent boundary layer at separation and fairly simple geometry. The step Reynolds number is quite large ($Re_H = 4.2 \times 10^4$) and the ratio of boundary layer thickness to step height is moderate ($\delta/H = 0.4$). Two additional cases were desired which would provide substantially different reattachment lengths than the baseline case; one was to give a longer reattachment length and one shorter.

Series 2c was selected to provide the longer reattachment distance (a 10% increase in X_r over the baseline case). The duct angle is sufficiently small to still be considered a small perturbation of the baseline flow, and is not at the edge of the facility's capability (the 15° case bounds the attainable angles). Reynolds number, boundary layer thickness, and area ratio are precisely as for the baseline case. This will be designated as case B.

For the short reattachment length, series 4b was selected (it gives a 15% decrease in reattachment length over the baseline case). The spanwise uniformity of the reattachment line is better than in series 4a and the effect on reattachment length is nearly as large as with the larger generators. This case (labeled as case C) is otherwise identical to the baseline case. Case 1a would have provided as large a decrease in reattachment length, but the cases with imbedded inlet vorticity promised a more intriguing and radical change in shear layer structure.

Table 4-1

SUMMARY OF PRELIMINARY EXPERIMENTS[a]

Series	Description	$Re_H \times 10^{-4}$	δ/H	$\alpha°$
1	Variable Inlet Boundary Layer Thickness			
a	Thin laminar boundary layer	4.2	0.06	0
b	Turbulent boundary layer	4.2	0.2	0
c	Turbulent boundary layer	4.2	0.4	0
2	Angled Downstream Duct			
a	Straight case[b]	4.2	0.4	0
b	Small angle	4.2	0.4	5
c	Moderate angle	4.2	0.4	10
d	Large angle	4.2	0.4	15
3	Variable Free-stream Velocity			
a	Thin boundary layer	2-8.8	0.06[c]	0
b	Angled duct	3-5.7	0.4	10
4	Imbedded Inlet Vorticity			
a	Large triangular generators	4.2	0.4[d]	0
b	Small triangular generators	4.2	0.4	0

Notes:

a. Area ratio AR = 1.67 and aspect ratio is 12 for all preliminary tests.

b. Series 2(a) and 1(c) were performed using different test sections, but are nominally the same case otherwise.

c. Boundary layer thickness for all cases of variable free-stream velocity cases is quoted at $Re_H = 4.2 \times 10^4$.

d. Boundary layer thickness for all cases with vortex generators is that which would occur if the generators were not present.

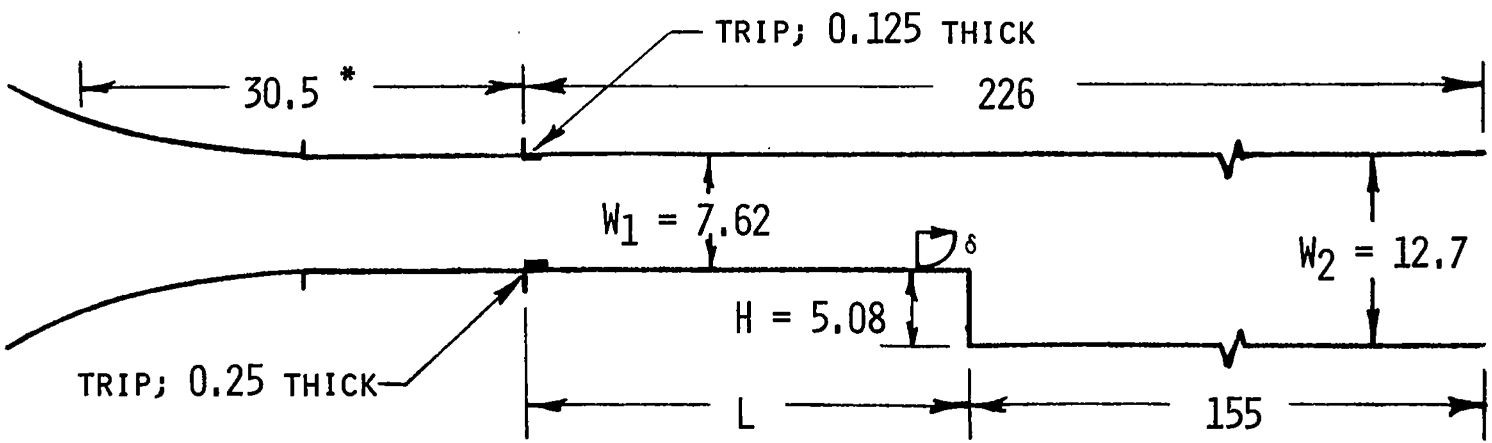

* EFFECTIVE FLAT-WALL UPSTREAM LENGTH

NOTES :

- STEP WALL TRIP USED ONLY FOR 1B AND 1C
- DIMENSIONS ARE GIVEN IN CM

SERIES	L CM	δ/H
1A	0	0.06
1B	30.5	0.2
1C	76.2	0.4

Fig. 4-1. Test section schematic for series 1 experiments.

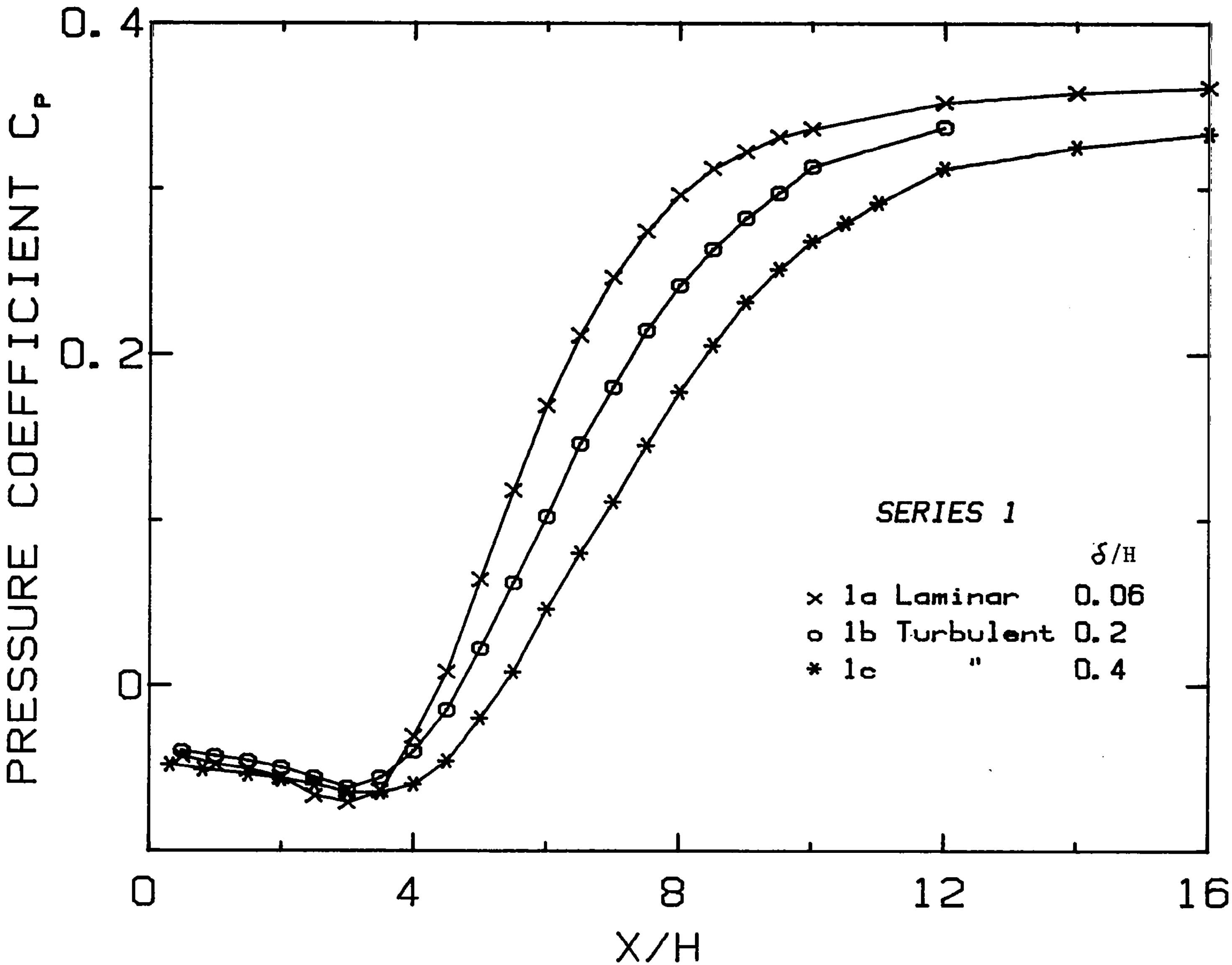

Fig. 4-2. Pressure coefficient, series 1.

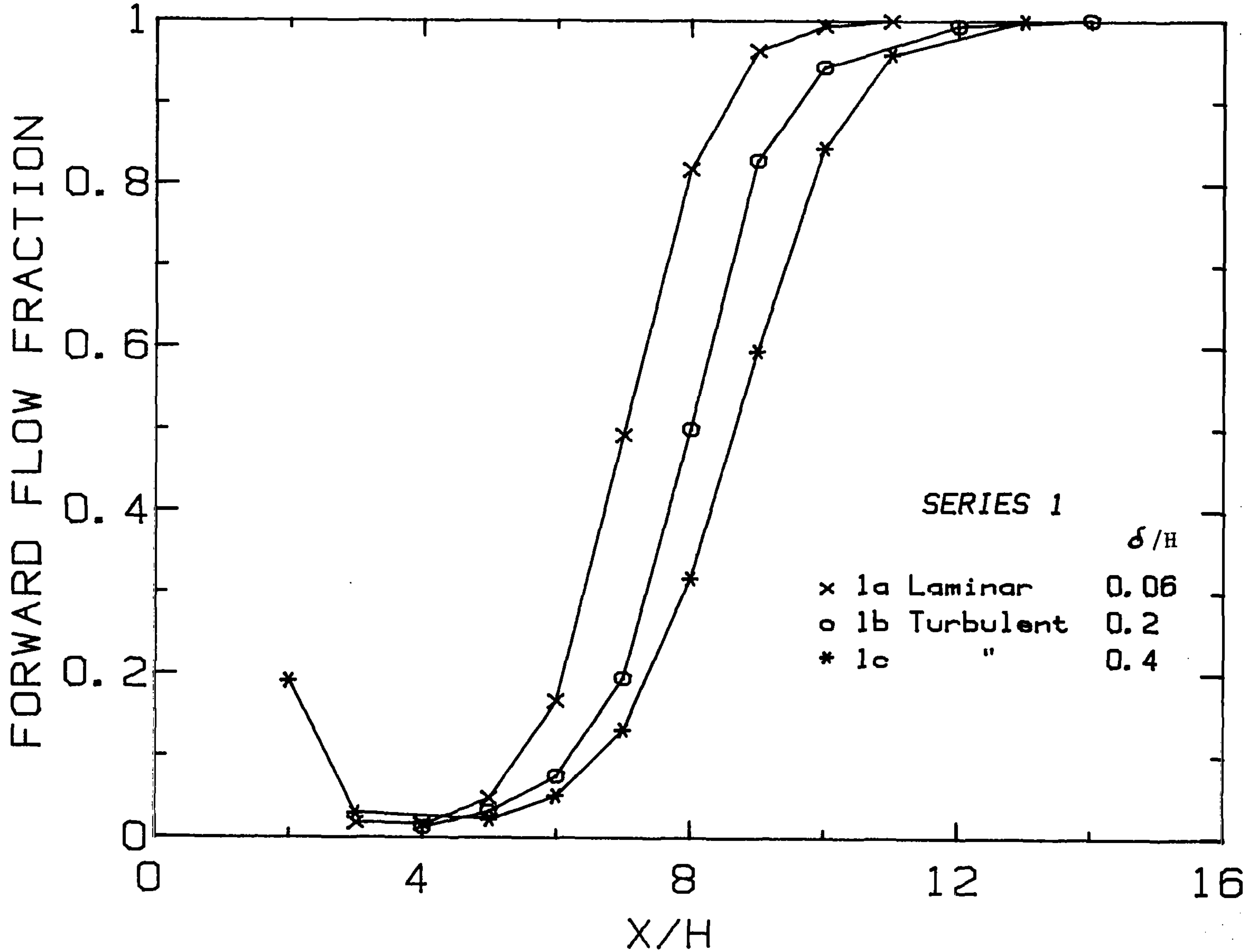

Fig. 4-3. Forward-flow fraction, series 1.

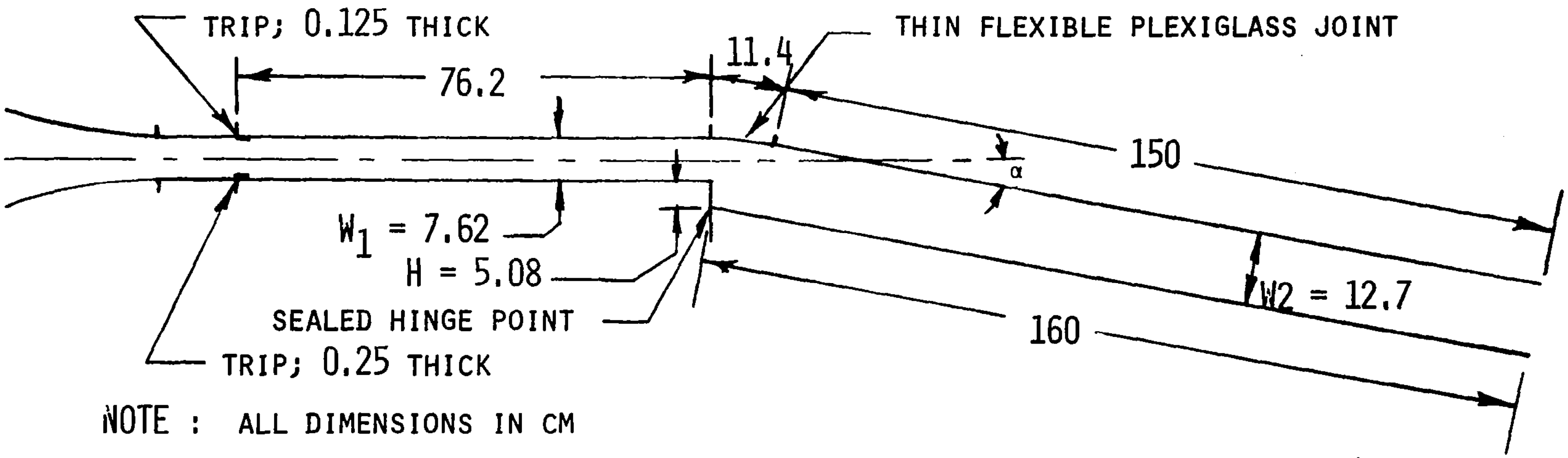

Fig. 4-4. Test-section schematic for series 2 experiments.

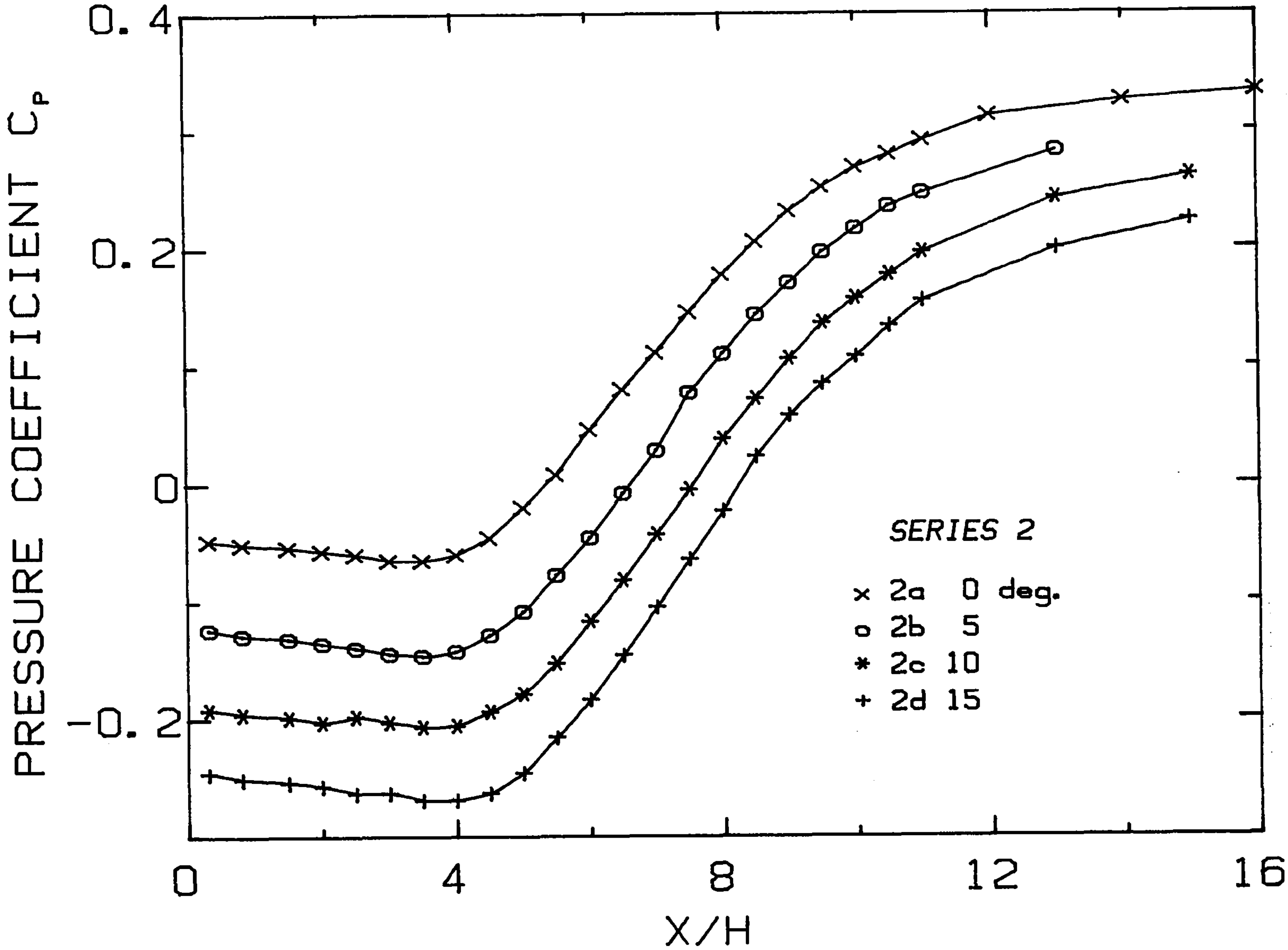

Fig. 4-5. Pressure coefficient, series 2.

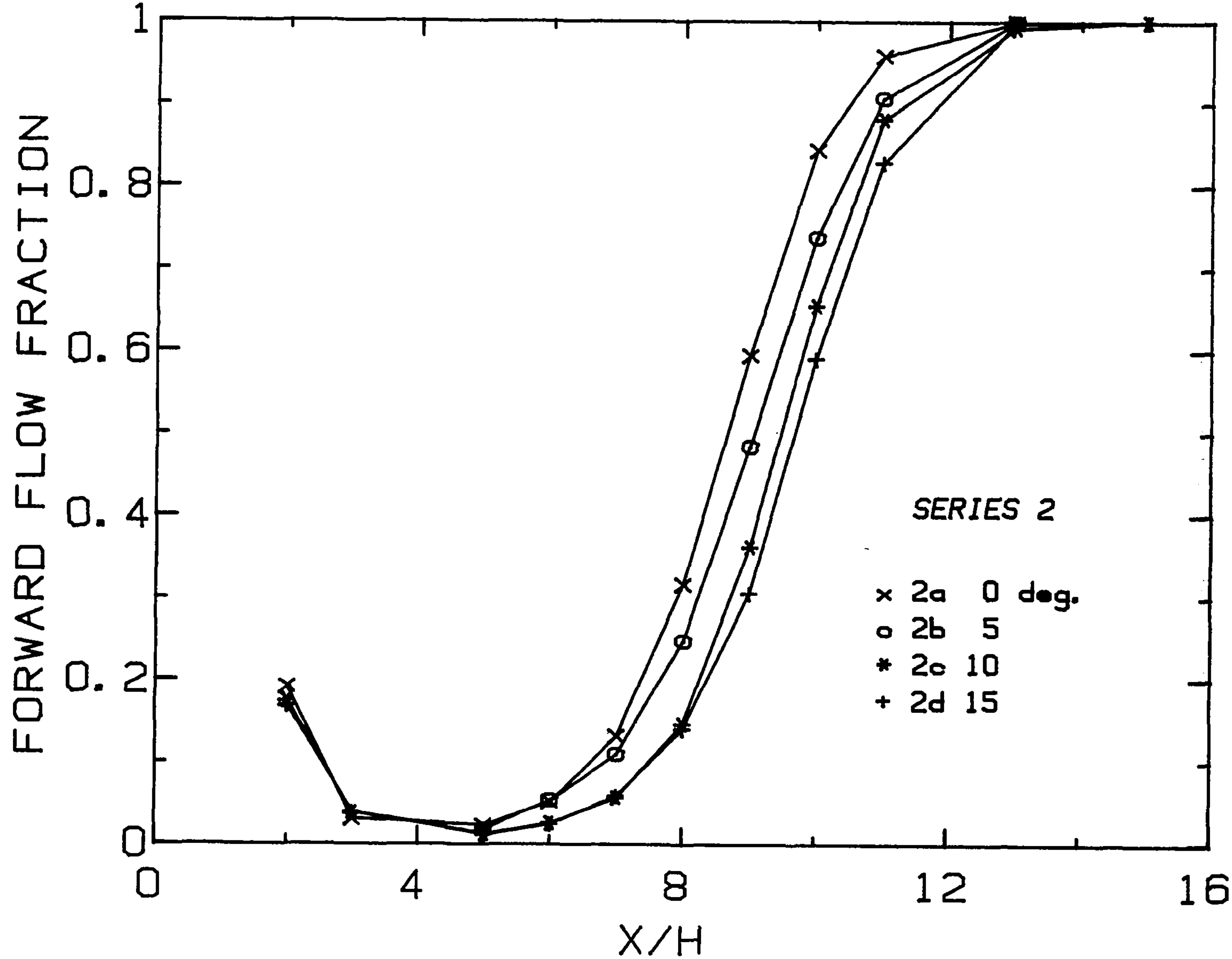

Fig. 4-6. Forward-flow fraction, series 2.

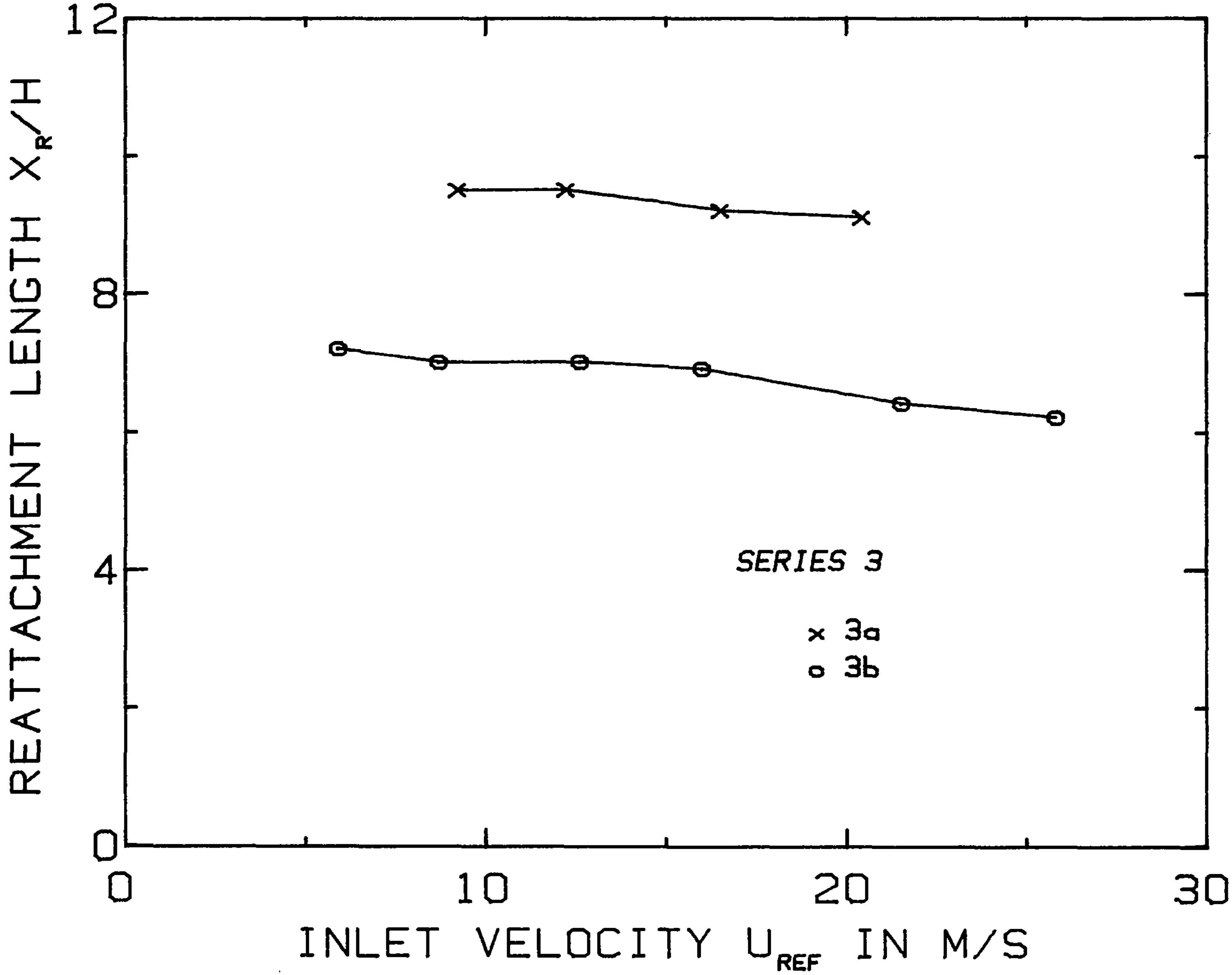

Fig. 4-7. Reattachment length vs. inlet velocity, series 3.

PLAN VIEW OF ELEMENT ARRANGEMENT

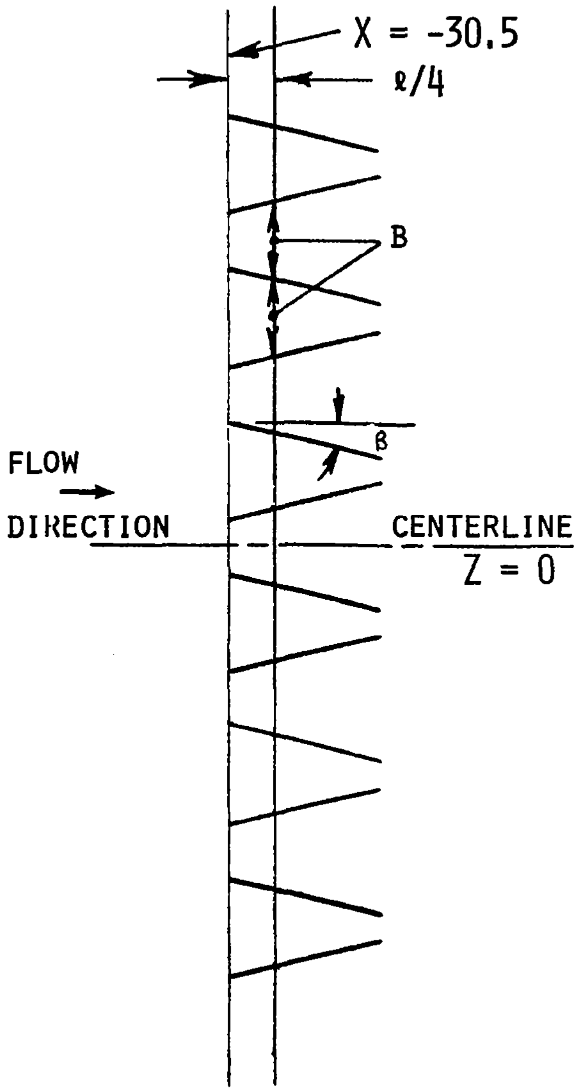

DETAIL OF A SINGLE GENERATOR

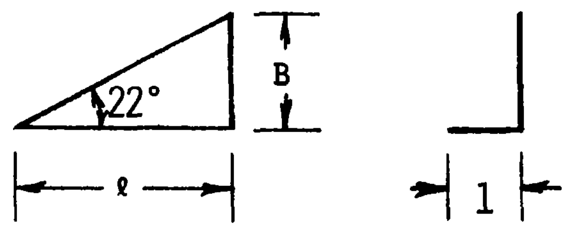

SERIES	β DEG.	B CM	ℓ CM	N
4A	12	2.0	5	14
4B	12	1.0	2.5	28

NOTES :

- N IS THE TOTAL NO. OF GENERATORS ACROSS THE SPAN
- ELEMENTS ARE MADE OF 0.2 THICK ALUMINUM
- GENERATORS ARE AFFIXED TO SURFACE WITH DOUBLE-STICK TAPE
- ALL DIMENSIONS GIVEN IN CM

Fig. 4-8. Vortex generators for series 4 experiments.

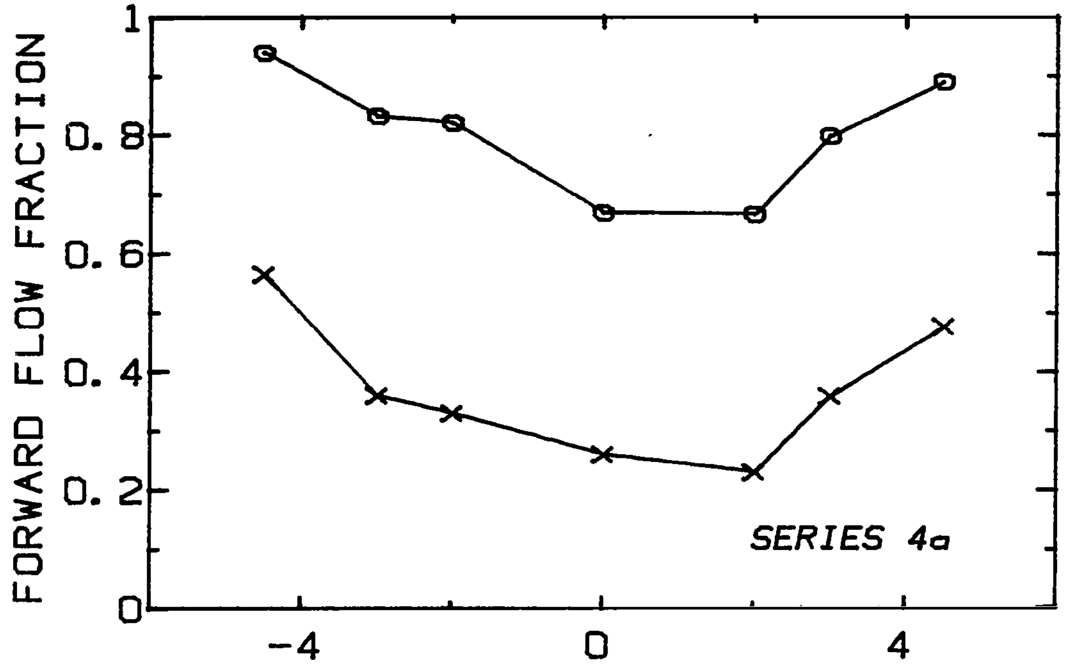

(a) Profile for series 4a, showing substantial nonuniformity.

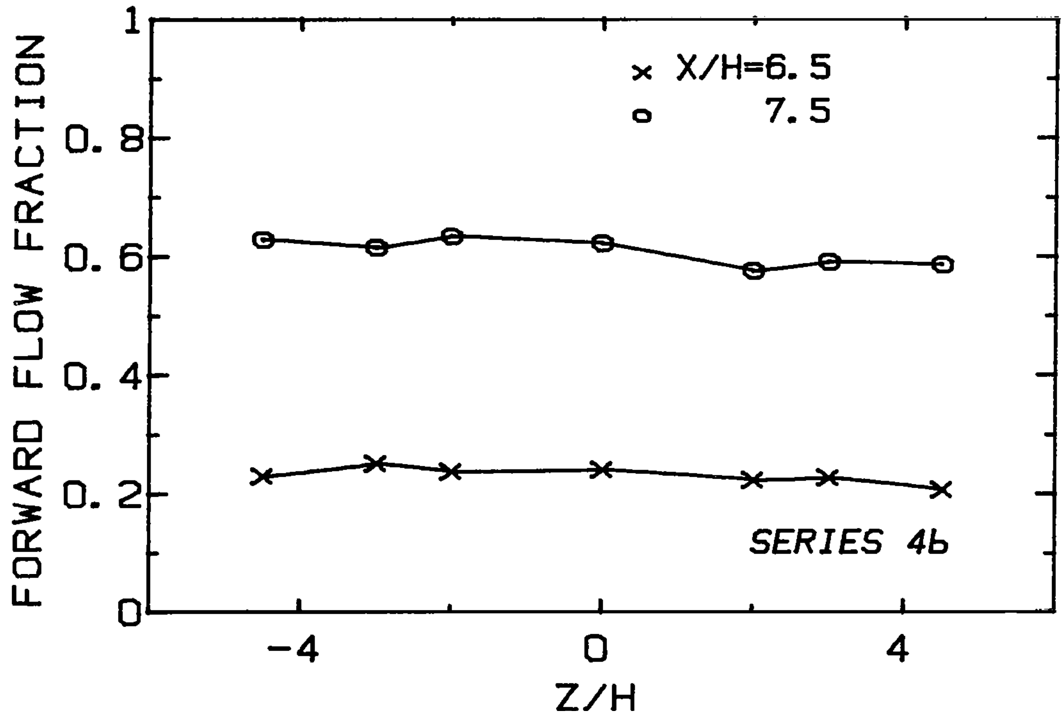

(b) Profile for series 4b, showing good uniformity.

Fig. 4-9. Spanwise profiles of forward-flow fraction, series 4.

Chapter 5

RESULTS OF MAIN EXPERIMENTS

The results of three main experiments selected from the preliminary tests described in Chapter 4 are given here. Geometry and nomenclature for the configurations are summarized in Fig. 5-1. Recall that the baseline configuration (Case A) is a single-sided expansion with a boundary layer thickness of $\delta/H = 0.4$, $Re_H = 4.2 \times 10^4$, and area ratio $AR = 1.67$. For Case B, the duct downstream of the step is set at an angle of 10° to the inlet duct. Case C uses precisely the configuration of Case A with vortex generators placed within the boundary layer upstream of separation. Inlet conditions, pressure distributions, visualization, forward-flow fraction near reattachment, skin friction, and streamwise velocity distributions are presented in this chapter. The results (including those of Chapter 4) are discussed in the following chapter.

5.1 Inlet Conditions

All three cases use the same inlet duct and boundary layer trip arrangement; the only difference in inlet conditions arises in Case C, in which vortex generators have been taped to the wall upstream of the step edge. It was felt that the use of trips would assure better uniformity of flow across the span--hence the use of trips on both surfaces. Note that a smaller trip is used on the wall opposite the step. The step-side trip was selected to be as large as possible to yield a thicker separating boundary layer, while still leaving a sufficient length of wall downstream of the trip to allow the boundary layer to recover from the effects of being tripped. The following will first consider the inlet conditions without the generators, then present a characterization of the effects of the generators on the inlet flow. Note that the free-stream velocity at $X/H = -3$ $(X/W_1 = -2)$ is U_{ref} = 12 m/s ± 0.3 m/s for all the tests. The actual value of U_{ref} is used to normalize all results.

Spanwise uniformity of the flow approaching the step was assessed in Appendix A using a continuous traverse of spanwise total pressure.

As a further verification, hot-wire profiles at three spanwise locations are shown in Fig. 5-2, again indicating that variations of mean velocity across the span at the inlet are very small indeed (about 1% variation in mean velocity across the center half-span). The measured free-stream turbulence intensity (u'/U_e) on the tunnel centerline at $X/H = -9.5$ was 0.17%.

Profiles of $\overline{U}$ and u' for the boundary layer upstream of separation were measured. Figure 5-3 shows profiles of $\overline{U}$ and u' at several locations upstream of separation. The following figure (5-4) compares the boundary layer profile at the selected inlet plane $(X/H = -3)$ with accepted profile shapes for flat-wall turbulent boundary layers. Figure 5-5 shows a complete profile of mean velocity and turbulence intensity across the duct at the same location. It will be noted that, due to the thinner trip used, the boundary layer on the opposite wall is somewhat thinner than that of the step side. Table 5-1 provides a summary of integral and shape parameters for the upstream flow.

With the vortex generators installed, the spanwise total pressure-traverse mechanism described in Appendix A was used to measure spanwise variation of total pressure caused by the generators. The plane of measurement was about 2 cm upstream of the step edge, and the test wall downstream of the step was removed for these tests. The leading edge of the generators was about 30 cm upstream of the step. Figure 5-6 shows the very regular and repeatable total pressure variation caused by the generators. One profile of mean and rms velocity was taken on the centerline $(Z = 0)$ with the generators in place--see Fig. 5-7. Since this is a "downwash" region, directly downstream of convergent trailing edges of adjacent generators (see Fig. 4-8), the profile appears much thinner than when no generators are installed. Subsequent visualization verified the strength, height, and spacing of the vortices implied by the total pressure and velocity profiles.

A few comments regarding the inlet conditions derive from the information cited above. Firstly, the two-dimensionality of the inlet flow has been assured by the continuous total pressure traverses cited in Appendix A, as well as the discrete boundary layer profiles of Fig. 5-2. The use of trips probably has improved the spanwise uniformity of the flow very near the walls. Without tripping, one might expect transition to take place at varying streamwise locations across the span, giving rise to an apparent spanwise non-uniformity downstream. The trip also gives a thicker separating boundary layer, but there remains some concern that the tripped layer is structurally different from a "natural" one, notwithstanding the fact that the step is nearly 300 trip heights from the trip position. Turbulence intensity u'/U_e measured in the upstream boundary layer was somewhat higher than Klebanoff's data at the outer edge of the boundary layer (see Fig. 5-4), which may be evidence of the slight effects of tripping. Also, a Coles-style analysis (see Coles, 1968) yielded a small value for the wake parameter $\pi = 0.3$ compared to a typical value of 0.6 for high-Re smooth wall boundary layers (see Table 5-1). This may be further evidence of trip effects.

5.2 Visualization

Smoke-wire visualization was performed to investigate the scales of turbulent motion present in the shear layer upstream of the reattachment region. This visualization also provides a quick verification of the thickness and structure of the separating boundary layer, as well as showing the interface between shear layer and free-stream fluid just after separation. The visualization was typically performed at somewhat lower reference velocity--U_{ref} = 8-10 m/s--to simplify setting the control electronics and allow use of a larger diameter smoke-wire (see Appendix B).

The first results presented will be a visual characterization of the embedded streamwise vortices generated for Case C. Figure 5-8 shows two views of the vortices--(b) is a plan view (X-Z plane) which shows how straight and evenly spaced the vortices remain. The first view (a) looks upstream (using a mirror) at a section (Y-Z plane) of the vortices, showing their approximate shape. The first view is somewhat fuzzy, due to the difficulty of obtaining a very narrow plane of light. The visualization confirms the rough estimates from the pressure profiles as to the shape of the vortices--they are of oval cross-section, about 2 cm wide and 3 cm high.

With a wire placed at $X/H = -3$, the upstream boundary layer and flow just after separation were visualized. This view is shown in Fig. 5-9 for each of the three main cases. Note that the wire is on the tunnel centerline, so for Case C the wire is in a "downwash" zone and thus the separating shear layer appears thinner than in the other two cases. No "roll-up" of the shear layer into discrete spanwise vortices is apparent; the separated region (at least the near-field) appears quite similar to the outer region of the separating boundary layer. Both observations suggest that the entrainment in the separated shear layer can be strongly affected by the thickness, state, and upstram history of the separating boundary layer.

A wire placed approximately in the center of the recirculation region allows the strong backflow near the surface to be visualized. This view is shown in Fig. 5-10 for all three cases. Note that slightly different distances were used to place the wire as near the center of the recirculation region as practical, given the differences in reattachment length for the three cases. In addition to showing the strong backflow near the surface, this view also emphasizes that spanwise motions exist which are quite strong and tend to move smoke out of the focal plane; these motions were noted in all three cases. In fact, this observation motivated the idea that using embedded streamwise vorticity (as in Case C) could significantly alter shear-layer entrainment.

In the region near but upstream of the reattachment point, instantaneous backflow is mostly confined to a thin region near the surface. Figure 5-11 shows this view using a smoke-wire placed just upstream of reattachment for all three cases. Strong motions containing significant large-scale streamwise vorticity are seen in all cases--note the out-of-focus smoke in the photographs. The views shown in Figs. 5-10 and 5-11 were chosen to be "typical" from 10 or 20 nominally identical realizations. However, different realizations at these locations did occasionally yield a substantially different visual impression. Figure 5-12 is an example of the variation found in random realizations at $X/H = 5$ for Case B. Similar differences were seen in the photos for the other cases at both the locations examined for Figs. 5-10 and 5-11. This is in sharp contrast to the consistency of photos of the separating boundary layer and near-field separated shear layer.

5.3 Wall Static Pressure

Distributions of wall static pressure have been measured along both surfaces for all three main cases. These data appear as Figs. 5-13, 5-14, and 5-15, showing C_p vs. distance normalized by step height in the range $0 < X/H < 20$. In all cases, the pressure coefficient C_p is defined as follows:

$$C_p = \frac{P(x) - P_{ref}}{\frac{1}{2}\rho U_{ref}^2}$$

where P_{ref} is the wall static pressure measured on the wall opposite the step at $X/W_1 = -2$ $(X/H = -3)$, and U_{ref} is velocity measured on the centerline of the inlet duct at $X/W_1 = -2$.

Considering first the baseline Case A of Fig. 5-13 and Case C of Fig. 5-15, the overall pressure rise is about $C_{p,max} = 0.35$ compared to the ideal* value of 0.48. The difference in pressure coefficient between corresponding points on the two surfaces never exceeds about 0.05, except in the turning region of Case B $(X/H < 2)$. The change in sense of flow curvature--from "stabilizing" upstream of reattachment to "destabilizing" downstream--is evidenced in each figure by the change in sign of pressure difference between the same X location on the two surfaces. The "crossover" (location of equal wall pressure on the two surfaces) appears to occur about one step height upstream of reattachment in all three cases. The obvious similarity in the shapes of the pressure rise curves will be explored more fully in the discussion of Chapter 6.

---

*The Borda-Carnot pressure recovery is that which obtains if an "ideal" sudden expansion is assumed--i.e., the base pressure is assumed equal to the upstream pressure, uniform inlet and exit flow is assumed, and wall and turbulence stresses are neglected:

$$C_{p_{ideal}} = 2(1 - 1/AR)/AR = 0.48 \quad \text{for} \quad AR = 5/3 \quad .$$

5.4 Forward-Flow Fraction

The thermal tuft was used to measure forward-flow fraction distributions (γ vs. X/H) for each case as a means of locating the reattachment point and assessing the two-dimensionality of the reattachment region. Figure 5-16 shows γ vs. distance normalized by step height, H, for each of the main cases. Only the reattachment region is shown, the reseparation region of the corner eddy near the step is not probed, because the convective velocities there are very small. One would expect the curves to turn up and give a value of $\gamma = 0.5$ around X/H = 1. A certain similarity and symmetry in the shape of each curve is apparent; this feature is explored more fully in the discussion of the following chapter. From interpolation of these data, the location of $\gamma = 0.5$ has been deduced and is recorded below. For the purposes of this report, the reattachment point (X_R) will henceforth be taken as the location of $\gamma = 0.5$, unless otherwise stated. In Appendix C, several different measures of reattachment position are compared to give a general idea of the differences in X_R which can be attributed to the method used to deduce this important quantity. The differences in reattachment length determined by a variety of methods is seen to lie in a band of ± 0.2 step heights, which is about the uncertainty in any of the methods.

Case	Location of $\gamma = 0.5$
A	X/H = 8.55
B	9.47
C	7.23

Spanwise distributions of forward-flow fraction near the reattachment point were measured to determine the degree of two-dimensionality of the reattachment line. These data are shown for Cases A and B in Fig. 5-17 and were given for Case C in Fig. 4-9(b). Case A displays the best uniformity--spanwise variation in γ is about 1% across the center midspan. For Cases B and C, this variation is about ± 3%. The implied spanwise variation in reattachment length can be estimated as follows:

$$\delta(X_R) \approx \left.\frac{\partial X}{\partial \gamma}\right|_{X_R} \cdot \delta\gamma$$

From Fig. 5-16,

$$\left.\frac{\partial \gamma}{\partial X}\right|_{X_R} \approx \frac{0.35}{H}$$

and taking $\delta\gamma = 0.03$ yields

$$\delta(X_R) \approx 0.1\ H$$

Thus, the implied spanwise variation in reattachment length is about one-tenth step height for the worst cases. The cause of the poorer two-dimensionality in Case B is thought to be the difficulty in controlling the test section dimensions accurately as compared to the other cases (see Fig. 5-1). In Case C, the mean inlet flow was not two-dimensional, so the spanwise uniformity of the reattachment region was by no means assured.

5.5 Velocity Field

Mean and rms values of the streamwise component of velocity ($\overline{U}$ and u'*) were measured throughout the flowfield using a pulsed-wire anemometer (for the separation and reattachment regions) and a hot-wire anemometer (for the recovery zone and the opposite-wall boundary layer). A small mount of data was obtained using a total pressure probe in conjunction with a wall static pressure tap (in the far recovery region and along the opposite wall) for Case B only as a means of verifying the hot-wire results and qualifying the digital implementation of hot-wire data acquisition. At some locations, several different techniques were used to measure $\overline{U}$ and u'. By overlapping results in this manner, a better idea of the accuracy of the results is obtained. This matter is

---

*The shorthand notation used throughout this report should be noted:

$$u' = \sqrt{\overline{u^2}}\ .$$

treated in Appendix D. All velocity data presented below are normalized on U_{ref}, the velocity at $X/W_1 = -2$ on the centerline of the inlet duct. This reference velocity is always measured with the Keil probe and wall static pressure tap.

The first set of figures (5-18 through 5-23) give pulsed wire measurements of $\overline{U}$ and u' in the separation and reattachment regions. The origin for Y is the step surface; profiles extend to Y = 2H (i.e., 80% of the duct width is covered). The traverse mechanism is mounted in the wall opposite the step and operated manually. Note that the measured values of turbulence intensity in the high-speed core flow upstream of reattachment (where $1.5 < Y/H < 2$) are known to be higher than the true values, as explained in Chapter 2. Also, the maximum backflow velocities invariably occur very near the surface in all cases. Due to the probe geometry, it was not possible to get closer than $Y/H = 0.1$ to better investigate this region.

Recovery-region velocity profiles obtained with a single hot-wire are given in the second group of figures (5-24 through 5-32). In each case, five measurement locations are shown which cover the region extending for ten step heights downstream of the last pulsed-wire profile in the reattachment region. The profiles display the inflexional shape noted by previous workers (e.g., Bradshaw and Wong, 1972). When plotted in inner coordinates (Figs. 5-27 through 5-29), U^+ vs. Y^+, the mean profiles in the recovery region, display an "undershoot" of the log-law of the wall in the wake—this is also pointed out by Kim et al. (1978), Bradshaw and Wong (1972), and Chandrsuda and Bradshaw (1981). A very rapid diffusion of turbulence energy in the outer layer is noted as the flow develops downstream (see Figs. 5-30 through 5-31). Parameters deduced from the recovery region profiles are listed in Table 5-2.

At one recovery location (X/H = 12, Case A), profiles of $\overline{U}$ and u' were measured in the early recovery region at three spanwise locations. These measurements are shown in Fig. 5-33. Variation in measured mean velocity is about 2% of U_{ref}; variations in u' are less than 1% of U_{ref}. It was felt that a better and more practically functional means of characterizing the two-dimensionality of the flow after separation would be to check the results against the requirements of two-dimensional, time-averaged conservation equations; this analysis is presented in Appendix E. Conservation of mass is satisfied at each station tested within a few percent of the inlet mass flux for both Cases A and B. Conservation of momentum is satisfied within 5% for the only case checked (Case A). It may be remarked that the major components of uncertainty in these checks come from the duct dimensions (W_1, W_2) and from the inability to traverse the entire duct with a single probe.

Profiles showing the streamwise development of the boundary layer on the opposite wall for all three cases are shown in the final group of figures pertaining to the velocity field, Figs. 5-34 through 5-38. For Case A, nine measurement stations were probed, extending over $2 < X/H <= 18$. In Case B, seven stations covering $5 < X/H <= 17$ are given; only one station was examined for Case C. The normal coordinate for these plots is Y^*, which is distance normal to the surface with origin at the opposite wall surface ($Y^* = W_2 - Y$). Parameters deduced from the mean velocity profiles along the opposite wall are listed in Table 5-3. Generally, it will be noted that this boundary layer undergoes a moderate adverse pressure gradient in the reattachment region. Since turbulent flow fills the duct in all three cases somewhat upstream of the reattachment position, a well-defined boundary layer edge ceases to exist downstream (of about $X/H = 7$ for Cases A and B). The profiles of u' in this region appear as a superposition of the shape one would expect of a wall-bounded flow and that characteristic of the developing shear layer.

5.6 Wall Skin Friction

Surface skin friction is reported for Case A along the step surface in Fig. 5-39 and for the opposite wall in Fig. 5-40. For Case B, the same results are shown in Figs. 5-41 and 5-42. No skin friction data were obtained for Case C. Several techniques were used to obtain the reported results. The upstream reference dynamic pressure has been used to normalize all skin friction measurements:

$$\overline{C_f} = \frac{\overline{\tau_w}}{\frac{1}{2}\rho U_{ref}^2}$$

$$C_f' = \frac{\sqrt{\overline{\tau_w'^2}}}{\frac{1}{2}\rho U_{ref}^2}$$

Note that the skin-friction coefficient reported below is not defined in the manner usual for boundary layer flows (based on a local dynamic pressure), but is simply normalized by a constant quantity.

Wall skin friction in the reattachment zone has been measured for Cases A and B using the pulsed-wall probe described in Chapter 3. Mean ($\overline{C}_f$) and fluctuating (C_f') values of skin friction are both shown in Figs. 5-39 (for Case A) and 5-41 (for Case B). The "log-law of the wall" was also used to compute skin friction from velocity data near the wall in the recovery region and along the opposite wall, as well as for the separating flow upstream. These results are shown for the two cases in Figs. 5-39 through 5-42. For Case B, a set of Preston probes (tube diameters 0.5 mm to 3.1 mm) was used with the calibration of Patel (1965) to measure skin friction at locations where no instantaneous flow-direction reversals were present (including two locations in the backflow region where the tubes faced upstream). These data are included in Figs. 5-41 and 5-42.

The large negative mean skin friction in the backflow region (see Figs. 5-39 and 5-41) was, at first, a somewhat surprising result of the measurements using the pulsed-wall probe (see Westphal et al., 1981). Later work with the Preston probe placed in this region also showed fairly large negative mean skin friction in the backflow region (Fig. 5-41), as did the results of Driver and Seegmiller (1982). Peak values of fluctuating skin friction always seem to occur in the reattachment region, and high fluctuation levels (relative to the mean) persist in the recovering flow. As far as ten step heights downstream of reattachment, for example, $C_f'/\overline{C}_f > 0.4$ (compared to 0.2-0.3 for typical turbulent boundary layers). From the work of Dean (1978), the expected value of $\overline{C}_f$ for fully developed, two-dimensional duct flow at the Reynolds number of the study is found to be $\overline{C}_f = 0.0016$. The skin friction in the recovery region overshoots this value slightly, an occurrence also noted by Bradshaw and Wong (1972).

Table 5-1

INLET BOUNDARY LAYER PARAMETERS

X/H	U_e/U_{ref} (1)	δ_{99} cm	δ^* cm	$Re_\theta \times 10^{-3}$	H	$C_{fe} \times 10^3$ (2)	Π (3)
-9.75	0.95	1.12	0.145	1.05	1.36	4.79	-0.04
-3.0	1.0	1.68	0.243	1.71	1.41	4.06	0.17
-0.75	1.01	1.85	0.268	1.96	1.39	3.89	0.28
-0.75 (4)	1.00	0.66	0.085	0.59	1.47	5.46	0.08
-3.0 (5)	1.0	1.36	0.216	1.48	1.45	4.12	0.26

Notes:

1. U_e is the maximum (core) velocity at the specified station.

2. C_{fe} is the wall skin friction normalized by the local dynamic head:

$$C_{fe} \equiv \frac{\overline{\tau}_w}{\frac{1}{2}\rho U_e^2}$$

3. Π is Coles' wake parameter computed using a fit of Coles' law of the wall-wake over the region $Y+ > 50$ to $Y/\delta < 0.75$.

4. These data are taken downstream of the vortex generators, Case C, in the "downwash" region between adjacent counter-rotating vortices.

5. This profile is taken along the opposite wall for Cases A and B.

Table 5-2

RECOVERY REGION BOUNDARY LAYER PARAMETERS

Case	X/H	U_e/U_{ref} (1)	δ_{99} cm	δ^* cm	$Re_\theta \times 10^{-3}$	H	$C_{fe} \times 10^3$ (2)
A	12	0.82	7.9	2.5	11.2	1.84	1.1
	14	0.79	7.9	2.1	10.4	1.62	1.7
	16	0.76	7.5	1.8	9.0	1.49	2.2
	18	0.72	7.3	1.4	7.6	1.37	2.9
	20	0.69	6.9	1.0	6.1	1.30	3.4
B	13.8	0.79	8.2	2.5	11.4	1.74	1.4
	15.8	0.73	7.7	2.0	9.3	1.54	2.1
	17.8	0.72	7.8	1.5	7.8	1.39	2.8
	19.8	0.66	7.1	1.2	5.9	1.32	3.3
C	12	0.78	8.0	2.5	11.6	1.73	1.4
	14	0.76	8.0	2.2	10.6	1.59	1.8
	16	0.74	7.9	1.9	9.5	1.49	2.2
	18	0.72	7.8	1.6	8.2	1.41	2.6
	20	0.69	7.4	1.3	6.6	1.35	3.0

Notes:

1. U_e is the maximum (core) velocity at the specified station.

2. C_{fe} is the wall skin friction normalized b y the local dynamic head:

$$C_{fe} \equiv \frac{\bar{\tau}_w}{\frac{1}{2}\rho U_e^2}$$

Table 5-3

OPPOSITE-WALL BOUNDARY LAYER PARAMETERS

Case	X/H	U_e/U_{ref} (1)	δ_{99} cm	δ^* cm	$Re_\theta \times 10^{-3}$	H	$C_{fe} \times 10^3$ (2)	Π (3)
A	2	1.00	1.7	0.26	1.88	1.41	3.9	0.34
	4	1.00	1.9	0.31	2.28	1.40	3.6	0.47
	6	0.95	2.2	0.39	2.65	1.45	3.1	0.82
	8	0.89	2.6	0.54	3.31	1.52	2.5	1.42
	10	0.85	3.1	0.71	3.91	1.59	2.1	1.91
	12	0.81	3.4	0.83	4.27	1.62	2.0	2.09
	14	0.78	3.7	0.86	4.42	1.58	2.2	1.80
	16	0.75	3.8	0.82	4.22	1.51	2.4	1.39
	18	0.72	3.9	0.75	3.84	1.46	2.8	1.03
B	5	1.05	1.9	0.27	2.09	1.37	3.9	0.18
	7	1.00	2.4	0.37	2.58	1.41	3.3	0.58
	9	0.94	2.8	0.50	3.16	1.49	2.7	1.15
	11	0.87	3.1	0.62	3.52	1.53	2.5	1.48
	13	0.81	3.2	0.68	3.51	1.55	2.5	1.41
	15	0.75	3.7	0.70	3.50	1.49	2.7	1.14
	17	0.73	3.9	0.64	3.22	1.44	3.1	0.76
C	16	0.73	3.7	0.75	3.80	1.47	2.7	1.11

Notes:

1. U_e is the maximum (core) velocity at the specified station.
2. C_{fe} is the wall skin friction normalized by the local dynamic head:

$$C_{fe} \equiv \frac{\overline{\tau}_w}{\frac{1}{2}\rho U_e^2}$$

3. Π is Coles' wake parameter computed using a fit of Coles' law of the wall-wake over the region $Y+ > 50$ to $Y/\delta < 0.75$.

Note : Lengths in cm.

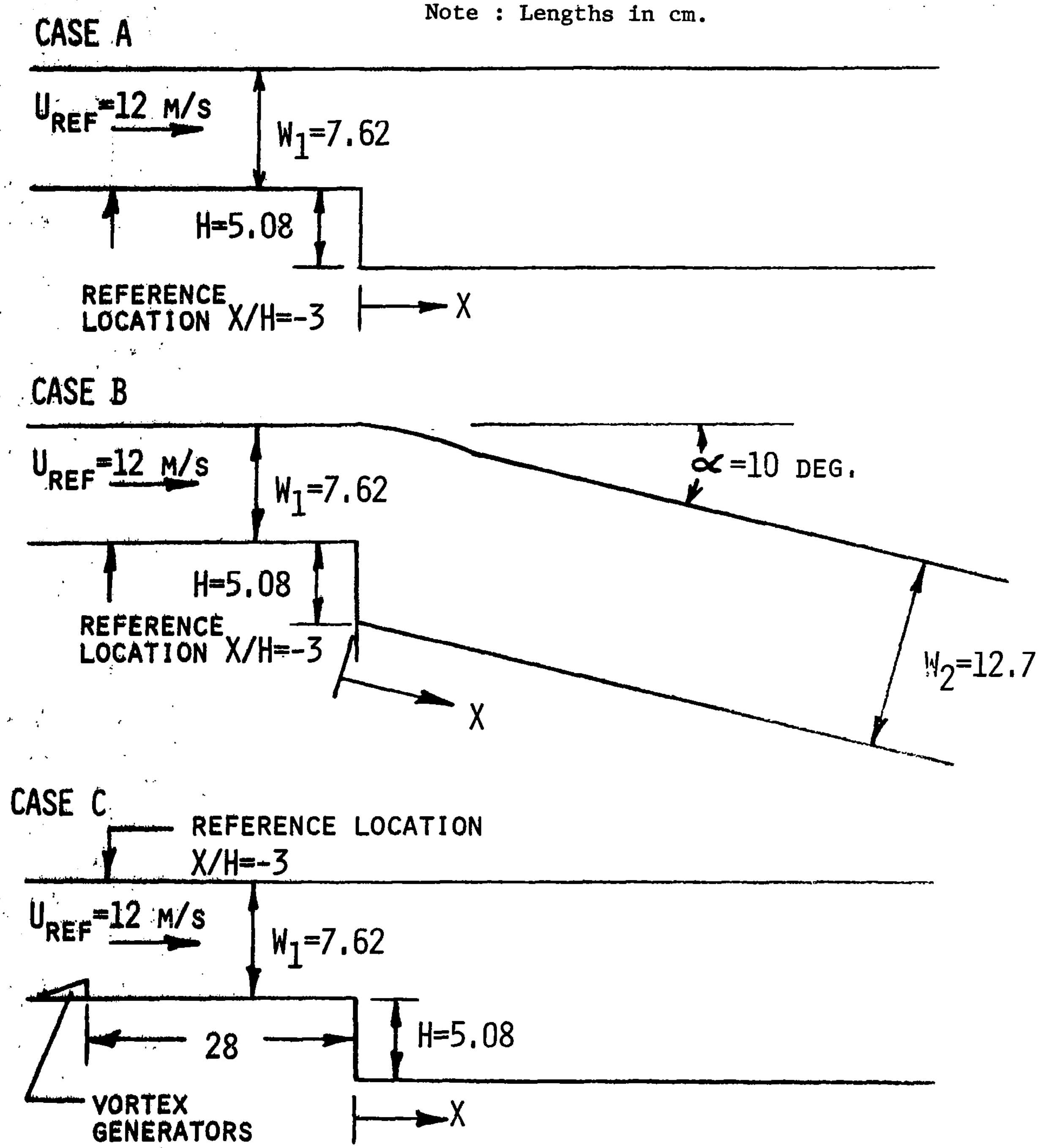

Fig. 5-1. Schematics and nomenclature for three main experiments.

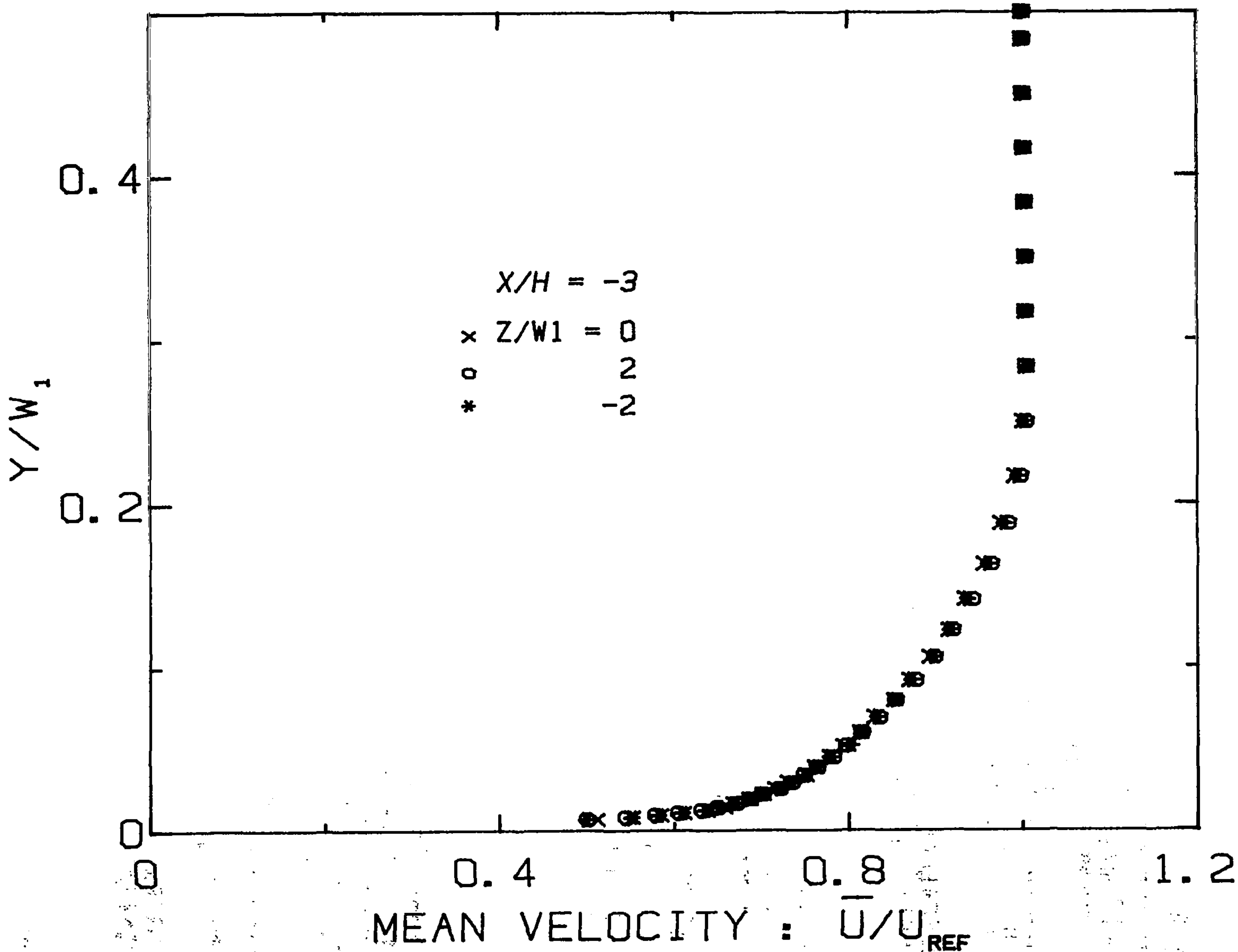

Fig. 5-2. Spanwise profiles at X/H = -3.

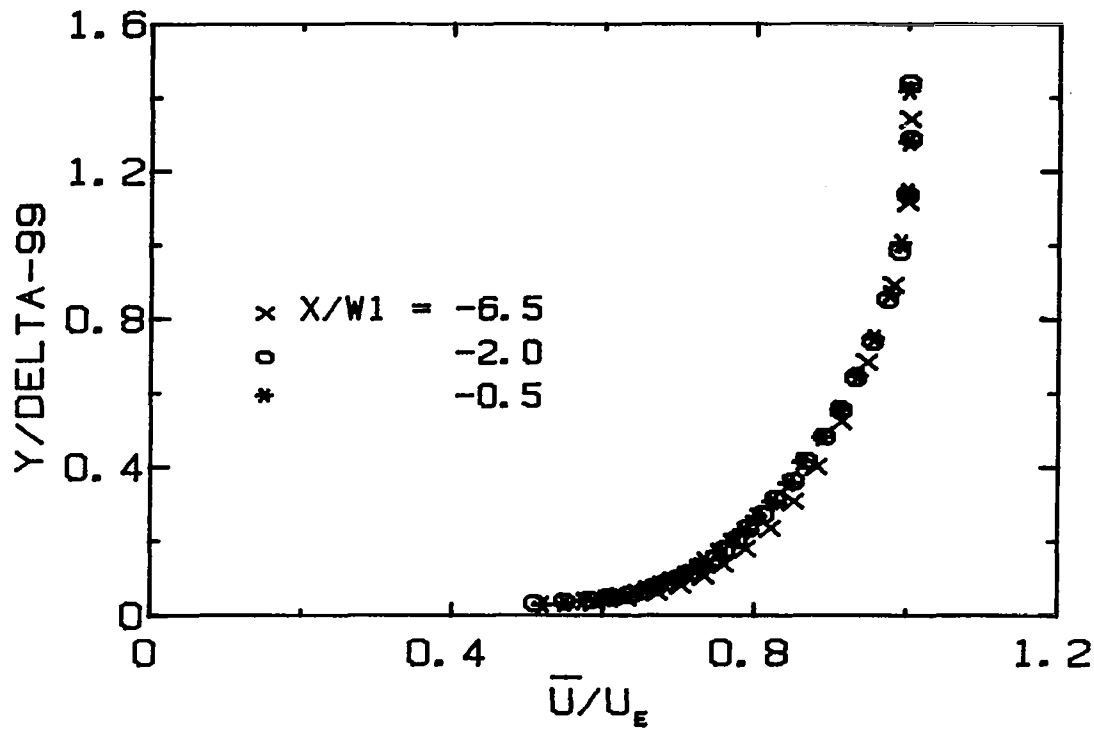

(a) Mean velocity profiles normalized by δ-99.

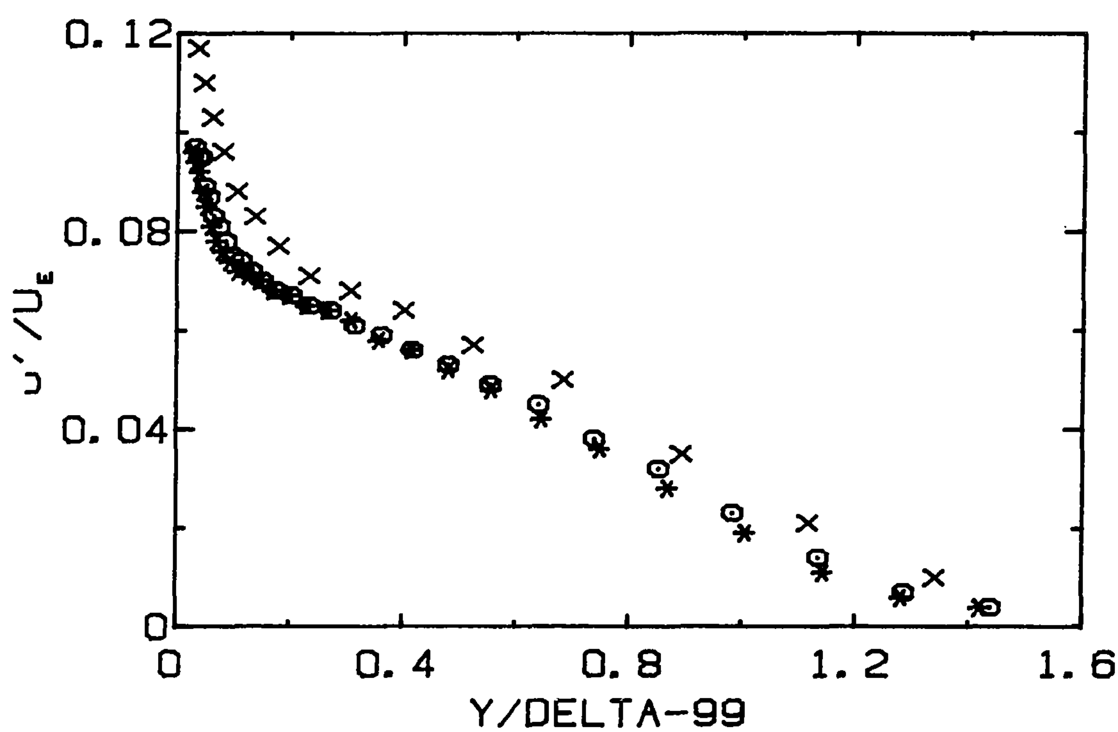

(b) Turbulence intensity profiles.

Fig. 5-3. Velocity profiles upstream of separation.

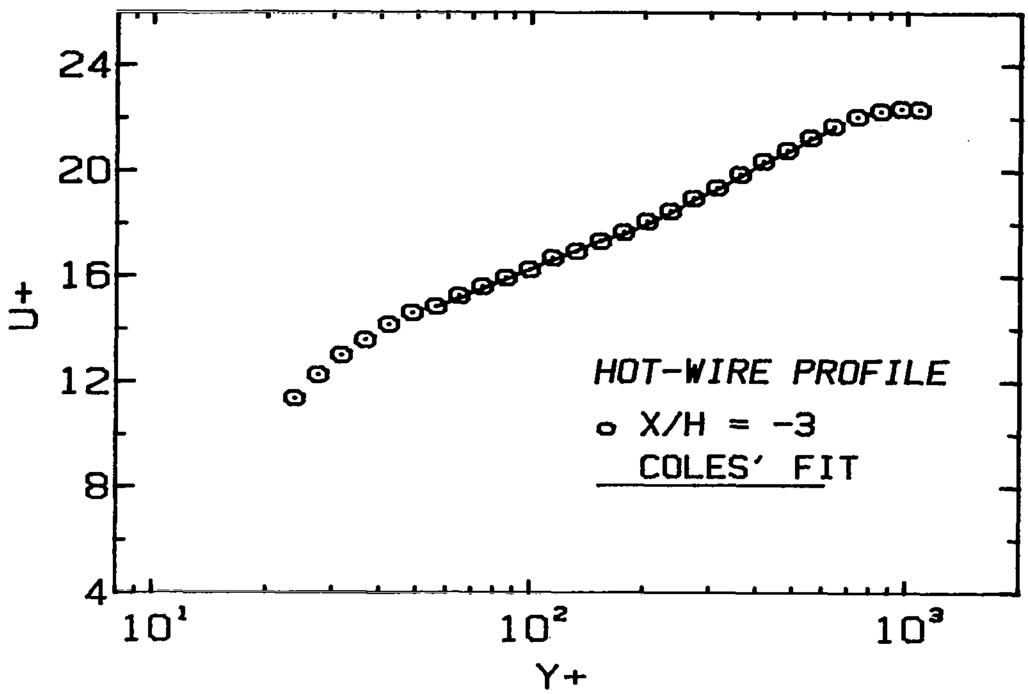

(a) Mean velocity plotted in inner coordinates compared to Coles' law of the wall-wake fit.

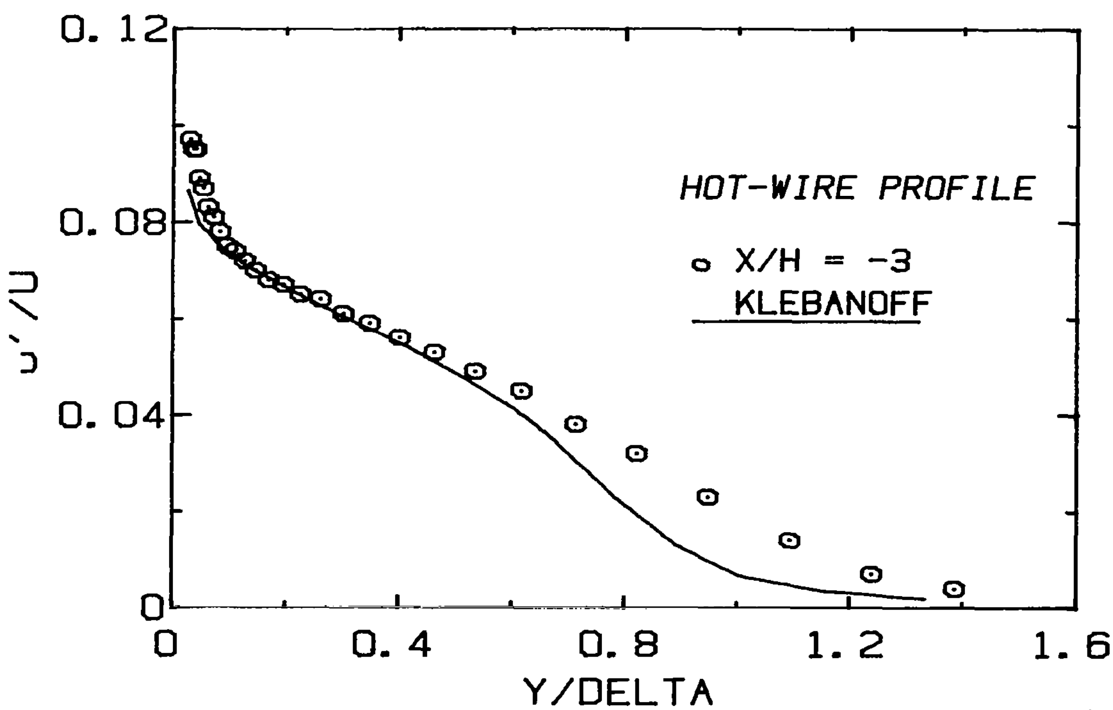

(b) Streamwise turbulence intensity normalized by U_e compared to Klebanoff's data.

Fig. 5-4. Comparison of upstream profile shapes with accepted curves for flat-wall turbulent boundary layers.

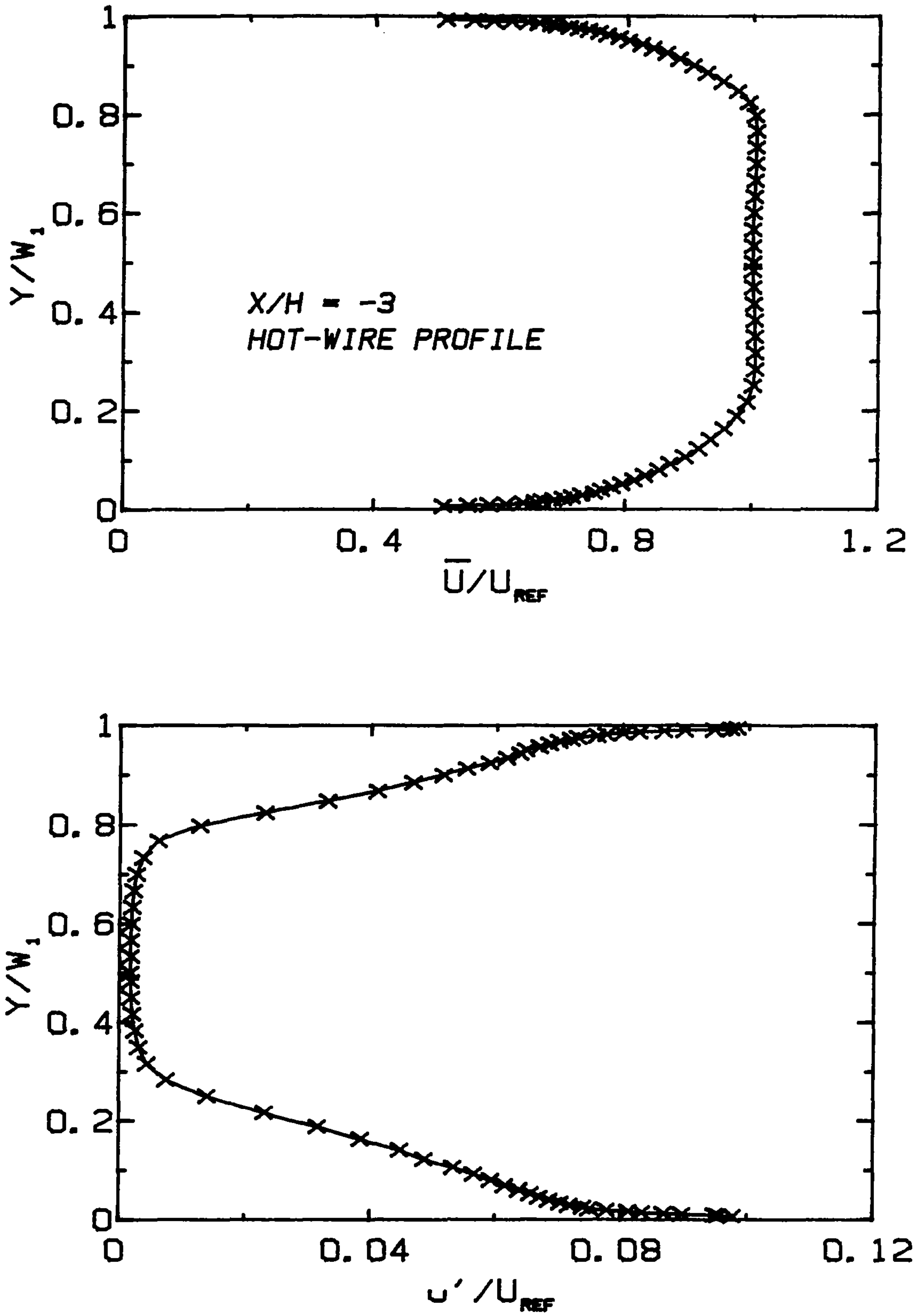

Fig. 5-5. Velocity profile across the duct at X/H = -3.

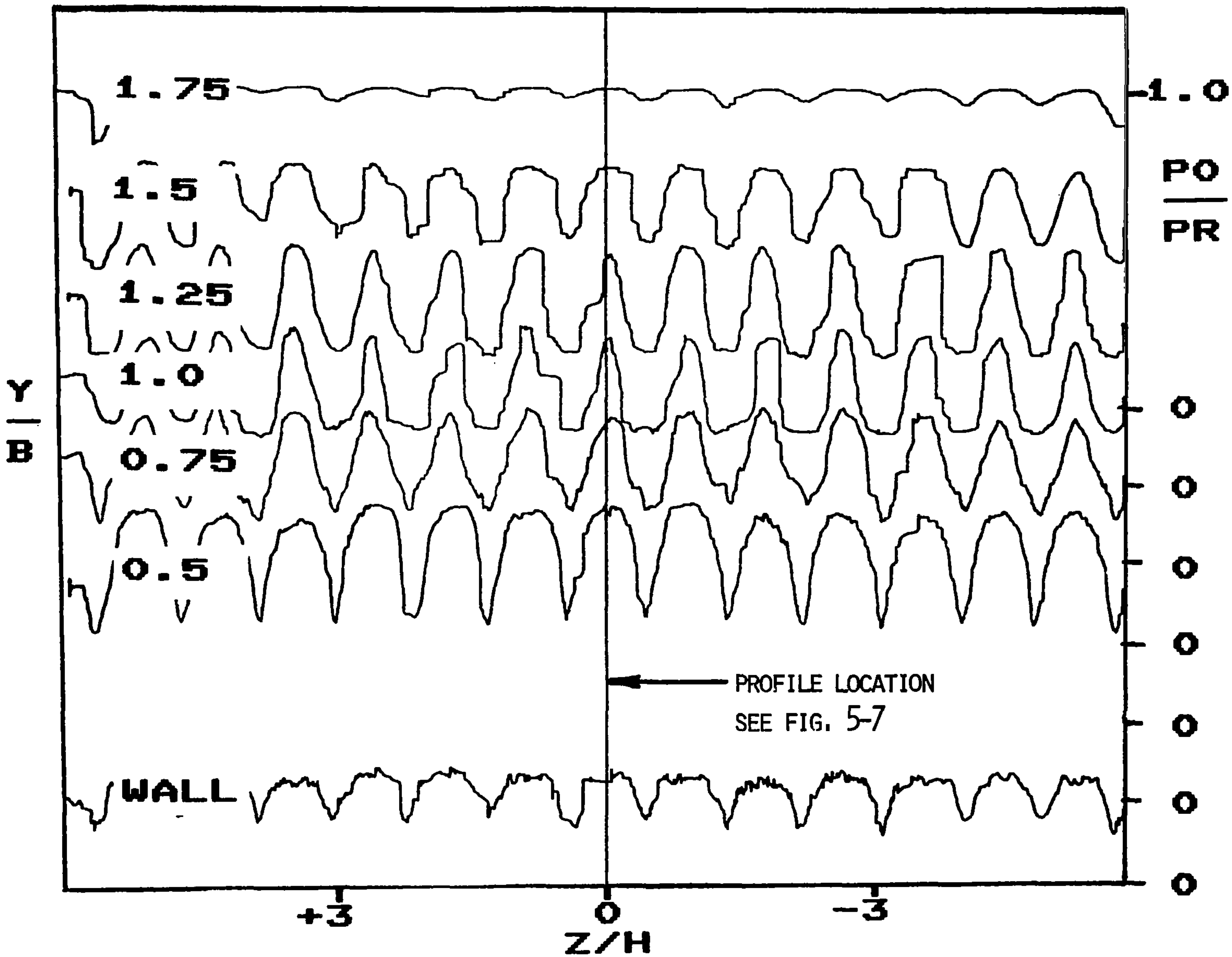

Fig. 5-6. Spanwise total pressure profiles for Case C. B is the generator height (1 cm).

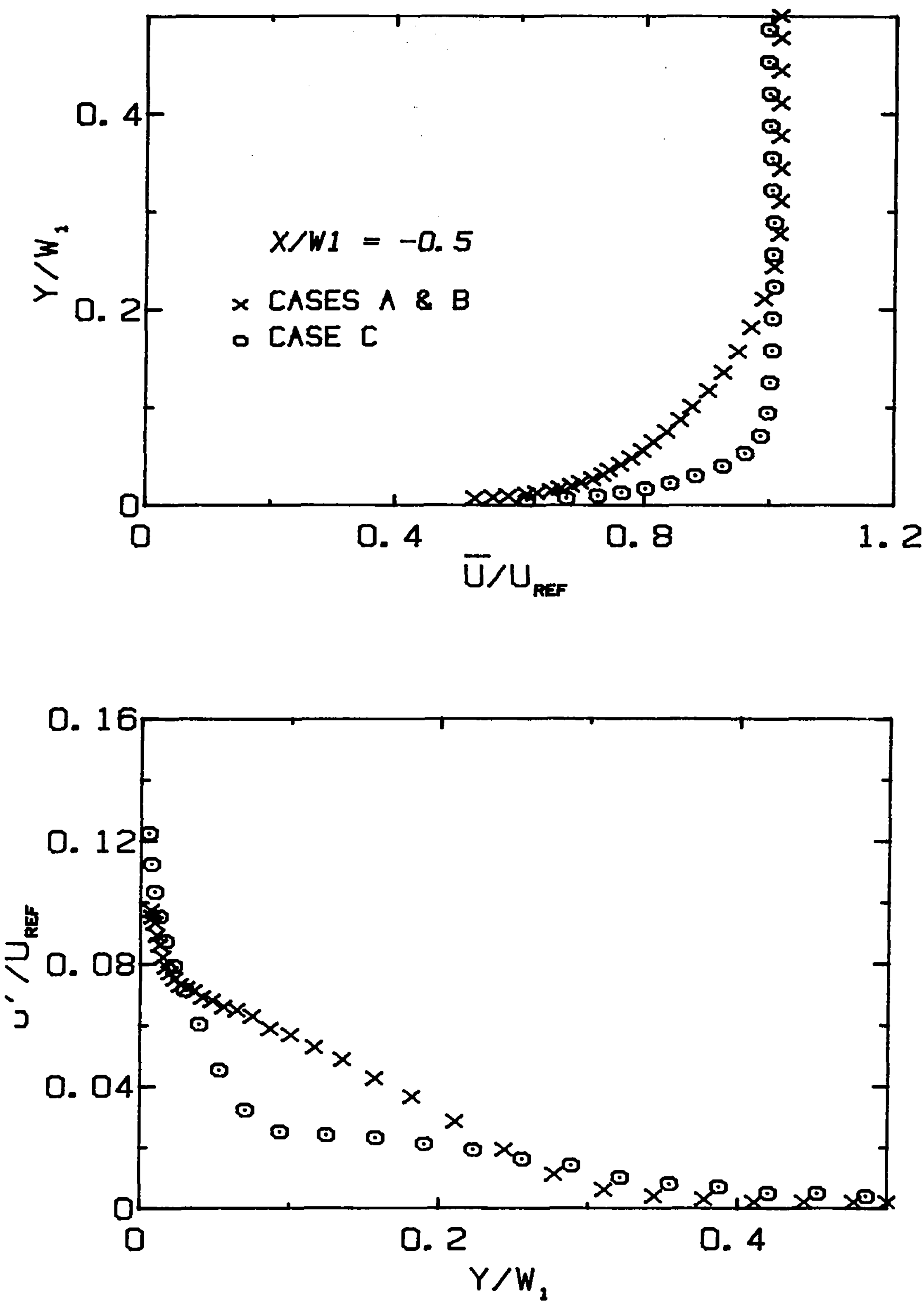

Fig. 5-7. Velocity profile at X/H = -0.75 for Case C.

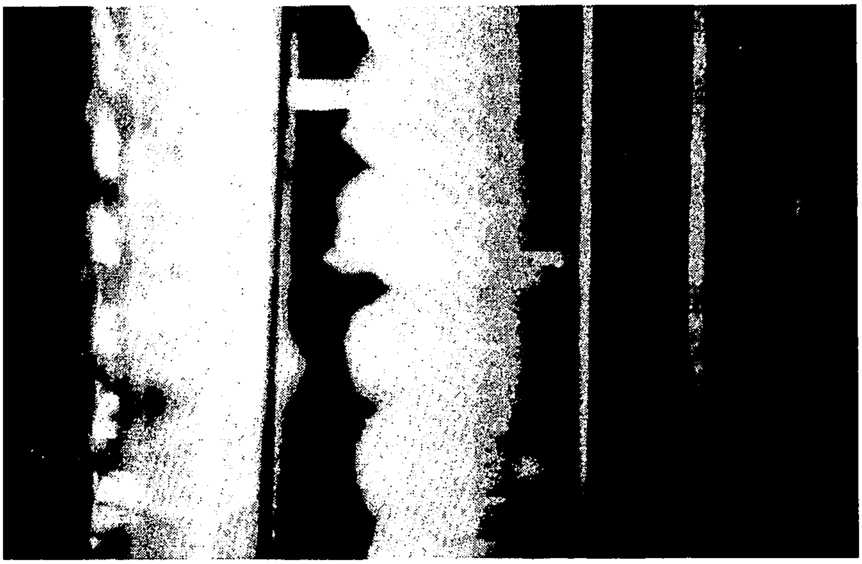

(a) Y-Z section showing the shape of the vortices; taken with the plane of lighting at X/H = -3.

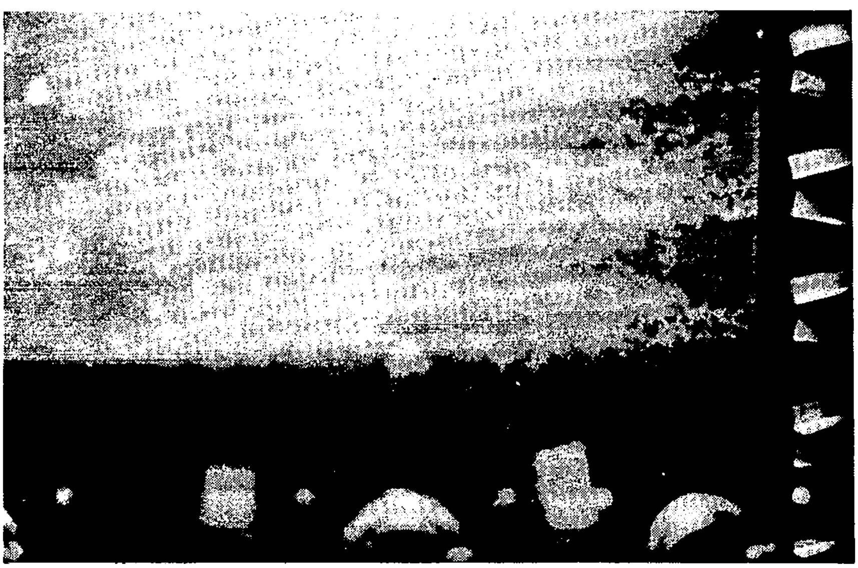

(b) Plan view of an X-Z plane with the wire at X/H = -5 and approximately 0.5 cm from the wall.

Fig. 5-8. Smoke-wire visualization of vortices upstream of separation for Case C.

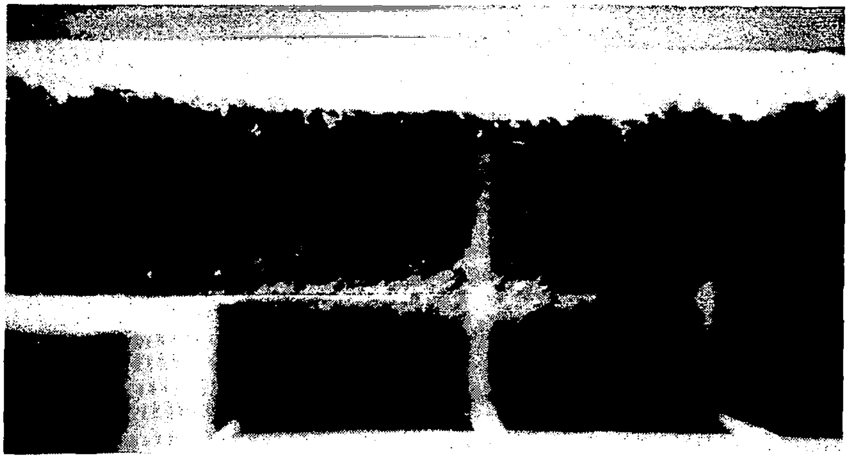

(a) Case A.

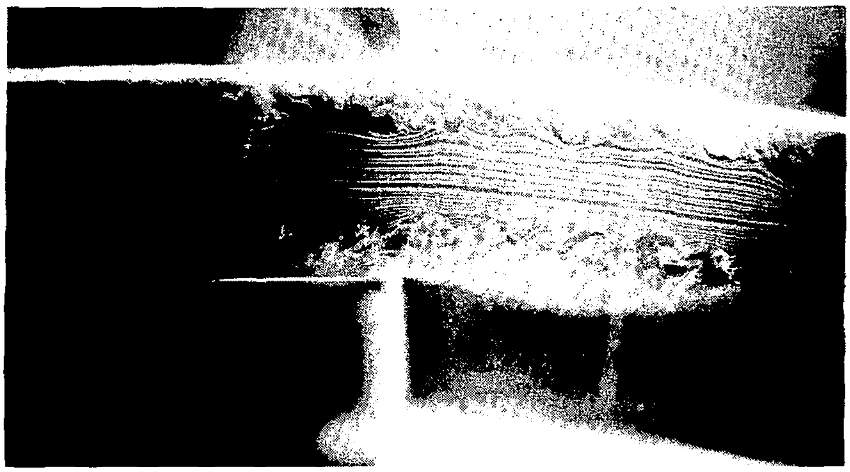

(b) Case B.

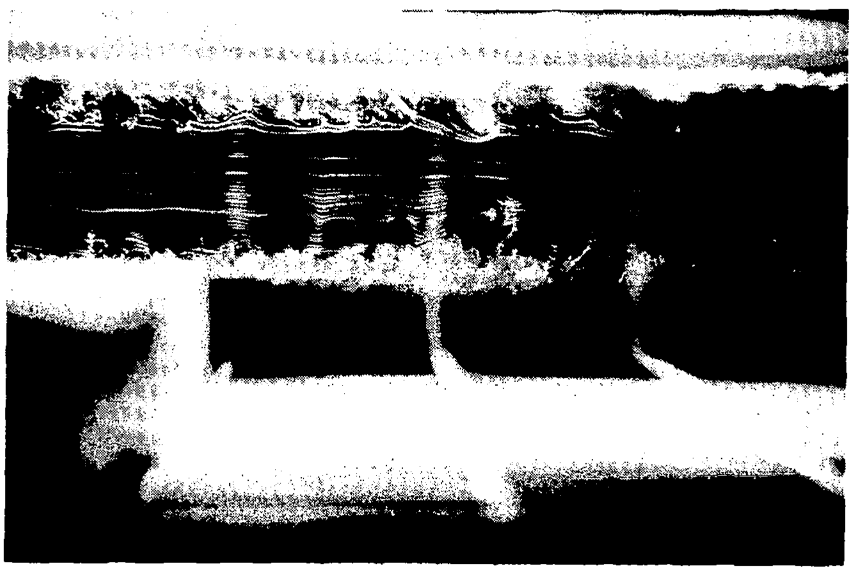

(c) Case C.

Fig. 5-9. Smoke-wire visualization of the separating boundary layer and shear layer just after separation using a smoke-wire at X/H = -3.

(a) Case A; X/H = 4.

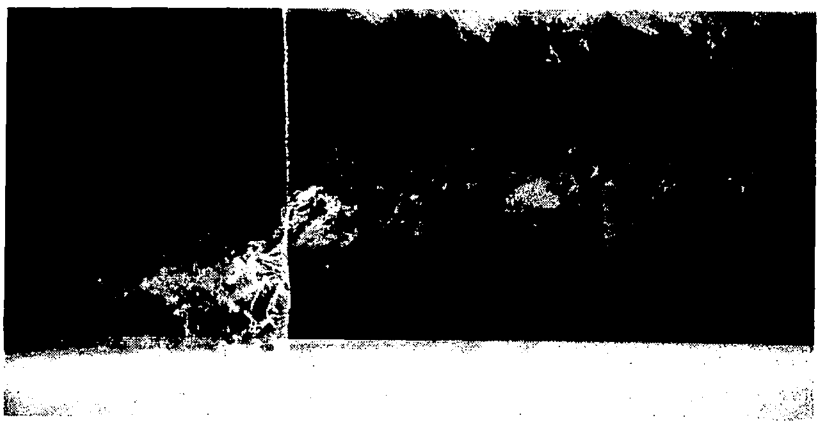

(b) Case B; X/H = 5.

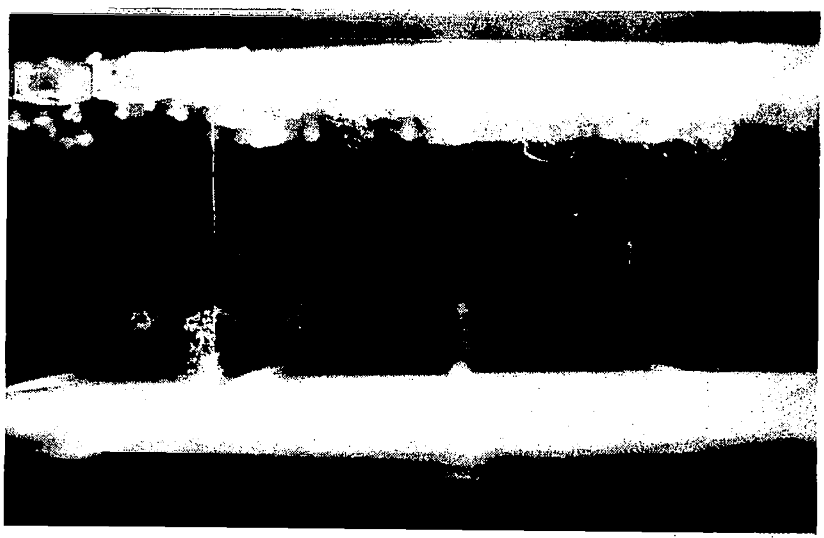

(c) Case C; X/H = 4.

Fig. 5-10. Smoke-wire visualization of the separated shear layer at approximately half the distance to reattachment.

(a) Case A; X/H = 8.

(b) Case B; X/H = 9.

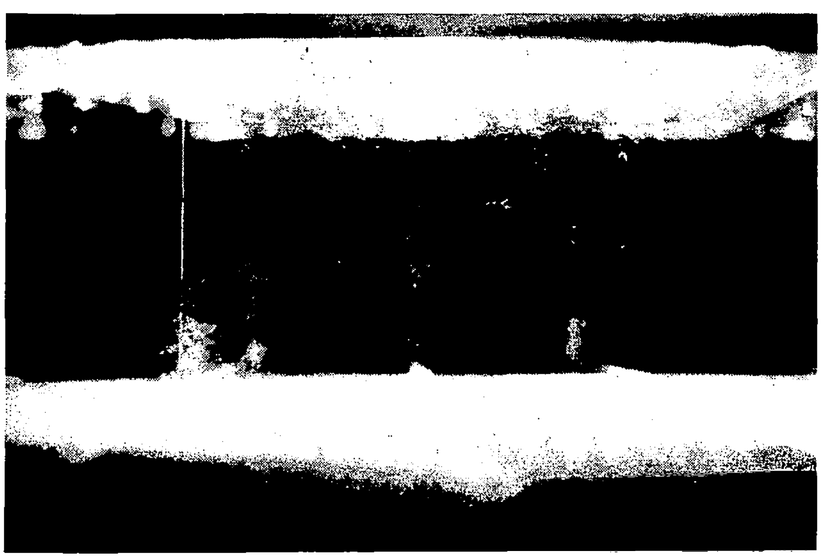

(c) Case C; X/H = 6.

Fig. 5-11. Smoke-wire visualization just upstream of the reattachment point.

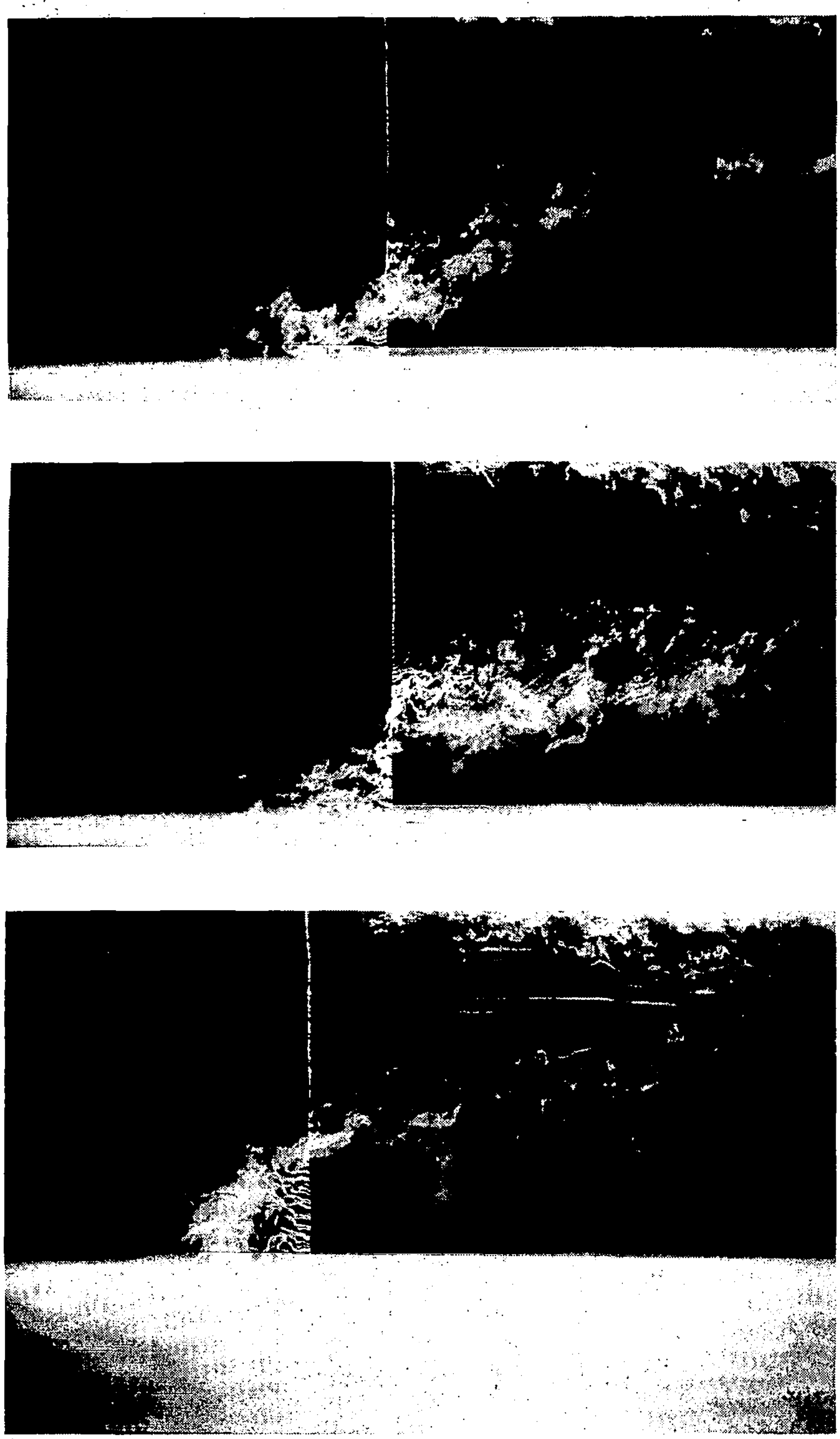

Fig. 5-12. Three photos from Case B at X/H = 5 showing the typical variation in nominally identical realizations.

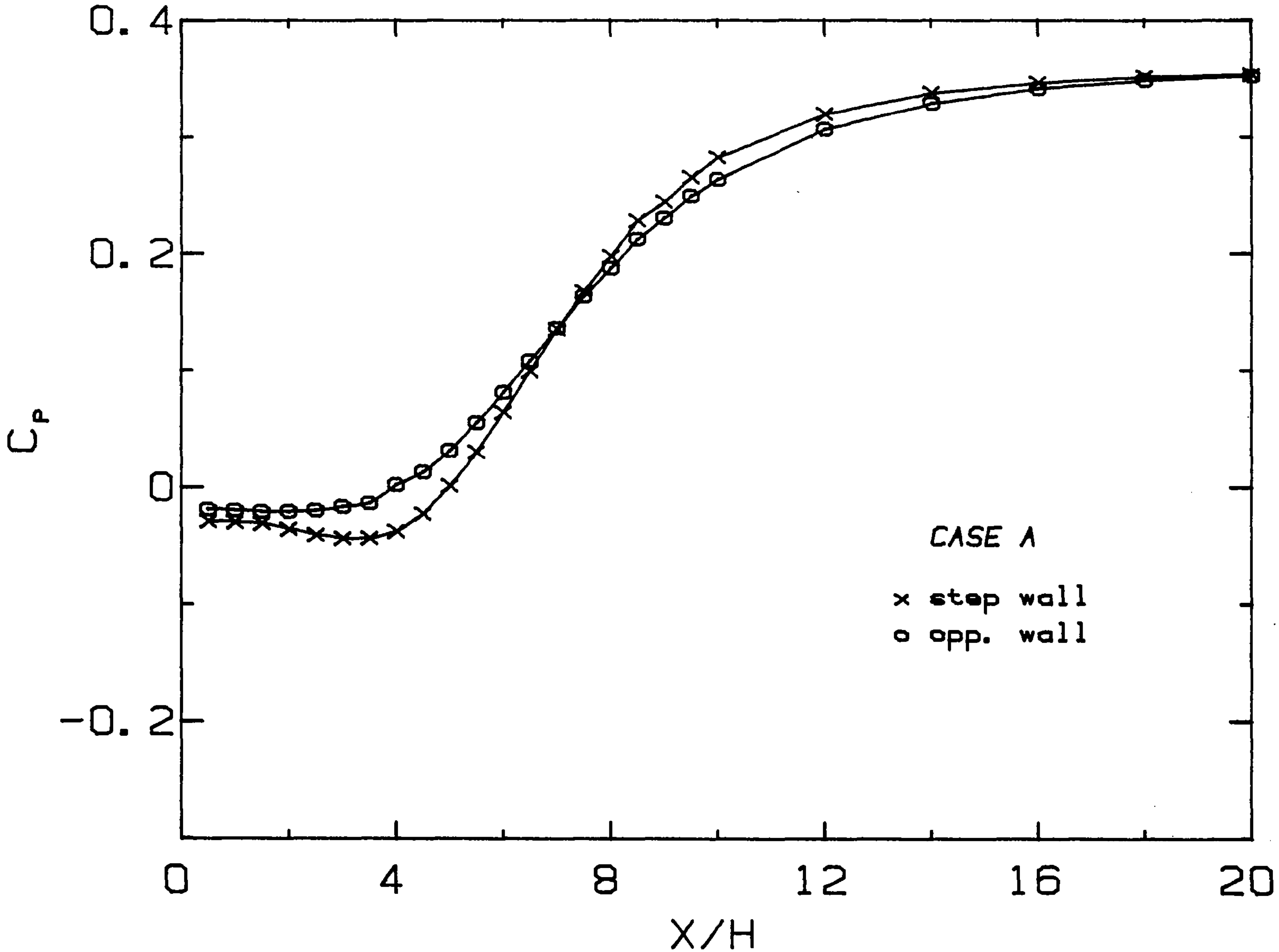

Fig. 5-13. Wall static pressure coefficient on both walls for Case A.

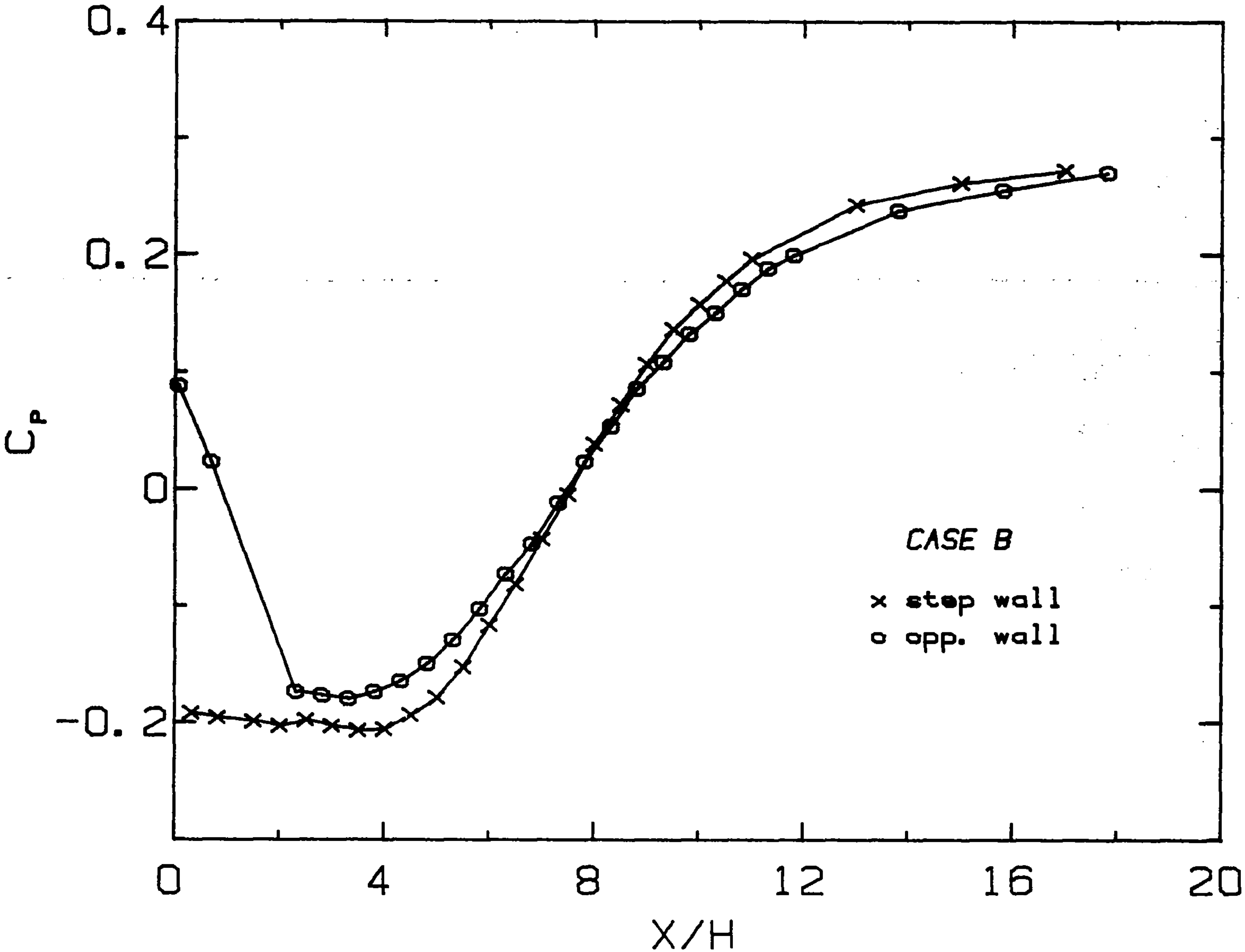

Fig. 5-14. Wall static pressure coefficient on both walls for Case B.

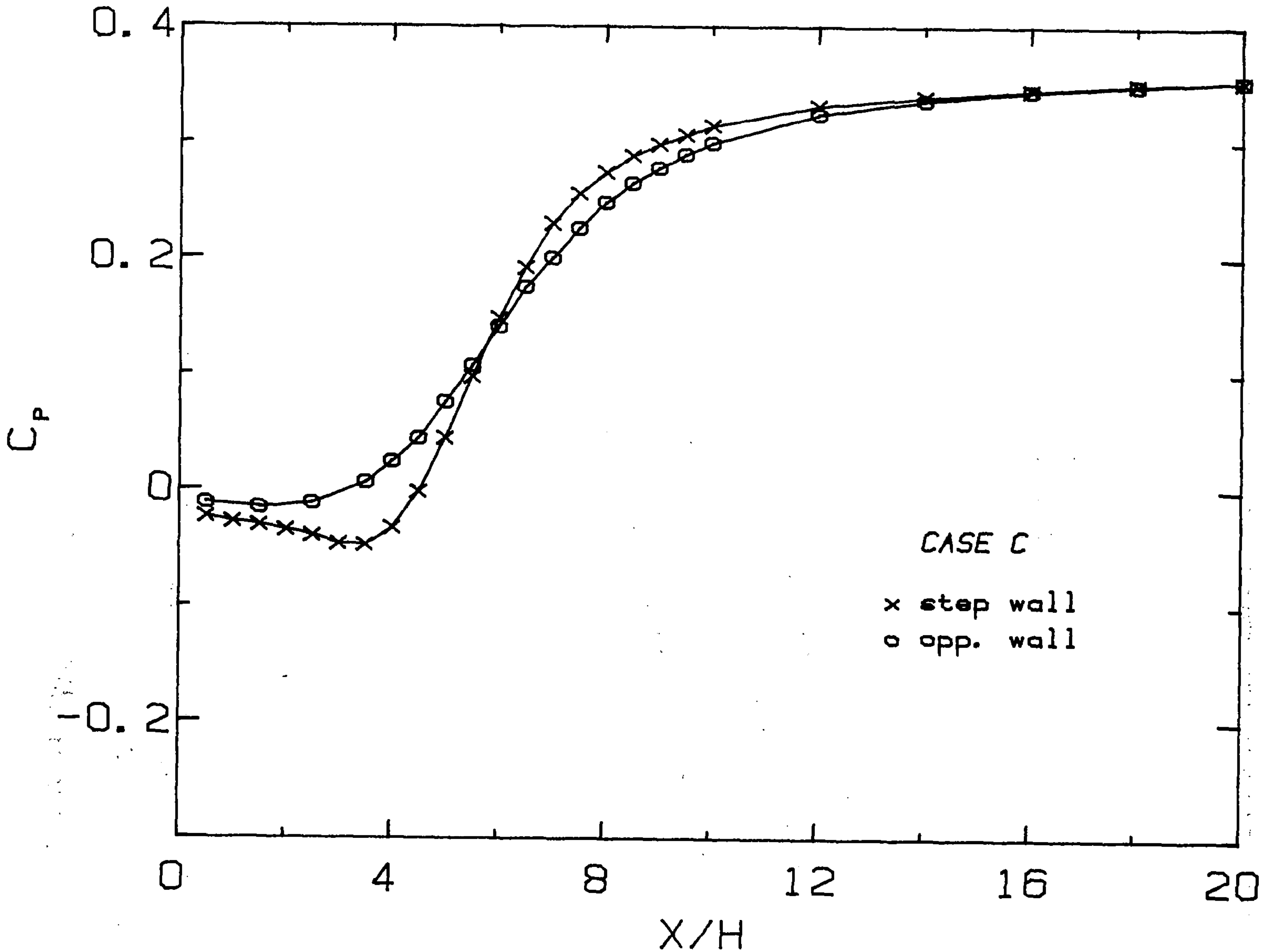

Fig. 5-15. Wall static pressure coefficient on both walls for Case C.

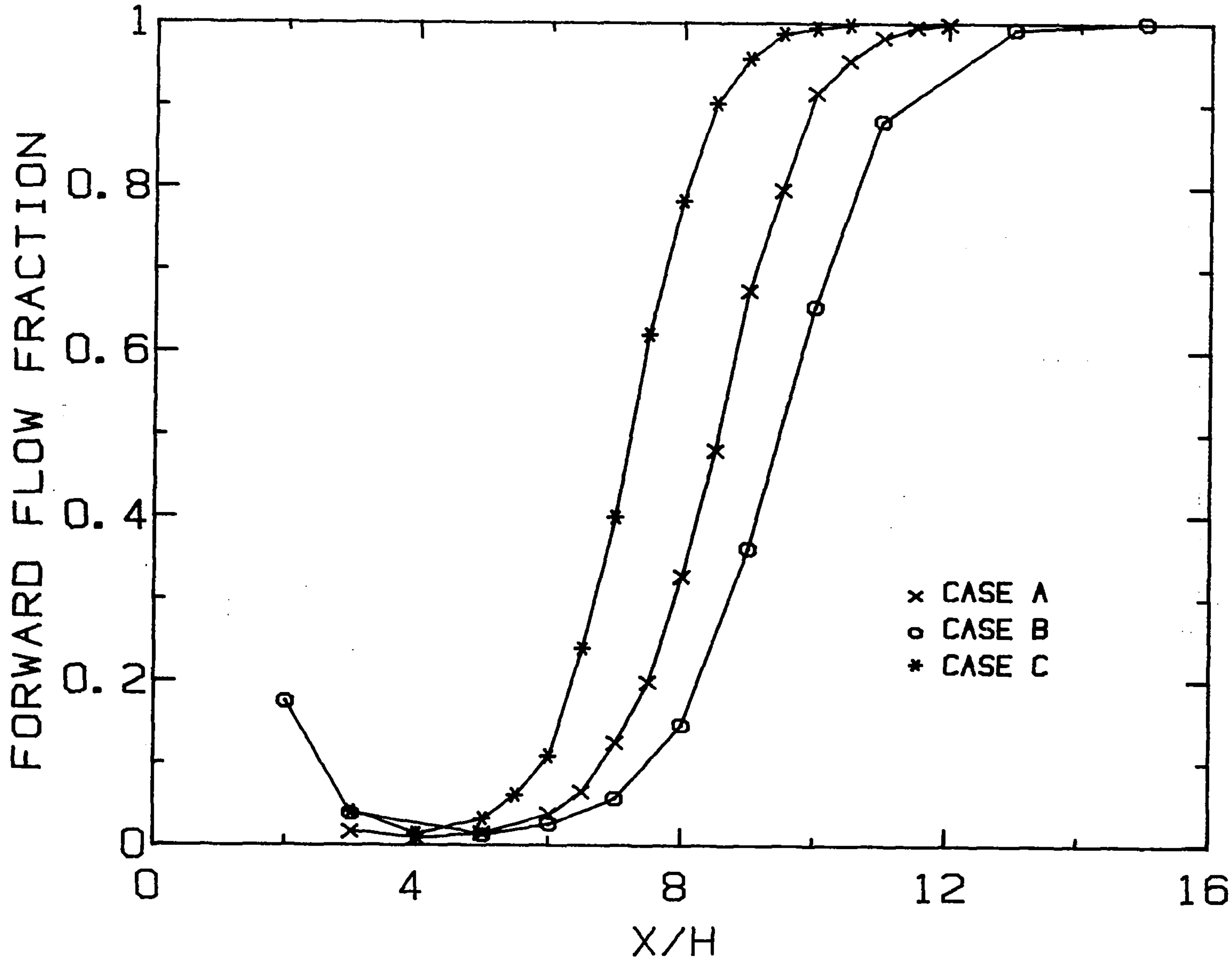

Fig. 5-16. Forward-flow fraction measured with a thermal tuft for the three main cases.

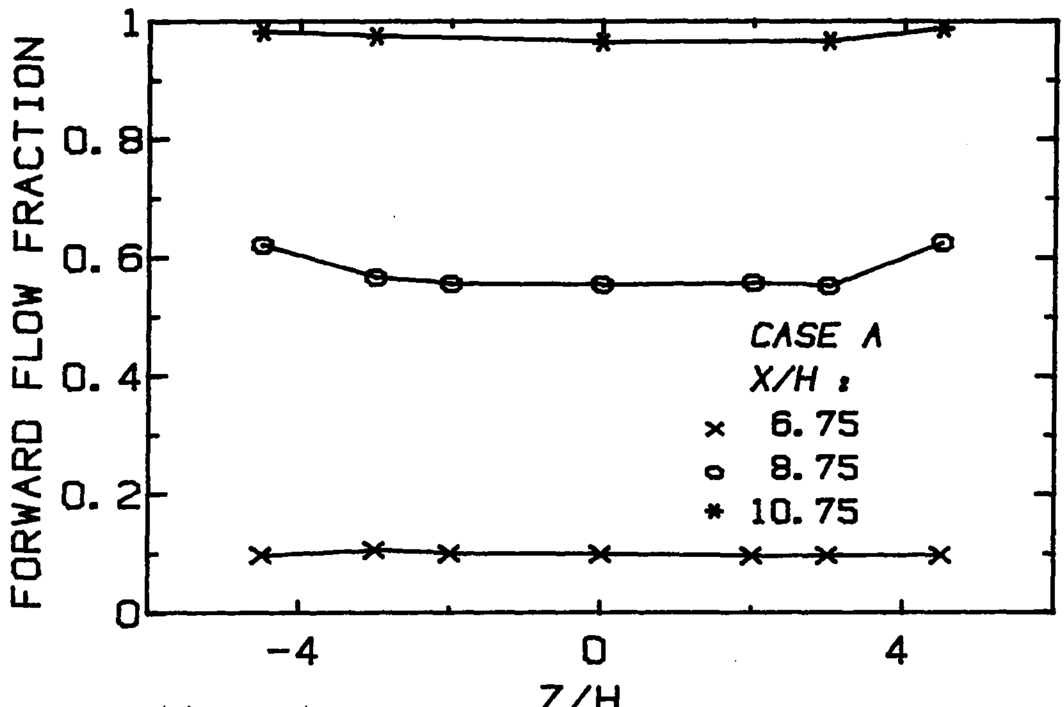

(a) Case A.

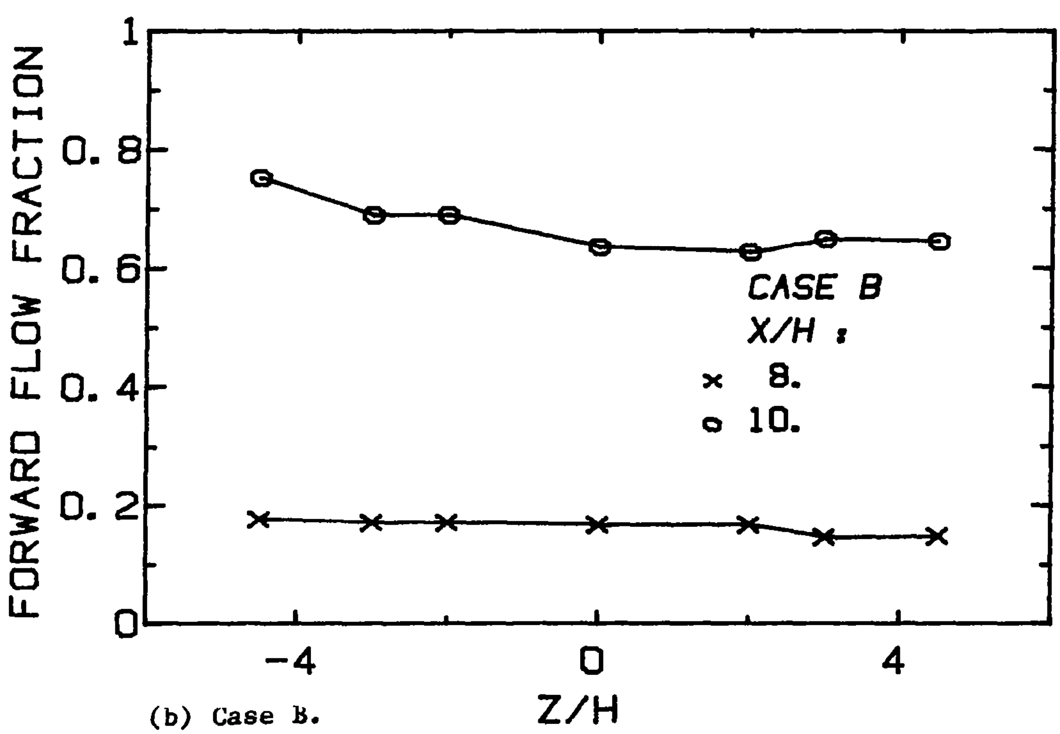

(b) Case B.

Fig. 5-17. Spanwise distributions of forward-flow fraction in near reattachment, indicating the degree to which the reattachment line is straight across the span.

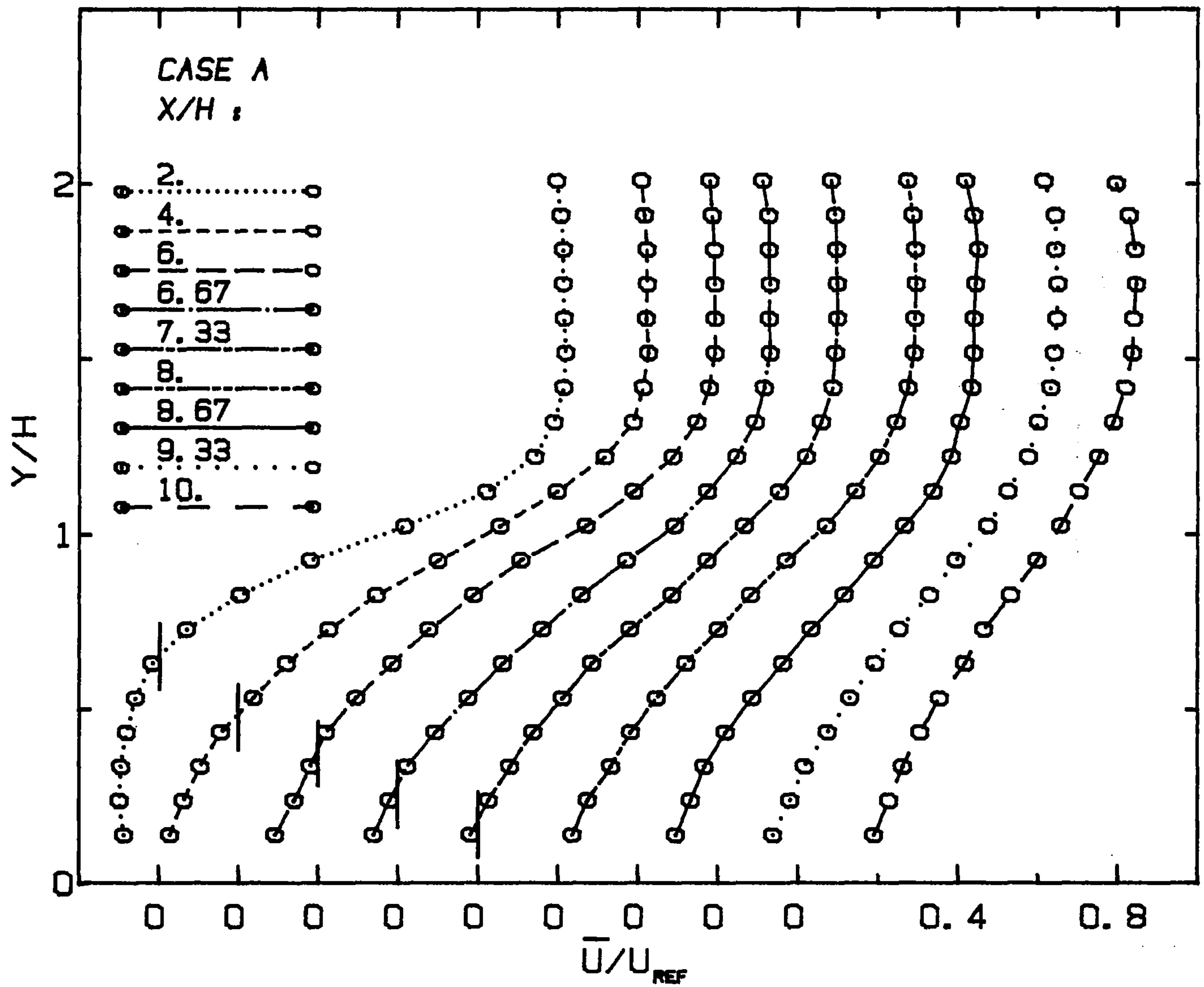

Fig. 5-18. Mean velocity distributions in the separation and reattachment regions measured with a pulsed-wire anemometer for Case A.

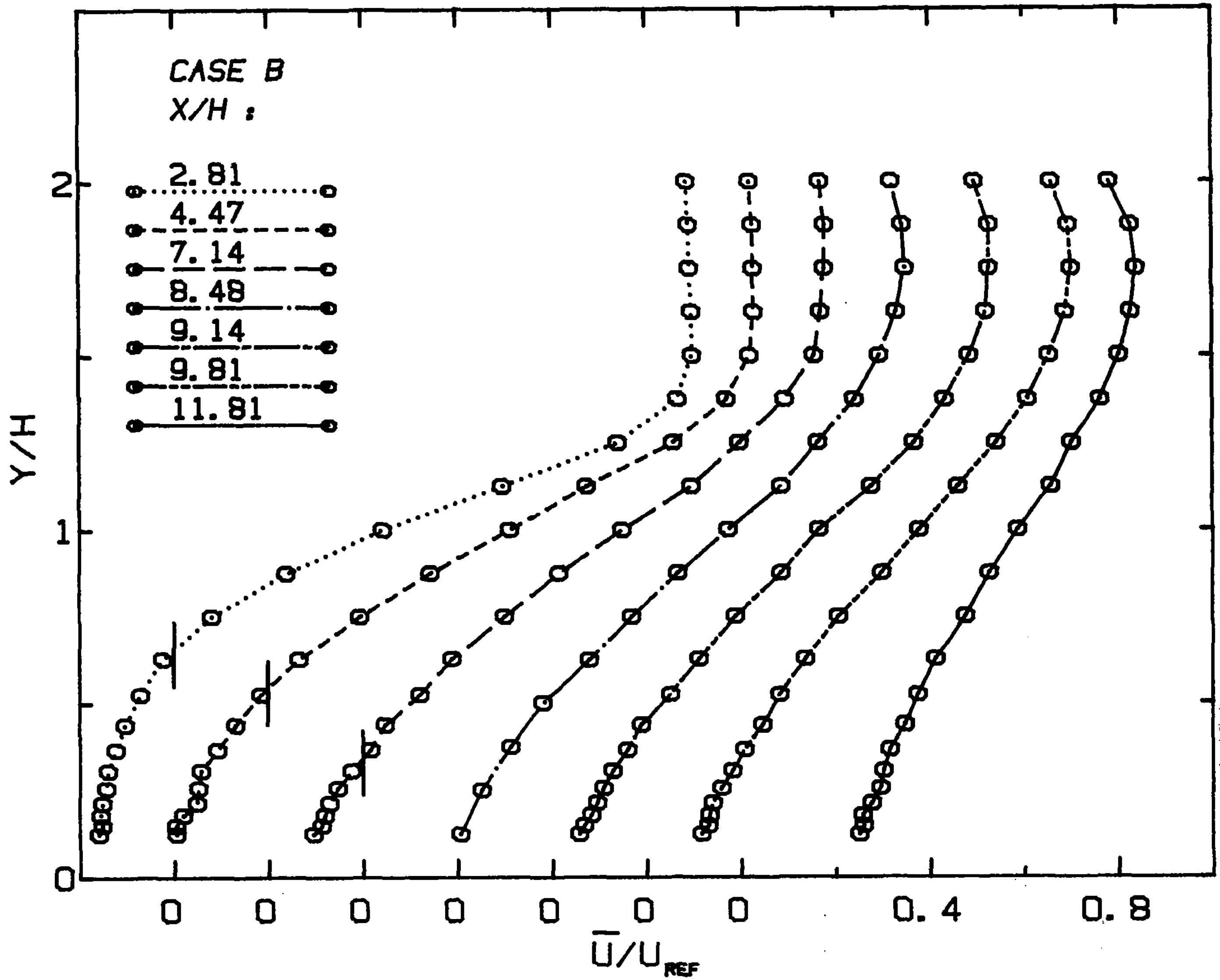

Fig. 5-19. Mean velocity distributions in the separation and reattachment regions measured with a pulsed-wire anemometer for Case B.

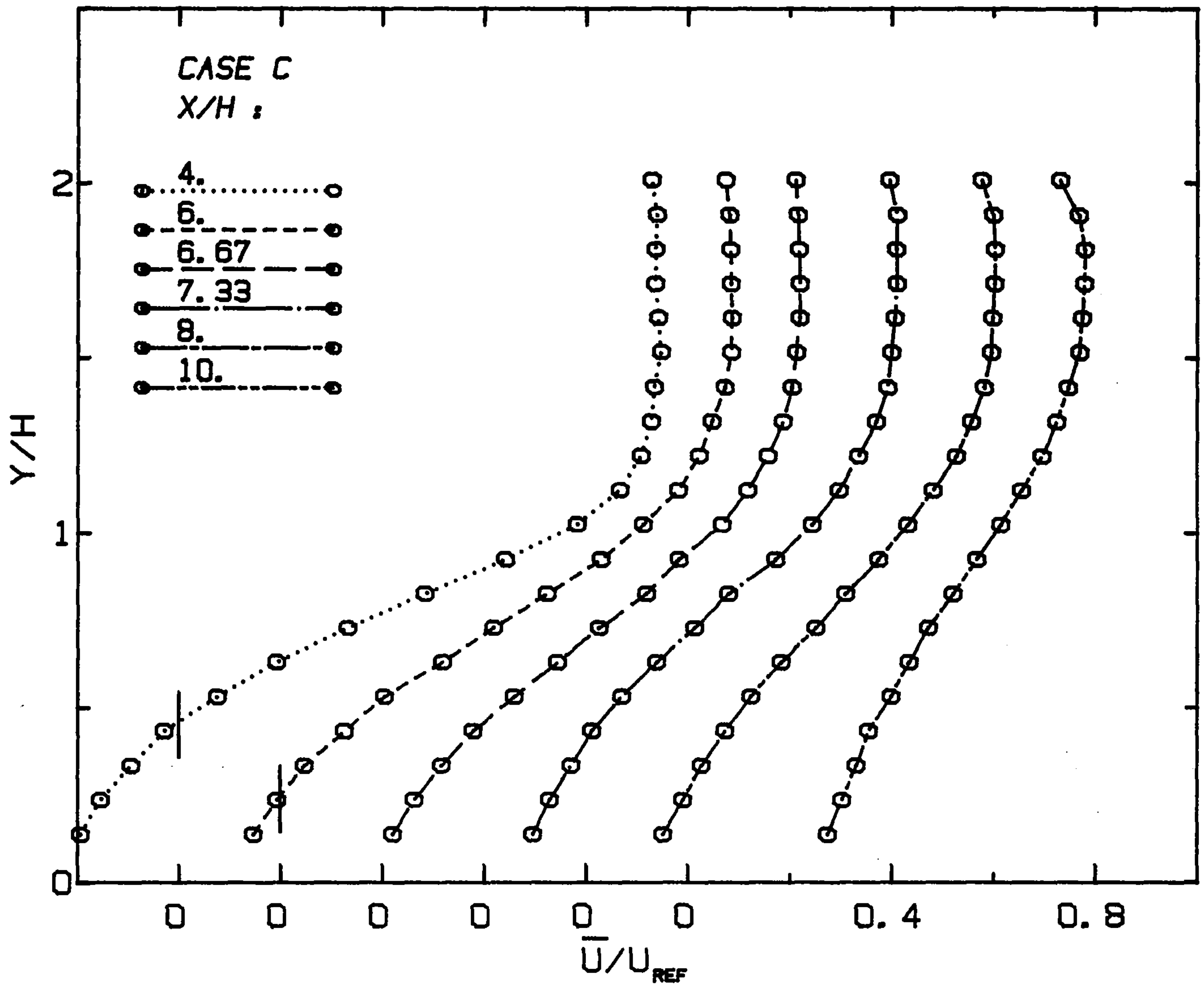

Fig. 5-20. Mean velocity distributions in the separation and reattachment regions measured with a pulsed-wire anemometer for Case C.

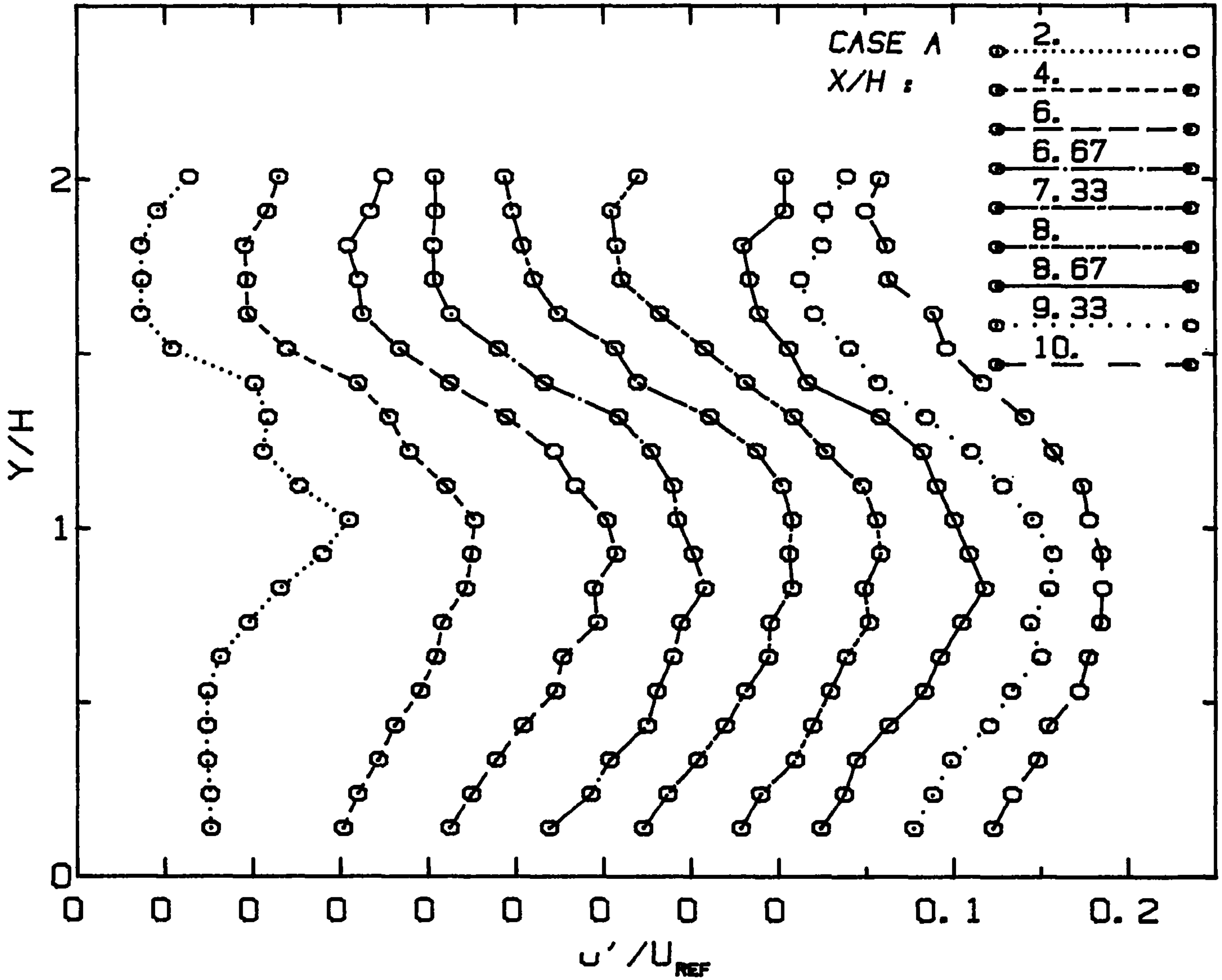

Fig. 5-21. RMS velocity distributions in the separation and reattachment regions measured with a pulsed-wire anemometer for Case A.

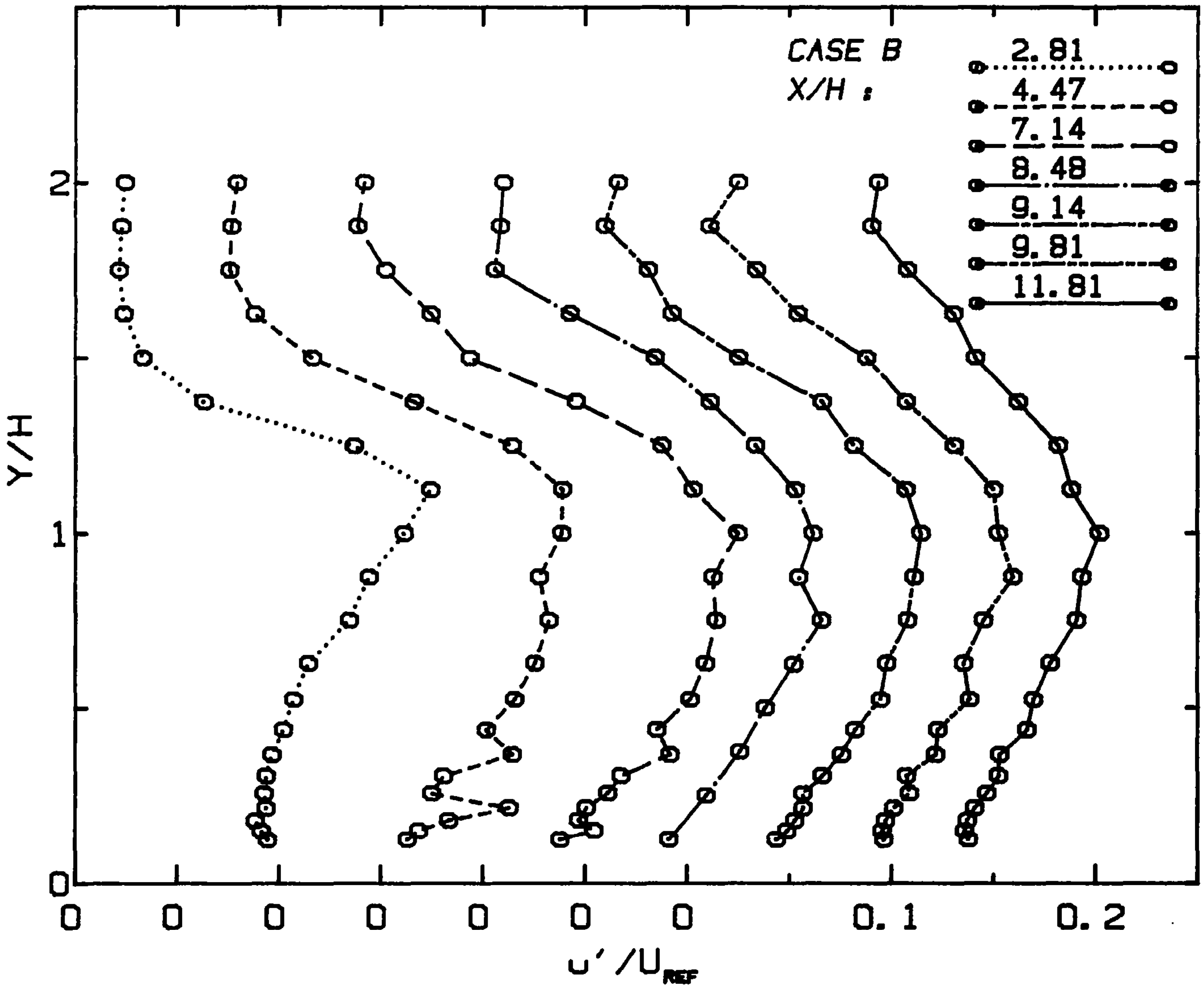

Fig. 5-22. RMS velocity distributions in the separation and reattachment regions measured with a pulsed-wire anemometer for Case B.

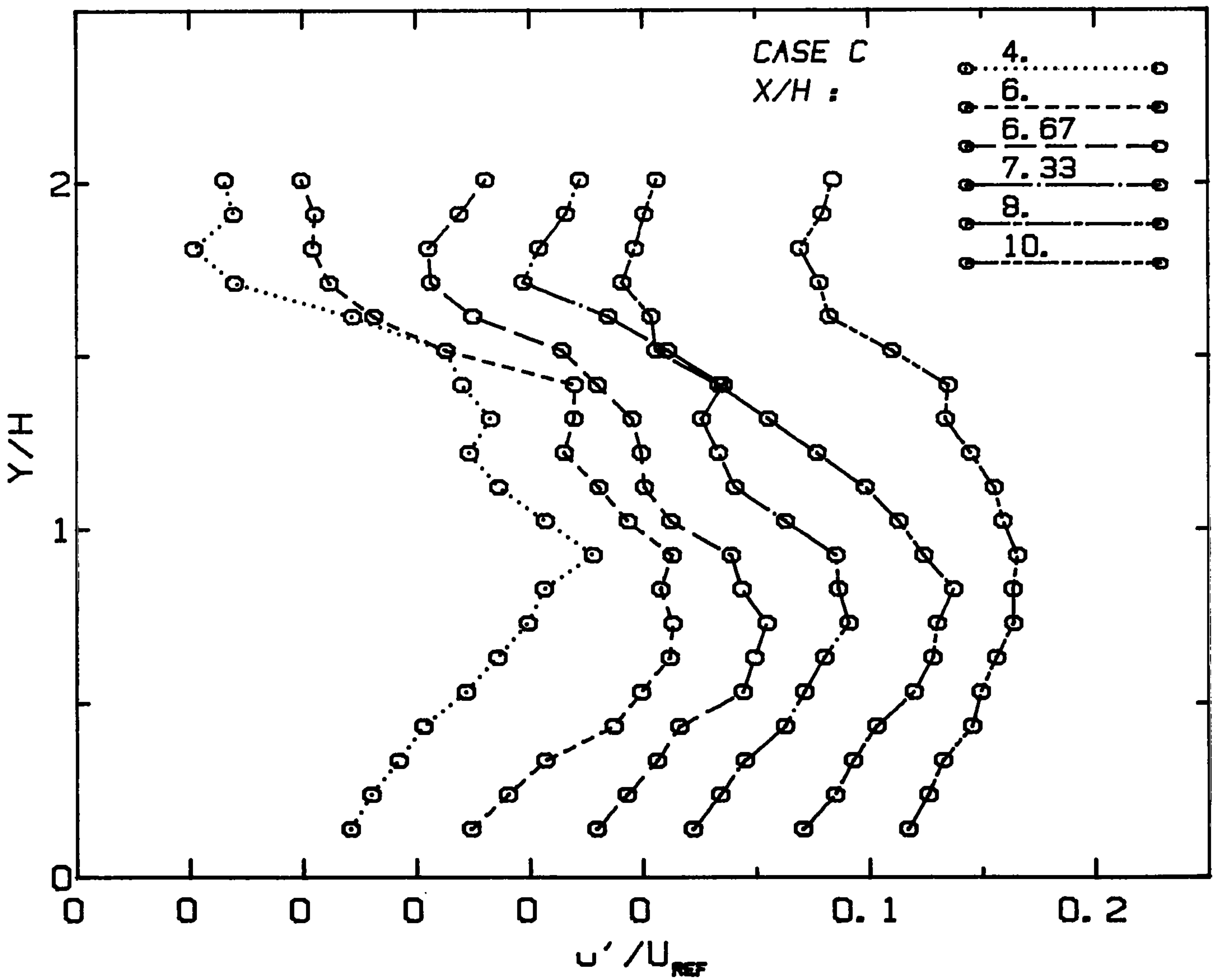

Fig. 5-23. RMS velocity distirbution in the saeparation and reattachment regions measured with a pulsed-wire anemometer for Case C.

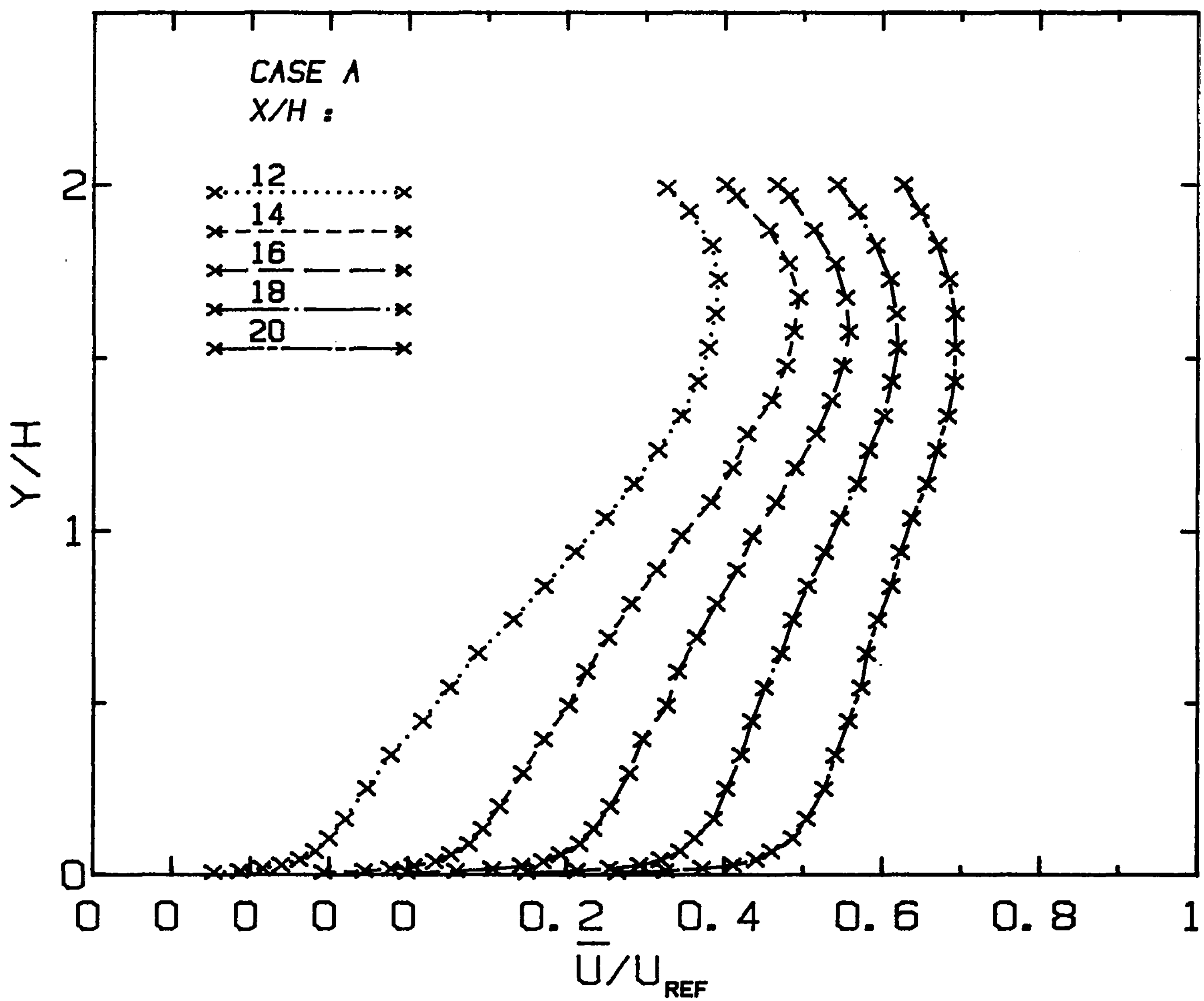

Fig. 5-24. Mean velocity distributions in the recovery region measured with a hot-wire anemometer for Case A.

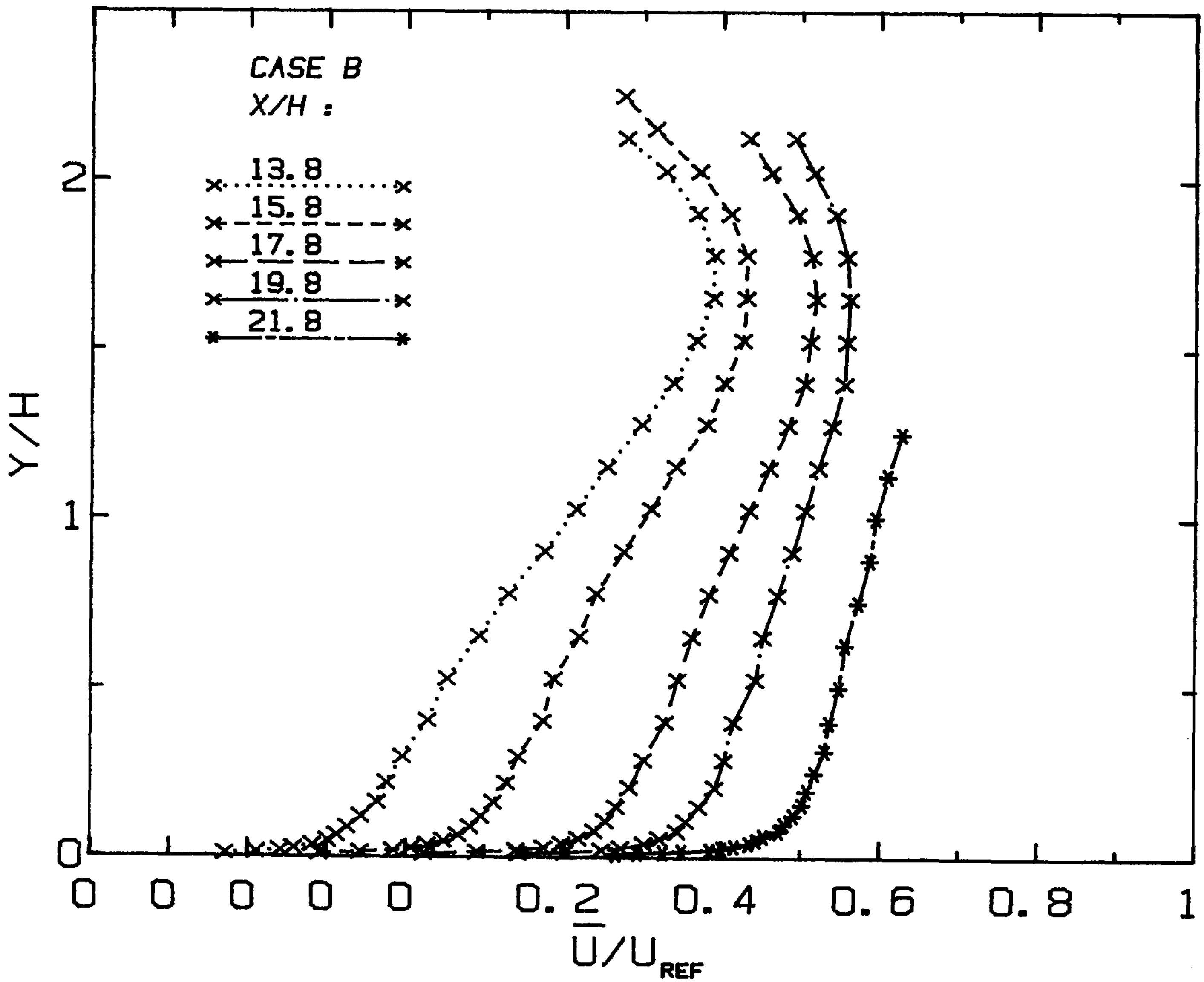

Fig. 5-25. Mean velocity distributions in the recovery region measured with a hot-wire anemometer (x), and with a total pressure probe (*), for Case B.

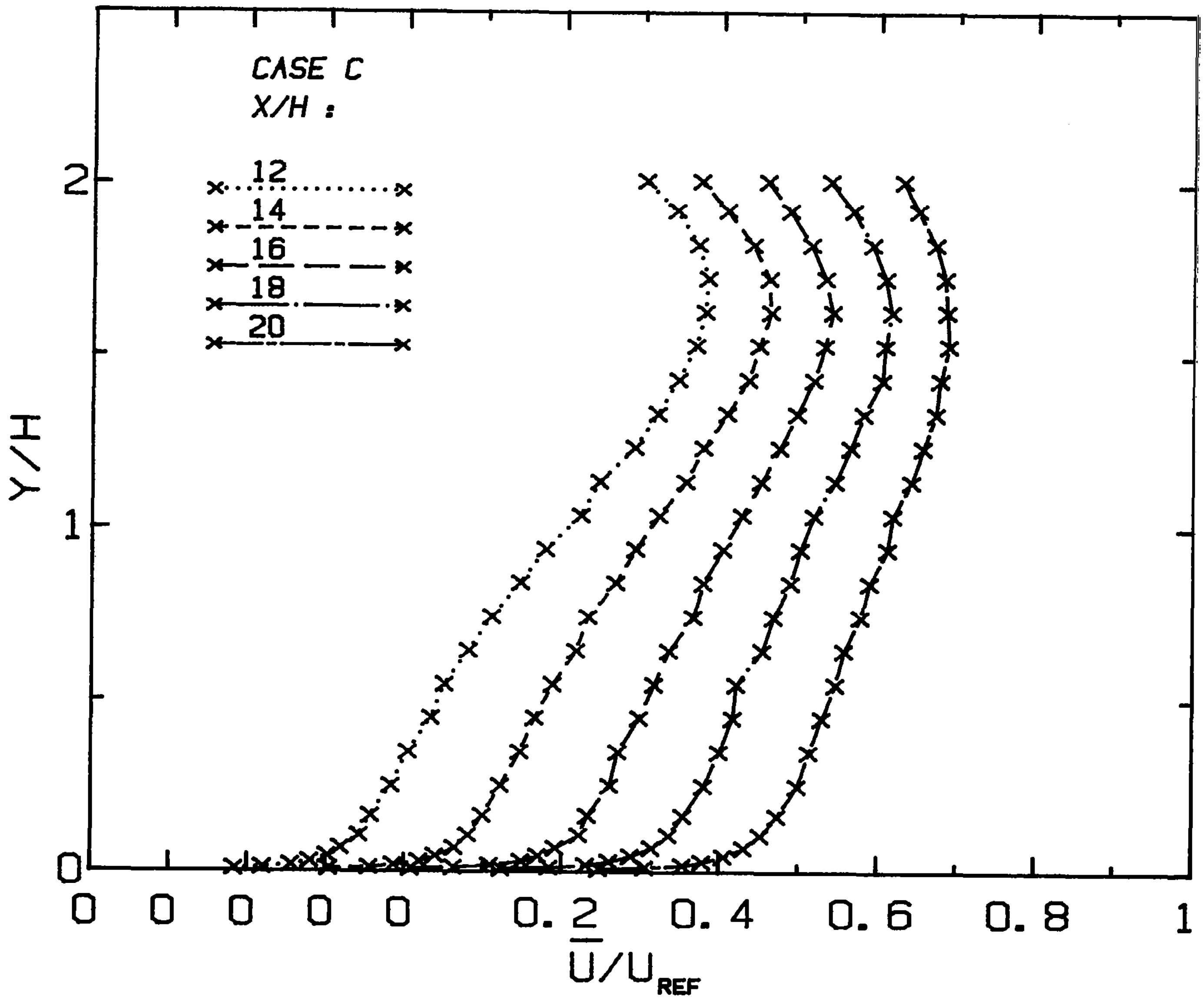

Fig. 5-26. Mean velocity distributions in the recovery region measured with a hot-wire anemometer for Case C.

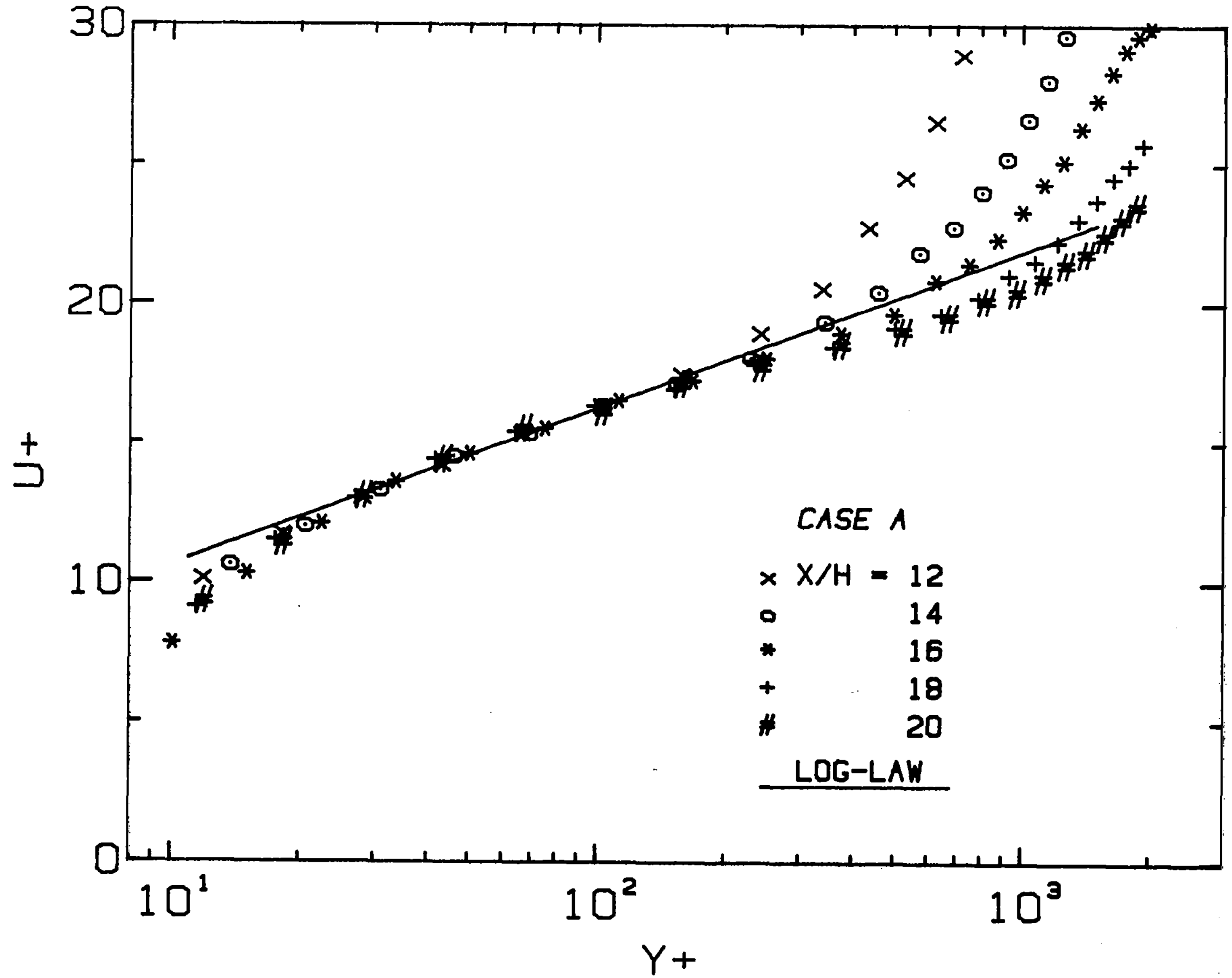

Fig. 5-27. Recovery region velocity profiles in inner coordinates U^+ vs. Y+ for Case A.

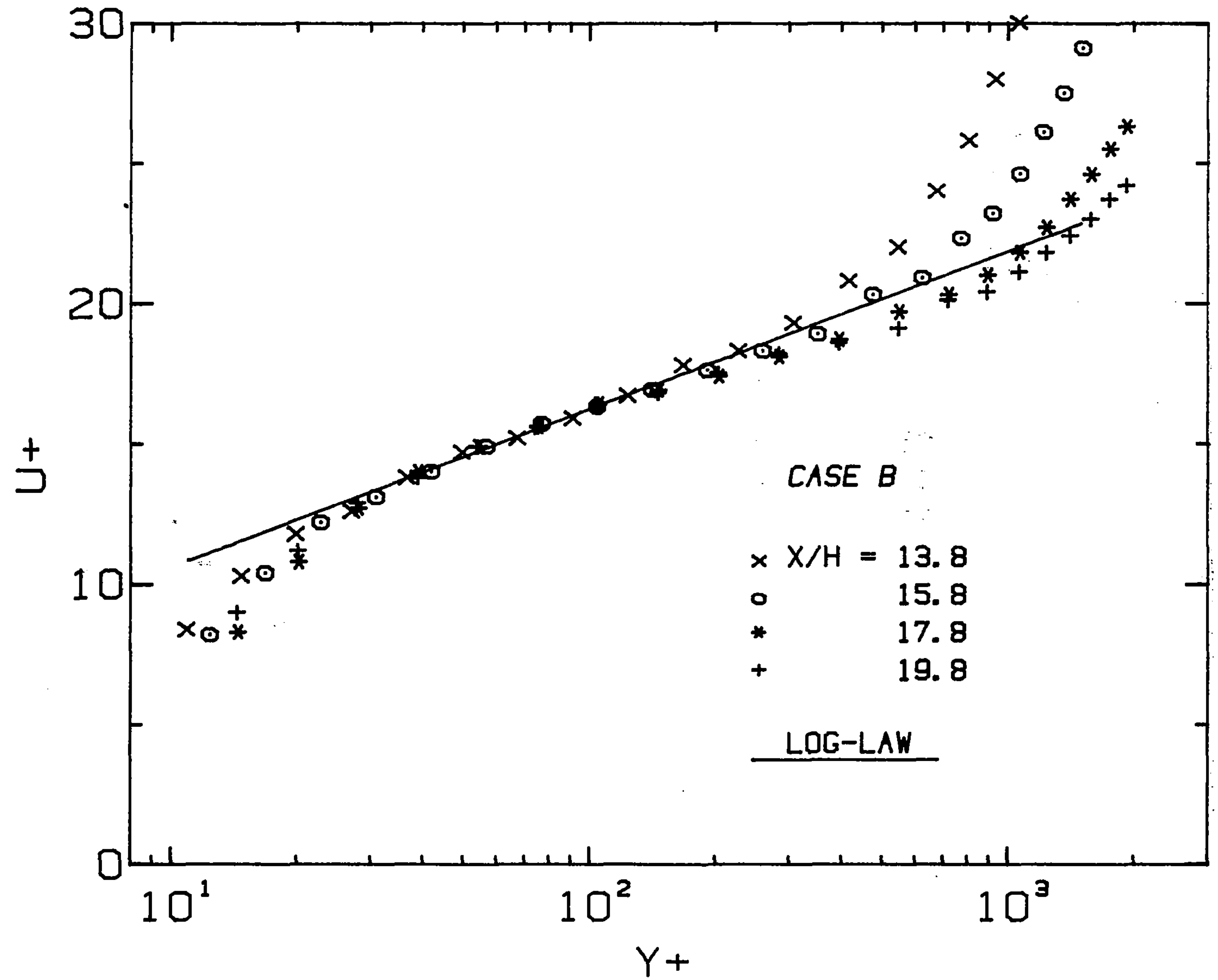

Fig. 5-28. Recovery region velocity profiles in inner coordinates for Case B.

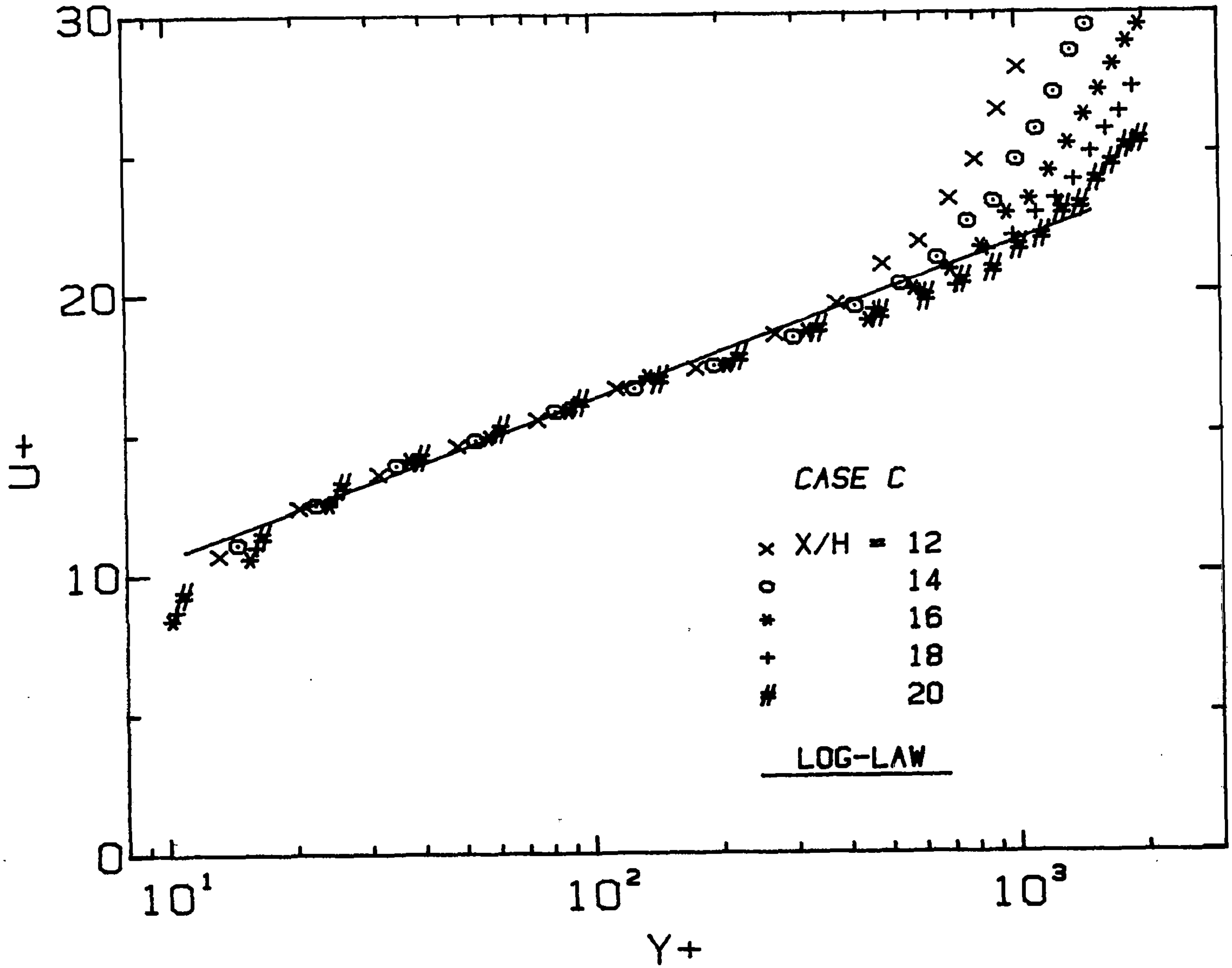

Fig. 5-29. Recovery region velocity profiles in inner coordinates for Case C.

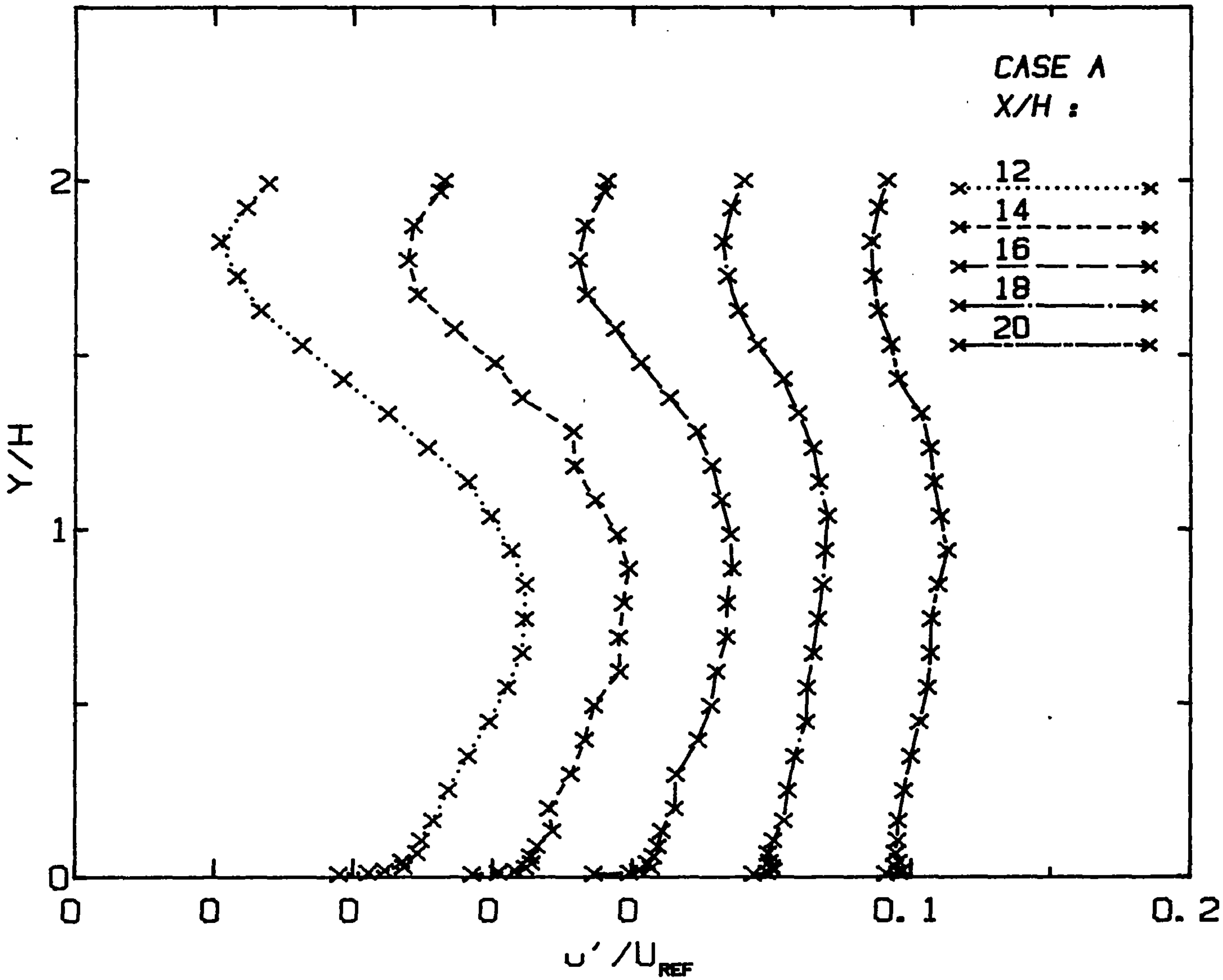

Fig. 5-30. RMS velocity distributions in the recovery region measured with a hot-wire anemometer for Case A.

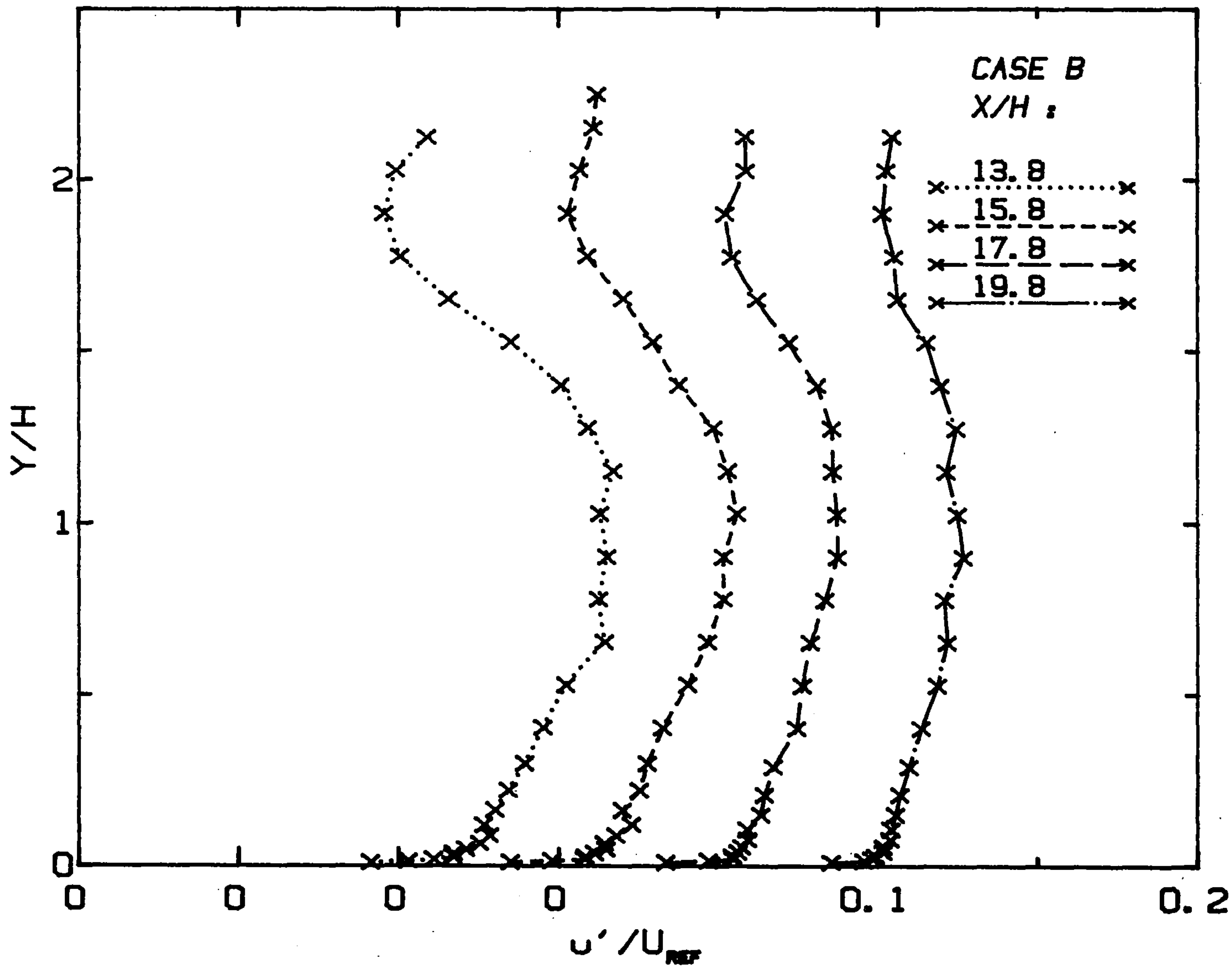

Fig. 5-31. RMS velocity distributions in the recovery region measured with a hot-wire anemometer for Case B.

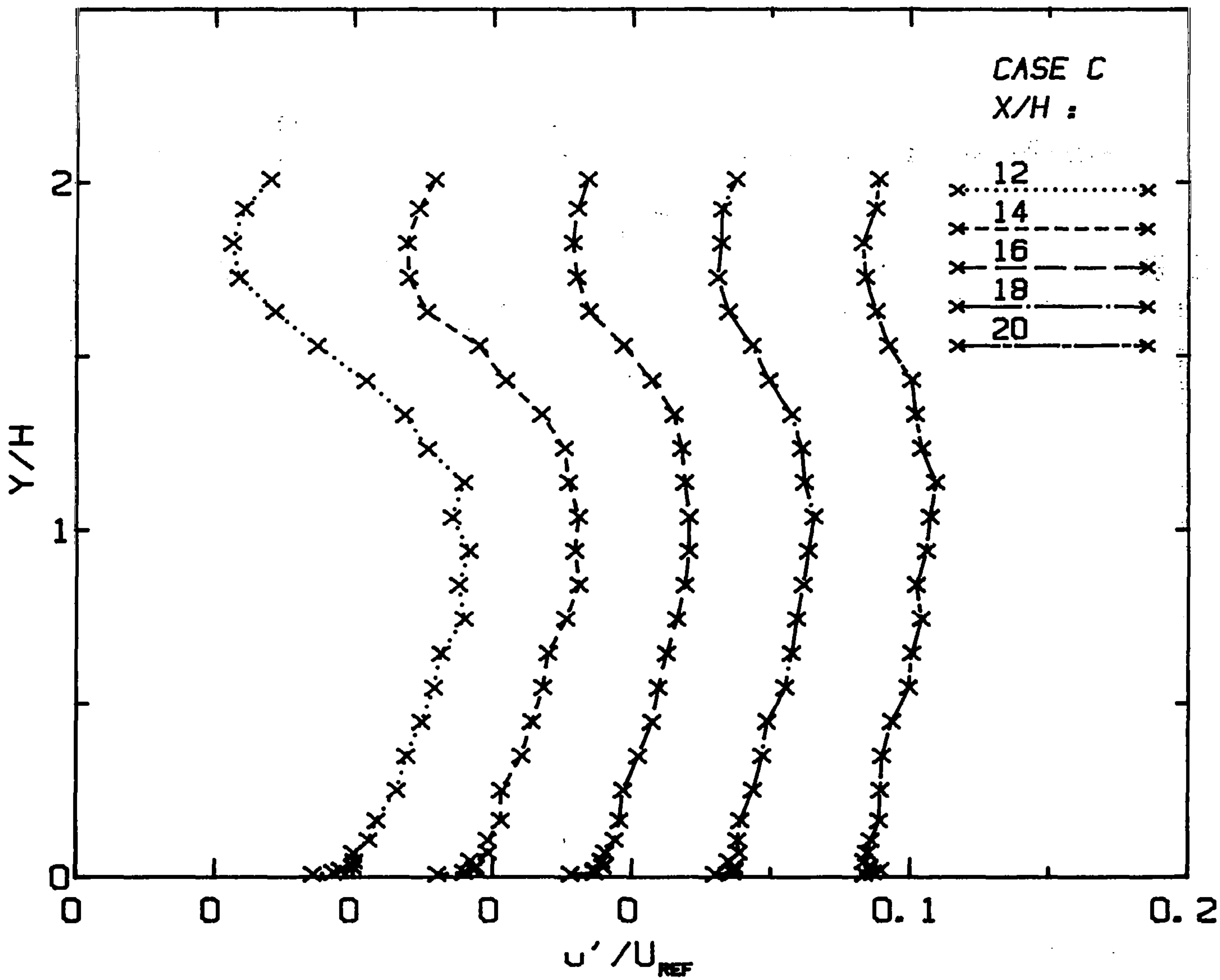

Fig. 5-32. RMS velocity distributions in the recovery region measured with a hot-wire anemometer for Case C.

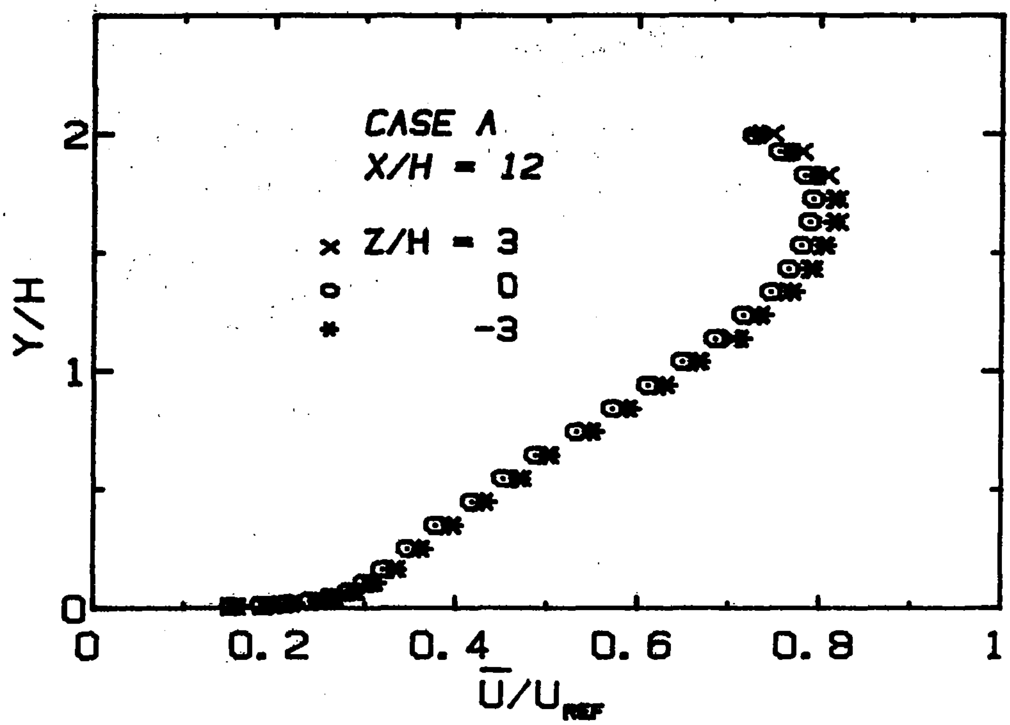

(a) Mean velocity at three spanwise stations.

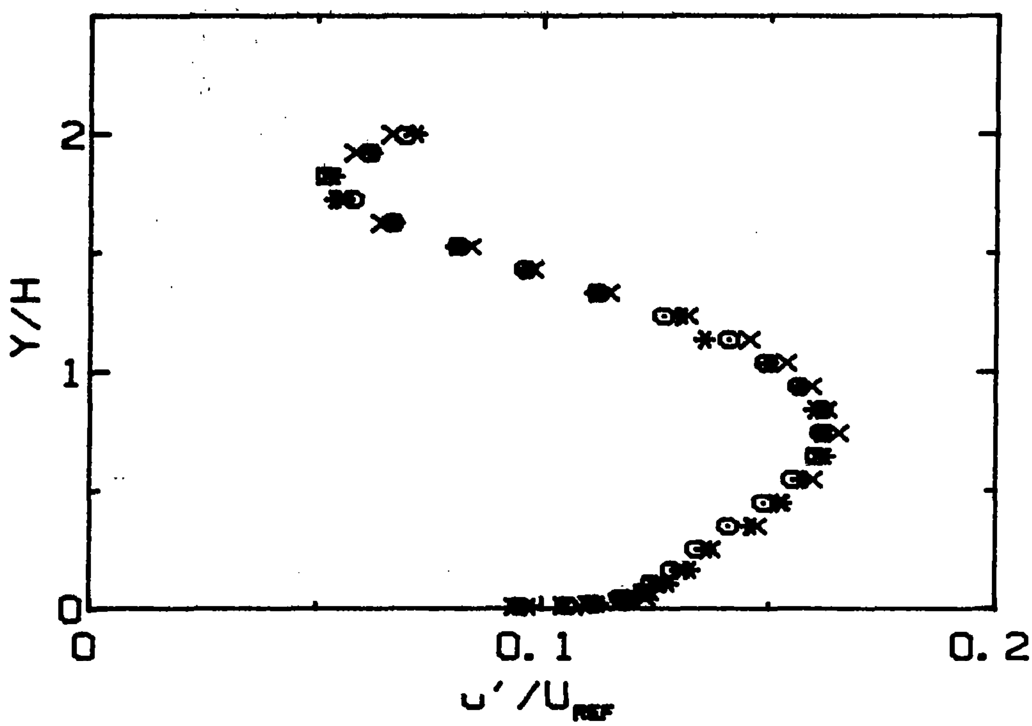

(b) Turbulence at three spanwise locations.

Fig. 5-33. Spanwise velocity profiles for Case A at X/H = 12 taken using a hot wire.

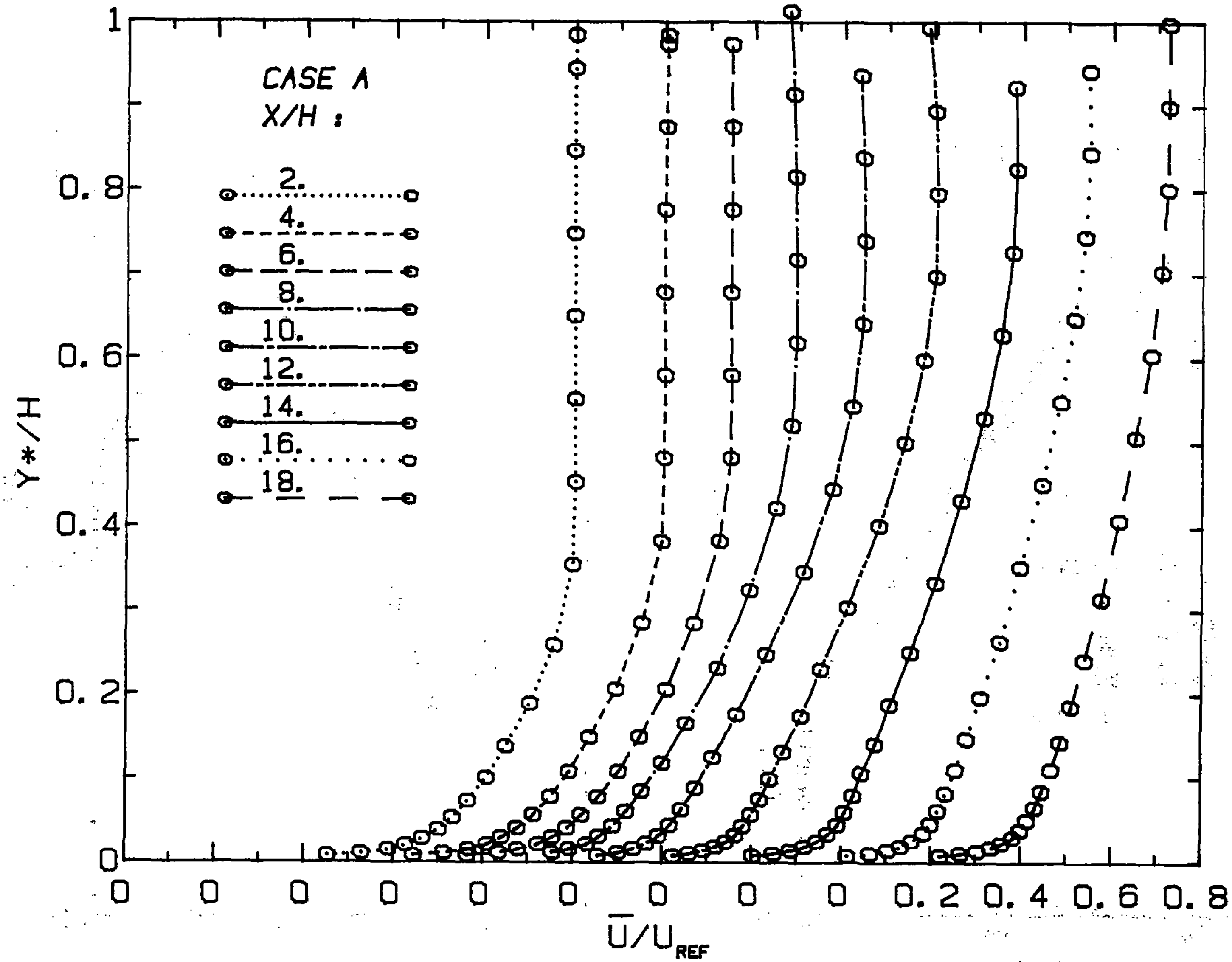

Fig. 5-34. Boundary layer development along the wall opposite the step: mean velocity profiles measured with a hot-wire for Case A.

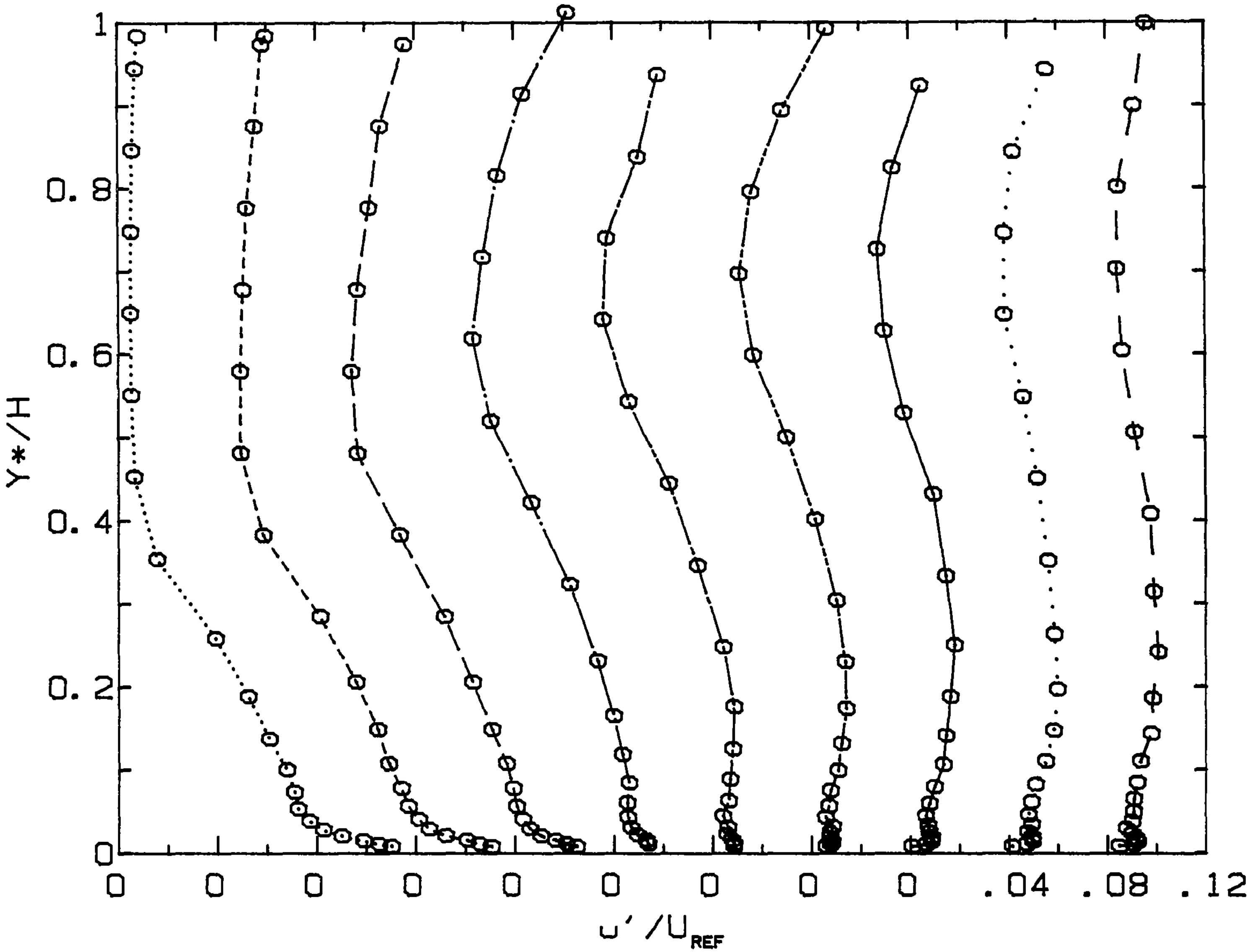

Fig. 5-35. Boundary layer development along the wall opposite the step: rms velocity profiles measured with a hot-wire for Case A. Legend as in Fig. 5-34.

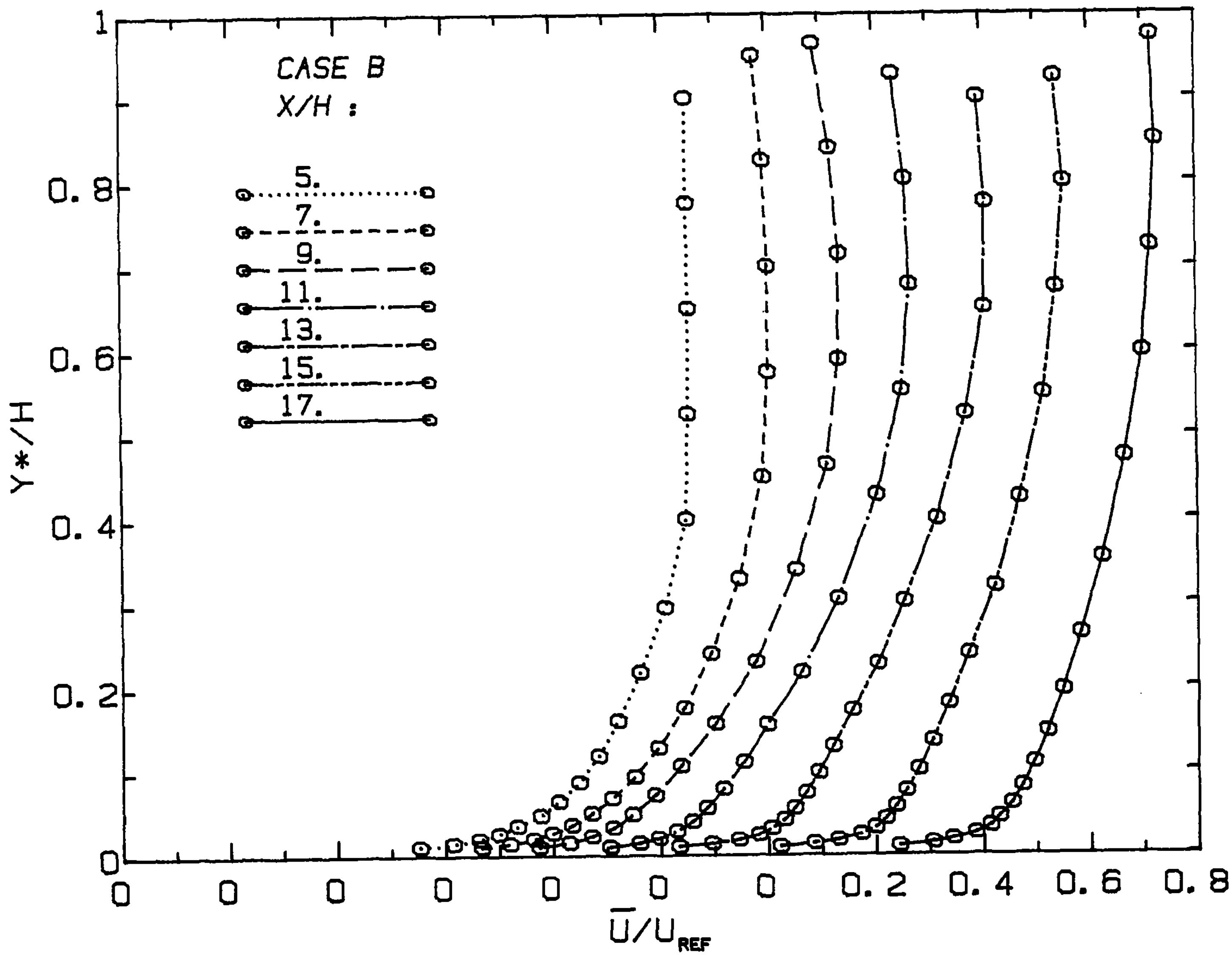

Fig. 5-36. Boundary layer development along the wall opposite the step: mean velocity profiles measured with a hot-wire for Case B.

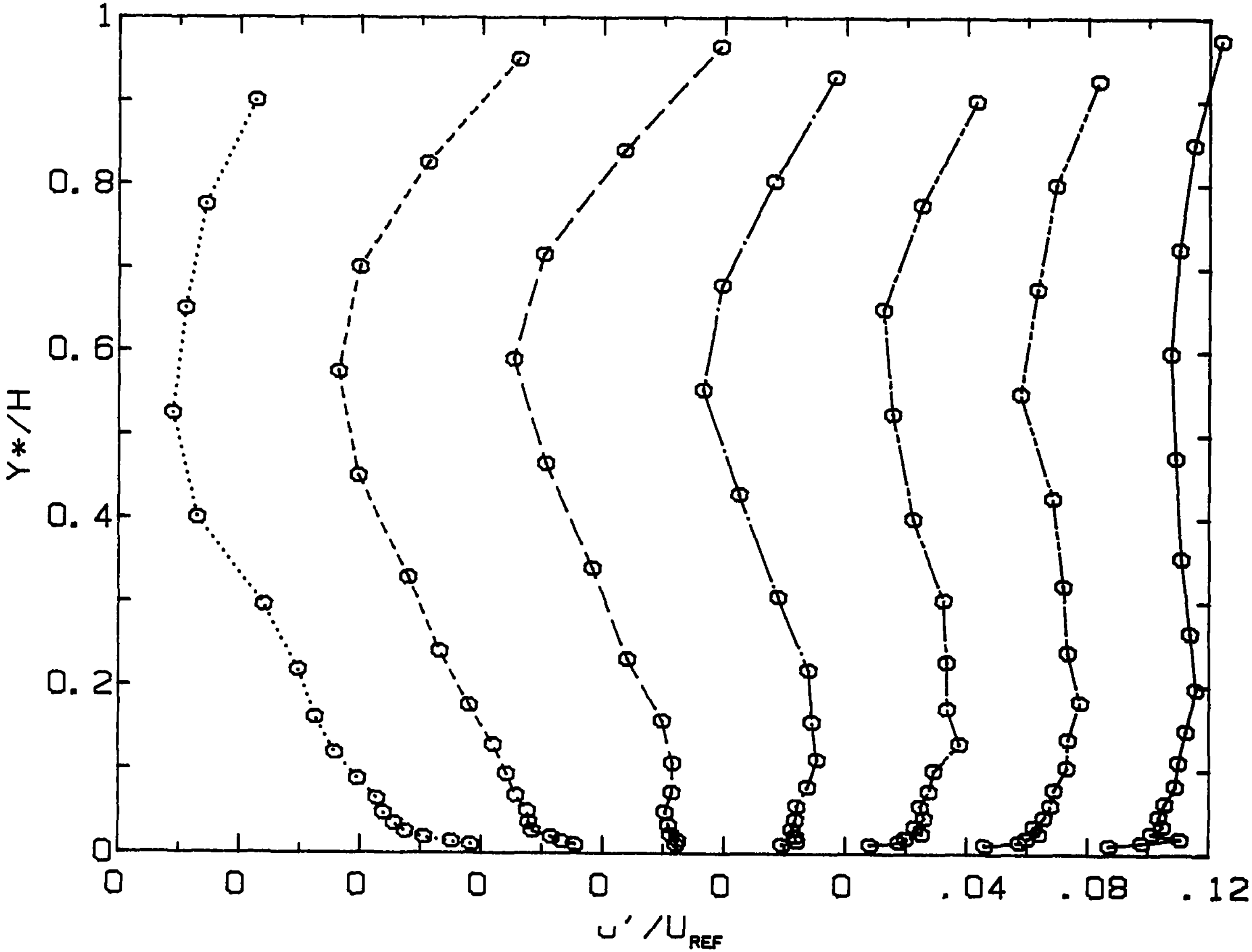

Fig. 5-37. Boundary layer development along the wall opposite the step: mean velocity profiles measured with a hot-wire for Case B. L gend as in Fig. 5-36.

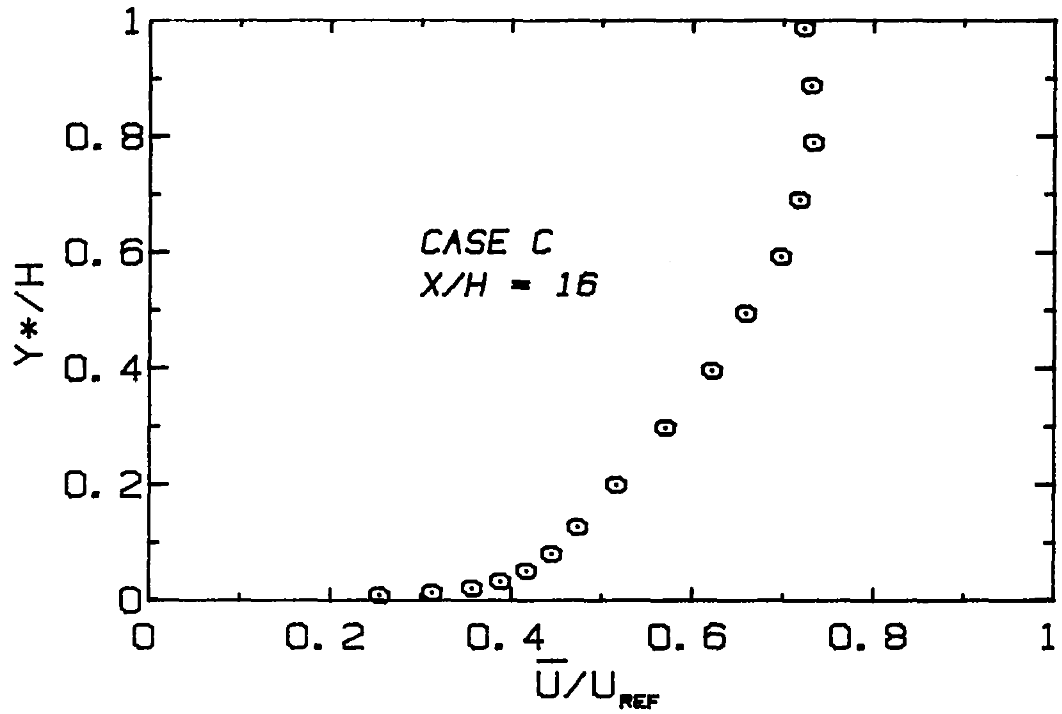

(a) Mean profile at X/H = 16.

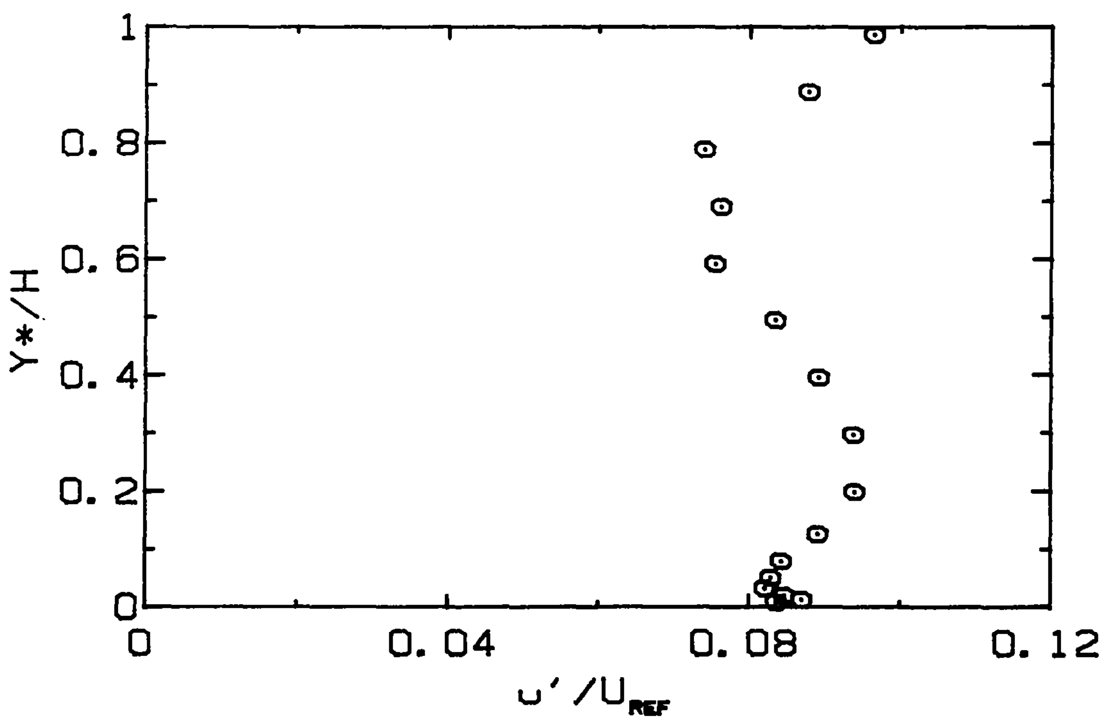

(b) Turbulence profile at X/H = 16.

Fig. 5-38. Boundary layer along the wall opposite the step: velocity measured with a hot-wire for Case C.

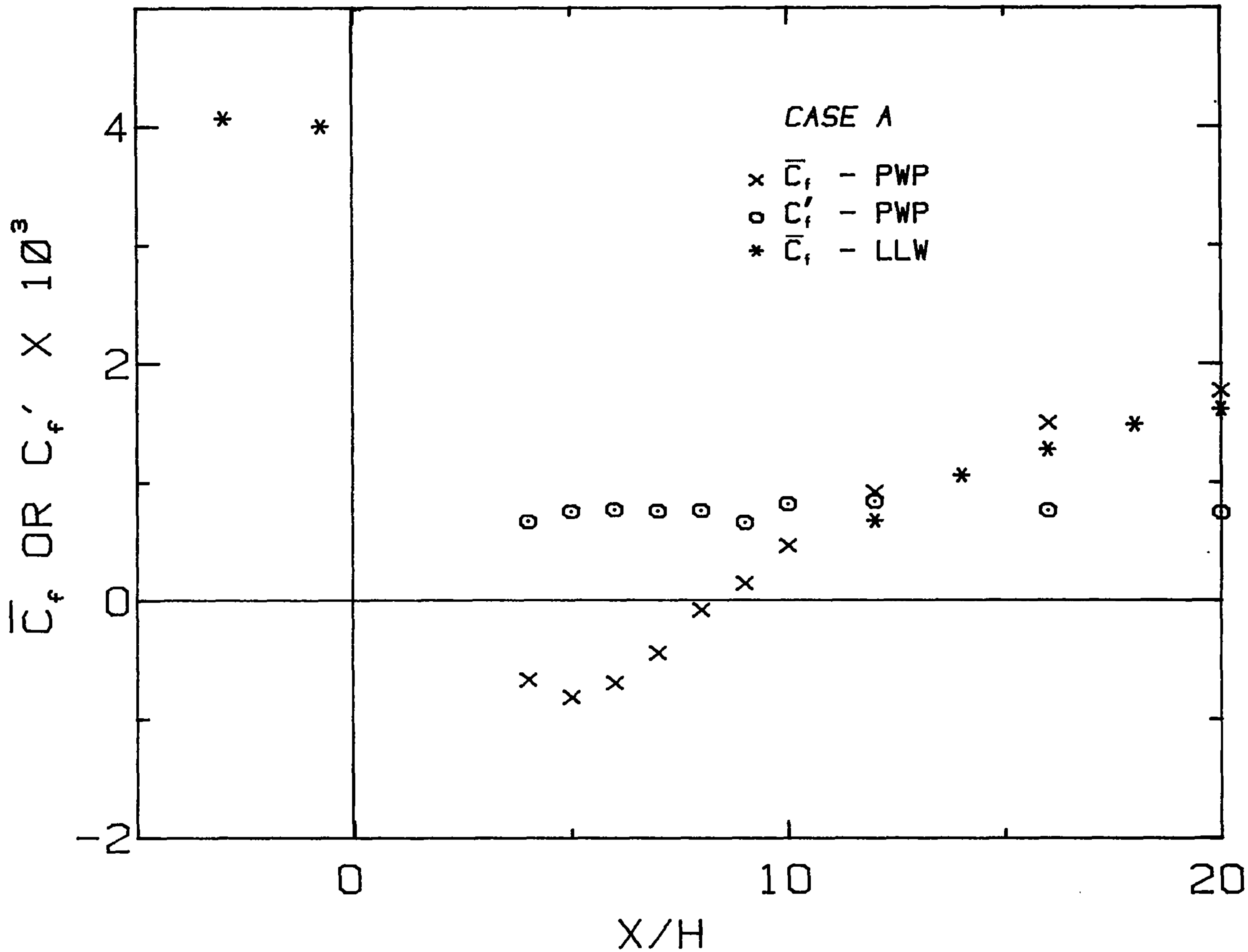

Fig. 5-39. Wall skin friction along the step wall for Case A. Legend: PWP, pulsed wall probe; LLW, log-law of the wall.

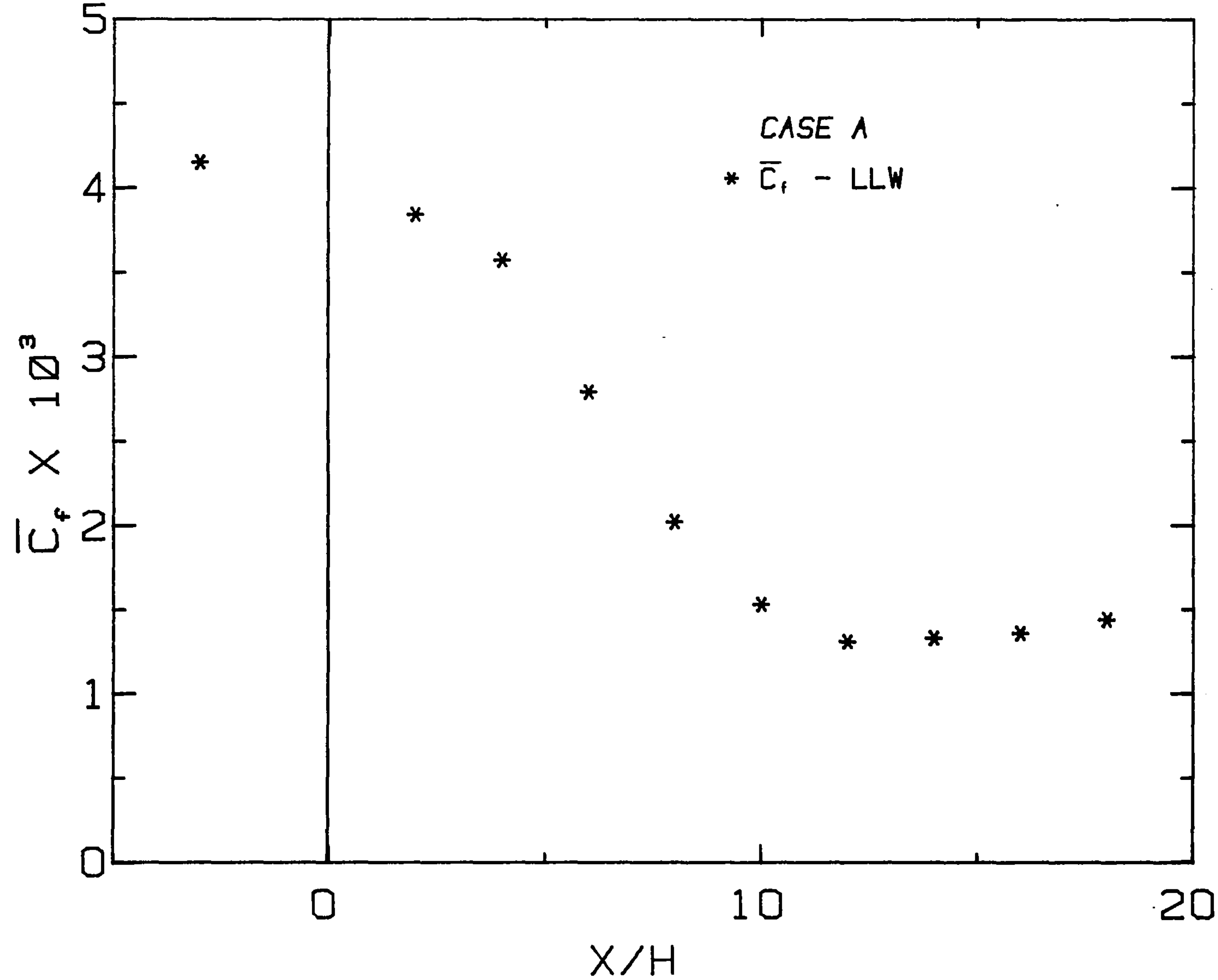

Fig. 5-40. Wall skin friction along the opposite wall for Case A. Legend as in Fig. 5-39.

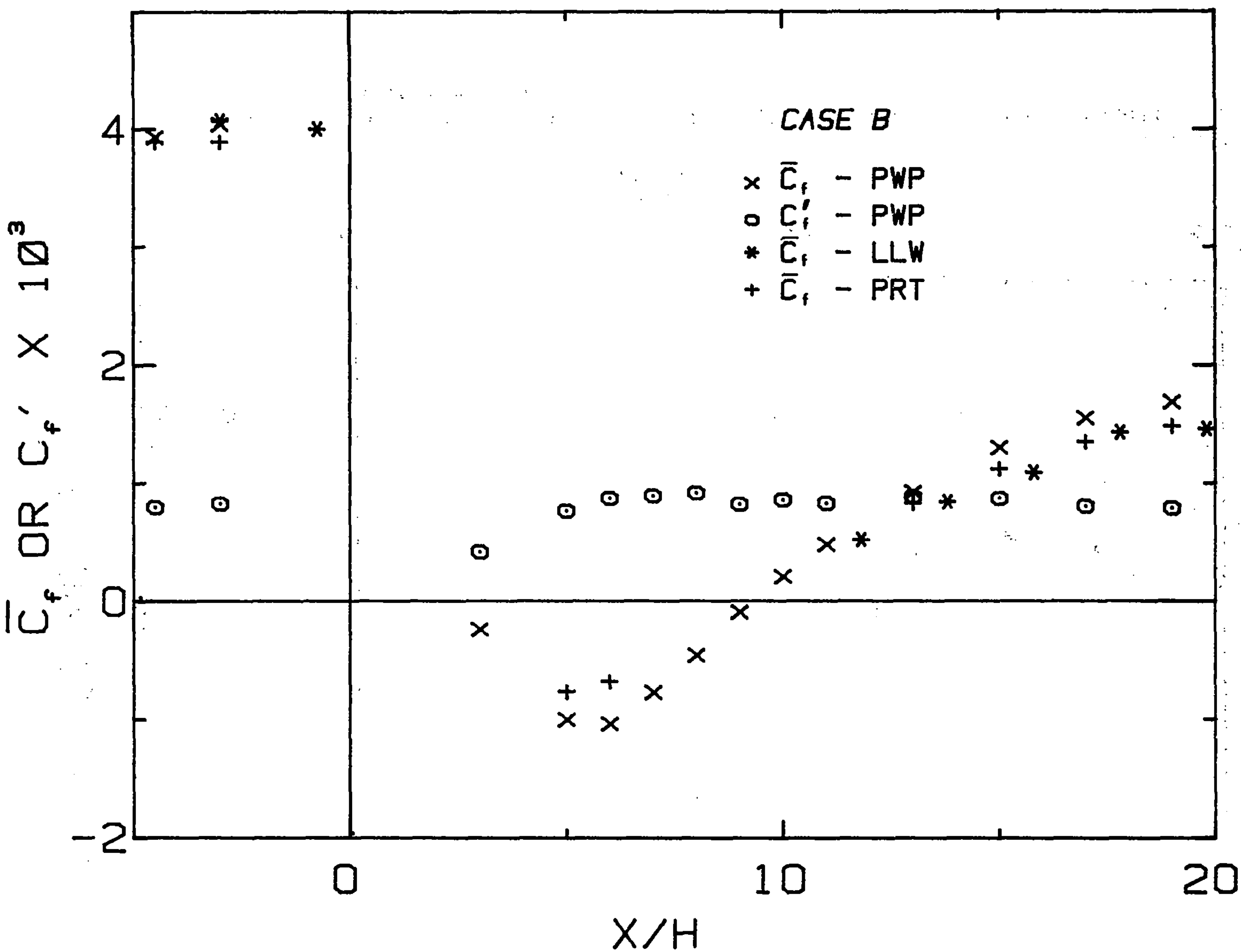

Fig. 5-41. Wall skin friction along the step wall for Case B. Legend: PWF, pulsed wall probe; LLW, log-law of the wall; PRT, Preston tube.

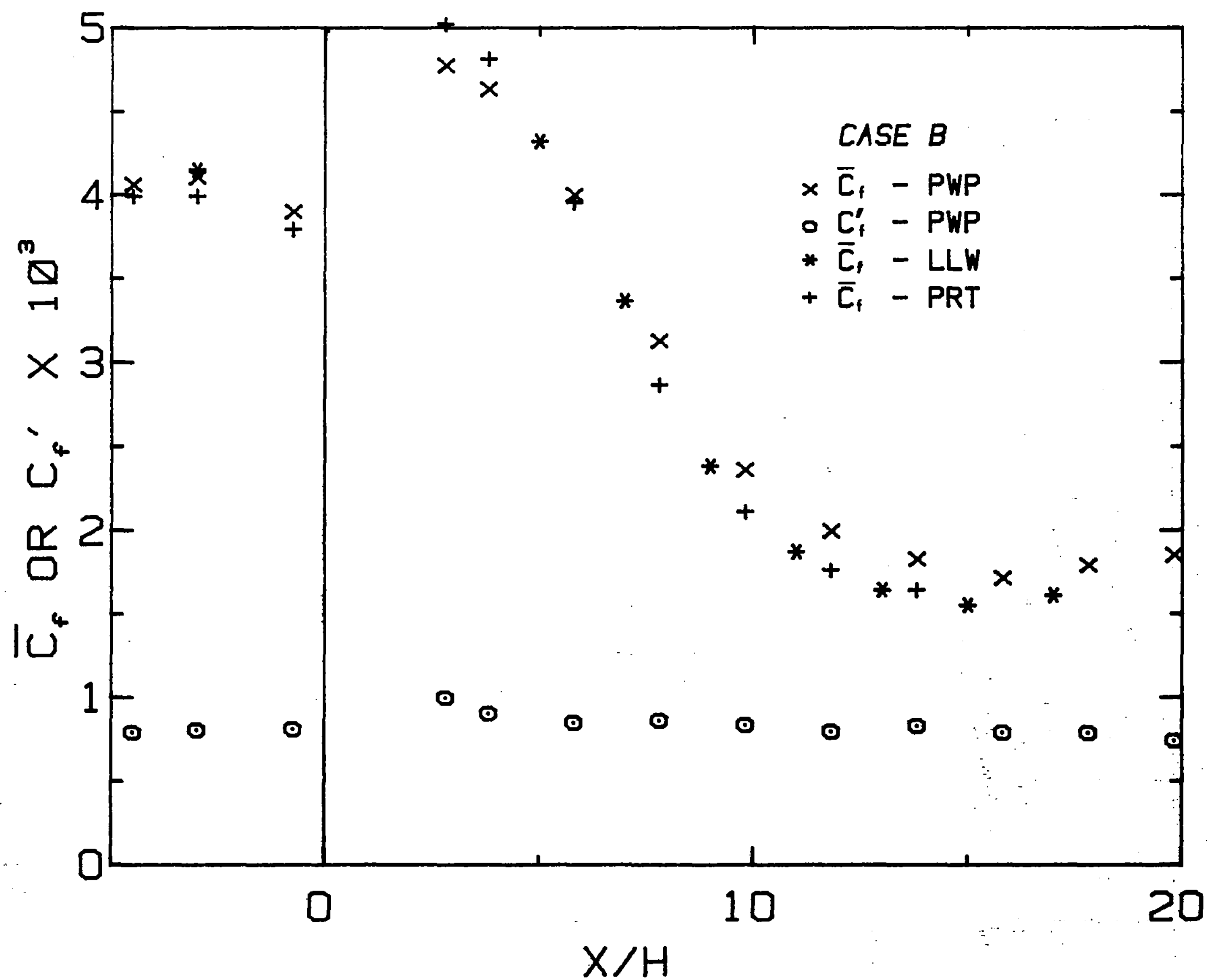

Fig. 5-42. Wall skin friction along the opposite wall for Case B. Legend as in Fig. 5-41.

Chapter 6

DISCUSSION

The discussion which follows will focus on two specific points: first, on observations regarding the measurements of skin friction in the backflow and reattachment regions, and second, on a description of the reattachment process. These two areas cover the first two main objectives outlined in Chapter 1; the third major objective (that of producing data for comparison with computation) has been implicitly treated in earlier chapters and will not receive specific discussion. Implications of the description of the reattachment process and specific effects of parameter variations are discussed in Section 6.3 below.

6.1 Wall-Region Flow Characteristics

The pulsed wall probe has enabled the first time-dependent measurements of skin friction in a reattaching flow. Two other sets of data wherein average skin friction has been measured are known: that of Chandrsuda and Bradshaw (1981) (obtained with a surface pressure tube), and those of Driver and Seegmiller (1982) (taken using the viscosity balance method). These two data sets are plotted (with streamwise distance normalized by step height H and average wall shear stress normalized by upstream dynamic pressure $\frac{1}{2}\rho U_{ref}^2$), along with Cases A and B from this study in Fig. 6-1. The reattachment distances are quite different for the four cases; however, considering the large uncertainties inherent in such data, considerable similarity in shape of the distributions can be seen.

In the region of strong backflow, we find $\overline{C}_f = -0.001$. In this plot, skin friction is normalized by the upstream dynamic pressure. For consideration of the local flow structure, it seems more reasonable to use a local value of dynamic pressure. If the maximum local backflow velocity is selected, the magnitude of the local skin-friction coefficient in the backflow region is about 0.025*—a very high value more typical of non-turbulent flows! This result suggests the hypothesis

*The magnitude of the maximum backflow velocity. $|U_{bf}|$, is assumed to be about $0.2\ U_{ref}$ for all cases, based on pulsed-wire data for Cases A and B.

that the reverse-flow region has the structure of a laminar-like near-wall flow, albeit a highly unsteady one (due to the "externally" imposed unsteadiness of the turbulent shear layer). A representative "boundary layer" Reynolds number may be computed based on the backflow region thickness and the magnitude of the reversed-flow velocity ($Re_{\delta bf}$). Using typical values,

$$Re_{\delta bf} = \frac{|U_{bf}|\delta_{bf}}{\nu} = Re_H \frac{|U_{bf}|}{U_{ref}} \frac{\delta_{bf}}{H} = Re_H \frac{1}{5} \cdot \frac{1}{20} = \frac{Re_H}{100}$$

Thus, for Re_H about 4×10^4, the effective boundary layer Reynolds number of the backflow region would be only a few hundred, as opposed to a few thousand normally required for transition in a flat-plate boundry layer.

The large C_f and relatively low effective Reynolds number of the near-wall flow in the backflow region are not characteristic of turbulent flow, and instead suggest an unsteady laminar-like flow. This implies that turbulent production $(\overline{u'v'})$ should be small in this region. However, no measurements of $\overline{u'v'}$ were available for this study. Attempts to visualize this region with a smoke-wire (using a spanwise wire at $X_R/2$) were unsuccessful, due to the limitations on visual access imposed by the facility design.

The tentative conclusion is that the backflow region seems laminar-like and that $\overline{u'v'}$ will be very small in this region. Since the backflow region "sees" an effectively favorable pressure gradient, is very thin, and has an effective local free-stream velocity of $0.2\ U_{ref}$, it seems plausible that the laminar-like flow structure in this region could persist to extremely high values of Re_H.

6.2 Description of the Reattachment Region

Measurements of pressure, forward-flow fraction, velocity, and skin friction in the reattachment region made for the various cases presented in Chapters 4 and 5 will now be compared. The objective here is to obtain a clearer quantitative picture of the reattachment process. Of key importance in the following discussion is the ability to accurately measure the reattachment length itself (refer to Appendix C).

Roshko and Lau (1965) proposed that pressure distributions for subsonic reattaching flows should be scaled by the reattachment length itself--i.e., a streamwise coordinate X* was proposed:

$$X^* = \frac{X - X_R}{X_R}$$

For the pressure-coefficient scaling, they extended the ideas of Chapman et al. (1958) to incompressiible flow:

$$C_p^* = \frac{(C_p - C_{p_{min}})}{(1 - C_{p_{min}})}$$

All seven cases from the current study for which pressure rise by reattachment was measured are plotted in these coordinates in Fig. 6-2. As noted by Tani et al. (1961), the ultimate pressure recovery is higher for thinner boundary layers. Note also that the downstream shape of these curves will be affected by the area ratio of the expansion. Notwithstanding these comments, the collapse is quite complete, covering a broad range of base pressures $\left(C_{p_{min}} = -0.04 \text{ to } -0.27\right)$. The pressure rise at reattachment (denoted C^*_{pR}) for all cases is approximately $C^*_{p_R} = 0.26\text{-}0.28$, which may be compared to a theory promulgated by Tanner (1976) and expected to be valid for two-dimensional reattaching flows with thin boundary layers at separation. (Tanner's (1976) model is an extension of the work of Chapman et al. (1958) to account for the empirical observation that flow along the mean dividing streamline is not isentropic. He gives a theory which is valid up to transonic Mach numbers; the result shown is for low Mach number only.) His equation gives:

$$C^*_{pR} = \frac{(0.27 - 0.25\, C_{p_{min}})}{(1 - C_{p_{min}})}$$

This equation is only weakly dependent on $C_{p_{min}}$ in the range of the present study $(-0.3 < C_{p_{min}} < 0)$. The result is a prediction of $C^*_{pR} = 0.27$ from this theory for the seven cases of the current study--in precise agreement with the data plotted in Fig. 6-2.

It must be emphasized that the collapse of pressure distribution data demonstrated above is expected to be valid only for thin separating boundary layers. Nash (1966) shows that base pressure is independent of separating boundary layer thickness only if θ/H at separation is less than 0.05, implying $\delta/H < 0.5$. For geometries other than the step flow, the effective thickness of the separating layer is generally quite small. For example, in the case of a normal plate with downstream splitter, the flow undergoes a strong acceleration near separation--effectively thinning the boundary layer. The same can often be said of the separating flow on the leading edge of a square-nosed plate, or flow about fences and ribs. So, for many cases of two-dimensional reattachment, the limitation of the above conclusions to thin separating boundary layers is not crucial.

In Chapter 1, it was observed that the reattachment zone is characterized by a balance between streamwise pressure gradient and gradient of stress normal to the surface. This fact, coupled with the apparent similarity of pressure distributions among the various cases examined, suggests that all aspects of the reattaching flow may display this same similarity. The extent of the region where this similarity is displayed would provide a natural, functional definition of the extent of the reattachment zone. Below, it will be shown that forward-flow fraction, velocity, and skin friction also attain universal distributions in the reattachment zone.

Figure 6-4 compares distributions of forward-flow fraction for the seven cases of this study, with the streamwise coordinate being X^*. By definition of X_R, all the curves must pass through the point $X^* = 0$, $\gamma = 0.5$. A collapse of the data is shown throughout the region of change in mean flow direction, $-0.5 < X^* < 0.5$. It should also be remarked that the measurement uncertainty for γ is very small--only about $\pm$ 0.02. It is of interest to note that over 90% of the variation in γ occurs in the region $\pm$ 0.3 X_R about the point $X^* = 0$.

Skin friction coefficients for the four cases described in the preceding section are shown in Fig. 6-5 with streamwise coordinate as X^* (quoted values of X_R/H were used to normalize the results of Driver and Seegmiller, 1982, and Chandrsuda and Bradshaw, 1981). Note that Re_H for these cases are all fairly close, so that the possible dependence of backflow skin friction on Reynolds number does not cloud comparison. Collapse of the data is again excellent (at least as far downstream as $X^* = 0.4$). One would expect that the far-downstream skin friction values would differ, due to the different downstream conditions imposed by the various geometries used.

Mean and rms velocity profiles for the three main cases are compared at nearly equivalent X^* locations in the six figures (6-6 through 6-11) covering approximately $-0.5 < X^* < 1.1$. In examining these figures, it must be emphasized that streamwise gradients are very large, so that differences in X^* of a few percent are significant. Nonetheless, the $\overline{U}$ and u' distributions compared at equivalent X^* do appear very similar for $Y/H < 1$. Farther from the surface, the differences in opposite-wall boundary layer development among the three cases obscure the comparison.

The evolution of maximum turbulence intensity at a given X^* through the reattachment region is shown in Fig. 6-12 for the three main cases. Two sets of data from previous studies in our lab are also shown on this plot. The first is that of Eaton and Johnston (1980), who also used a pulsed-wire anemometer in the reattachment region. The second, that of Kim et al. (1978) was obtained with a hot-wire. Again, the collapse of maximum values of $u'/\overline{U}$ on X^* is quite complete. The data of Kim et al. (1978) are somewhat lower than those of the current study and of Eaton and Johnston (1980), very probably due to their use of a hot-wire for making measurements in the reattachment zone.

Thus, the reattachment length seems to provide the necessary length scale for normalizing results. The implicit assumptions of linear shear-layer growth and the scaling of the extent of the reattachment region on the reattachment length itself seem to be justified. Remarkably, the region of validity for the collapse of pressure rise, forward-flow fraction, skin friction, and the velocity field seems to extend about $\pm 0.5\ X_R$ about the reattachment location. A functional definition of the reattachment region as the zone which extends $\pm 0.4\ X_R$ is proposed. Nearly all the pressure rise and variation in forward-flow fraction--features which strongly identify the reattachment region--

occur over this zone. This same quantitative description should be applicable to other cases which satisfy the implicit assumptions outlined above, such as flows over fences and ribs. The flows studied by Roshko and Lau (1965), for example, of which the single case shown in Fig. 6-2 is representative*, display the same similarity in pressure distribution found here.

A further implication from the above demonstration that X^* provides the appropriate normalized length for describing the reattachment zone is that the normalized distributions given above may actually prove useful for determining the reattachment length. For example, for previous studies wherein surface pressure distribution in the reattachment zone is provided, the reattachment length could be found by insisting that the data fit the distribution of Fig. 6-2†. It should be noted that a similar suggestion has been made by Chandrsuda (1975), but that neither he nor any other researcher has previously investigated the viability of the idea. Applying this idea to the data of Kim et al. (1978) shown in Fig. 6-2, a correction of about 10% (from the quoted value of $X_R = 7H$ to $7.6H$) is required to shift their pressure distribution to agree with the other data shown. This correction is within the authors' reported measurement uncertainty of ± 1H (14%).

6.3 Importance of Shear-Layer Structure

The discussion above has demonstrated that the quantitative properties of seven reattaching flows are similar, despite significant differences in reattachment length among the cases. Changes in X_R were obtained by alterations in the structure (i.e., entrainment rate) of the separated shear layer. Four parameters were varied in the experiments presented in Chapter 4: (i) inlet boundary layer thickness, (ii) streamwise curvature of the shear layer just after separation, (iii) free-

---

*These include reattachment on splitter plates downstream of blunt bodies and normal plates, as well as for the case of the square-nosed plate shown in Fig. 6-2.

†A simple procedure is to choose X_R such that C^*_{pR} $(X^* = 0) = 0.27$.

stream velocity, and (iv) strong streamwise vortices were embedded in the separating boundary layer. It now remains to discuss the effect of each parameter on shear layer structure. Throughout the following discussion, however, the important result of the previous section--that the quantitative features of the reattachment zone are similar in each case studied--must be borne in mind.

As the inlet boundary layer thickness is increased from 0.06 H to 0.4 H, the reattachment distance moves downstream by 1.6 H. This result may seem at odds with the conclusions of previous workers (e.g., Abbott and Kline, 1961, or Tani et al., 1961); however, this amount of shift is within the uncertainty in location of the reattachment point in these studies, which used earlier instrumentation and had different purposes. Chandrsuda and Bradshaw (1981) propose that such movement can be accounted for simply by including the added displacement thickness of the boundary layer with the step height to form an "effective" step height; but this accounts for only a quarter of the observed difference. Chuen et al. (1981) had reached a tentative conclusion that reattachment occurred sooner with $\delta/H = 0.14$ than when $\delta/H = 0.67$ in their experiments, but provided no quantitative measure of the difference.

Thinner separating boundary layers induce more vigorous mixing and higher rates of entrainment, so it appears instead that the shear layer spreads more slowly as the thickness of the separating boundary layer increases, giving a longer reattachment length. Abbott and Kline (1961) outline a model for the mechanics of reattachment which has been implicitly used in this study. The extent of the reattachment zone is determined by a balance between shear-layer entrainment and pressure-gradient-driven backflow. Since the pressure rise through the reattachment zone has been shown to be almost constant for the cases studied, total entrainment is also constant. Thus, changes in shear layer entrainment upstream of reattachment (spreading rate) must be accompanied by variations in reattachment length to give approximately <u>constant</u> overall entrainment. This idea may be generalized to help explain the manner in which other parameters can be altered to yield variations in reattachment length which are discussed below.

In the tests of Series 2, the duct downstream of the step was turned in order to provide some curvature (stabilizing sense) to the separated shear layer. The radius of curvature would be roughly 1.5 H for the geometry used (see Fig. 4-4), and the separating shear-layer thickness is 0.4 H, giving a nominal value of $\delta/R = 0.3$. By any criterion, this should be strong curvature (see, e.g, Castro and Bradshaw, 1976) insofar as its effect on shear-layer turbulence structure is concerned. However, the augmented curvature persists in the shear layer only immediately downstream of the step for a distance of about 1-2 step heights; stabilizing curvature in the upstream region should reduce mixing and entrainment and thus increase reattachment length. The reattachment length does increase from 8.6 H to 9.7 H as the turning angle of the duct is varied from 0 to 15°. This rather small change is interpreted to indicate that the effects of the rather abrupt curvature applied to the separated shear layer are confined to the curved region. Thus, curvature does not seem to have a persistent effect on shear-layer structure.

Increasing free-stream velocity while holding geometry constant (Series 3) was found to give a small decrease in reattachment length over the range of velocities tested. Since the Reynolds number for these tests was maintained quite high ($Re_H > 2 \times 10^4$), one would not expect that changes in shear-layer turbulence structure are responsible for the change in X_R with U_{ref}. A plausible explanation is that this change of reattachment length with free-stream velocity is a reflection of the dependence of reattachment length on boundary layer thickness at detachment; see the experiments of Series 1 ($\delta \propto U_{ref}^{-0.2}$ for a turbulent boundary layer with fixed development distance).

Streamwise vortices embedded in the separating shear layer act to enhance three-dimensional mixing markedly, in the manner addressed by Rothe and Johnston (1975). The increased entrainment reduces the reattachment length by about 1.4 H (compare Cases A and C). It was expected (and subsequently verified) that the highly three-dimensional separating flow would still produce a fairly straight, two-dimensional reattachment line. The reduction in reattachment length is slightly greater when a thinner separating boundary layer is used (Series 1a) than when using embedded streamwise vorticity.

The present results regarding the effects of parameter variation on reattachment length and flow structure have shown that the normalized properties of the flow in the reattachment region remain unaffected, even though reattachment length itself has been altered by as much as 30%. Verification of the interpretation that shear-layer entrainment (and thus turbulent shear stress, $\overline{u'v'}$) are different in these cases would require measurements with advanced anemometry capable of multi-component velocity cross-correlations. Significant new insight into the sensitivity of reattachment length to boundary layer thickness, downstream duct angle, Reynolds number, and inlet streamwise vorticity has been provided. Further explicit exploration of the effects of area ratio, thick separating boundary layers, and flow at higher Reynolds numbers would augment this study.

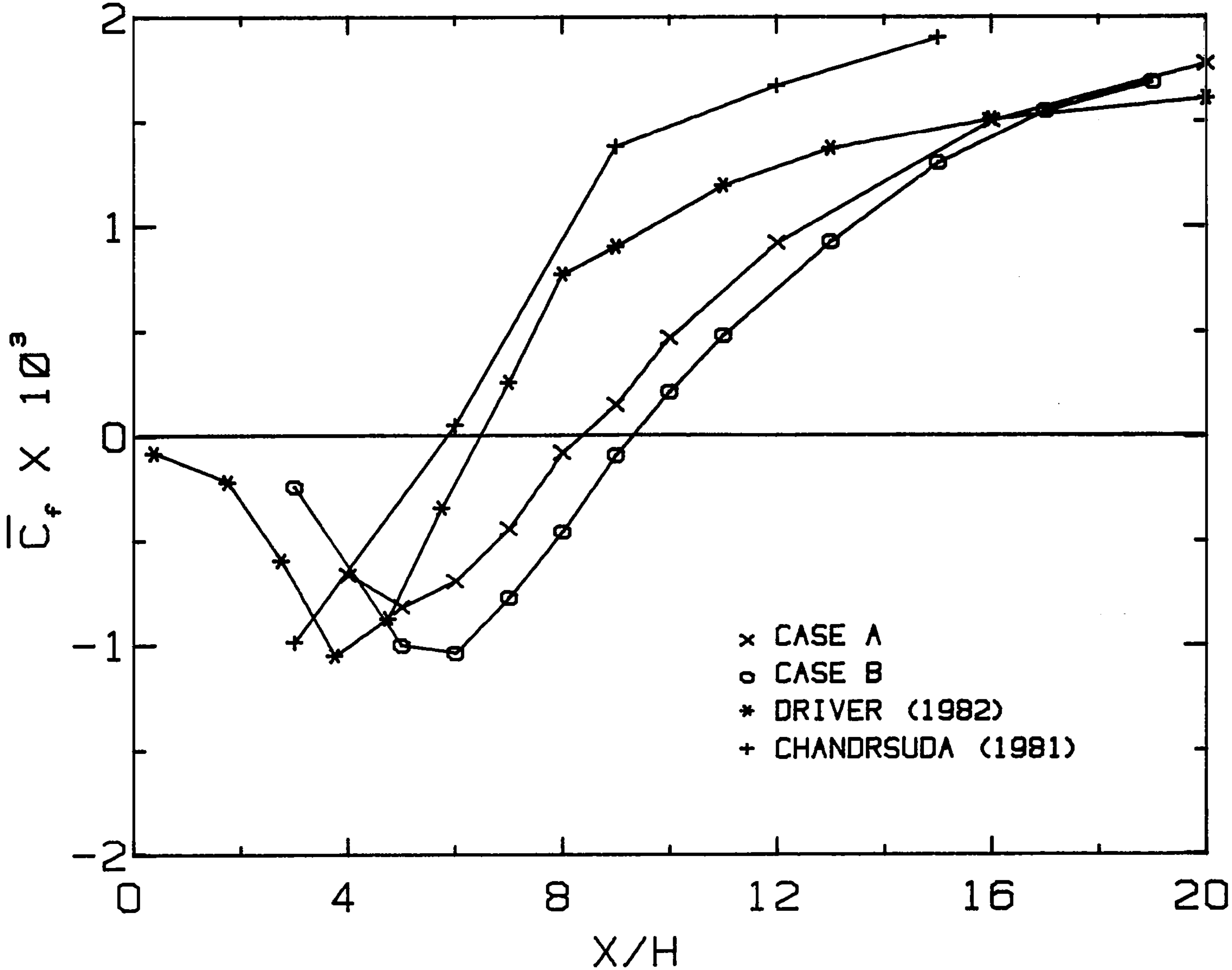

Fig. 6-1. Skin-friction coefficient measured in backward-facing step flows.

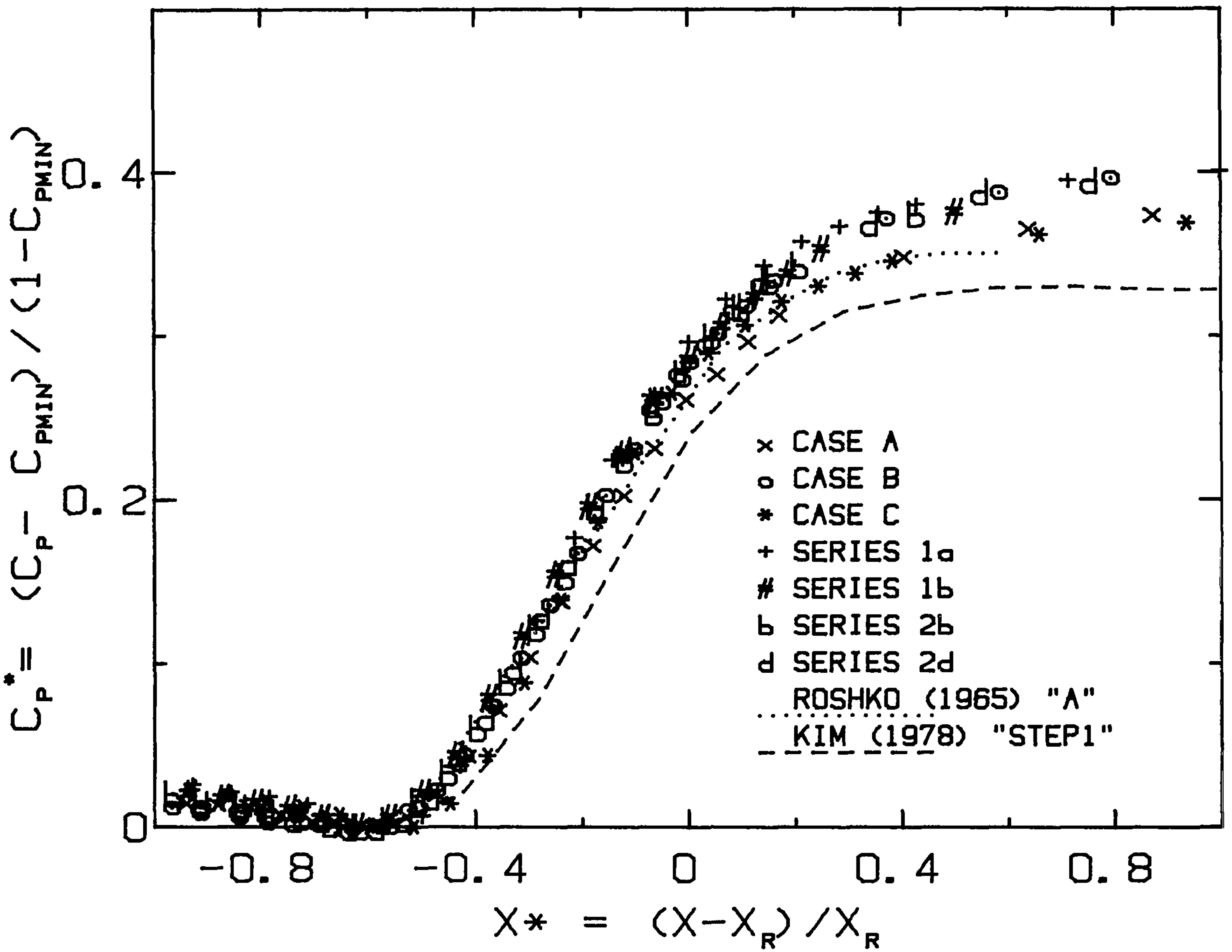

Fig. 6-2. Normalized pressure rise by reattachment, normalized as proposed by Roshko and Lau (1965).

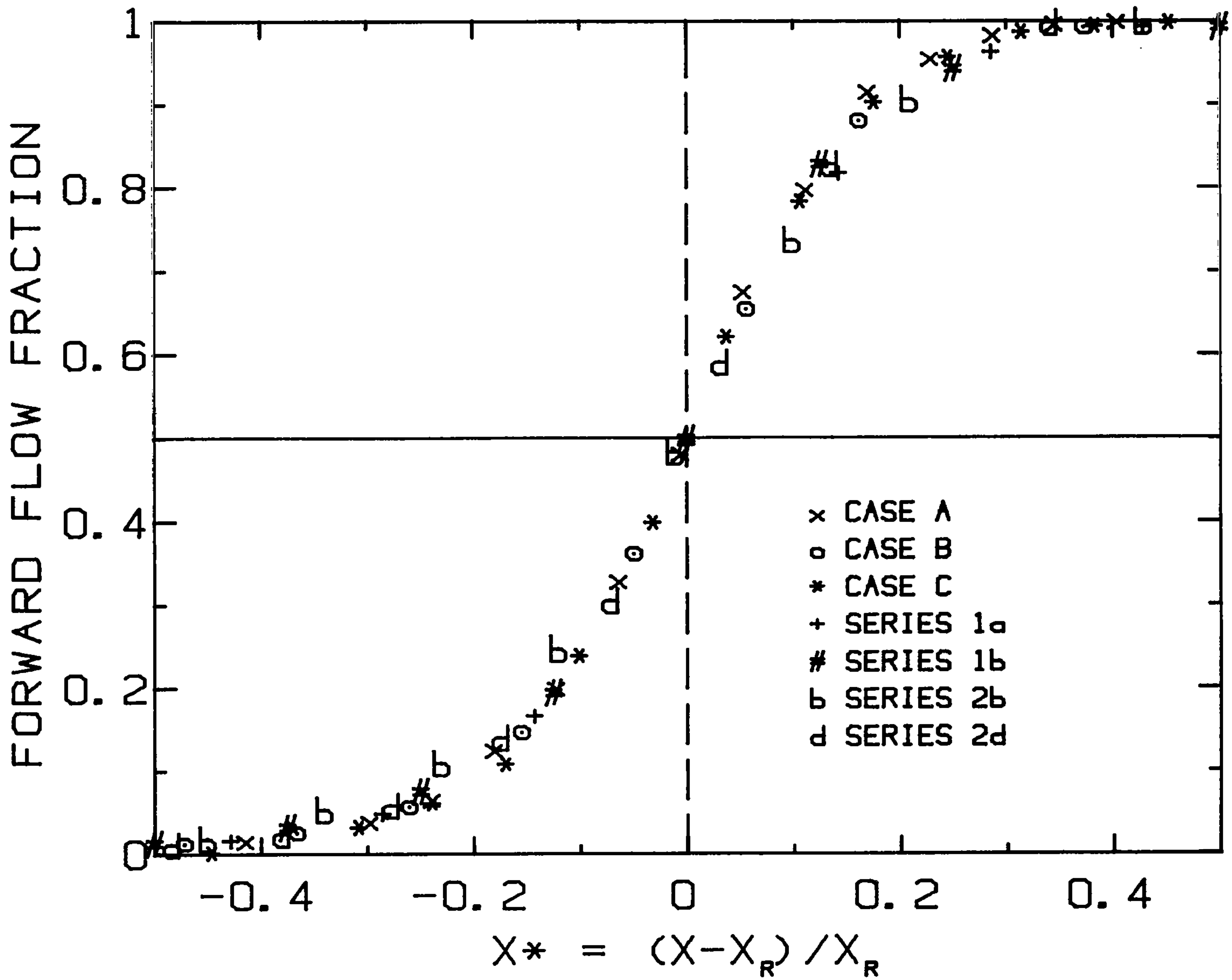

Fig. 6-3. Forward-flow fraction by reattachment for seven cases of the current study.

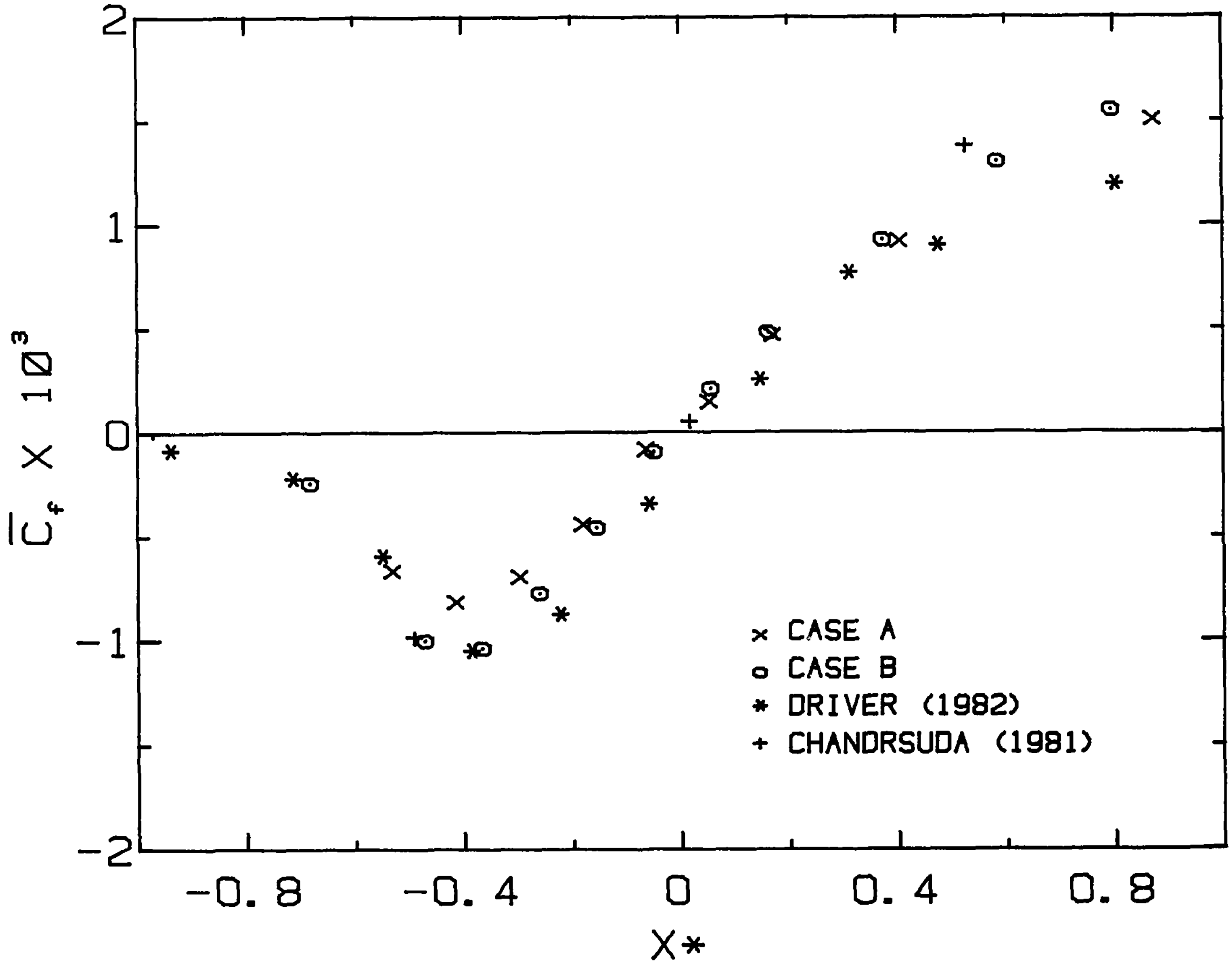

Fig. 6-4. Skin friction by reattachment; same data as in Fig. 6-1, but with normalized streamwise coordinate.

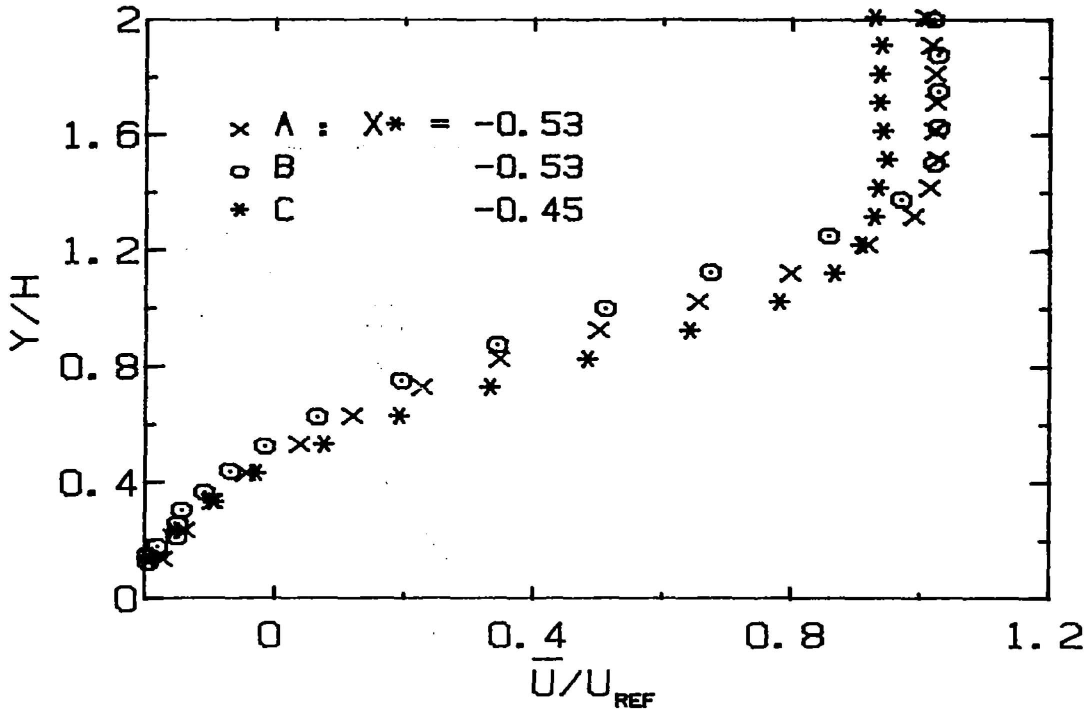

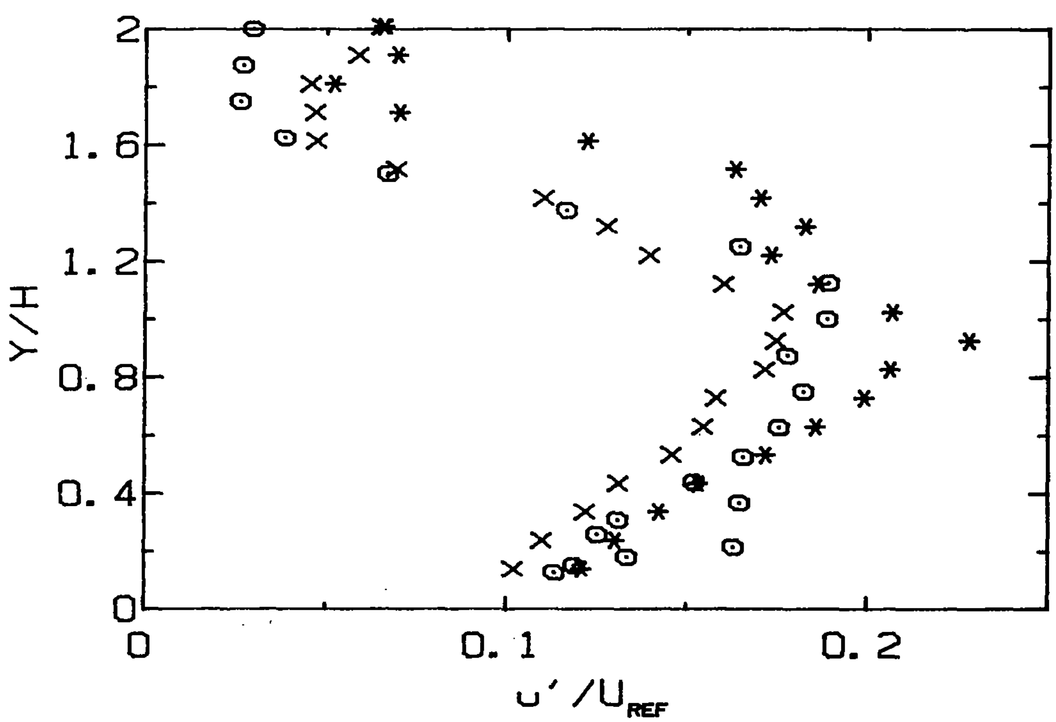

Fig. 6-5. Velocity profiles near X* = -0.5 measured with the pulsed-wire anemometer.

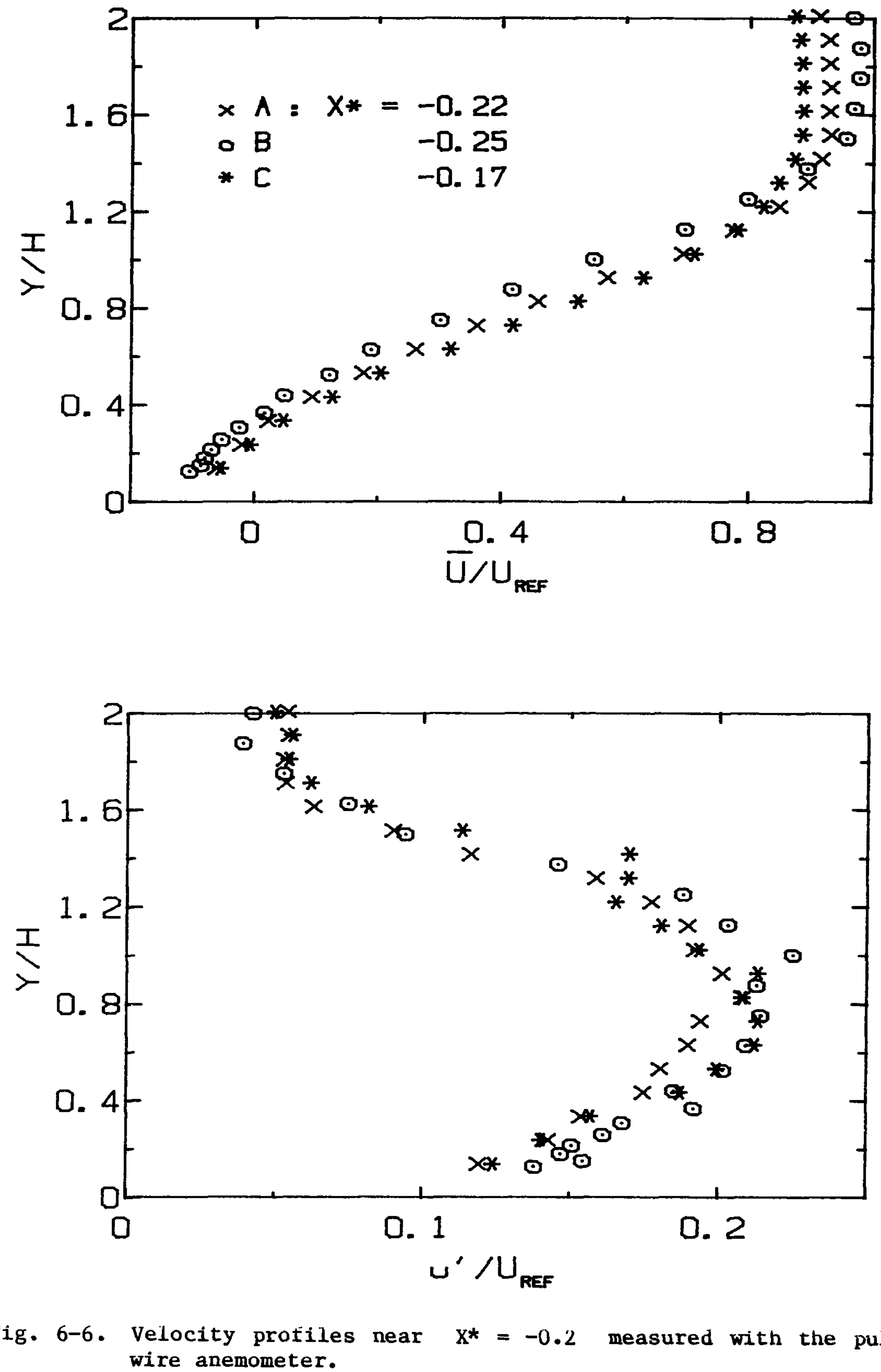

Fig. 6-6. Velocity profiles near X* = -0.2 measured with the pulsed-wire anemometer.

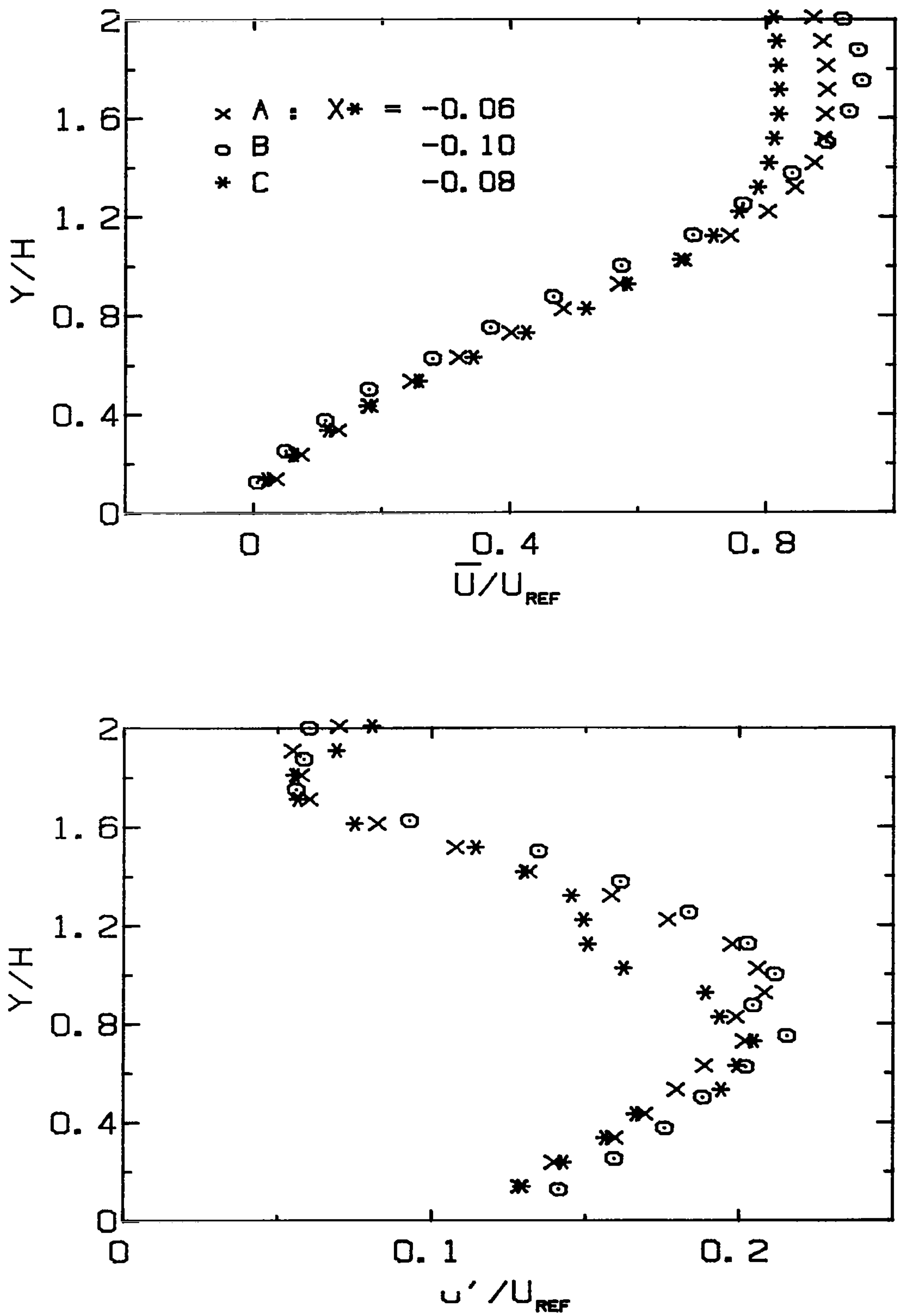

Fig. 6-7. Velocity profiles near X* = -0.1 measured with the pulsed-wire anemometer.

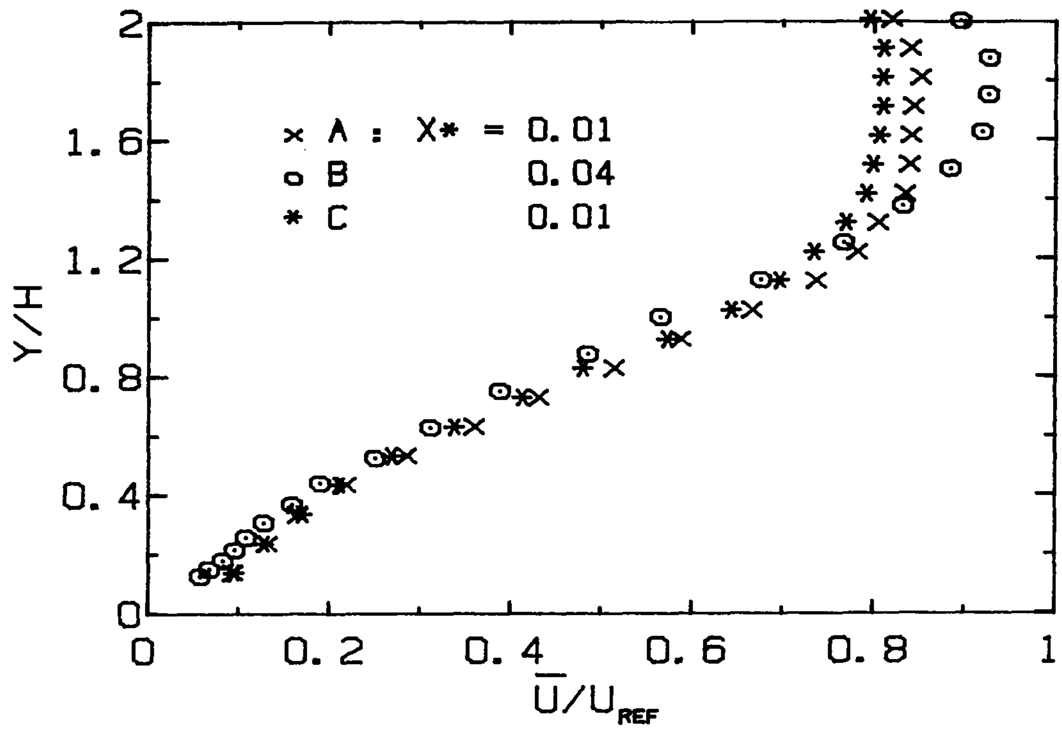

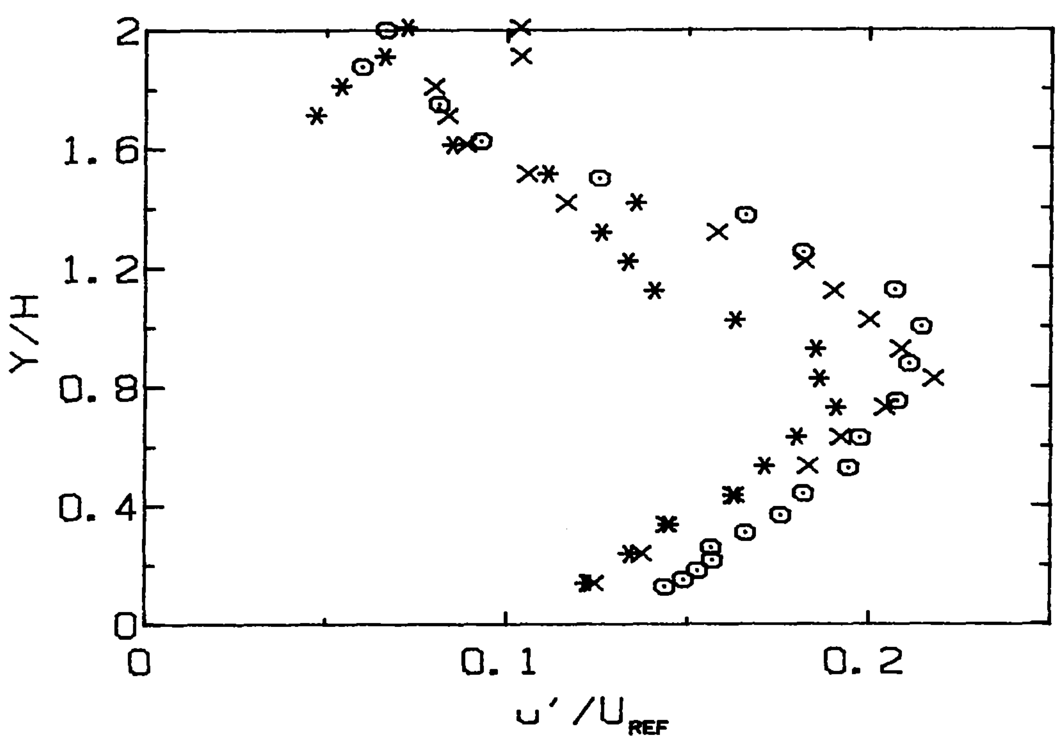

Fig. 6-8. Velocity profiles near X* = 0 measured with the pulsed-wire anemometer.

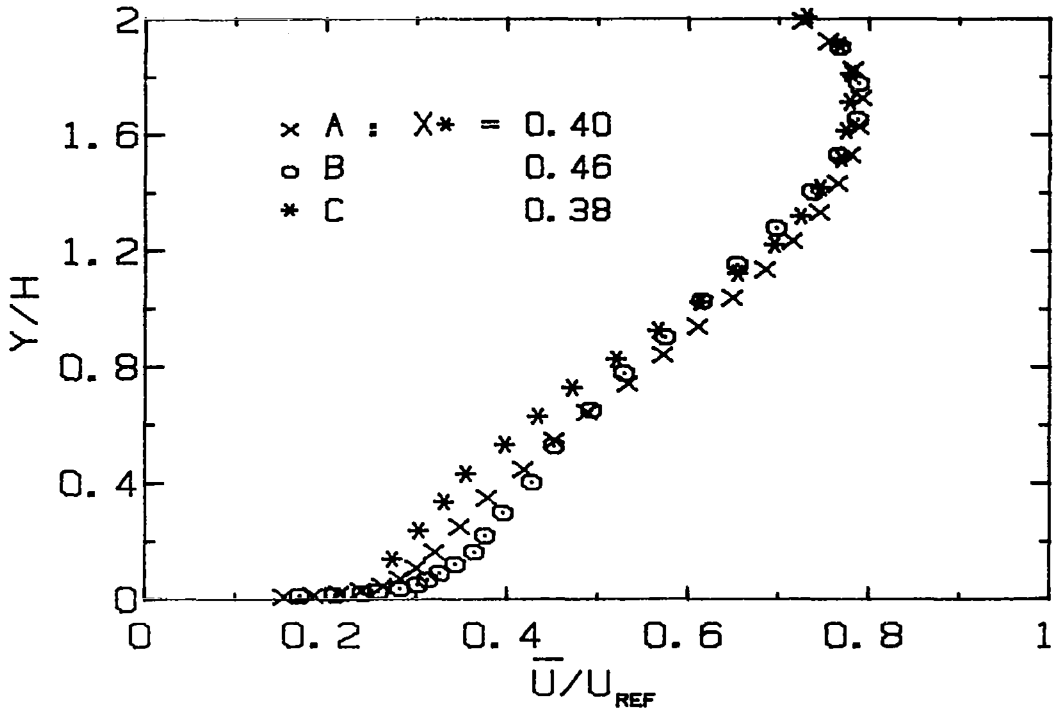

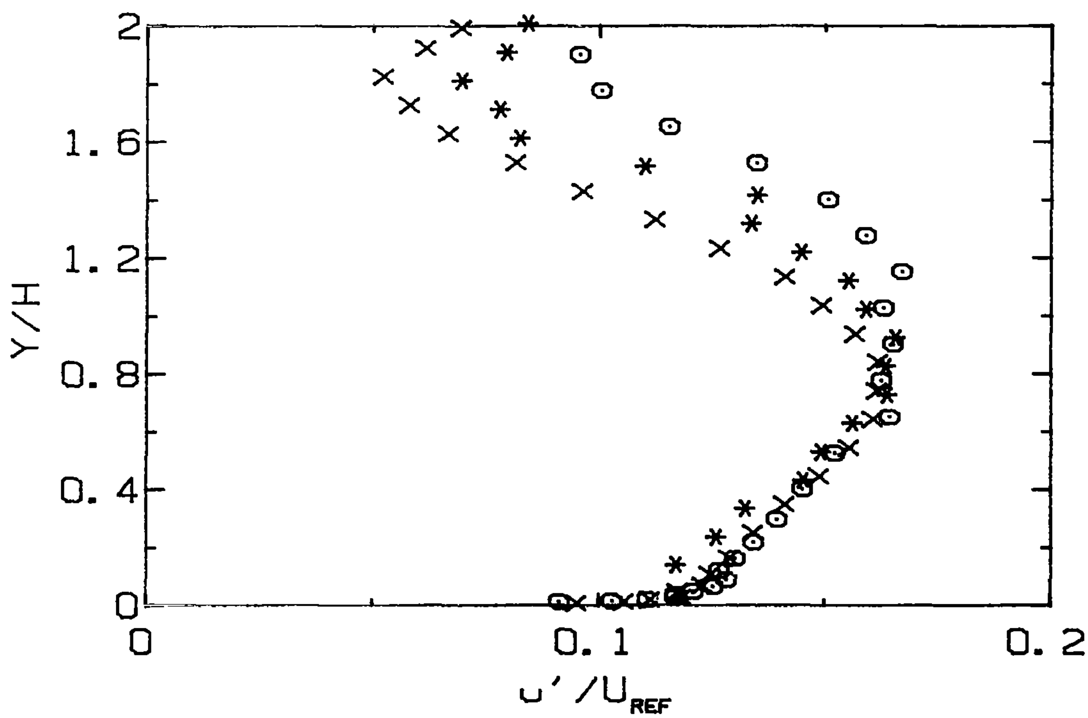

Fig. 6-9. Velocity profiles near X* = 0.4 measured with a hot wire.

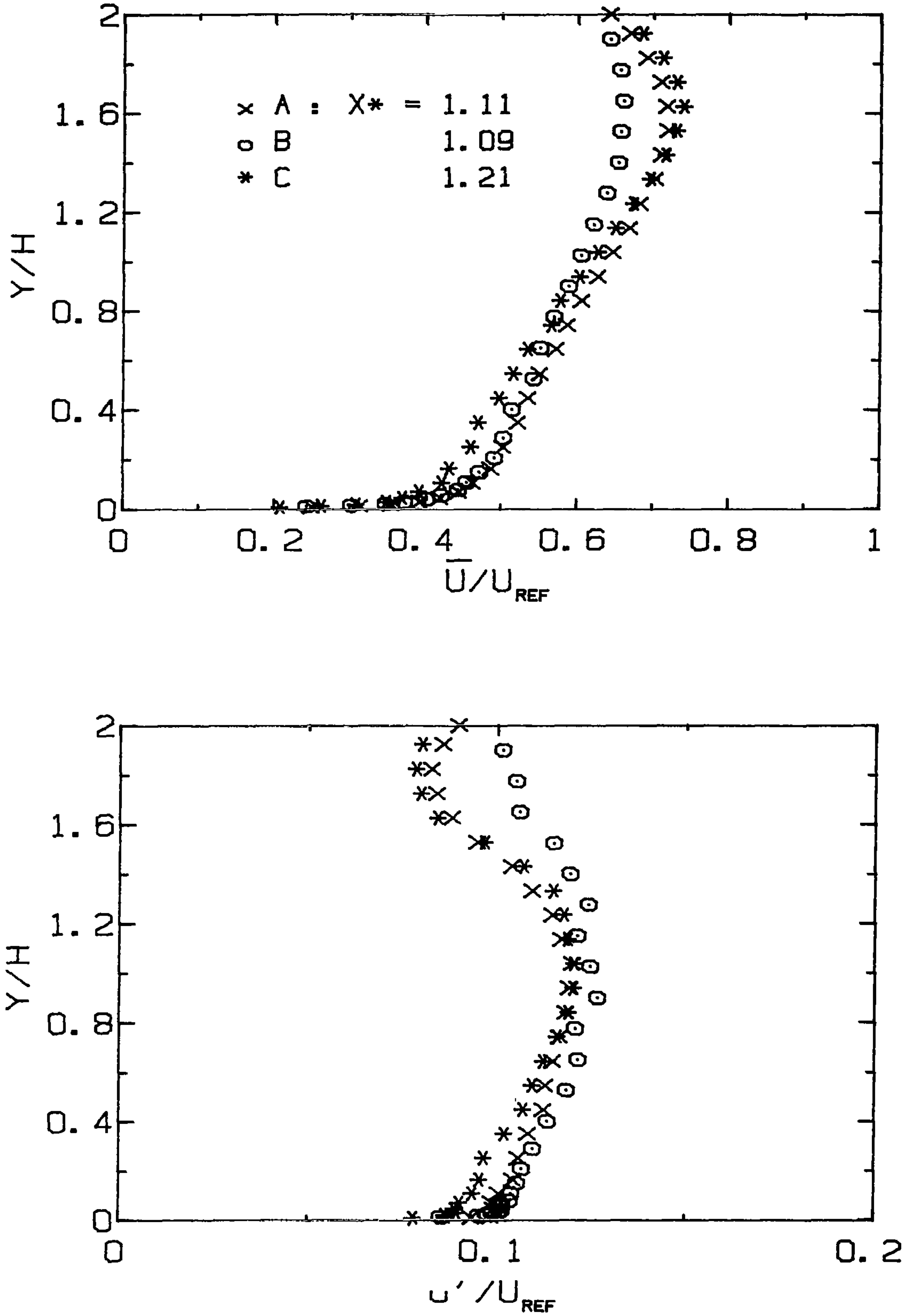

Fig. 6-10. Velocity profiles near X* = 1.1 measured with a hot wire.

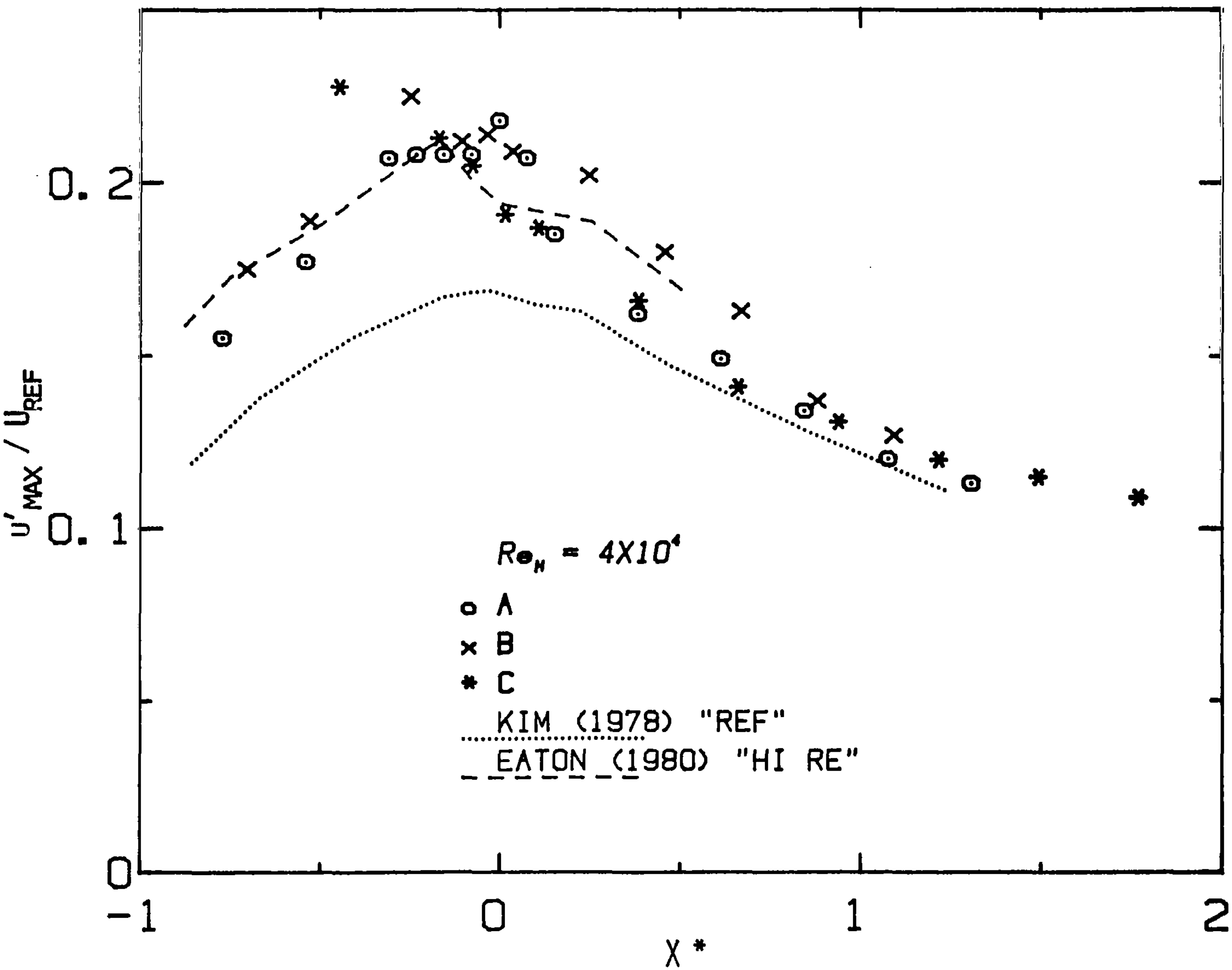

Fig. 6-11. Maximum value of velocity fluctuation u'/U_{ref} in the reattachment region for Cases A, B, and C of the present study compared to the results of Kim et al. (1978) and Eaton and Johnston (1980).

Chapter 7

CONCLUSIONS AND RECOMMENDATIONS

Conclusions and recommendations are distilled below from the discussion and results already presented. In both sections, major points are listed in their perceived order of importance.

7.1 Conclusions

1. The process and properties of two-dimensional reattachment may be universally scaled and usefully described using a streamwise coordinate $X^* = (X-X_R)/X_R$. For cases in which the separation provides a strong perturbation of the upstream boundary layer (δ/H small), a universal region has been identified extending $\pm 0.4\ X_R$ about the reattachment point.

2. For thin separating boundary layers, all measures of the properties of the reattachment zone (scaled on X^*) have been found to be independent of shear-layer structural modifications imposed by significant changes in (i) boundary layer thickness, (ii) streamline curvature in the separated region, and (iii) the introduction of strong streamwise vorticity into the separating boundary layer.

3. Reattachment length may be strongly affected by the changes in shear-layer structure enumerated above, even though the properties of the reattachment region itself are not strongly affected.

4. Strong backflow is present near the surface beneath the separated shear layer upstream of reattachment. The large magnitude of the backflow skin-friction coefficient suggests that the near-wall flow is behaving in a laminar-like fashion, at least for Reynolds numbers of this (and most previous) studies.

5. Data provided for Cases A and B are qualified for use as test cases for computational models of complex flows. Quality of the flow in the wind tunnel has been assured through extensive rework of flow conditioning upstream of the test section. Inlet conditions, two-dimensionality, and conservation law requirements have been explicitly checked and quantitatively characterized for these cases. Different experimental methods have been employed to measure the same quantities

where practical in order to verify uncertainty estimates. Tabular data appear in an appendix for reference.

6. In addition to the "test case" data sets, new results concerning gross effects of parametric variations of (i) boundary layer thickness (Series 1), (ii) duct angle (Series 2), and Reynolds number (Series 3) are made available.

7. Time-dependent, directionally resolved skin-friction measurements can be made with reasonable accuracy in low-speed turbulent air flows using the pulsed wall probe developed for this study.

7.2 Recommendations for Future Work

1. More turbulence stresses should be measured in the separation and reattachment regions. Of special interest would be measurement of $\overline{u'v'}$ in the region of strong backflow. Such data could illuminate structural features of this region, which has been characterized as "laminar-like" on the basis of results presented here.

2. The effect of varying the three main parameters of the backward-facing step geometry (δ/H, AR, Re_H) requires further study. Advanced instrumentation (e.g., laser-Doppler anemometry) must be used and accurate measurement of X_R is essential. Of greatest interest are cases with thicker separating boundary layers ($\delta/R > 1$) and very large Reynolds numbers ($Re_H > 10^5$).

3. Reattachment-length measurements using visual techniques such as the surface-oil-film method should be checked against one or more of the quantitative methods employed in this study to better calibrate this popular technique for measurement of reattachment length.

4. The pulsed-wire anemometer seems to be qualified for use in complex flows such as the one studied here. It should be employed to check other proposed instruments which are to be used in such flows (e.g., the laser-Doppler anemometer).

References

Abbott, D. E., and S. J. Kline (1961), "Theoretical and Experimental Investigation of Flow over Single and Double Backward-Facing Steps," Report MD-5, Dept. of Mech. Engrg., Stanford University, Stanford, CA.

Adams, E., and S. Honami (1980), "Smoke-Wire Technique," Rept. IL-28, Thermosciences Div., Dept. of Mech. Engrg., Stanford University, November.

Ajagu, C. O., P. A. Libby, and J. C. LaRue (1982), "Modified Gage for Time-Resolved Skin Friction Measurements," unpublished. To appear in Rev. Sci. Inst.

Arie, M., and H. Rouse (1956), "Experiments on Two-Dimensional Flow over a Normal Wall," JFM, 1, 129-141.

Armaly, B. F., F. Durst, and B. Schonung (1980), "Measurements and Predictions of Flow Downstream of a Single Backward-Facing Step," SFB80/ET/172, July.

Arvizu, D. E., and R. J. Moffat (1981), "Experimental Heat Transfer from an Array of Heated Cubical Elements on an Adiabatic Channel Wall," Rept. HMT-33, Thermosciences Division, Mechanical Engrg. Dept., Stanford University, December.

Asanuma, T (1977), "Flow Visualization," Proc. Intl. Symp. on Flow Visualization," Oct. 12-14, 1977, Tokyo, Japan.

Ashurst, W. T., F. Durst, and C. Tropea (1980), "Two-Dimensional Separated Flow: Experiment and Discrete Vortex Dynamics Simulation," SAND 79-8830, Sandia Laboratories, Albuquerque, NM, October.

Back, L. H., and E. J. Roschke (1972), "Shear Layer Flow Regimes and Wave Instabilities and Reattachment Lengths Downstream of an Abrupt Circular Channel Expansion," Trans. ASME, J. Appl. Mech., 94, 677-681, September.

Baker, S. (1977), "Regions of Recirculating Flow Associated with Two-Dimensional Steps," Ph.D. thesis, Dept. of Civil Engrg., Univ. of Surrey, Great Britain, December.

Banyopadhyay, P. (1977), "Combined Smoke-Flow Visualization and Hot-Wire Anemometry in Turbulent Boundary Layers," Lecture Notes in Physics, No. 75, Springer, New York, 205-216.

Batill, S. M., and T. J. Mueller (1981), "Visualization of Transition in the Flow over an Airfoil Using the Smoke-Wire Technique," AIAA J., 19, No. 3, 340-345, March.

Bearman, P. W. (1965), "Investigation of the Flow Behind a Two-Dimensional Model with a Blunt Trailing Edge and Fitted with Splitter Plates," JFM, 21, Pt. 1, 241-255.

Bellhouse, G. J., and D. L. Schultz (1966), "Determination of Mean and Dynamic Skin Friction, Separation, and Transition in Low-Speed FLow with a Thin-Film Heated Element," JFM, 24, 379-400.

Bradbury, L. J. S. (1978), "Examples of the Use of the Pulsed-Wire Anemmeter in Highly Turbulent Flows," Proc. Dynamic Flow Conf., 489-509.

Bradbury, L. J. S., and I. P. Castro (1971), "A Pulsed-Wire Technique for Velocity Measurements in Highly Turbulent Flows," JFM, 49, 657-691.

Bradshaw, P. (1967), "A Low-Turbulence Wind Tunnel Driven by a Centrifugal Blower," J. Royal Aero. Soc., 71, 132.

Bradshaw, P. (1968), "Simple Wind Tunnel Design," NPL Aero Rept. #1258, March.

Bradshaw, P., and F.Y.P. Wong (1972), "The Reattachment and Relaxation of a Turbulent Shear Layer," JFM, 52, Pt. 1, 113-135.

de Brederode, V., and P. Bradshaw (1972), "Three-Dimensional Flow in Nominally Two-Dimensional Separation Bubbles. I. Flow behind a Rearward-Facing Step," I.C. Aero Report #72-19.

Bremmer, R. J. (1980), "An Experimental and Numerical Comparison of Turbulent Flow over a Step," M.S. thesis, Purdue University, August.

Castro, I. P. (1971), "Wake Characteristics of Two-Dimensional Perforated Plates Placed Normal to an Airstram," JFM, 46, Pt. 3, 599-609.

Castro, I. P. (1981), "Measurements in Shear Layers Separating from Surface-Mounted Bluff Bodies," J. Wind Engr. and Ind. Aero, 7, 253-272.

Castro, I. P., and P. Bradshaw (1976), "The Turbulence Structure of a Highly Curved Mixing Layer," JFM, 73, Pt. 2, 265-3-4.

Castro, I. P., and B. S. Cheun (1982), "The Measurement of Reynolds Stresses with a Pulsed-Wire Anemometer," JFM, 118, 41-58.

Castro, I. P., and J. E. Fackrell (1978), "A Note on Two-Dimensional Fence Flows, with Emphasis on Wall Contraint," J. Ind. Aero., 3, No. 1, 1-20, March.

Castro, I. P., and A. G. Robbins (1977), "The Flow around a Surface-Mounted Cube in Uniform and Turbulent Streams," JFM, 79, Pt. 2, 307-335.

Chandrsuda, C. (1975), "A Reattaching Turbulent Shear Layer in Incompressible Flow," Ph.D. thesis, Imperial College of Sci. and Tech., Dept. of Aeronautics.

Chandrsuda, C., and P. Bradshaw (1981), "Turbulence Structure of a Reattaching Mixing Layer," JFM, 110, 171-194.

Chang, P. K. (1980), "Recent Developments in Flow Separation," AFOSR-TR-81-0451.

Chapman, D. R., D. H. Kuehn, and H. K. Larson (1958), "Investigation of Separated Flows in Supersonic and Subsonic Streams with Emphasis on the Effect of Transition," NACA TN3869.

Cherdron, W., F. Durst, and J. H. Whitelaw (1978), "Asymmetric Flows and Instabilities in Symmetric Ducts with Sudden Expansions," JFM, 84, Pt. 1, 13-31.

Cheun, B. S., N. Toy, and W. D. Moss (1981), "The Effect of Upstream Boundary Layer Thickness upon Flow Past a Backward-Facing Step," from the 1981 conference at the Univ. of Missouri-Rolla.

Chilcott, R. E. (1967), "A Review of Separated and Reattaching Flows with Heat Transfer," Int. J. Heat Transfer, 10, 783-797.

Coles, D. (1968), "The Young Person's Guide to the Data," appears in Proc. of the 1968 AFOSR-Stanford Conference on Computation of Turbulent Boundary Layrs. Vol. II (D. Coles and E. Hirst, eds.), 1-19.

Coles, D., and A. J. Wadcock (1978), "A Flying Hot-Wire Study of Two-Dimensional Mean Flow Past a NACA 4412 Airfoil at Maximum Lift," AIAA 11th Fluids and Plasma Dynamics Conf. paper #78-1196.

Corke, T. C. (1981), "A New View on Origin, role, and Manipulation of Large Scales in Turbulent Boundary Layers," Ph.D. thesis, Dept. of Mechanics, Mechanical and Aerospace Engrg., Illinois Inst. of Technology, Chicago, Dec.

Corke, T. C., D. Koga, R. Drubka, and H. Nagib (1977), "A New Technique for Introducing Controlled Sheets of Smoke Streaklines in Wind Tunnels," ICIASF, 1977 Record, 74-80.

Counihan, J., J. C. R. Hunt, and P. S. Jackson (1974), "Wakes behind Two-Dimensional Surface Obstacles in Turbulent Boundary Layers," JFM, 64, Pt. 3, 529-563.

Dean, R. B. (1978), "Reynolds Number Dependence of Skin Friction and Other Bulk Flow Variables in 2-Dimensional Rectangular Duct Flow," J. Fluids Eng., 100, No. 2, June, 715-223.

Driver, D. M., and H. L. Seegmiller (1982), "Features of a Reattaching Turbulent Shear Layer," AIAA paper No. 82-1029 (to be published in the AIAA J).

Dryden, H. L., and G. B. Schubauer (1949), "Appendix to the Effect of Wire Gauze on Small Disturbances in a Uniform Stream," Quart. J. Mech. and Appl. Mech., 2, No. 1, p. 1 (see also Taylor and Batchelor (1949).

Durst, F., A. Melling, and J. H. Whitelaw (1974), "Low Reynolds Number Flow over a Plane Symmetric Sudden Expansion," JFM, 64, Pt. 1, 111-128.

Durst, F., and A. K. Rastogi (1979), "Theoretical and Experimental Investigations of Turbulent Flows with Separation," Turbulent Shear Flows I, Springer-Verlag, NY, 208-219.

Durst, F., and A. K. Rastogi (1980), "Turbulent Flow over Two-Dimensional Fences," Turbulent Shear Flows II, Springer-Verlag, NY, 218-232.

Durst, F., and C. Tropea (1981), "Turbulent, Backward-Facing Step Flows in Two-Dimensional Ducts and Channels," Proc. Third Symp. on Turbulent Shear Flows, Univ. of California-Davis, Sept. 9-11, 1981, 18.1-18.6.

Eaton, J. K., and J. P. Johnston (1981), "A Review of Research on Subsonic Turbulent Flow Reattachment," AIAA J., 19, 1092-1100, September.

Eaton, J. K., R. V. Westphal, and J. P. Johnston (1981), "Two New Instruments for Flow Direction and Skin Friction Measurements in Separated Flows," ISA Trans., 21, No. 1, 69-78.

Eaton, J. K., and J. P. Johnston (1980), "Turbulent Flow Reattachment: An Experimental Study of the Flow and Structure behind a Backward-Facing Step," Report No. MD-39, Thermosci. Div. of Mech. Engrg. Dept., Stanford University, June.

Eaton, J. K., A. J. Jeans, J. Ashjaee, and J. P. Johnston (1979), "A Wall-Flow Direction Probe for Use in Separating and Reattaching Flows," J. Fluids Engrg., 101, 364-366.

Etheridge, D. W., and P. M. Kemp (1978), "Measurements of Turbulent Flow Downstream of a Rearward-Facing Step," JFM, 86, Pt. 3, 545-566.

Filetti, E. G., and W. M. Kays (1967), "Heat Transfer in Separated, Reattached, and Redevelopment Regions behind a Double Step at Entrance to a Flat Duct," Trans. ASME J. Heat Transfer, 89, 163-168, May.

Fletcher, L. S., D. H. Briggs, and R. H. Page (1974), "Heat Transfer in Separated and Reattached Flows: An Annotated Review," Israel J. Tech., 12, 236-261.

Flow Visualization Systems (1980), "Vertical Smoke Wire Instrument," operating manual and parts list, December.

Freeman, A. R. (1978), "Measurements of Velocity and Temperature in the Region Downstream of a Sudden Pipe Expansion," CEGB Rept. #RD/B/N4306, July.

Gaviglio, J., J. P. Dussauge, and A. Favre (1977), "Behavior of Turbulent Flow, Strongly out of Equilibrium, at Supersonic Speeds," Phys. Fluids Suppl., 20, No. 10, Pt. 11, S179-S192.

Ginder, R. B., and L. J. S. Bradbury (1973), "Preliminary Investigation of a Pulsed Gauge Technique for Skin Friction Measurements in Highly Turbulent Flows," #34-488, FM 4394, Aeronautics Dept., Imperial College.

Goldstein, R. J., V. L. Erickson, R. L. Olson, and E.R.G. Eckert (1970), "Laminar Separation, Reattachment, and Transition of the Flow over a Downstream-Facing Step," J. Basic Engrg., 92, 732-741, December.

Good, M. C., and P. N. Joubert (1968), "The Form Drag of Two-Dimensional Bluff Plates Immersed in Turbulent Boundary Layers," JFM, 31, 547-582.

Grant, I., F. A. Barnes, and C. A. Greated (1975), "Velocity Measurements Using the Photon Correlation Technique in a Separated Boundary Layer," Phys. Fluids, 18, 504-507, May.

Ha Minh, H. H., and P. Chassaing (1979), "Perturbations of Turbulent Pipe Flows," Turbulent Shear Flows I, Springer-Verlag, NY, 178-197.

Hastings, R. C. (1963), "Turbulent Flow Past Two-Dimensional Bases in Supersonic Streams," RAE TN Aero 2931.

Higuchi, H., and D. J. Peake (1978), "Bi-Directional, Buried-Wire Skin-Friction Gage," NASA-TM-78531, Nov.

Hsu, H. (1950), "Characteristics of Mean Flow and Turbulence at an Abrupt Two-Dimensional Expansion," Ph.D. thesis, Dept. of Mech. and Hydraulis, Univ. of Iowa, February.

Hussain, A.K.M.F., and W. C. Reynolds (1975), "Measurements in a Fully Developed Turbulent Channel Flow," Trans. ASME, J. Fluids Engrg., 97, 568-579, Dec.

Kasagi, N., M. Hirata, and S. Yokobari (1977), "Visual Studies of Large Eddy Structures in Turbulent Shear Flows by Means of Smoke-Wire Method," Proc. Int. Symposium on Flow Visualization (T. Asanuma, ed.), Oct. 12-14, 1977, Tokyo, Japan.

Kim, J., S. J. Kline, and J. P. Johnston (1978), "Investigation of Separation and Reattachment of a Turbulent Shear Layer: Flow over a Backward-Facing Step," Rept. No. MD-37, Thermosci. Div., Mech. Engrg. Dept., Stanford University, April.

Kim, J., S. J. Kline, and J. P. Johnston (1980), "Investigation of a Reattaching Turbulent Shear Layer: Flow over a Backward-Facing Step," Trans. ASME, J. Fluids Engrg., 102, No. 3, 302-308, September.

Kline, S. J., B. J. Cantwell, G. M. Lilley (eds.) (1981), Proceedings of the 1980-81 AFOSR-HTTM-Stanford Conference on Complex Turbulent

Flows, Vol. 1, "Ad Hoc Committee Report on Hot-Wire Anemometry at Low Mach Numbers," 582-585.

Kline, S. J., and F. A. McClintock (1953), "Describing Uncertainty in Single-Sample Experiments," Mech. Engrg., January.

Korst, H. H. (1956), "A Theory for Base Pressure in Transonic and Supersonic Flow," Trans. ASME, J. Appl. Mech., 23, No. 4, 593-600, December.

Kuehn, D. M. (1980), "Some Effects of Adverse Pressure Gradient on the Incompressible Reattaching Flow over a Backward-Facing Step," AIAA J., 18, No. 3, 343-344, March.

Laws, E. M., and J. L. Livesy (1978), "Flow through Screens," Ann. Rev. Fluid Mech., 10, p. 247.

Leal, L. G., and A. Acrivos (1969), "The Effects of Base Bleed on the Steady Separated Flow past Bluff Objects," JFM, 39, Pt. 4, 735-752.

Ligrani, P. M., and B. Gyles (1981), "Hot-Wire Thermal Tuft Development for Measurement of Flow Reversal near a Compressor Blade," VKI #1981-7, from Measurement Techniques in Turbomachines, May 18-22, 1981.

Loerke, R. I., and H. M. Nagib (1972), "Experiments on Management of Freestream Turbulence," AGARD Rept. #598, September.

Loerke, R. I., and H. M. Nagib (1976), "Control of Free-Stream Turbulence by Means of Honeycombs: A Balance between Suppression and Generation," J. Fluids Engrg., 98, No. 3, p. 342.

McCroskey, W. J., and E. J. Durbin (1972), "Flow Angle and Shear Stress Measurements Using Heated Films and Wires," Trans. ASME, J. Basic Engrg., 94, No. 1, 46-52, March.

Mehta, R. D., and P. Bradshaw (1979), "Design Rules for Small, Low-Speed Wind Tunnels," Aero. J. of Royal Aero. Soc., 443-449, November. Mehta and Bradshaw (1977) is the expanded version, this is Mehta's Imperial College Report reprinted by Pergammon Press in Prog. Aero. Sci., 18, 59-120, 1977.

Mikhail, M. N. (1979), "Optimum Design of Wind Tunnel Contractions," AIAA J., 17, No. 5, 471-477, May.

Mitchell, J. E., and T. J. Hanratty (1966), "A Study of Turbulence at a Wall Using an Electrochemical Wall Shear-Stress Meter," JFM, 26, Pt. 1, 199-221.

Moffat, R. J. (1981), "Contributions to the Theory of Uncertainty Analysis for Single-Sample Experiments," Proc. 1980-81 AFOSR-HTTM-Stanford Conference o Complex Turbulent Flows, Vol. 1 (S. J. Kline, B. J. Cantwell, and G. M. Lilley, eds.), 40-55.

Monson, D. J., and H. Higuchi (1981), "Skin Friction Measurements by a New Non-Intrusive Laser Beam-Oil Viscosity Balance Technique," AIAA J., 19, No. 6, 739-744.

Moore, T.W.F. (1960), "Some Experiments on the Reattachment of a Laminar Boundary Layer Separating from a Rearward-Facing Step on a Flat Plate Airfoil," J. Royal Aero. Soc., 64, 668-672, November.

Moss, W. D., S. Baker, and L.J.S. Bradbury (1979), "Measurements of Mean Velocity and Reynolds Stresses in some Regions of Recirculating Flow," Turbulent Shear Flows I, Springer Verlag, NY, 193-207.

Mueller, T. J. (1961), "On Separation, Reattachment, and Redevelopment of Turbulent Boundary Layers," Ph.D. thesis, Dept. of Mech. Engrg., University of Illinois.

Mullin, T., C. A. Greated, and I. Grant (1980), "Pulsating Flow over a Step," Phys. Fluids, 23, No. 4, 669-674, April.

Narayanan, B., M. A. Khadge, and P. T. Viswanath (1974), "Similarities in Pressure Distribution in Separated Flow behind a Backward-Facing Step," Aero. Quart., 25, Pt. 4, 305-312, November.

Nash, J. F. (1966), "Experiments on Two-Dimensional Base Flow at Subsonic and Transonic Speeds," Aero Res. Council R&M #3427.

Naysmith, A. (1958), "Heat Transfer and Boundary Layer Measurements in a Region of Supersonic Flow Separation and Reattachment," RAE TN Aero 2558.

Patel, V. C. (1965), "Calibration of the Preston Tube and Limitations on Its Use in Pressure Gradients," JFM, 23, No. 1, 185-208.

Perry, A. E., and B. D. Fairlie (1975), "A Study of Turbulent Boundary-Layer Separation and Reattachment," JFM, 69, Pt. 4, 657-672.

Plate, E. J ., and C. W. Lin (1965), "The Velocity Field Downstream of a Two-Dimensional Model Hill," Pt. 1, CER62EJP14, Fluid Dynamics Laboratory, Colorado State University, August.

Pontikos, N., and P. Bradshaw (1981), "Miniature Pressure Probe for Measuring the Surface Shear Stress Vector in Turbulent Flow," Aero. Quart., 32, Pt. 1, 43-47, Feb.

Ranga Raju, K. G., and R. J. Garde (1970), "Resistance of an Inclined Plate Placed on a Plane Boundary in Two-Dimensional Flow," Trans. ASME, J. Basic Engrg., 92 21-31, March.

Ranga Raju, K. G., J. Loeser, and E. J. Plate (1976), "Velocity Profiles and Fence Drag for a Turbulent Boundary Layer along Smooth and Rough Flat Plates," JFM, 76, Pt. 2, 383-399.

Reda, D. C., and R. H. Page (1969), "Supersonic Turbulent Flow Reattachment Downstream of a Two-Dimensional Backstep," AFOSR #69-1592TR, May.

Restivo, A., and J. H. Whitelaw (1978), "Turbulence Characteristics of the Flow Downstream of a Symmetric, Plane Sudden Expansion," Trans. ASME, J. Fluids Engrg., 100, 308-310, September.

Roshko, A., and J. C. Lau (1965), "Some Observations on Transition and Reattachment of a Free Shear Layer in Incompressible Flow," Proc. 1965 Heat Transfer and Fluid Mech. Inst. (A. F. Charwat, ed.), Stanford University Press, 157-167.

Rothe, P. H., and J. P. Johnston (1975), "The Effects of System Rotation on Separation, Reattachment, and Performance in Two-Dimensional Diffusers," Rept. PD-17, Thermosci. Div., Mech. Engrg. Dept., Stanford University.

Sandborn, V. A. (1979), "Evaluation of the Time-Dependent Sruface Shear Stress in Turbulent Flows," ASME WAM 79-WA/FE-17 preprint.

Scheiman, J. (1981), "Comparison of Experimental and Theoretical Turbulence Reduction Characteristics for Screens, Honeycomb, and Honeycomb-Screen Combinations," NASA-TP-1958 L-14628, December.

Schlichting, H. (1979), Boundary Layer Theory, seventh edition, McGraw-Hill, New York.

Seban, R. A., A. Emery, and A. Levy (1959), "Heat Transfer to Separated and Reattached Subsonic Turbulent Flows Obtained Downstream of a Step," J. Aero/Space Sci., 26, No. 12, 809-814, December.

Seban, R. A. (1964), "Heat Transfer to the Turbulent Separated Flow of Air Downstream of a Step in the Surface of a Plate," Trans. ASME J. Heat Trans., 86, 259-264, May.

Seki, N., S. Fukusako, and T. Hirata (1976a), "Effect of Stall Length on Heat Transfer in the Reattached Region behind a Double-Step and Entrance to an Enlarged Flat Duct," Int. J. Heat Mass Trans., 19, No. 6, 700-702, May.

Seki, N., S. Fukusako, and T. Hirata (1976b), "Turbulent Fluctuations and Heat Transfer for Separated Flow Associated with a Double Step at an Entrance to an Enlarged Flat Duct," Trans. ASME, J. Heat Trans., 98, 588-593, November.

Settles, G. S., B. K. Baca, D. R. Williams, and S. M. Bogdonoff (1980), "A Study of Reattachment of a Free Shear Layer in Compressible Turbulent Flow," paper presented at AIAA 13th Fluids and Plasma Dynamics Conf. in Snowmass, Colo., July 14-16.

Shivaprasad, B. G., and R. L. Simpson (1982), "Evaluation of a Wall-Flow Direction Probe for Measurements in Separated Flows," J. Fluids Engrg., 104, No. 2, 162-166.

Simonich, J. C., and R. J. Moffat (1982), "Local Measurements of Turbulent Boundary Layer Heat Transfer on a Concave Surface Using Liquid Crystals," Ph.D. thesis, Mech. Engrg. Dept., Stanford University.

Sinha, S. N., A. K. Gupta, and M. M. Oberai (1981), "Laminar Flow over Backsteps and Cavities, Part I: Backsteps," AIAA J., 19, No. 2, 1527-1530, December.

Sirkar, K. K., and T. J. Hanratty (1970a), "Relation of Turbulent Mass Transfer to a Wall at High Schmidt Numbers to the Velocity Field," JFM, 44, Pt. 3, 589-603.

Sirkar, K. K., and T. J. Hanratty (1970b), "The Limiting Behavior of the Turbulent Transverse Velocity Component Close to a Wall," JFM, 44, Pt. 3, 605-614.

Smits, A. J. (1979), "A Critical Preliminary Review of Literature Relating to Bluff Bodies with Splitter Plates," Rept. #FM10, Dept. Mech. Engrg., Univ. of Melbourne.

Smits, A. J. (1981), "Scaling Parameters for a Time-Averaged Separation Bubble," Trans. ASME J. Fluids Engrg., 104, No. 2, 178-184, June.

Smyth, R. (1979), "Turbulent Flow over a Plane Symmetric Sudden Expansion," Trans. ASME J. Fluids Engrg., 101, 348-353, September.

Stevenson, W. H., H. D. Thompson, and R. Bremmer (1979), "Laser Velocimeter Measurements in Turbulent and Mixing Flows, Part II," Purdue Univ. Report #AFAPL-TR-79-2009.

Tani, I. (1974), "Low-Speed Flows Involving Bubble Separations," Prog. Aero. Sci., 5, 70-103.

Tani, I., M. Iuchi, and H. Komoda (1961), "Experimental Investigation of Flow Separation Associated with a Step or Groove," Aeronautics Research Institute, Univ. of Tokyo, Rept. #364, 119-137, April.

Tanner, L. H., and L. G. Blows (1976a), "A Study of the Motion of Oil Films on Surfaces in Air Flow, with Application to the Measurement of Skin Friction," J. Phys. E.: Sci. Inst., 9, No. 3, 194-202, Mar.

Tanner L. H., and V. G. Kulkarni (1976b), "The Viscosity Balance Method of Skin Friction Measurement: Further Developments Including Applications to Three-Dimensional Flows," J. Phys. E.: Sci. Inst., 9, No. 12, 1114-1121, March.

Tanner, L. H. (1977a), "A Skin Friction Meter, Using the Viscosity Balance Principle, Suitable for Use with Flat or Curved Metal Surfaces," J. Phys. E: Sci. Inst., 10, No. 3, 278-284, March.

Tanner, L. H. (1977b), "A Comparison of the Viscosity Balance and Preston Tube Methods of Skin Friction Measurement," J. Phys. E: Sci. Inst., 10, No. 6, 627-632, June.

Tanner, M. (1976), "The Pressure Rise at the Reattachment Point in Subsonic Two-Dimensional Steady Base Flow," Aero Quart., 55-65, Feb.

Taylor, G. I., and G. K. Batchelor (1949), "The Effect of Wire Gauze on Small Disturbances in a Uniform Stream," Quart. J. Mech. and Appl. mech., 2, No. 1, p. 1. See also Dryden and Schubauer (1949).

Teyssandier, R. G., and M. P. Wilson (1974), "An Analysis of Flow through Sudden Enlargements in Pipes," JFM, 64, Pt. 1, 85-95, June.

Tutu, N. K., and R. Chevray (1975), "Cross-Wire Anemometry in High-Intensity Turbulence," JFM, 71, Pt. 4, 785-800.

Vagt, J. D., and H. Fernholz (1973), "Use of Surface Fences to Measure Wall Shear Stress in Three-Dimensional Boundary Layers," Aero. Quart., 26, 87-91.

Westphal, R. V. (1982), "MINC Software for Operating the Malvern Pulsed-Wire Anemometer," Report #IL-61, Thermosciences Div., Dept. of Mechanical Engrg., Stanford University, November.

Westphal, R. V., J. K. Eaton, and J. P. Johnston (1981), "A New Probe for Measurement of Velocity and Wall Shear Stress in Unsteady, Reversing Flow," J. Fluids Engrg., 103, No. 3, 478-482, Sept.

Wigeland, R. A., M. Ahmed, and H. M. Nagib (1978), "Management of Swirling Flows with Application to Wind Tunnel Design," AIAA J., 16, No. 11, 1125-1131, November.

Winter, K. G. (1977), "An Outline of the Techniques Available for the Measurement of Skin Friction in Turbulent Boundary Layers," Prog. Aero Sci., 18, 1-57.

Young, A. D., and J. N. Maas (1936), "The Behavior of a Pitot Tube in a Transverse Total-Pressure Gradient," Report #1770, Aero. Res. Council, London.

Zemanick, P. P., and R. S. Dougall (1970), "Local Heat Transfer Downstream of an Abrupt Circular Channel Expansion," ASME J. Heat Trans., 92, 53-60, February.

Appendix A

WIND TUNNEL MODIFICATIONS AND FACILITY PERFORMANCE

Introduction

Recent investigations uncovered severe spanwise nonuniformity of the mean velocity within the test section of the backstep flow facility located in the upstrairs laboratory of Building 500. Complete redesign of the facility was undertaken to provide a uniform mean flow at the test section entrance, as well as to lower the free-stream turbulence intensity. This appendix contains diagnostic data for the old facility, a description of components used for the modifications, and the resulting flow characteristics after modifications were completed. Professor Hassan Nagib (while at Stanford on sabbatical leave from Illinois Institute of Technology in Chicago) provided guidance for much of the redesign, and he deserves credit for the success of the work.

I. The Old Backstep Facility

A schematic of the old backstep facility (before any modifications were implemented) is shown in Fig. A-1. This is the same facility used by Eaton and Johnston (1980), which is described in some detail in this reference. Several mild symptoms of the problems eventually diagnosed were noted during the course of preliminary experiments during the summer of 1980. These were:

- High free-stream turbulence intensity (u'/U_∞ = 0.5% about 15 cm upstream of the step on the tunnel centerline for U_∞ = 12 m/s).
- A small but measurable spanwise variation in free-stream velocity (1% difference in U_∞ at a location 15 cm above tunnel centerline vs. the value 15 cm below centerline at U_∞ = 12 m/s).
- Long integration times (> 20 sec) were needed within the boundary layer 15 cm upstream of the step. Experience in other facilities indicated that under similar conditions only 10 sec were typically required. This symptom indicated the presence of low-frequency unsteadiness.

These observations prompted the more thorough investigations of spanwise nonuniformity described below.

A simple device was installed to obtain spanwise profiles of total pressure about 2.5 cm upstream of the step edge (see Fig. A-4). The device allowed a continuous spanwise traverse from 27.5 cm above centerline to 27.5 cm below (the center 55 cm of the total 61 cm span). The probe could be positioned at a fixed Y location anywhere in the inlet duct, whose width is 7.62 cm. A square-ended total pressure probe made of a hypodermic needle soldered into stainless stell tubing was mounted in the traverse. The probe had a tip diameter of 0.71 mm (0.028 in.). The reference pressure was taken at a wall static tap 2.5 cm upstream of the step. Note that the step wall was removed for these tests, so that the static pressure was very nearly atmospheric at the step edge and at the plane where the total pressure was being mapped. The probe holder rode smoothly on a lubricated aluminum bar which was fitted with flanges on the end so that it could be clamped to the test section side walls. A home-made Nichrome slidewire (diameter 0.25 mm) was used as a linear position transducer by applying a small voltage (50-100 mV) to the entire length and measuring the variation in voltage between a sliding pick-off and one end of the wire.

Spanwise total pressure profiles are shown in Fig. A-5(a) for various values of Y/H with the free-stream velocity at the design speed of about 12 m/s. A small free-stream total pressure variation is noted, but profiles within each boundary layer display an even more marked spanwise nonuniformity. Moreover, as luck would have it, the worst problems seem to be right on the tunnel centerline, where all the instrument ports are located!

II. Diagnosis and Conceptual Redesign

It was felt that the existing upstream separating boundary layer was not adequately two-dimensional to be considered a "normal" two-dimensional turbulent boundary layer. A further concern was that this severely three-dimensional flow might produce substantially different entrainment in the separated shear layer compared to that produced with a truly two-dimensional mean flow at separation. It was also thought that a much lower free-stream turbulence intensity than the measured 0.5% value would be quite easily obtained. There seemed ample reason to believe that improved inlet flow quality would be necessary if a canonical experiment was to be performed in the step configuration.

Several shortcomings in the old facility were supposed to be responsible for the poor flow quality. Firstly, there was no flow conditioning between the blower and the diffuser. One may expect that the particular diffuser design used (a multi-vaned device of area ratio 4.5 and with large opening angle) would be quite sensitive to inlet flow quality. Some inter-vane cells might stall, and the vanes would be expected to produce wakes. If stall did occur, a highly skewed flow would result at the honeycomb, causing it, in turn, to operate with some stalled cells. In any case, the honeycomb in use at the time seemed to have much too large a cell size and length (ref. Mehta & Bradshaw, 1979, or Loerke & Nagib, 1976). Finally, no turbulence-reducing screens were employed downstream of the honeycombs.

The blower exit-flow profile was checked by disconnecting the blower from the diffuser and measuring the exit-flow total pressure distribution--see Fig. A-3(a). Note the large region of no flow adjacent to the region of highest velocity; this appeared to be caused by the irregular geometry of the exit. This test verified the need to improve the uniformity of the flow to the diffuser, as such a distorted flow is bound to impair the performance of even well-designed diffusers of such high opening angle and area ratio as this.

The advice of Prof. Nagib, based on his experience in performance of flow-conditioning components at Illinois Institute of Technology, was used very heavily in the redesign of the facility. His unique observation was the idea that deices designed to improve flow uniformity (e.g., grids or screens) must be sized to address the length scales of the nonuniformity by promoting turbulent mixing at these scales, not just to improve uniformity through the well-known effects of pressure drop. These considerations often yield much larger mesh sizes than are conventionally used and tend to rule out the use of high-solidity devices (e.g., plates with small perforations or very dense screens). Other contributions of Nagib and co-workers included design data for honeycombs and for relative positioning of wind tunnel components.

III. Modifications

The modified facility is shown in Fig. A-2. The changes implemented are summarized below.

- A short duct containing two coarse grids and a small-celled, short honeycomb followed by a screen was installed directly downstream of the blower (just upstream of the diffuser). It functions to radically improve flow uniformity to the diffuser inlet (via the grids) and to reduce inlet swirl (the honeycomb accomplishes this). The screen at the diffuser inlet prevents separation at this location of abrupt change in wall shape, and breaks up the small shear layers formed by the honeycomb.
- The diffuser vanes were removed, and two coarse grids were installed. The grids were designed and positioned to prevent any pressure recovery (and thus stall) within the diffuser and to promote the mixing necessary to yield a uniform flow in the settling chamber. The second grid was placed right at the diffuser exit--another location of abrupt change in wall shape.
- The strange, large, long-celled phenolic honeycomb along with the 0.6 m long duct which housed it were removed. Plastic soda straws were installed to act as a honeycomb in the remaining settling chamber duct.
- Three 24-mesh screens were placed downstream of the straw pack, the first acting to restrain the straws from traveling into the test section. These screens were tensioned using a home-built screen stretcher, then fastened to specially constructed wooden ducts which were designed to act as frames. Screens were clamped between flanges of adjacent ducts. However, the screens tended to sag perceptibly after installation, so that the stretcher was left in place after installing the farthest-downstream screen. A better screen-holding design should incorporate a method for maintaining continuous tension on the screens.

- The nozzle suction assembly was removed and the joint between the last settling chamber and the nozzle was smoothed by hand, using an epoxy filler.

A list of the materials used in the modifications and the suppliers appears as Table A-1. The total cost of all materials for the modifications was about $400, and a few days of shop time were required to fabricate the wooden ducts and to reassemble the contraction. Thus the total cost of modifications was about $1000. The facility was inoperative for about four months for diagnosis, redesign, and requalification.

IV. New Facility Performance

Initially, there was some concern that the flow conditioning components would contribute significant pressure losses to the overall system, resulting in a higher blower loading at a given flow rate. Estimation of the component pressure losses (see Table 2) showed that less than one inch of water additional pressure loss would be incurred--the largest single pressure loss accrues due to the honeycomb used in the blower exit duct. The flow conditioning devices located in the settling chamber make a small contribution to the pressure loss, because this is a region of very low dynamic pressure. It seems safe to generalize that most open-loop blower facilities with flow conditioning in the settling chamber can be modified without much regard for the additional pressure losses incurred. In the current case, the comparatively large loss incurred from the small flow-conditioning duct upstream of the diffuser was quite tolerable, because the blower was running lightly loaded anyway. The honeycomb is not a critical component in the redesign in any case, and could probably be omitted with little degradation in system performance.

The flow to the diffuser inlet was checked to verify its uniformity. For these tests, the short duct with two grids was installed downstream of the blower, but the diffuser was disconnected and the screen-honeycomb assembly removed. An amazing improvement in flow quality is shown by comparing the total pressure maps of Figs. A-3(a) and (b). It is even more pleasing to realize that the improvement shown was accomplished with so little cost in terms of pressure loss (only about 0.28 inches of water at design velocity of 12 m/s).

Again, spanwise total pressure profiles were recorded at the test section for four values of Y/W_1. These are shown in Fig. A-5(b), and reveal that spanwise total pressure is uniform across the center mid-span within about 2%, translating to mean velocity uniformity within 1%. The worst profiles in Fig. A-5(a) show spanwise nonuniformity in total pressure of about 10-20%; thus, spanwise uniformity has been improved by an order of magnitude. Inlet turbulence intensity was now about 1/4%--reduced by a factor of two.

V. Conclusions

1. Nonuniformities in spanwise velocity, high free-stream turbulence intensity, and low-frequency phenomena (manifested by long integration times) are reliable indicators of poor performance in flow-conditioning components of open-loop blower facilities.

2. The cost (in terms of pressure loss) of improving test-section flow in open-loop blower facilities with contractions will usually be small when modifications are made in the settling chamber.

3. Inlet-flow quality is best assessed by taking <u>continuous</u> spanwise traverses, some of which should be within the boundary layers. Measuring boundary-layer parameters at a few discrete spanwise locations <u>will not suffice</u>.

4. The publications of Nagib and co-workers should be consulted for component performance data. The general guidelines set forth by Mehta and Bradshaw, 1976, are also helpful.

5. Vaned diffusers have no place in low-speed wind tunnel design. The potential performance benefits (in terms of pressure recovery) are far outweighed by the undesirable vane wakes and possibility that inter-vane cells may stall. Constant-pressure designs should be used instead.

4. Blower-exit flows are likely to be of very poor quality and should undergo conditioning before the settling chamber--especially if the flow must pass through a diffuser first!

ITEM	DESCRIPTION	SUPPLIER	COST
1. Screen 4ftX15ft	24-mesh stainless wire screens; 70% open area 0.19 mm dia. wire 4 ft. wide rolls	Howard Wire Cloth 935 Howard St. San Francisco, CA 392-4778	$208
2. Perforated Plate 4ftX8ft	16 ga. mild steel 0.5in sq. perfs on 0.625in centers 64% open area	Duus Perforating 242 Phelan Ave San Jose, CA 293-5717	$96
3. Soda Straws 1 case	0.25in OD, 7.25in long unwrapped plastic bulk No. 5258 1 case is 50 boxes of 250 each	Palo Alto Egg & Fruit Co. 897 Commercial Ave Palo Alto, CA 494-7550	$22
4. Epoxy 2 kits	HYSOL 2-part Kit 1-C "EZ Patch" 4 oz. per kit	K. R. Anderson Co. 136 Wolfe Rd. Sunnyvale, CA 736-6730	$8
5. Misc. (obtained from stock, EE stores, or hardware store) 0.125in thick rubber No. 10 1.25in FH wood screws 1/4-20 Hex bolts, nuts, and washers 1/2 AD plywood, 4ftX8ft sheet 3/4 particle board, 4ftX8ft sheet 1/4 cell X 3in phenolic honeycomb, 10inX14in approx total cost of misc. hardware: $75			

Table A-1 : Materials used for facility modifications.

DEVICE (1)	"K" FACTOR (2) K	AREA FACTOR (3) AF	LOSS FACTOR (4) LF	PRESSURE DROP AT 0 35 INS WATER TEST SECTION HEAD
1 grid	1.2	0 33	0 4	0 14
2 "	"	"	"	0 14
3 honeycomb		"		
4 screen	5	"	1 65	0 58
5 grid	1 2	0 049	0 059	0 021
6 grid	1.5	0.016	0 024	0 008
7 straw pack		"		
8 screen	5	"	0 08	0 028
9 "	0 8	"	0 013	0 005
10 "	0 8	"	0 013	0 005
TOTAL FOR MODIFICATIONS				0 95 INS WATER
COMPONENTS				
NOZZLE (8:1)			1	0 35
TEST SECTION (1 67 EXPANSION)			-0 3	-0 11
DIFFUSER (4 5 AREA RATIO)			-0 05	-0 018
FILTER AT BLOWER INLET			(5)	0 25
COMPONENT TOTAL				0 47 INS WATER

TOTAL BLOWER PRESSURE RISE - NEW FACILITY 1 4 INS WATER

NOTES

(1) Device numbers as in Figure A-2

(2) K factors are defined as

$$K = \frac{\text{pressure drop across device}}{\text{local dynamic head}}$$

(3) Area factor is the ratio of test section area to device area, squared

$$AF = \left(\frac{\text{test section area (72 square inches)}}{\text{device area}}\right)^2$$

(4) The loss factor is the pressure loss normalized by the dynamic head in the test section.

$$LF = K \times AF$$

(5) For the 5 micron (nominal) filter material used, the pressure drop is computed from

$$LF = \frac{0.02 \text{ (ins water per m/s)} \times U \text{ test section}}{\text{test section dynamic head}}$$

e.g., for U = 12 m/s, head = 0.35 ins. water and LF = 0.7

Table A-2 : Pressure-loss estimates for new wind tunnel facility

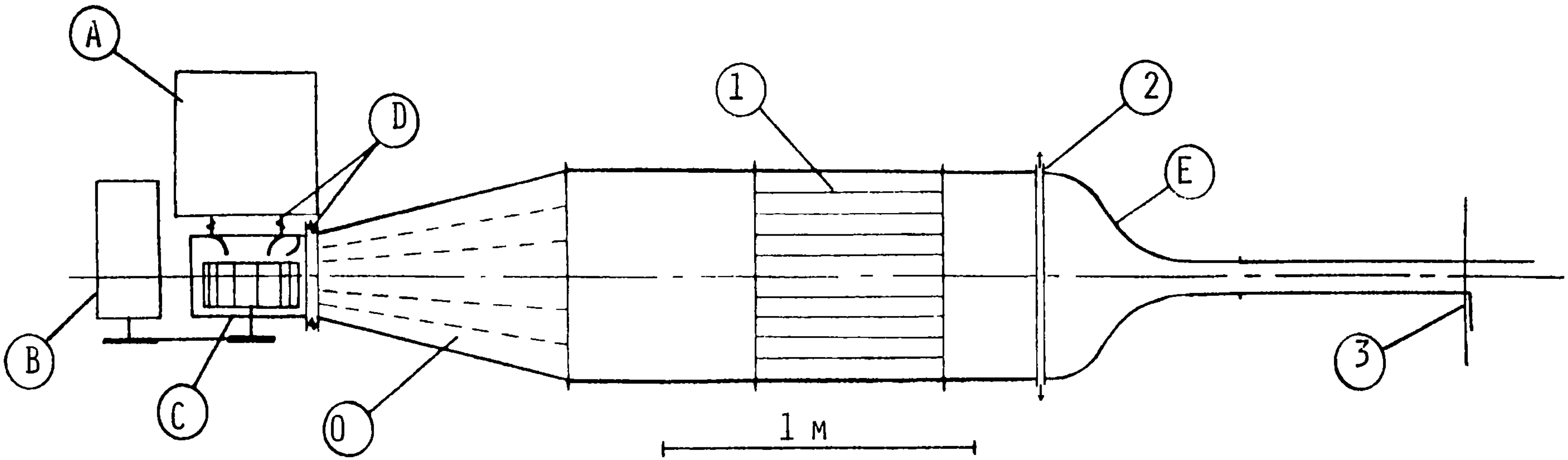

A Filter box, 5 micron nominal, 4 sq. meters area
B 3-phase motor, eddy-current clutch and speed control
C Airfoil-blade blower
D Flexible joints
E 8:1 contraction
F Plane of spanwise traverses (2.5 cm upstream of step edge)

0 Multi-vaned diffuser; 4.5 area ratio
1 Honeycomb; 1.25 cm cell size by 60 cm long
2 Nozzle suction assembly

Fig. A-1. Original (unmodified) wind-tunnel facility.

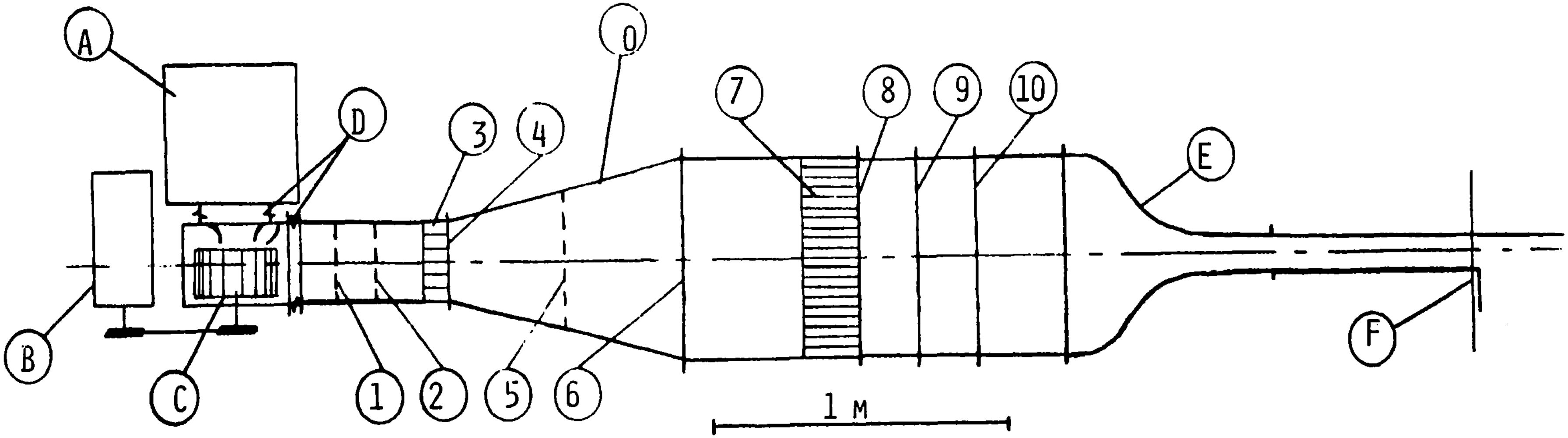

Lettered components as in Figure 1

0 Constant pressure diffuser; 4.5 area ratio
1 Grid 1.25 cm square perfs on 1.6 cm centers (64% open area)
2 Grid "
3 Honeycomb 0.6 cm cell, 7.5 cm long phenolic
4 Screen 24 mesh, 70% open area
5 Grid (as item 1)
6 Grid "
7 Straw Pack 0.64 cm cell OD, 18.4 cm long
8 Screen (as item 4)
9 Screen "
10 Screen "

Fig. A-2. Wind-tunnel facility after modifications.

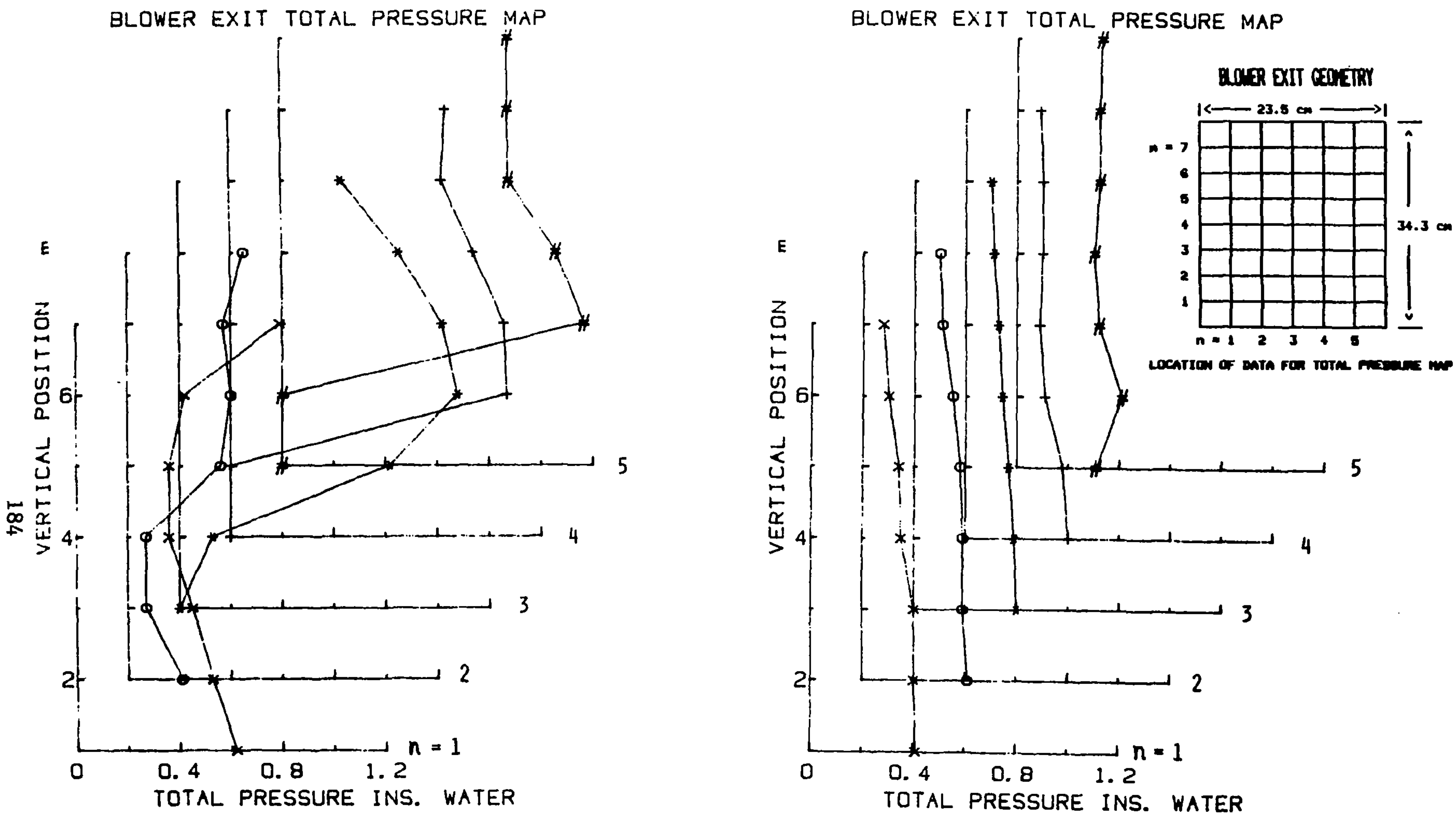

(a) Blower exit with no flow conditioning

(b) Blower with two grids downstream

Fig. A-3. Blower exit flow total pressure maps with and without flow-conditioning grids.

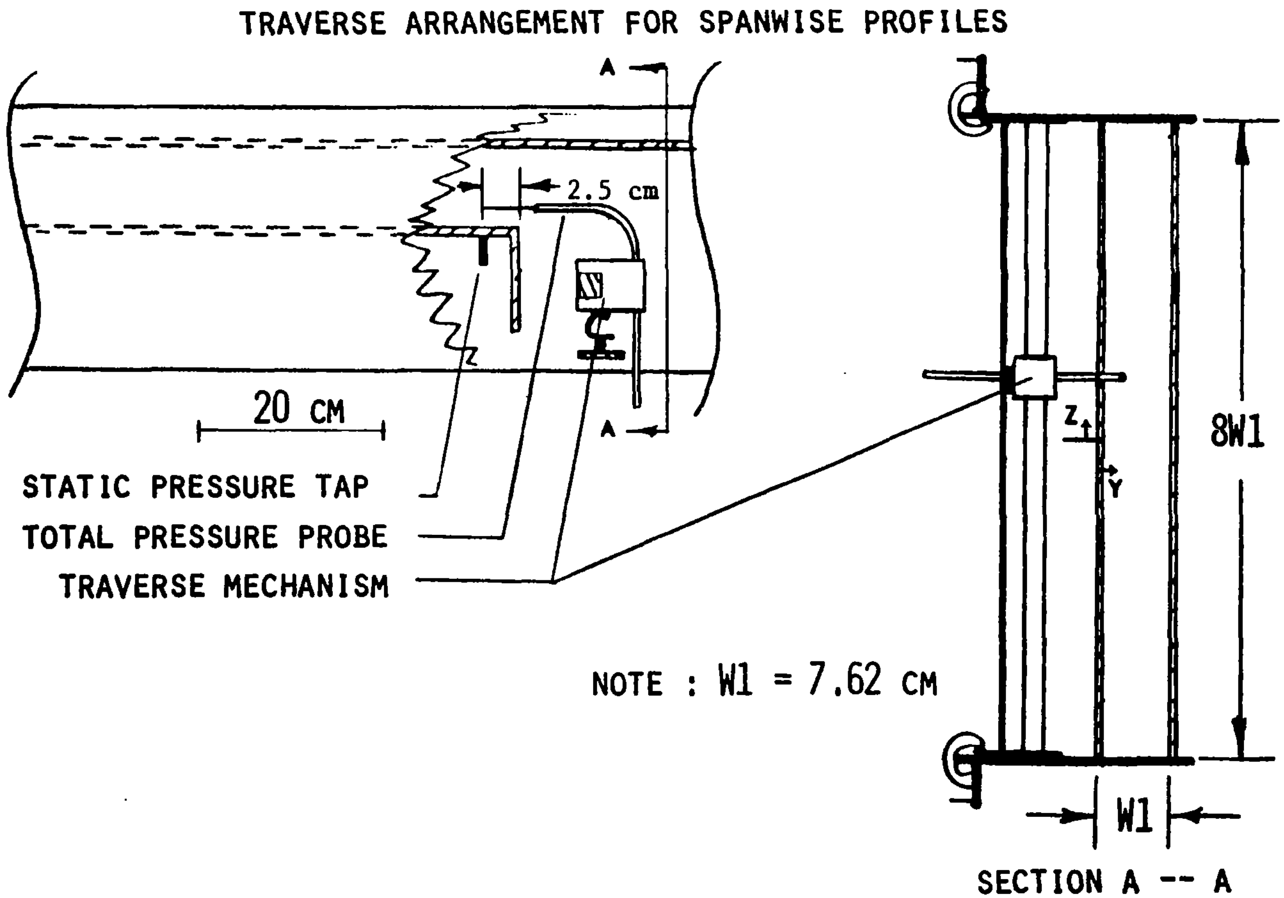

Fig. A-4. Traverse location and arrangement for spanwise total pressure profiles.

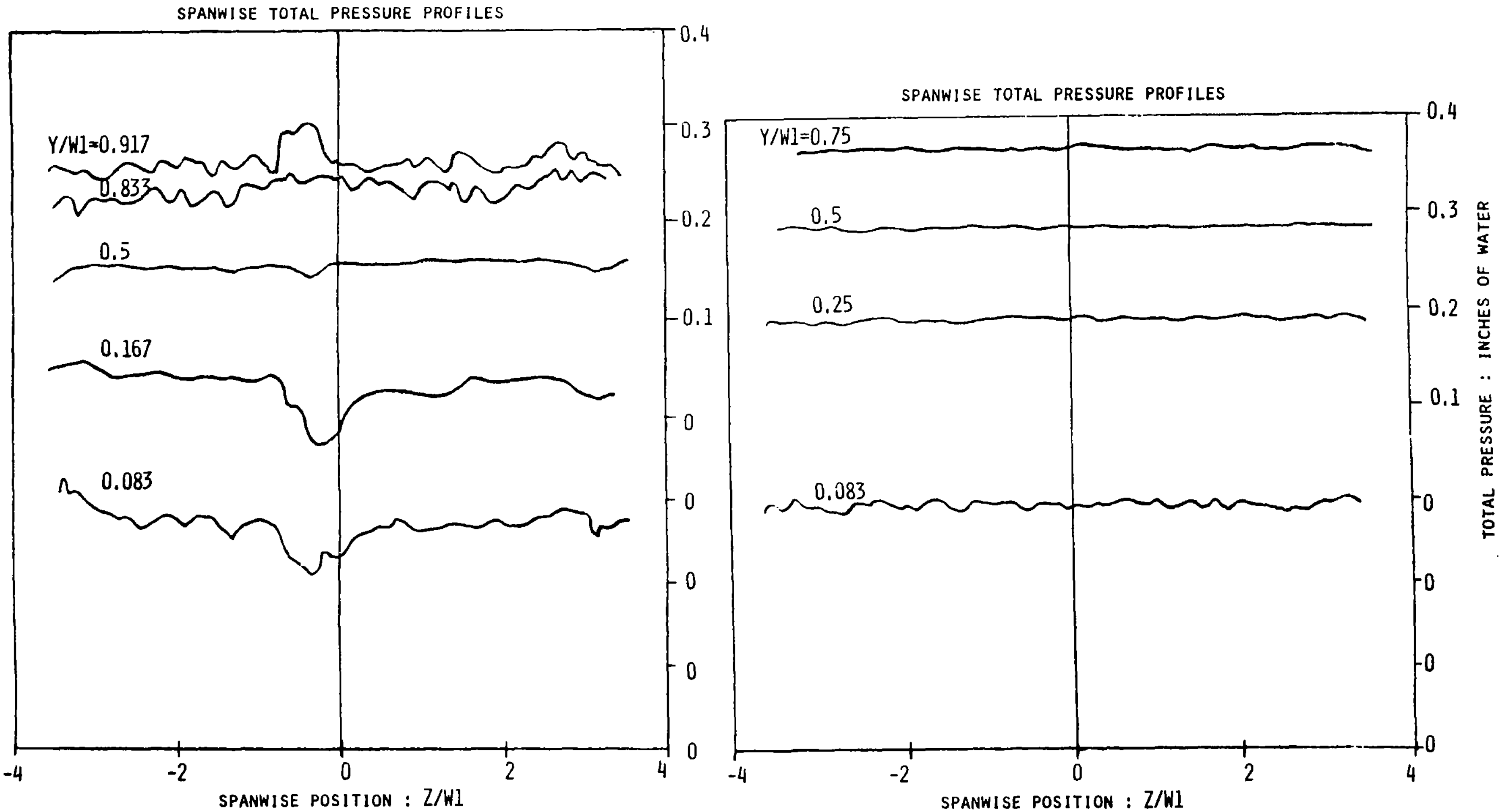

(a) Spanwise traverse - old facility

(b) Spanwise traverse - new facility after modifications

Fig. A-5. Spanwise total pressure profiles before and after facility modifications.

Appendix B

SMOKE-WIRE TECHNIQUE

B.1 Introduction

The methods and equipment used to perform smoke-wire visualization in the single-sided sudden expansion are briefly discussed. Although the technique is quite widely used in other laboratories, little use had been made of this visualization method in our research group at Stanford. Adams and Honami (1980) detail the first experience with the smoke wire in our group. They encountered severe difficulties, many of which have been eliminated with the technique discussed here. This appendix, then, is mainly intended to record relevant experience for future workers, pointing up areas where critical parameters must be controlled for best results.

Batill and Mueller (1981) provide an interesting discussion of the history of the smoke-wire technique and some general guidelines for its use. Corke et al. (1977) describe a clever control circuit and automatic wire oil-coating system which is now sold commercially and was purchased for this study. An idea of the possible uses of the technique is provided by Corke (1981), who obtained very high-resolution smoke-wire photographs of a quality suitable for digital image processing to examine near-wall structural details of turbulence! Kasagi et al. (1977) show some examples of the technique applied to a case similar to the current study.

The discussion below will consider many factors which influence the quality of the resulting visualization. These include preparation of the facility, wire materials and oiling procedures, the synchronization of camera shutter and strobe with the presence of smoke, and photographic techniques. A schematic of the equipment used is shown in Fig. B-1, and an itemized list of equipment has been provided in Table B-1. Special care was needed to deal with problems encountered in this study, due to complicating factors such as a fairly high velocity (10 m/s) and the extreme gradients in velocity present in the separated flow. Although some high-speed motion pictures were taken, this subject will not be taken up here, because, with such high flow speeds, the duration of smoke burn was quite small (only 0.2 sec). Thus, less than a few hundred frames of film are exposed. Still photographs seemed to provide better resolution and as much information.

B.2 Apparatus and Techniques

B.2.1 Preparation of the Facility

Optical access to the test section is of course needed for lighting the smoke sheet and photographing the result. Less obvious is the need to eliminate all stray light sources and reflections from surfaces. The camera and strobe are always perpendicular to each other, so that two optical access areas are required. The surface directly behind the plane of smoke streaklines must be blackened. Other interior surfaces of the facility should be black for best results, leaving only openings for required optical access. It was found convenient to use double-stick tape and large sheets of heavy black paper cut to fit for covering the Plexiglass surfaces of the facility used here. More black paper was draped on the exterior surfaces of the facility to prevent stray light from entering the test section.

Some means of holding the smoke wire in the flow and coating it with oil must be provided. If the wire is vertical, the possibility of using the gravity feed probe designed by Corke et al. (1977) exists; note that this method cannot be used if flow velocity exceeds about 7 m/s, since the oil droplet is blown off the wire by the airstream. The probe supports would presumably be mounted through a hole in the test section. If the wire is horizontal, it could be coated using a motor-driven swab (this is done at Illinois Institute of Technology by Prof. H. Nagib and his students) or simply by hand. The latter was the method used in this study. Instrument ports were constructed with metal inserts through which the wire was inserted into the test section. Then the wire was made extra long and attached by spring clamps so that it could be quickly pulled through, coated with oil, and repositioned in the test section.

B.2.2 Wire, Oils, and Heating the Wire

The wire used should have good strength at high temperatures; thus either Nichrome or stainless steel are usually used. When extremely large gradients in mean velocity occur, some areas of the wire will get much hotter than others. This can cause wire breakage, so Nichrome should be used for these applications. Note that there will usually be some part of the wire near each end which "sees" a velocity near zero—thus, with a high flow speed (> 8 m/s for the 0.1 mm wire), there again appears a tendency for extreme temperature differences along the wire span.

Wire diameter must be small enough to avoid producing an unstable smoke streakline due to Reynolds number effects. An excellent example of the effect of using too large a wire diameter can be found in Schlichting (1979) on page 18. For Reynolds number based on diameter (Re_D) less than about 20, the wire wake remains straight and stable. In the range $20 < Re_D < 60$, instability begins, and at higher values of Re_D a large-scale pattern of vortex structures persists. Consistent with this picture, we found that reasonably coherent streaklines could be obtained as long as $Re_D < 60$. For a 0.1 mm wire in air, this implies a limiting flow velocity below 10 m/s. The wire diameter should always be as large as possible within the criterion for Re_D to give a long smoke burn and less chance of breakage.

Oils used should produce dense white smoke and must have proper surface tension to give an appropriate streakline spacing. Model train smoke or kerosene works well; for this study the former was used. Coating of the wire must be done carefully, especially with high flow speed, because thick coatings increase the effective wire diameter (producing an unstable wire wake) and require higher wire temperaturs to vaporize the oil. A cloth, cotton swab, or brush can be used, but best repeatability was obtained when thumb and forefinger were used to wipe off excess oil after coating with a brush.

A DC voltage is applied to the wire to heat it and thus vaporize the oil. A variable voltage supply was needed, because a slightly different optimal voltage must be used, depending on flow conditions and wire length, material, and diameter. The lower limit of required wire voltage can be determined at zero-velocity conditions. For 0.1 mm Nichrome wire about 20 cm long, 25 volts is a typical value. The voltage obviously need only be applied until all the oil is vaporized; this time can vary tremendously, depending on flow speed. Smoke duration is typically around 0.25 sec at 10 m/s, while a much longer duration is possible for lower speeds (more than 2 sec at 3 m/s). Either a 115V AC variac and rectifier or a DC power supply can be used, although either should be equipped with a large capacitor and be capable of supplying several amps. An HP model 6290A capable of supplying 3 amps at 40 volts was used.

B.2.3 Synchronizing Camera and Strobe with Smoke

Control circuitry consisting of several adjustable time-delay relays is used to synchronize the camera and strobe with the presence of smoke. A commercial unit manufactured by Flow Visualization Systems (precisely the design of Corke et al., 1977) was purchased. It provides several relays with various time delays for applying the voltage to the smoke wire and triggering the camera shutter. For the current work, the strobe was triggered by the camera, using "X"-synchronization. The camera shutter was initially actuated using a large solenoid to drive a cable release (this is the same as described by Corke et al., 1977). Later in the work, a new camera with motor drive was purchased which allowed the shutter to be triggered directly by a relay closure.

Typically, a delay of 0.1-0.5 seconds was employed from the time that the smoke wire was energized until the camera shutter was actuated. This delay is found by trial and error; with practice, this can be done without actually photographing the smoke but by simply varying the delay and viewing the result by eye. The delay setting was probably the most sensitive parameter, and considerable practice was required to get an idea of the appropriate delay. Of course, this setting is very easy to make at lower flow speeds, since the duration of smoke presence is so much longer.

B.2.4 Photographic Technique

Proper lighting is essential to produce high-quality photographs. Care in preparing the facility to eliminate reflections and stray light is important, as described above. Also, a strobe of extremely high intensity and very short duration will effectively "freeze" the action and give good contrast. The strobe light should be made nearly planar by using a slit covering the light; a double slit is even more effective. A black cover with a narrow slit was affixed to the strobe itself, and a second slit was made in the black paper for lighting access in the test section. A new strobe (General Radio type 1540) was purchased for this work; it gave a flash duration of only about 15 microseconds from a very bright quartz flash lamp. The accessory controller (General Radio type 1540-P1) allowed external triggering directly compatible with a camera "X-sync" connection.

Since the strobe light is very bright, and if care is taken to blacken the test section itself, the exposure is controlled by the strobe duration, brighness, and the f-stop selected. With the synchronization strategy described above, this means that the laboratory itself needn't be completely darkened to perform the visualization--subdued laboratory light is acceptable. This is a vast improvement over strategies such as described by Adams and Honami (1980), which require the shutter to be open for long periods (thus necessitating a totally darkened laboratory) and trigger only the strobe flash. A shutter speed setting of 1/60 sec and f-stop of 1.8-3.5 were used. Lenses with focal lengths of 50-85 mm were used. The longer focal length was often preferred to minimize parallax effect in photographs.

Tri-X ASA 400 black and white film was used for all photography. The film speed can be effectively pushed to 1200 with Acufine developer (this can often be done by commercial services on request) or to 1600 with Diaphine two-part developer. Both were used for this study, the latter being done in the darkroom in Building 500 (summary instructions appear as Fig. B-2). The negatives are printed on heavy bond paper of high contrast; if care is taken to produce high-quality negatives, the printing process is not too critical.

B.3 Summary and Conclusions

The smoke-wire technique described above has proved viable in air at flow speeds up to 10 m/s. Careful attention is especially warranted in preparing the test section, selecting the appropriate wire diameter, and coating the wire lightly and uniformly. High flow speed and large velocity gradient along the wire have made the current application somewhat more challenging than usual. Motion pictures did not prove too useful, due to the short duration of smoke. Improvement in the quality of results compared to that obtained by Adams and Honami (1980) in their earlier work in our group was mostly due to a better technique for synchronizing the camera, strobe, and smoke. Further improvements accrued from using a more suitable wire diameter, a brighter strobe with shorter flash duration, and processing the film with a faster developer.

ITEM	DESCRIPTION	SUPPLIER
A	Control electronics Time-delay relays for camera & strobe synchronization	Flow Visualization Systems 19 W. 401 Frontage Rd. Lemont, ILL 60439 (312) 567-3217
B	Smoke wire 0.1 mm Nichrome or 0.05 mm Nichrome	Clancy Associates 3303 Harbor Blvd. Suite H-5 Costa Mesa, CA 92626 (714) 957-1162
C	Strobe light, power supply, and controller General Radio Type 1540 and 1540 P-1	General Radio Corporation 300 Baker Avenue Concord, MASS 01742 (403) 727-4400
D	35 mm SLR camera system a - Nikon FE body b - " MD-12 motor drive c - " 50 mm f1.4 lens d - " 85 mm f2.0 "	Keeble & Schucat 290 California Ave Palo Alto, CA (415) 327-8996
Miscellaneous items -		
E	DC power supply for wire power HP6290A DC supply, 3 amps at 40 volts	lab check-out item
F	Wire oil "SEE-NIKS" train smoke oil	San Antonio Hobby
G	KODAK Tri-X ASA 400 Black & White film	Keeble & Schucat
H	Diaphine 2-part developer	"

Table B-1 : Smoke-wire equipment list

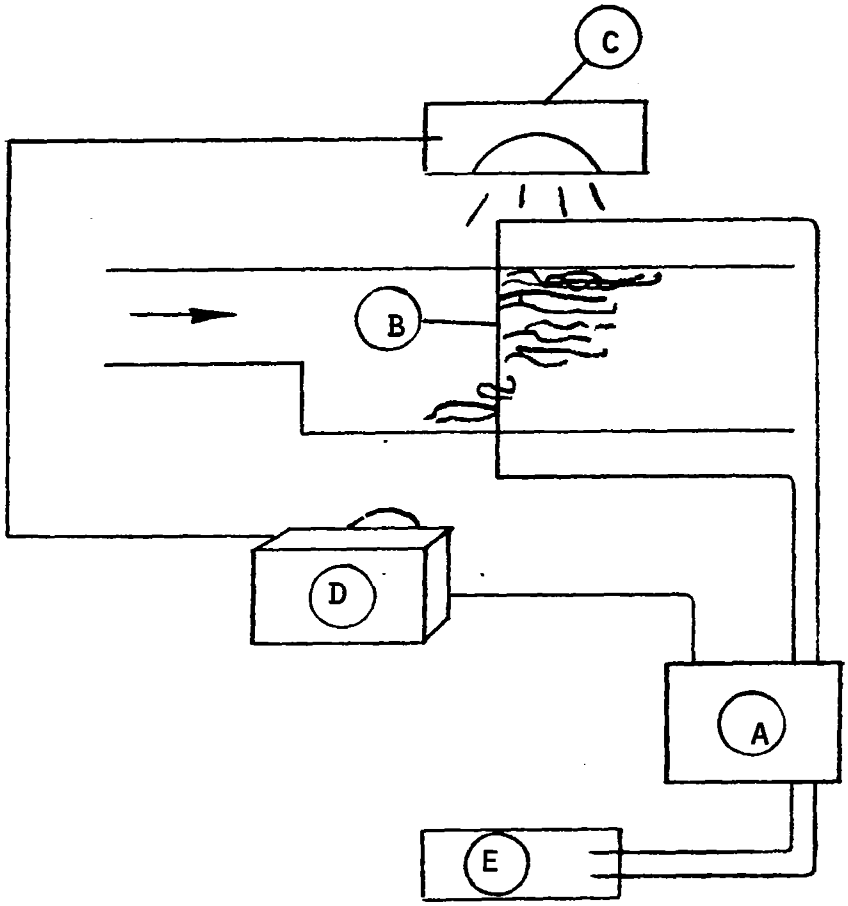

Fig. B-1. Schematic arrangement of smoke-wire visualization equipment (refer to Table B-1 for a description of the various components.

INSTRUCTIONS FOR PROCESSING TRI-X 400 WITH DIAPHINE DEVELOPER

IN DARKNESS

1. Remove exposed film from case and load onto Patterson tank ratcheting reel.
2. Insert reel into tub and set white light seal ring in place. Screw lid onto Patterson tank.

LIGHTS ON

1. Pour full quart of Diaphine part A quickly into tank. Agitate once each minute for a few seconds, leaving part A on the film 3 minutes. Pour A quickly back into the container.
2. Pour full quart of Diaphine part B quickly into tank. As with A, leave for 3 minutes and agitate for a few seconds every minute. Note that A and B should last for at least 5 rolls and turn cloudy and colored when spent.
3. Rinse with water for 5 minutes.
4. Fix with "rapid fixer" for about 4 minutes.
5. Rinse with water for 1 minute.
6. Cleanse using hypoeliminator for 2 minutes.
7. Remove developed film from Patterson tank and reel. Rinse in a bath of water for a few minutes, then wipe away water with the rubberized squeegee.
8. Hang to dry in film closet for an hour or so.

Fig. B-2. Summary of instructions for using Diaphine developer.

Appendix C

DETERMINATION OF REATTACHMENT LENGTH

The generally accepted definition of the reattachment point for two-dimensional flow is the location of zero average wall skin friction. However, as explained in Chapter 3, there were no techniques suitable for making skin-friction measurements in the reattachment region when this study began. Several techniques had been used by previous investigators, but it has been unclear how results obtained with these are related to the unambiguous definition of the two-dimensional reattachment point, $\overline{C}_f = 0$. Due to the development of the pulsed wall probe, it has been possible to compare direct measurement of the reattachment location with several other methods in the same experimental facility under carefully controlled conditions.

Three methods for determining reattachment length will be compared. These are listed below, then each is explained in more detail. Results of applying these different methods for determination of the reattachment location for the three main cases of this study are then compared in Table C-1.

1. $\overline{C}_f = 0$; the pulsed wall probe is used to measure $\overline{C}_f$.
2. $\gamma = 0.5$; γ is determined by three methods:
   - thermal tuft,
   - pulsed wall probe,
   - extrapolation of pulsed-wire anemometry data to the wall.
3. $X/H \to \overline{U}(Y \to 0) = 0$. Extrapolate the loci of points where $\overline{U} = 0$ (as measured by the pulsed-wire anemometer) to the surface.

Streamwise distributions of measured skin friction for Cases A and B (shown in Figs. 5-39 and 5-41) are interpolated to yield the location of $\overline{C}_f = 0$. Distributions of γ obtained with the thermal tuft were shown in Fig. 5-16 for each of the three cases. By interpolation of these data, the location of $\gamma = 0.5$ was determined. γ was also determined (using the pulsed wall probe) as the fraction of samples sensed by the downstream wire compared to the total number of samples sensed by either wire. The resulting distribution of γ vs. X/H was then interpolated as with the thermal tuft data. A third method for measuring γ is to extrapolate profiles of the γ versus Y measured with the pulsed-wire anemometer to the surface. These profiles are shown at each location in the reattachment region for all three cases in Figs. C-1, C-2, and C-3. Simple linear extrapolation of these curves was performed to yield γ distributions along the surface which were interpolated to give the streamwise location of $\gamma = 0.5$. For Case A, γ distributions determined from all three methods are shown in Fig. C-4. The thermal tuft and pulsed wall probe agree very closely, whereas the extrapolation of pulsed-wire data falls up to 5% from these. This is expected, because the extrapolation is rather steep, and the data do not extend very near the surface ($Y/H > 0.13$ for the pulsed-wire data).

Figure C-5 shows that the location of $\gamma = 0.5$ very nearly coincides with that of $\overline{C}_f = 0$ for Cases A and B. Values of skin friction in the reattachment region are plotted versus γ determined by the thermal tuft. In both cases, the location of $\overline{C}_f = 0$ coincides with $\gamma \approx 0.45$. Thus, the location of $\overline{C}_f = 0$ is less than that of $\gamma = 0.5$ by about 0.1-0.2H (see Table C-1).

From the mean velocity profiles measured with the pulsed-wire anemometer (see Figs. 5-18 through 5-20), the distance from the surface at which $\overline{U} = 0$ can be determined for successive streamwise locations. Plotted in Fig. C-6, these data were then linearly extrapolated to the surface for each case. This is the technique recently used by Durst and Tropea (1981), who were able to obtain considerably better definition near the surface with their laser anemometer. Notwithstanding the lack of near-wall velocity data in the current study, the extrapolated loci of points where $\overline{U} = 0$ gives results amazingly close to the other methods included in Table C-1.

The conclusion of this comparison is that all three methods examined can be used to measure reattachment length with an uncertainty of 0.2H, i.e., X_R/H can be measured with less than 3% uncertainty in all the cases reported here. The spread of the various values given in Table C-1 is about ± 0.2H for each case. The reattachment location determined by the pulsed wall probe is the most unambiguous, but since the values agree rather closely, it was decided to use the thermal tuft measurement as the reattachment location for consistency. The thermal tuft is considerably easier to use; further, other workers have used the device, so comparisons of current results will be on a sounder basis.

It is worth noting that all of the methods described above share three characteristics which are thought to be crucial--all are quantitative, time-dependent, and directionally sensitive. Methods which do not share these characteristics seem to be much less accurate. For example, Abbott and Kline (1961) and Kim et al. (1978) used visual methods in their step flows in water and air, respectively. Both report uncertainties of $\pm$ 1 step height in their determination of reattachment length (compared to $\pm$ 0.2H for the current study). It is also believed that extrapolation of $\overline{C}_f$ measurements made with a Preston tube downstream of reattachment (see, e.g., Bradshaw and Wong, 1972, or Smits, 1981) are very likely to contain similar uncertainties due to lack of directional sensitivity or time-dependent measurement capability. The curvature of the $\overline{C}_f$ vs. X/H distribution downstream of reattachment is substantial, as indicated in Figs. 5-39 and 5-41.

Many workers (e.g., Narayanan et al., 1974, and Brederode and Bradshaw, 1972) have used the surface oil-film method to determine reattachment length. Typical uncertainty in visual location of the reattachment position is given as a few tenths of a step height in the references cited above. In the current study, the test surface was vertical, so it wasn't possible to use this technique. It would be most desirable, however, to compare surface oil-film results with one of the techniques used here to verify its accuracy.

Method	$\gamma = 0.5$			$\tau_f = 0$	$\bar{U} = 0$
Case	**Thermal tuft**	**Pulsed wall probe**	**Pulsed wire**		
A	8.55	8.50	8.24	8.35	8.61
B	9.47	9.38	9.26	9.31	9.22
C	7.23	----	6.99	----	7.00

Table C-1 : Comparison of reattachment lengths measured by different techniques

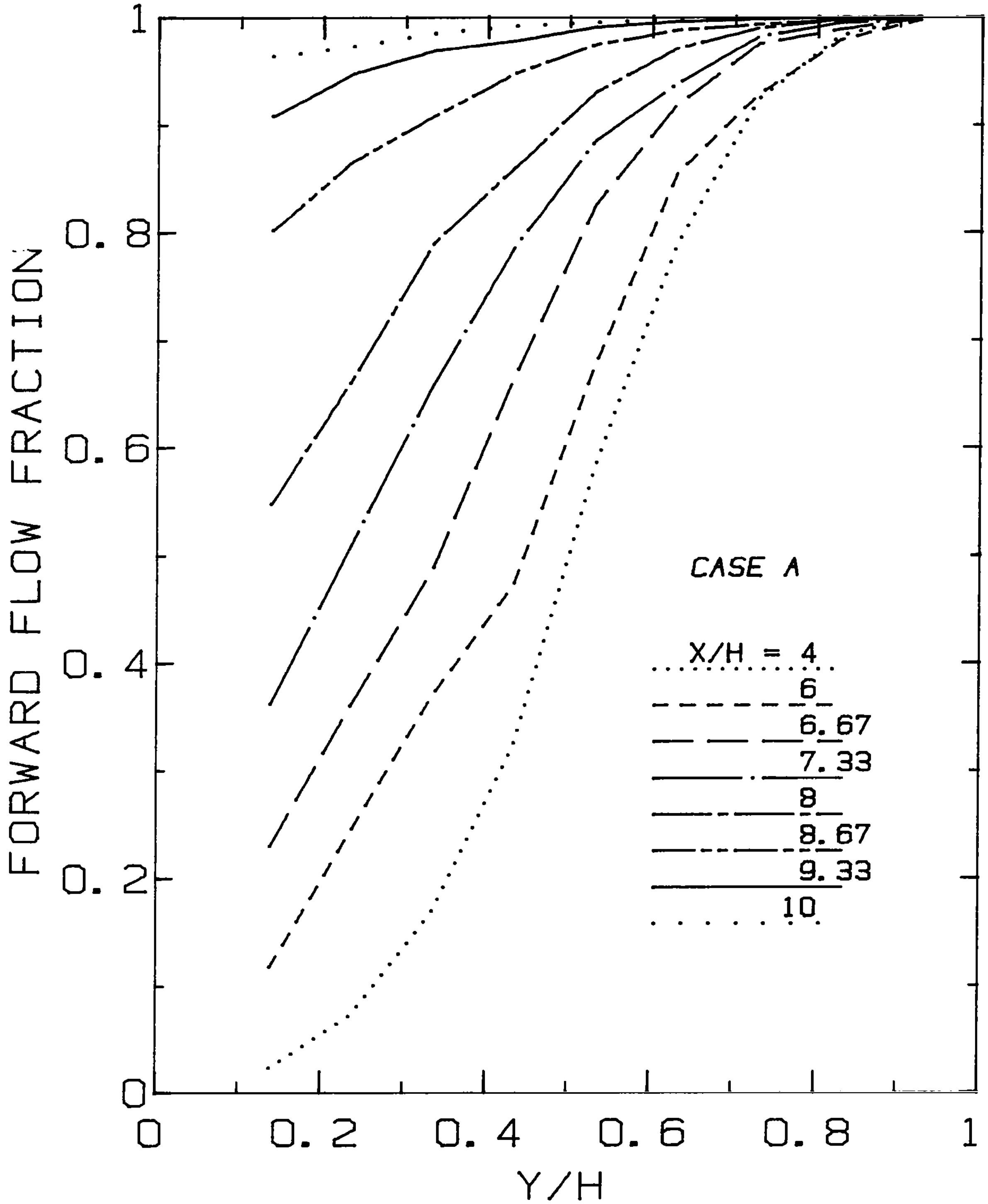

Fig. C-1. γ profiles for Case A from the pulsed-wire anemometer.

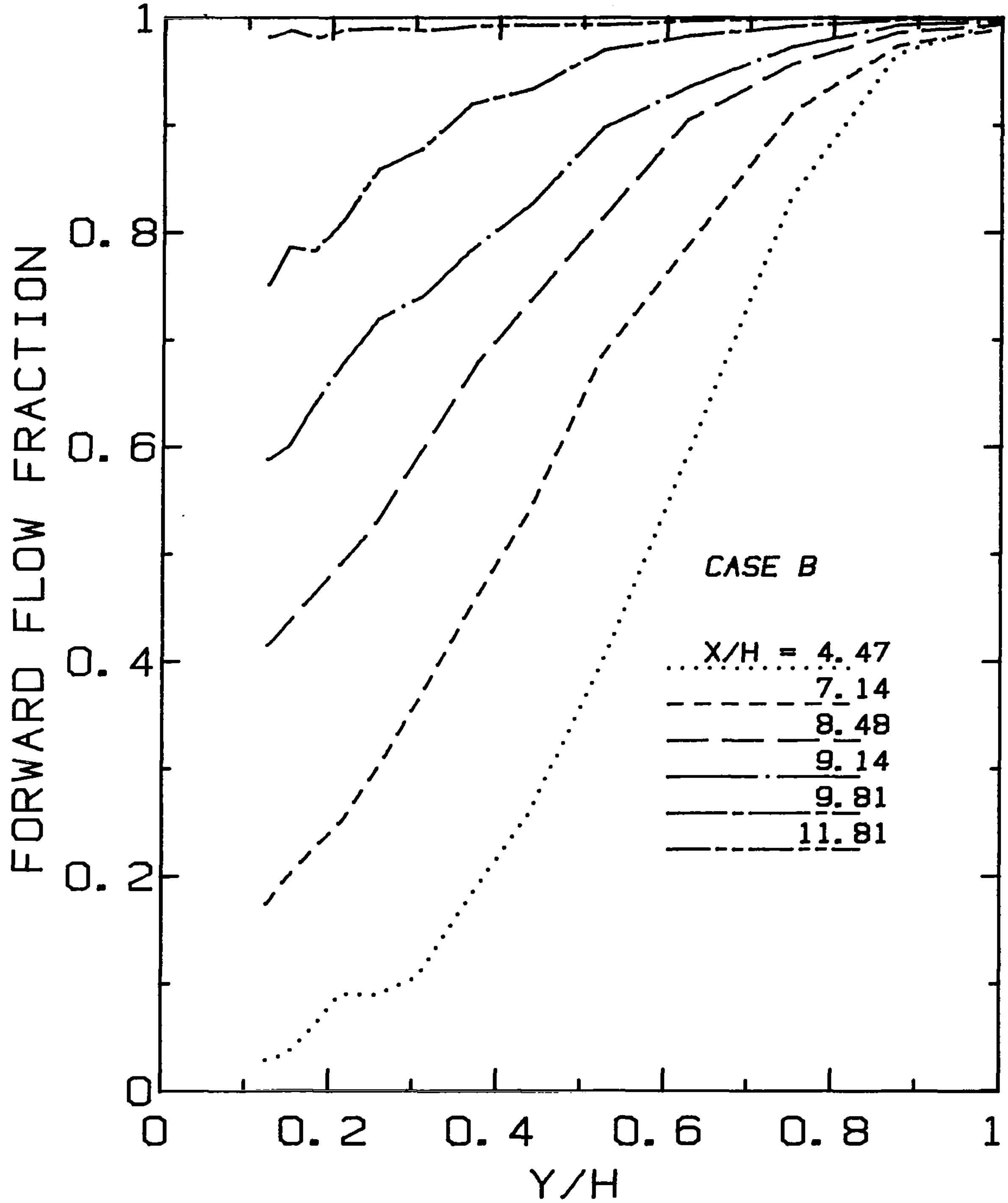

Fig. C-2. γ profiles for Case B from the pulsed-wire anemometer.

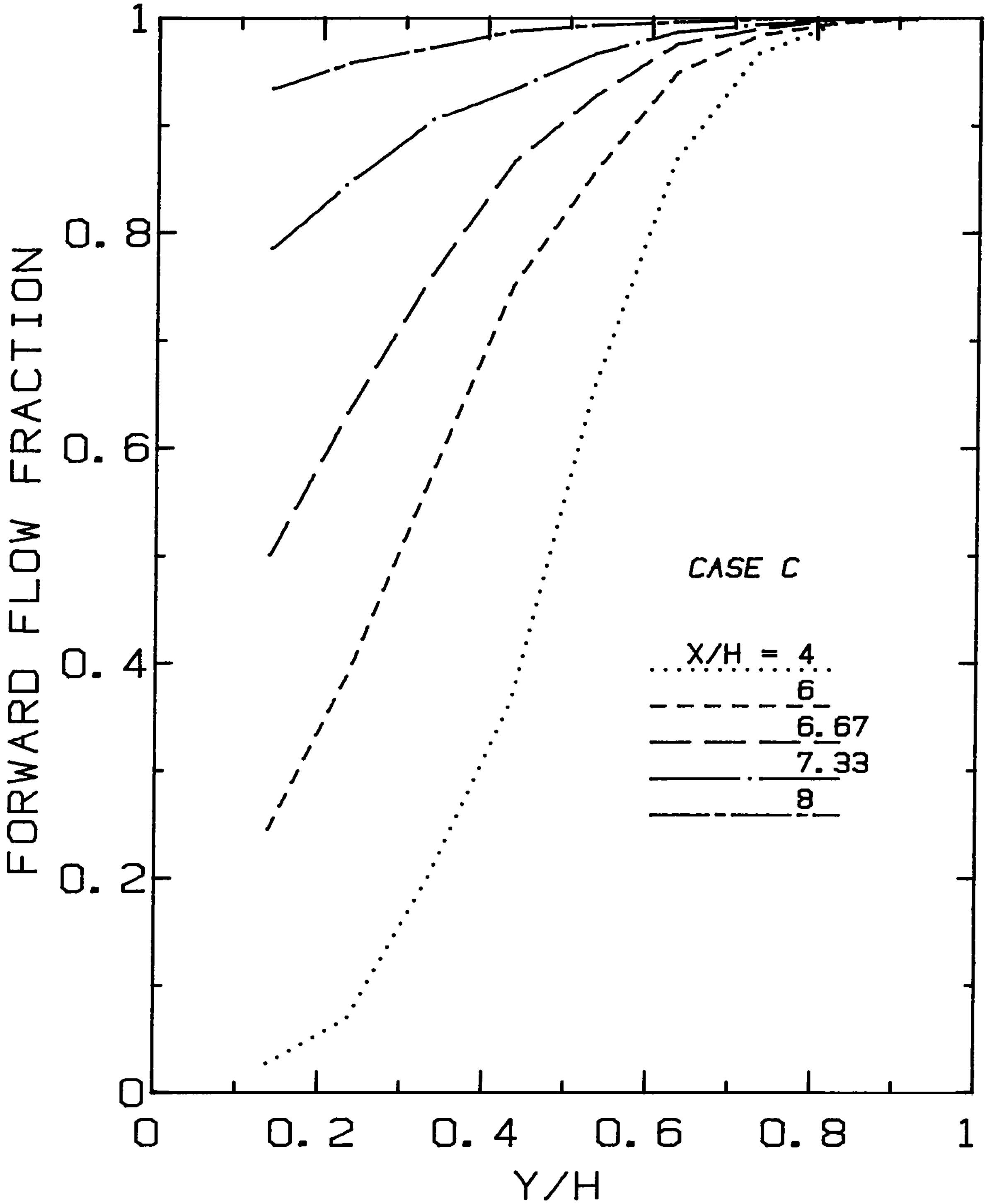

Fig. C-3. γ profiles for Case C from the pulsed-wire anemometer.

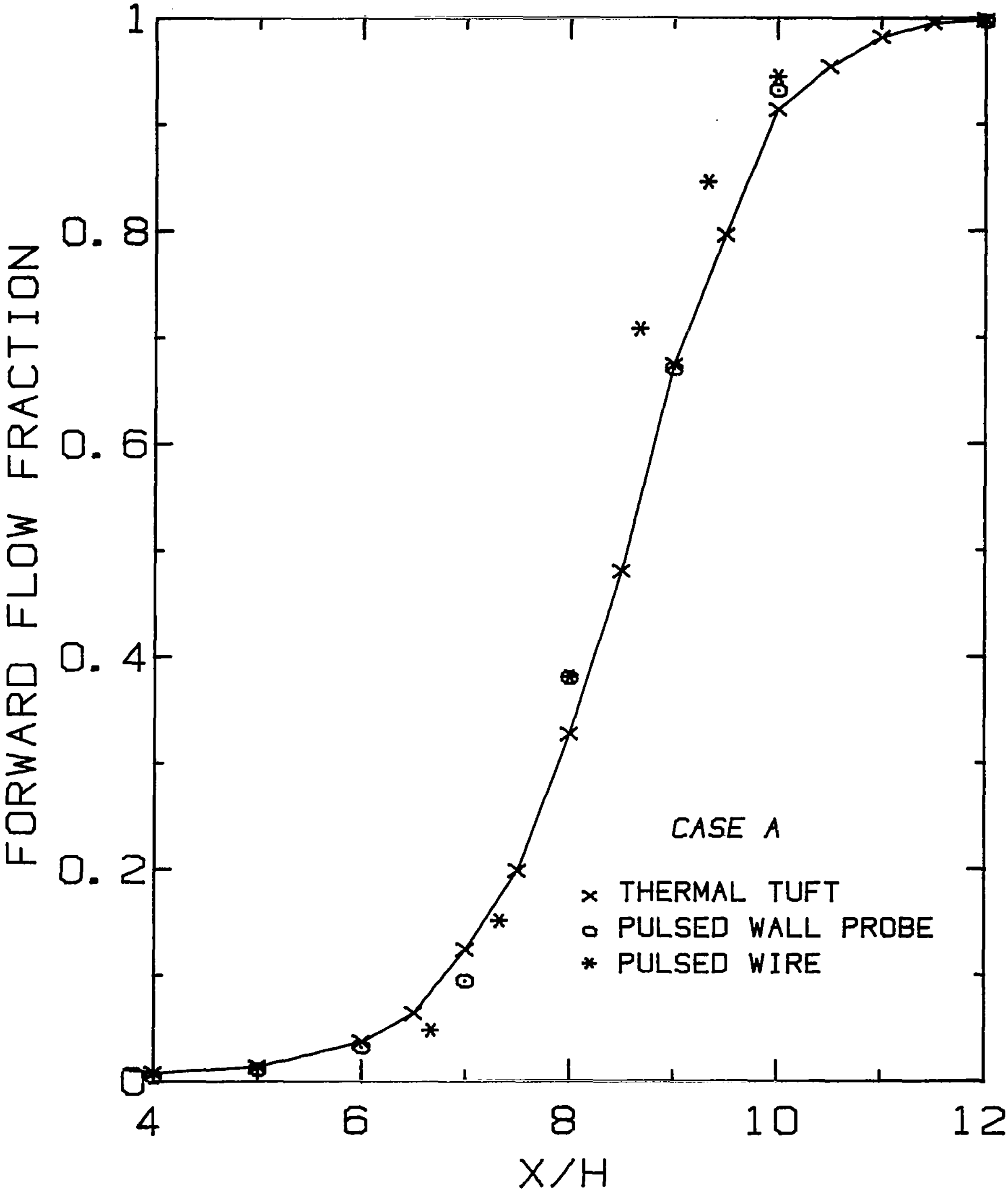

Fig. C-4. Comparison of three methods for measuring forward-flow fraction (γ) for Case A.

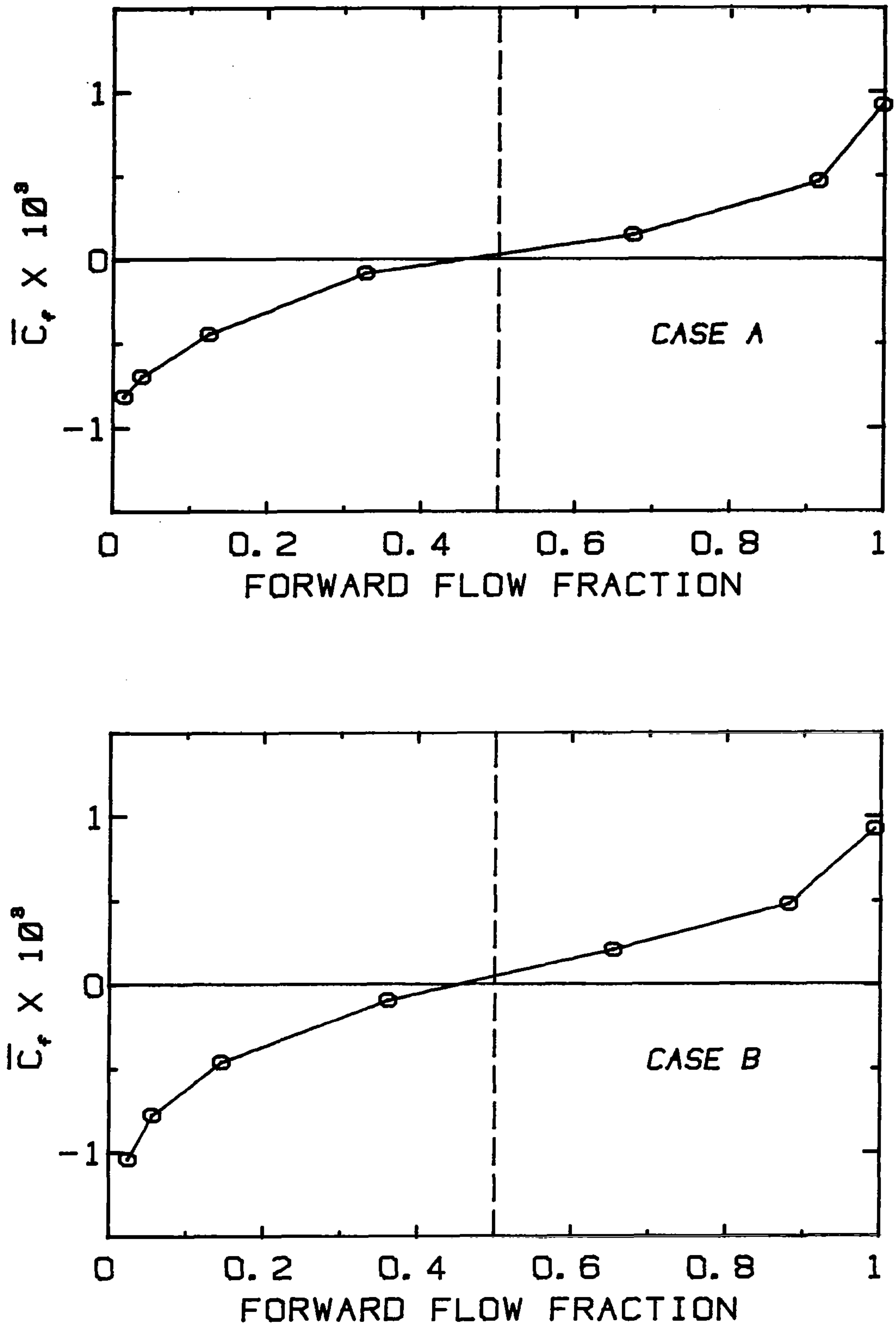

Fig. C-5. Skin-friction coefficient measured with the pulsed wall probe vs. forward-flow fraction, γ, measured with the thermal tuft. Only data in the reattachment region are plotted.

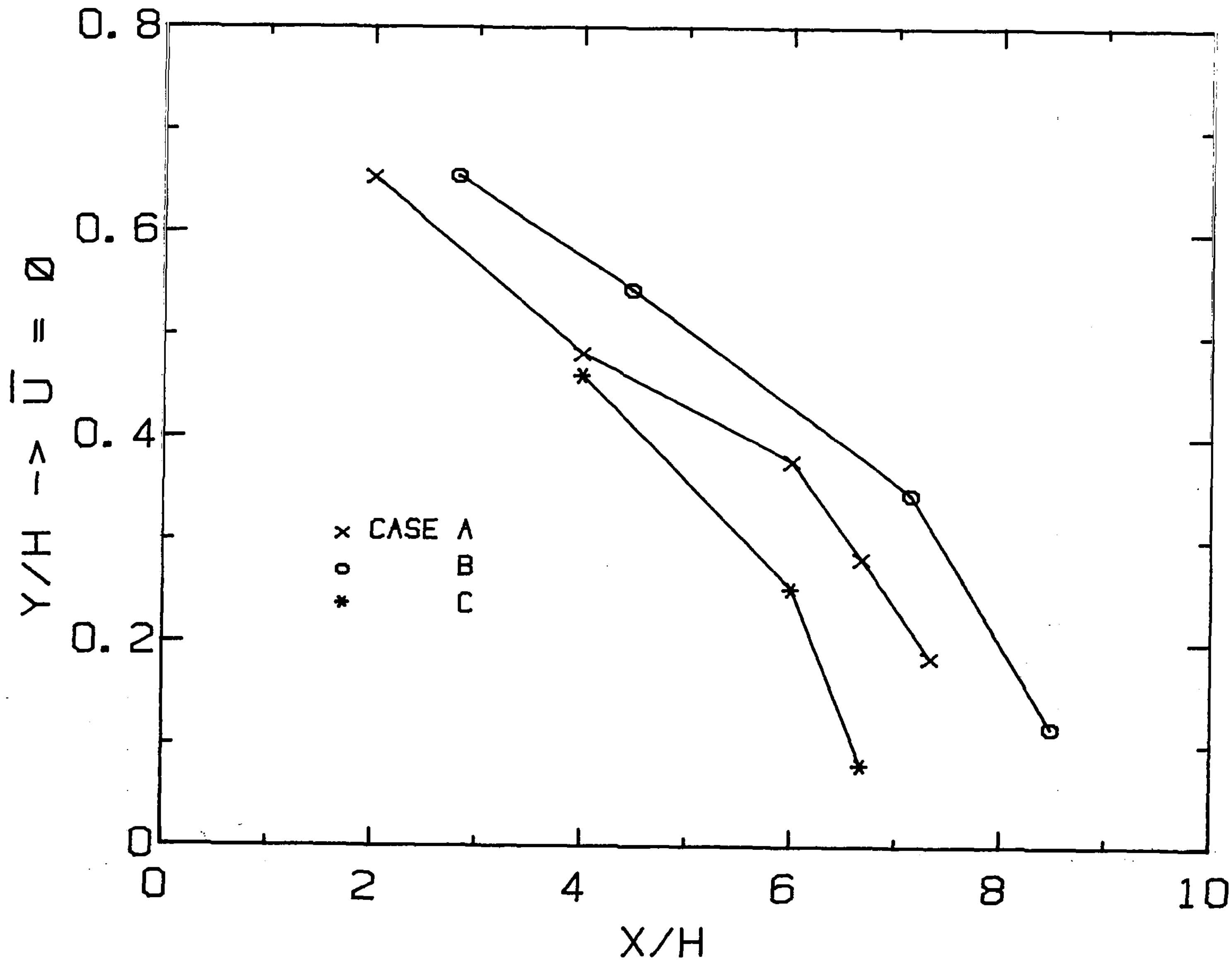

Fig. C-6. Loci of points where $\bar{U} = 0$, determined from mean velocity profiles upstream of reattachment measured with the pulsed-wire anemometer.

Appendix D

COMPARISON OF HOT-WIRE AND PULSED-WIRE PERFORMANCE

The performance of hot-wire anemometers in turbulent free shear layers has been questioned by many authors. For example, Tutu and Chevray (1975) point out that large errors in X-wire results can accrue in flows with local turbulence intensities $(u'/\overline{U})$ over 30%. Chandrsuda and Bradshaw (1981) caution against placing too much faith in hot-wire measurements in the backstep flow in regions of high turbulence intensity. However, many workers have used hot-wire anemometers in the reattaching flow, and it is therefore desired to investigate the expected errors in these data.

The pulsed-wire anemometer provides the potential for overcoming the difficulty of resolving the direction as well as the sign of the velocity component. However, this technique has not been widely employed, and some evaluation of the results in regions where other methods can be confidently used seemed in order. Baker (1977) has performed very similar tests with comfortingly similar results.

Three figures are presented to summarize the conclusions. These compare hot-wire and pulsed-wire measurements of $\overline{U}$ and u' in the reattachment region (where local values of $u'/\overline{U}$ exceed 0.5), the early recovery zone (with $u'/\overline{U}$ around 0.3-0.5), and farther downstream $(u'/\overline{U} \sim 0.25)$. The two methods agree very closely in the measurement of $\overline{U}$ at all locations (note that the hot-wire was not used very near the surface in the first two cases, because reversals of flow direction were known to exist there). however, u' measurements do not agree well, especially near the reattachment location. Far from the wall, where turbulence intensities are quite low $(u'/\overline{U} < 0.05)$, the pulsed-wire is expected to be in error, as discussed in Chapter 2. But within the shear layer, the hot-wire undermeasures u' by as much as 0.03 U_{ref}. This conclusion agrees with Baker's (1977) comparisons made in similar situations. The implication, then, is that previous results which have been obtained with a hot-wire anemometer may give erroneously low values of the peak Reynolds stresses which exist in the reattachment zone.

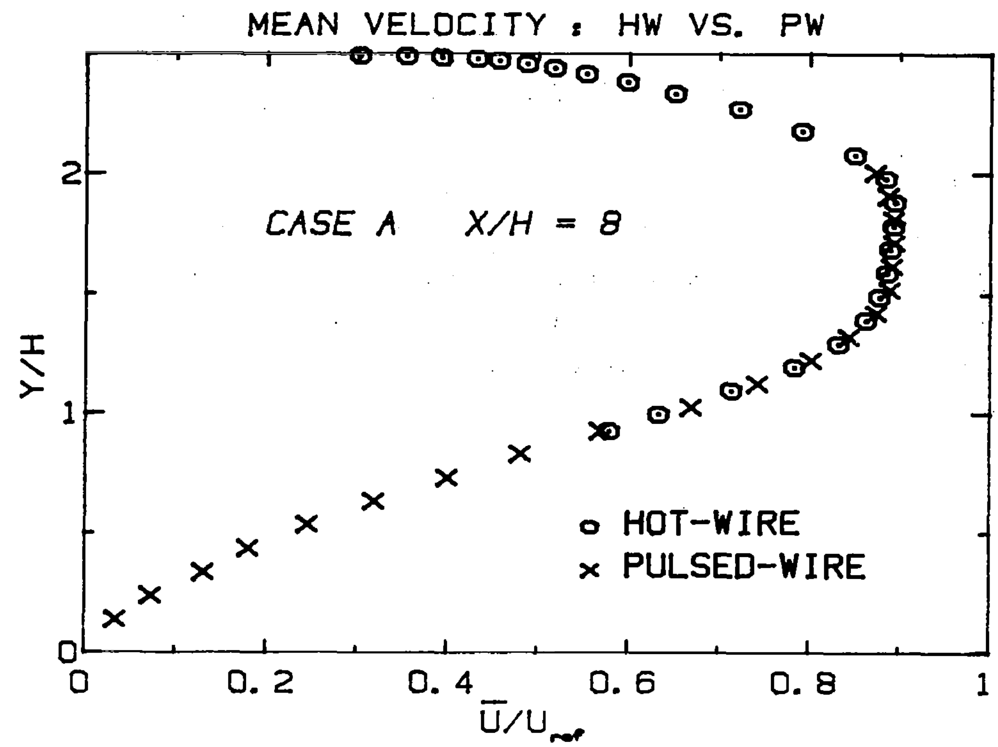

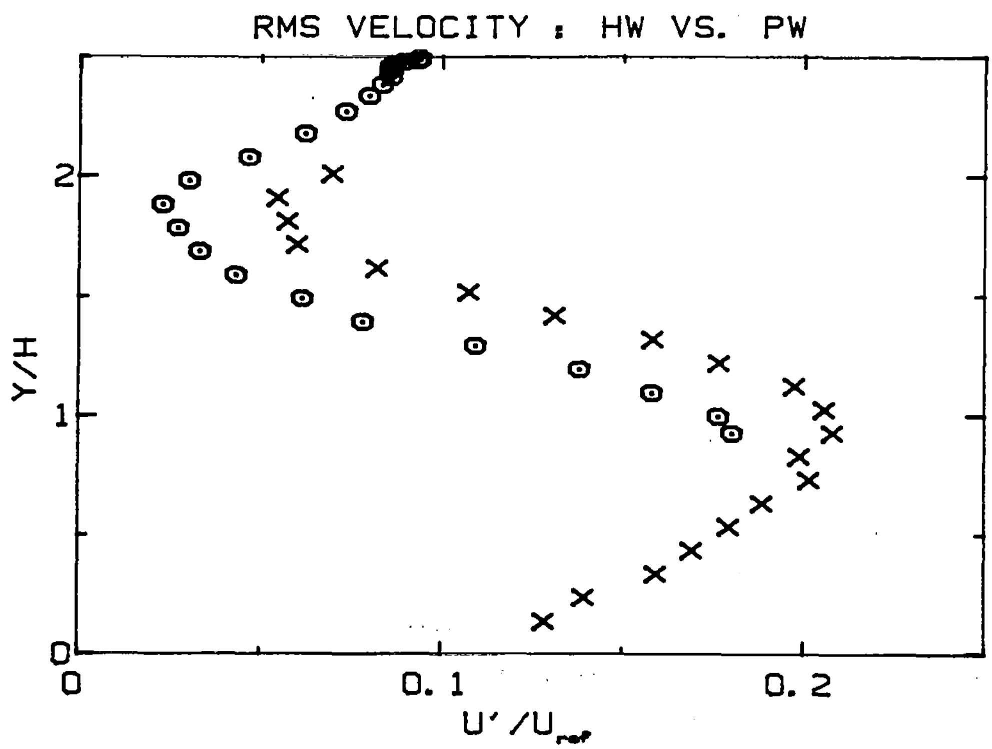

Fig. D-1. Comparison of hot-wire and pulsed-wire measurements near reattachment.

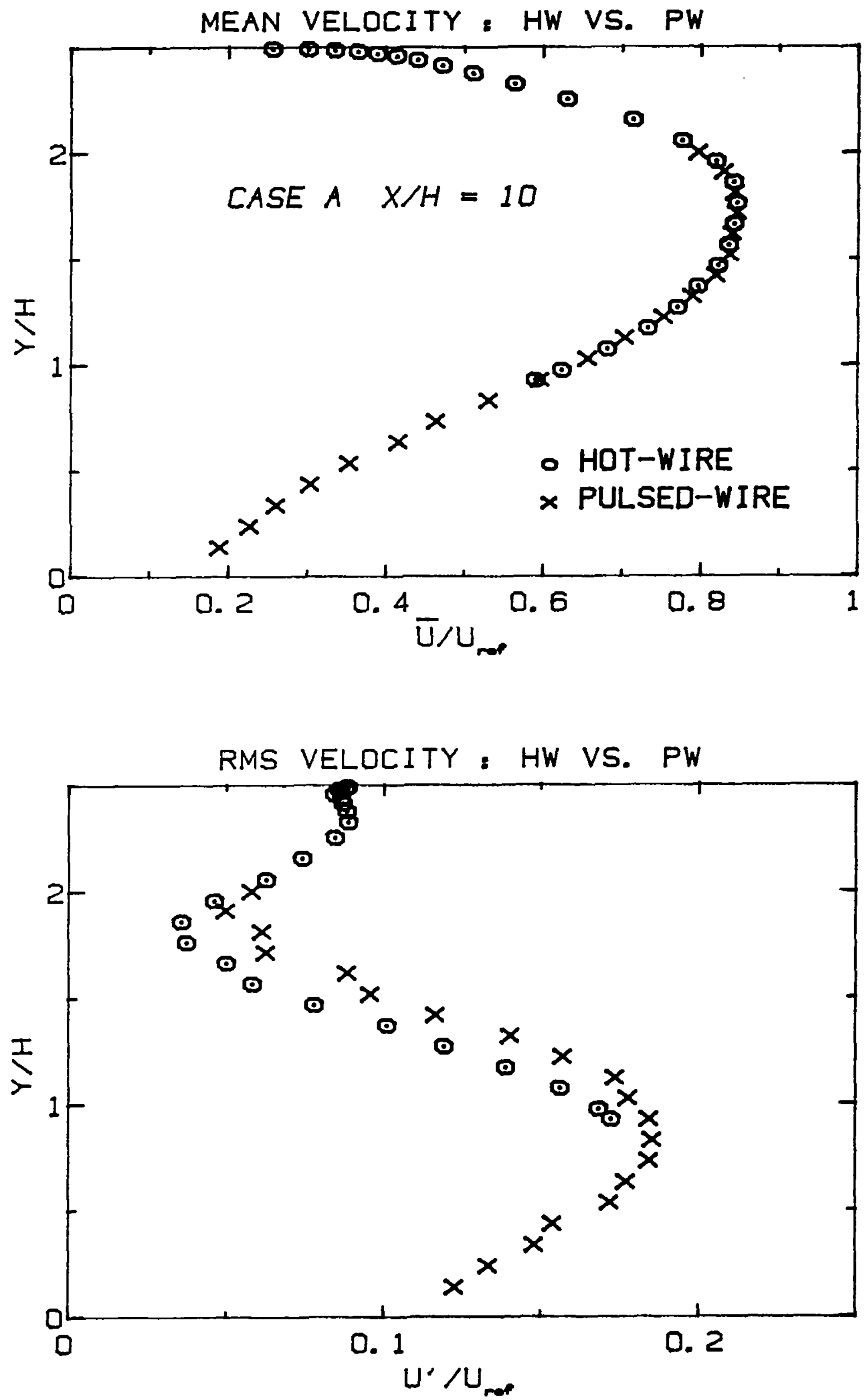

Fig. D-2. Comparison of hot-wire and pulsed-wire measurements in the early recovery region.

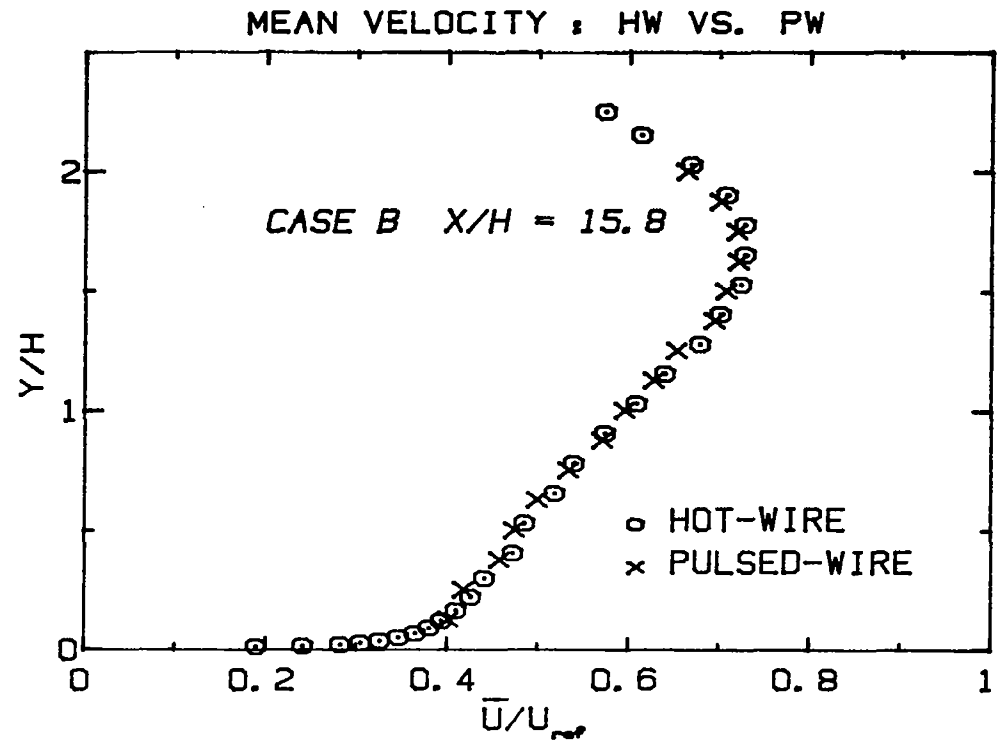

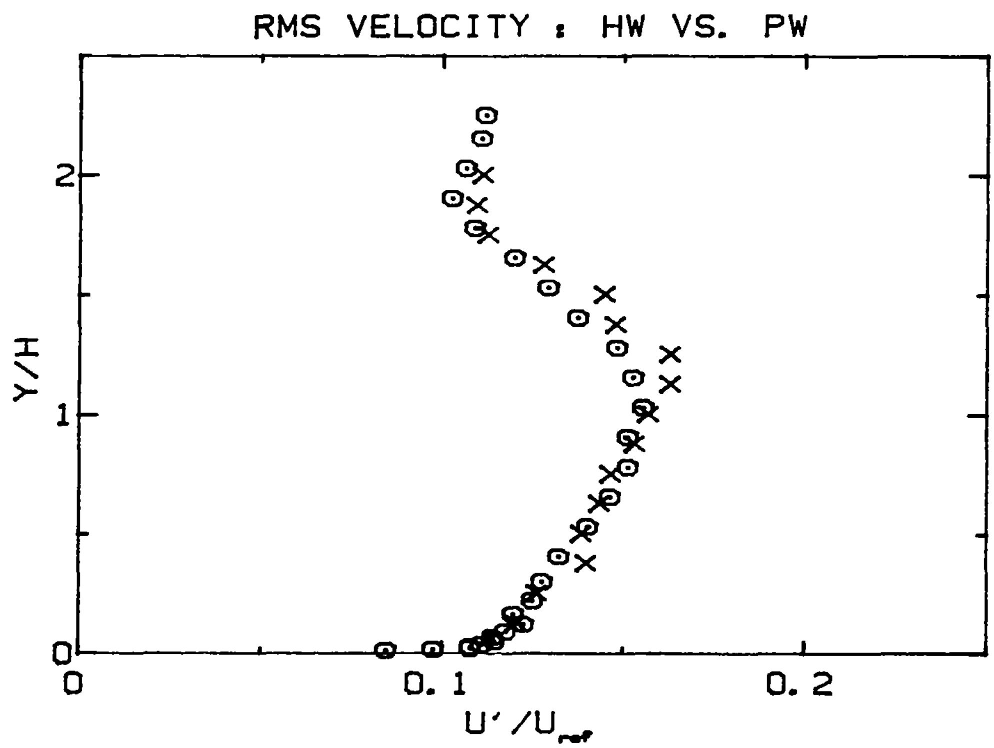

Fig. D-3. Comparison of hot-wire and pulsed-wire measurements in the far recovery region.

Appendix E

EVALUATION OF FLOW TWO-DIMENSIONALITY FROM CONSERVATION EQUATIONS

The configurations studied in Cases A and B have been designed to produce two-dimensional flows. Presumably, any computation of these flows would satisfy conservation of mass and momentum requirements for two-dimensional flow. Thus it is of interest (considering the objectives of Chapter 1) to examine the degree to which the data presented actually satisfy these requirements. Only then can comparison of computations with these results be on a sound basis.

Moreover, checking the data against the requirements of conservation laws helps "close" the experiment, providing a means for evaluating uncertainty estimates and the two-dimensionality of the actual flow. It is in this spirit that the following analysis is presented. Continuity requirements will be tested for Cases A and B; a momentum balance will also be performed for Case A.

The conservation law requirements will be tested at eight streamwise locations for the two cases. Velocity profiles do not span the entire cross-section, so data taken along the opposite wall must be pieced together with profiles taken along the test wall. Where these profiles have not been obtained at precisely the same X location, linear interpolation of values of the integrals at adjacent stations along the opposite wall has been performed.

Stations at Which Conservation Laws Will Be Tested

Case	X/H
A	-3, 2, 4, 6, 8, 10, 12, 16, 20
B	-3, 1.8, 4.5, 7.1, 8.5, 9.8, 11.8, 15.8, 19.8

For the continuity check, the integrated velocity profile at each station is normalized by $U_{ref}W_1$, then compared to the normalized value at the inlet plane $(X/H = -3)$ in Table E-1. The quantities appearing in the momentum integral equation for two-dimensional duct flow are all normalized by $U_{ref}^2 W_1$; of course, all forces are then given per unit density. Four terms are explicitly given, then the net deficit is listed in Table E-2. All the terms are given with respect to the inlet reference value (at $X/H = -3$). The four terms are (i) the net momentum flux, (ii) the net turbulent normal stress, (iii) the net pressure force, and (iv) the skin-friction drag.

The results generally show a few percent imbalance in the continuity equation (a few percent of the inlet mass flux) for each of Cases A and B, and a similar imbalance in the momentum equation for Case A. Considering the uncertainties reported for velocity measurements in Chapter 2, these values may be considered to be within the expected range. Additional contributions to the uncertainty in the overall balance arise from variations in the duct dimensions; for Case B, this could contribute as much as 1.5% to the apparent imbalance in the continuity law check. In Case A, the contribution from uncertainty in duct dimensions is estimated to be 0.5%-1%. Different methods used to align the test-section geometries in the two cases are responsible for the difference.

A further comment on the relative magnitude of the terms in the momentum equation may be of interest. From Table E-2, it can be seen that the net momentum flux is substantially balanced by the pressure rise in the reattachment region. Terms arising due to skin friction and the streamwise turbulent normal stress are a few percent of the inlet momentum flux. Thus, accurate measurement of pressure and mean velocity are critical for doing this check, while estimates of skin friction and turbulent normal stress would suffice.

Table E-1

MASS BALANCE RESULTS

Case A

X/H	M_1^*	$\Delta M_1^\dagger$
-3	.942	___
2	.949	.008
4	.978	.038
6	.966	.025
8	.962	.021
10	.962	.021
12	.971	.031
16	.988	.049
20	.984	.044

Case B

X/H	M_1	ΔM_1
-3	.942	___
2.8	.948	.006
4.5	.959	.018
7.1	.964	.023
8.5	.970	.030
9.8	.959	.017
11.8	.955	.014
15.8	.969	.029
19.8	.960	.019

*Normalized mass flowrate:

$$M_1 \triangleq \frac{1}{W_1} \int_0^W \frac{\bar{U}}{U_{ref}} \, dy \quad .$$

†Mass flow imbalance:

$$\Delta M_1 \triangleq \frac{M_1 - M_{1,ref}}{M_{1,ref}} \quad ; \qquad M_{1,ref} = M_1 \, (X/H = -3) \quad .$$

Table E-2

MOMENTUM BALANCE RESULTS - CASE A

X/H	M_2	MT	CP	CF	ΔM_2
2	0.000	0.010	0.019	-0.010	.001
4	0.010	0.019	0.010	-0.013	.032
6	-0.071	0.027	-0.065	-0.014	.035
8	-0.187	0.031	-0.164	-0.016	.024
10	-0.251	0.027	-0.230	-0.017	.023
12	-0.282	0.022	-0.263	-0.018	.021
16	-0.287	0.019	-0.289	-0.022	.043
20	-0.304	0.015	-0.297	-0.026	.034

$$M_2 = \text{net momentum flux} = \frac{1}{W_1}\left[\int_o^{W_2} \frac{\bar{U}^2}{U_{ref}^2}\,dy - \left.\int_o^{W_1} \frac{\bar{U}^2}{U_{ref}^2}\,dy\right|_{X/H\,=\,-3}\right]$$

$$MT = \text{net turbulent normal stress} = \frac{1}{W_1}\left[\int_o^{W_2} \frac{\overline{u'^2}}{U_{ref}^2}\,dy - \left.\int_o^{W_1} \frac{\overline{u'^2}}{U_{ref}^2}\,dy\right|_{X/H=-3}\right]$$

$$CP = \text{net pressure} = \frac{-\frac{W_2}{W_1} P_X + P_{X/H\,=\,-3} + \frac{H}{W_1} P_{X=o}}{\rho U_{ref}^2}$$

$$CF = \text{skin friction drag} = \frac{1}{W_1}\left[\left.\int_{X/H=-3}^{X} \frac{\tau_w(y)}{\rho U_{ref}^2}\,dx\right|_{\text{step wall}} + \left.\int_{X/H=-3}^{X} \frac{\bar{\tau}_w(x)}{\rho U_{ref}^2}\,dx\right|_{\text{opp. wall}}\right]$$

$$\Delta M_2 = \text{net imbalance in momentum equation} = M_2 + MT - CP - CF$$

Appendix F

BIBLIOGRAPHY ON SKIN-FRICTION MEASUREMENT TECHNIQUES

The list of references below was compiled to assess the viability of various skin-friction measurement techniques for use in the reattachment region of low-speed air flow. Note that many of the references were not mentioned in the overview of techniques in Chapter 3.

Ajagu, C. O., P. A. Libby, and J. C. LaRue (1982), "Modified Gage for Time-Resolved Skin Friction Measurements," unpublished. To appear in Rev. Sci. Inst.

Allen, J. M. (1977), "Experimental Study of Error Sources in Skin-Friction Balance Measurements," Trans. ASME J. Fluids Engrg., 197-204, March.

Bellhouse, G. J., and D. L. Schultz (1966), "Determination of Mean and Dynamic Skin Friction, Separation, and Transition in Low-Speed Flow with a Thin-Film Heated Element," JFM, 24, 379-400.

Chambers, F. W., and H. D. Murphy (1981), "Turbulent Wall Shear Stress Fluctuations in Fully-Developed and Accelerating Flows," Rept. #LA-8781-MS, Los Alamos Scientific Labs, New Mexico.

Dewey, C. J., Jr., and P. W. Huber (1982), "Measurement Methods for Fluid Shear Stress," Rept. #82-4, Fluids Laboratory, Dept of Mech. Engrg., M.I.T., March.

Escudier, M. P., J. Bornstein, M. Acharya, and V. Vokura (1982), "Development of a Floating Element for Measurement of Surface Shear Stress," unpublished.

Frei, D., and H. Thomann (1980), "Direct Measurements of Skin Friction in a Turbulent Boundary Layer with Strong Adverse Pressure Gradients," JFM, 101, Pt. 1, 79-95, November.

Ginder, R. B., and L. J. S. Bradbury (1973), "Preliminary Investigation of a Pulsed Gauge Technique for Skin Friction Measurements in Highly Turbulent Flows," #34-488, FM 4394, Aeronautics Dept., Imperial College.

Higuchi, H., and D. J. Peake (1978), " Bi-Directional, Buried-Wire Skin-Friction Gage," NASA-TM-78531, November.

McAllister, J. E., F. J. Pierce, and M. H. Tenant (1982), "Preston Tube Calibrations and Direct Force Floating Element Measurements in a Two-Dimensional Turbulent Boundary Layer," unpublished. To appear in Trans. ASME, J. Fluids Engrg.

McCroskey, W. J., and E. J. Durbin (1972), "Flow Angle and Shear Stress Measurements Using Heated Films and Wires," Trans. ASME, J. Basic Engrg., 94, No. 1, 46-52, March.

Mitchell, J. E., and T. J. Hanratty (1966), "A Study of Turbulence at a Wall Using an Electrochemical Wall Shear-Stress Meter," JFM, 26, Pt. 1, 199-221.

Monson, D., D. Driver, and J. Szodruch (1981), "Application of a Laser Interferometer Skin-Friction Meter in Complex Flows," ICIASF Record '81, 232-243, October.

Monson, D. J., and H. Higuchi (1981), "Skin Friction Measurements by a New Non-Intrusive Laser Beam-Oil Viscosity Balance Technique," AIAA J., 19, No. 6, 739-744.

Nitsche, W. (1981), "Measuring Skin Friction with Preston Tubes in Boundary-Layer Flows with Additional Parameters," #0077-5606, Canada Inst. for Scientific and Technical Information (1981 translation).

Owen, F. K., and D. A. Johnson (1980), "Separated Skin Friction Measurement--Source of Error, and Assessment, and Elimination," AIAA 13th Fluids and Plasma Conf., July 14-16, 1980, Snowmass, Colo.

Patel, V. C. (1965), "Calibration of the Preston Tube and Limitations on Its Use in Pressure Gradients," JFM, 23, No. 1, 185-208.

Pontikos, N., and P. Bradshaw (1981), "Miniature Pressure Probe for Measuring the Surface Shear Stress Vector in Turbulent Flow," Aero. Quart., 32, Pt. 1, 43-47, February.

Rubesin, M. W., A. F. Okuno, G. G. Mateer, and A. Brosh (1975), "A Hot-Wire Surface Gage for Skin Friction and Separation Detection Measurements," NASA TMX-62,465, Ames Research Center.

Sandborn, V. A. (1979), "Evaluation of the Time-Dependent Surface Shear Stress in Turbulent Flows," ASME WAM 79-WA/FE-17, preprint.

Sirkar, K. K., and T. J. Hanratty (1970), "Relation of Turbulent Mass Transfer to a Wall at High Schmidt Numbers to the Velocity Field," JFM, 44, Pt. 3, 589-603.

Sirkar, K. K., and T. J. Hanratty (1970), "The Limiting Behavior of the Turbulent Transverse Velocity Component Close to a Wall," JFM, 44, Pt. 3, 605-614.

Sivasegaram, S. (1971), "The Evaluation of Local Skin Friction in Compressible Flow," J. Royal Aero. Soc., 75, 793-795.

Smith, D. W., and J. H. Walker (1958), "Skin Friction Measurements in Incompressible Flow," NACA TN 4231, March.

Tanner, L. H., and L. G. Blows (1976a), "A Study of the Motion of Oil Films on Surfaces in Air Flow, with Application to the Measurement of Skin Friction," J. Phys. E.: Sci. Inst., 9, No. 3, 194-202, Mar.

Tanner, L. H., and V. G. Kulkarni (1976b), "The Viscosity Balance Method of Skin Friction Measurement: Further Developments, Including Applications to Three-Dimensional Flows," J. Phys. E.: Sci. Inst., 9, No. 12, 1114-1131, March.

Tanner, L. H. (1977a), "A Skin Friction Meter, Using the Viscosity Balance Principle, Suitable for Use with Flat or Curved Metal Surfaces," J. Phys. E.: Sci. Inst., 10, No. 3, 278-284, March.

Tanner, L. H. (1977b), "A Comparison of the Viscosity Balance and Preston Tube Methods of Skin Friction Measurement," J. Phys. E.: Sci. Inst., 10, No. 6, 627-632, June.

Tennant, M. H., F. J. Pierce, and J. E. McAllister (1980), "An Omnidirectional Wall Shear Meter," Trans. ASME, J. Fluids Engrg., 102, March.

Tillman, W., and G. Haubinger (1978), "Wall Shear Stress Measurements in Heart Valves with Hot-Film Probes," Proc. Dyn. Flow Conf., Marseille and Baltimore, 1978, 737-743.

Tillman, W., M. Waschmann, M. Herold, and G. Haubinger (1981), "Hot-Film Probe for Measurements at Flexible Walls," J. Phys. E: Sci. Inst., 14.

Vagt, J. D., and H. Fernholz (1973), "Use of Surface Fences to Measure Wall Shear Stress in Three-Dimensional Boundary Layers," Aero Quart., 26, 87-91.

Voisinet, R. L. P. (1979), "Influence of Roughness and Blowing on Compressible Turbulent Boundary Layer Flow," Rept. TR79-153, Naval Surface Weapons Center.

Westphal, R. V., J. K. Eaton, and J. P. Johnston (1981), "A New Probe for Measurement of Velocity and Wall Shear Stress in Unsteady, Reversing Flow," J. Fluids Engrg., 103, No. 3, 478-482, September.

Winter, K. G. (1977), "An Outline of the Techniques Available for the Measurement of Skin Friction in Turbulent Boundary Layers," Prog. Aero. Sci., 18, 1-57.

APPENDIX G -- TABULAR DATA FOR THREE MAIN CASES

WALL STATIC PRESSURE DISTRIBUTIONS - 3 MAIN CASES

For all cases:

Uref = 12.2 m/s
AR = 5/3
H = 5.08 cm

Cp = (Pwall - Pref)/(ref dyn head),

where ref is at X/H = -3 on the opposite wall and the origin for X is the step base.

CASE A

Step wall X/H	Step wall Cp	Opposite wall X/H	Opposite wall Cp
-3.	0.001	-2.5	-0.002
-1.	-0.010	-1.5	-0.007
-0.25	-0.017	-0.25	-0.015
0.5	-0.029	0.5	-0.019
1.	-0.030	1.	-0.020
1.5	-0.031	1.5	-0.021
2.	-0.036	2.	-0.021
2.5	-0.041	2.5	-0.020
3.	-0.044	3	-0.017
3.5	-0.044	3.5	-0.014
4.	-0.038	4.	0.002
4.5	-0.023	4.5	0.013
5.	0.001	5.	0.031
5.5	0.030	5.5	0.055
6.	0.064	6.	0.081
6.5	0.099	6.5	0.108
7	0.135	7.	0.136
7.5	0.167	7.5	0.163
8.	0.197	8.	0.187
8.5	0.228	8.5	0.212
9	0.244	9.	0.230
9.5	0.265	9.5	0.249
10.	0.282	10.	0.263
12	0.319	12.	0.306
14.	0.337	14.	0.328
16.	0.346	16	0.341
18	0.351	18.	0.348
20.	0.353	20.	0.352

CASE B

Step wall X/H	Step wall Cp	Opposite wall X/H	Opposite wall Cp
-4.	-0.002	-2.5	-0.006
-3.5	-0.009	-2.	-0.012
-3	-0.017	-1.5	-0.015
-2.5	-0.027	-1.	-0.015
-2	-0.042	-0.63	-0.006
-1.75	-0.051	-0.37	0.006
-1.5	-0.069	-0.13	0.023
-1.25	-0.098	0.06	0.088
-0.25	-0.189	0.68	0.023
0.31	-0.192	2.31	-0.174
0.81	-0.196	2.81	-0.177
1.5	-0.199	3.31	-0.180
2.	-0.203	3.81	-0.174
2.5	-0.198	4.31	-0.165
3.	-0.203	4.81	-0.150
3.5	-0.207	5.31	-0.130
4	-0.206	5.81	-0.103
4.5	-0.194	6.31	-0.073
5.	-0.179	6.81	-0.047
5.5	-0.153	7.31	-0.012
6	-0.117	7.81	0.023
6.5	-0.082	8.31	0.053
7	-0.043	8.81	0.085
7.5	-0.005	9.31	0.108
8	0.038	9.81	0.132
8.5	0.072	10.31	0.150
9	0.106	10.81	0.170
9.5	0.136	11.31	0.188
10.	0.157	11.81	0.199
10.5	0.177	13.81	0.237
11	0.196	15.81	0.255
13	0.242	17.81	0.270
15.	0.261		
17	0.272		

CASE C

Step wall X/H	Step wall Cp	Opposite wall X/H	Opposite wall Cp
-6.75	0.05	-6.75	0.041
0.5	-0.024	-4.5	0.008
1.0	-0.028	-2.5	-0.005
1.5	-0.031	-2.	-0.007
2.0	-0.035	-1.	-0.007
2.5	-0.040	-0.5	-0.008
3.0	-0.047	0.5	-0.012
3.5	-0.048	1.5	-0.016
4.0	-0.033	2.5	-0.012
4.5	-0.002	3.5	0.006
5.0	0.044	4.	0.024
5.5	0.097	4.5	0.044
6.0	0.147	5.	0.075
6.5	0.191	5.5	0.107
7.0	0.229	6.	0.140
7.5	0.255	6.5	0.174
8.0	0.273	7.	0.199
8.5	0.288	7.5	0.225
9.0	0.298	8.	0.247
9.5	0.306	8.5	0.264
10.	0.314	9.	0.277
12.	0.331	9.5	0.289
14.	0.339	10.	0.299
16.	0.345	12.	0.324
18.	0.350	14.	0.336
20.	0.353	16.	0.344
		18.	0.349
		20.	0.353

FORWARD FLOW FRACTION - 3 MAIN CASES

For all cases:

Uref = 12.2 m/s
AR =5/3
H = 5.08 cm

CASE A

X/H	GAMMA
3.	0.016
4.	0.008
5.	0.014
6.	0.037
6.5	0.064
7.	0.124
7.5	0.198
8.	0.327
8.5	0.480
9.	0.674
9.5	0.796
10.	0.914
10.5	0.954
11.	0.982
11.5	0.995
12.	0.998

CASE B

X/H	GAMMA
2.	0.174
3.	0.038
5.	0.012
6.	0.025
7.	0.056
8.	0.146
9.	0.361
10.	0.654
11.	0.880
13.	0.992
15.	1.00

CASE C

X/H	GAMMA
3.	0.041
4.	0.013
5.	0.032
5.5	0.061
6.	0.108
6.5	0.239
7.	0.399
7.5	0.621
8.	0.783
8.5	0.902
9.	0.957
9.5	0.987
10.	0.994
10.5	0.998

SKIN FRICTION DATA - CASES A & B

Pulsed wall probe skin friction measurements
Laminar channel calibration

Cfbar - mean Cf based on Uref
Cfpri - rms Cf " " "
gamma - forward flow fraction (misses not counted)

Uref = 12.2 m/s

CASE A

X/H	Cfbar x1000	Cfpri x1000	Gamma
4.	-0.665	0.671	0.004
5.	-0.817	0.754	0.011
6.	-0.694	0.769	0.032
7.	-0.443	0.756	0.094
8.	-0.080	0.761	0.380
9.	0.147	0.659	0.670
10.	0.466	0.817	0.932
12.	0.920	0.843	0.997
16.	1.503	0.762	1.0
20.	1.774	0.747	1.0

CASE B

X/H	Cfbar x1000	Cfpri x1000	Gamma
-4.5	3.93	0.793	1.0
3.	4.04	0.824	1.0
3.	-0.242	0.415	0.013
5.	-1.004	0.763	0.009
6.	-1.040	0.870	0.019
7.	-0.774	0.891	0.051
8.	-0.459	0.915	0.154
9.	-0.094	0.817	0.392
10.	0.209	0.856	0.679
11.	0.479	0.827	0.885
13.	0.926	0.384	0.996
15.	1.301	0.868	1.0
17.	1.549	0.801	1.0
19.	1.685	0.784	1.0
21.	1.738	0.732	1.0
23.	1.851	0.700	1.0

PULSED-WIRE DATA FOR CASE A

X/H=2

NOM. UREF : 12.20 M/S
FLOW TEMP : 22.40 C
ATM. PRES : 75.95 CM HG

NO. DATA PTS. : 20

PT.	Y-CM	UBAR/UREF	URMS/UREF	GAMMA
1	0.7000	-0.0881	0.0761	0.0443
2	1.2000	-0.0988	0.0756	0.0341
3	1.7000	-0.0954	0.0741	0.0312
4	2.2000	-0.0814	0.0737	0.0555
5	2.7000	-0.0579	0.0742	0.1313
6	3.2000	-0.0179	0.0815	0.3580
7	3.7000	0.0691	0.0973	0.7860
8	4.2000	0.2036	0.1156	0.9646
9	4.7000	0.3795	0.1395	0.9980
10	5.2000	0.6170	0.1549	1.0000
11	5.7000	0.8218	0.1263	1.0000
12	6.2000	0.9412	0.1059	1.0000
13	6.7000	0.9895	0.1085	1.0000
14	7.2000	1.0134	0.1010	1.0000
15	7.7000	1.0185	0.0539	1.0000
16	8.2000	1.0146	0.0361	1.0000
17	8.7000	1.0117	0.0369	1.0000
18	9.2000	1.0125	0.0360	1.0000
19	9.7000	1.0067	0.0457	1.0000
20	10.2000	0.9952	0.0638	1.0000

X/H=4

NOM. UREF : 12.20 M/S
FLOW TEMP : 22.60 C
ATM. PRES : 75.95 CM HG

NO. DATA PTS. : 20

PT.	Y-CM	UBAR/UREF	URMS/UREF	GAMMA
1	0.7000	-0.1730	0.1017	0.0228
2	1.2000	-0.1383	0.1097	0.0724
3	1.7000	-0.0966	0.1217	0.1686
4	2.2000	-0.0455	0.1309	0.3223
5	2.7000	0.0370	0.1456	0.5811
6	3.2000	0.1190	0.1543	0.7890
7	3.7000	0.2265	0.1579	0.9243
8	4.2000	0.3465	0.1714	0.9829
9	4.7000	0.5001	0.1745	1.0000
10	5.2000	0.6547	0.1765	1.0000
11	5.7000	0.7974	0.1600	1.0000
12	6.2000	0.9170	0.1393	1.0000
13	6.7000	0.9887	0.1275	1.0000
14	7.2000	1.0137	0.1100	1.0000
15	7.7000	1.0263	0.0691	1.0000
16	8.2000	1.0214	0.0470	1.0000
17	8.7000	1.0226	0.0466	1.0000
18	9.2000	1.0222	0.0453	1.0000
19	9.7000	1.0160	0.0585	1.0000
20	10.2000	1.0071	0.0650	1.0000

X/H=6

NOM. UREF : 12.18 M/S
FLOW TEMP : 26.22 C
ATM. PRES : 75.69 CM HG

NO. DATA PTS. : 20

PT.	Y-CM	UBAR/UREF	URMS/UREF	GAMMA
1	0.7000	-0.1094	0.1124	0.1171
2	1.2000	-0.0605	0.1245	0.2438
3	1.7000	-0.0201	0.1387	0.3699
4	2.2000	0.0178	0.1541	0.4725
5	2.7000	0.0945	0.1725	0.6763
6	3.2000	0.1841	0.1765	0.8545
7	3.7000	0.2770	0.1965	0.9286
8	4.2000	0.3891	0.1944	0.9789
9	4.7000	0.5064	0.2070	0.9975
10	5.2000	0.6701	0.2019	0.9995
11	5.7000	0.7898	0.1836	1.0000
12	6.2000	0.8875	0.1716	1.0000
13	6.7000	0.9479	0.1443	1.0000
14	7.2000	0.9790	0.1123	0.9995
15	7.7000	0.9933	0.0838	1.0000
16	8.2000	0.9936	0.0624	1.0000
17	8.7000	0.9921	0.0602	1.0000
18	9.2000	0.9915	0.0542	1.0000
19	9.7000	0.9859	0.0672	1.0000
20	10.2000	0.9793	0.0747	1.0000

PULSED-WIRE DATA FOR CASE A

X/H=6 67

NOM. UREF : 12. 17 M/S
FLOW TEMP : 22. 20 C
ATM. PRES : 76. 20 CM HG

NO. DATA PTS. : 20

PT.	Y-CM	UBAR/UREF	URMS/UREF	GAMMA
1	0. 7000	-0. 0623	0. 1191	0 2289
2	1. 2000	-0. 0221	0. 1426	0. 3614
3	1. 7000	0. 0219	0. 1535	0. 4874
4	2. 2000	0. 0921	0. 1747	0. 6647
5	2. 7000	0. 1750	0. 1803	0. 8262
6	3. 2000	0. 2604	0. 1896	0. 9187
7	3. 7000	0. 3590	0. 1939	0. 9753
8	4. 2000	0. 4574	0. 2079	0. 9888
9	4 7000	0. 5702	0. 2010	0. 9985
10	5. 2000	0. 6924	0. 1920	1. 0000
11	5. 7000	0. 7746	0. 1895	1. 0000
12	6. 2000	0. 8476	0. 1771	0. 9995
13	6. 7000	0. 8937	0. 1585	1. 0000
14	7. 2000	0. 9155	0. 1160	0. 9995
15	7. 7000	0. 9303	0. 0897	1. 0000
16	8. 2000	0. 9287	0. 0627	1. 0000
17	8. 7000	0. 9301	0. 0533	1. 0000
18	9. 2000	0. 9279	0. 0528	1. 0000
19	9. 7000	0. 9275	0. 0543	1. 0000
20	10 2000	0. 9112	0. 0538	0. 9995

X/H=7. 33

NOM. UREF : 12. 17 M/S
FLOW TEMP : 21. 96 C
ATM. PRES : 76. 20 CM HG

NO. DATA PTS. : 20

PT.	Y-CM	UBAR/UREF	URMS/UREF	GAMMA
1	0. 7000	-0. 0204	0. 1228	0. 3613
2	1. 2000	0. 0255	0. 1365	0. 5106
3	1. 7000	0. 0793	0. 1538	0. 6584
4	2. 2000	0. 1368	0. 1693	0. 7865
5	2. 7000	0. 2111	0. 1812	0. 8857
6	3. 2000	0. 2829	0. 1742	0. 9384
7	3. 7000	0. 3786	0. 1950	0. 9822
8	4. 2000	0. 4851	0. 2077	0. 9945
9	4. 7000	0. 5724	0. 2058	0. 9970
10	5 2000	0. 6663	0. 2077	0. 9995
11	5. 7000	0. 7535	0 2017	1. 0000
12	6. 2000	0. 8201	0. 1876	0. 9990
13	6. 7000	0. 8577	0. 1606	0. 9995
14	7. 2000	0. 8863	0. 1193	1. 0000
15	7 7000	0. 8925	0. 1064	0. 9985
16	8. 2000	0. 8988	0. 0738	1. 0000
17	8. 7000	0. 8968	0. 0598	1. 0000
18	9. 2000	0. 8961	0. 0535	1. 0000
19	9. 7000	0. 8931	0. 0479	1. 0000
20	10. 2000	0. 8822	0. 0435	1. 0000

X/H=8

NOM. UREF : 12. 22 M/S
FLOW TEMP : 24. 03 C
ATM. PRES : 75. 69 CM HG

NO. DATA PTS. : 20

PT.	Y-CM	UBAR/UREF	URMS/UREF	GAMMA
1	0. 7000	0. 0348	0. 1286	0. 5467
2	1. 2000	0. 0737	0. 1395	0. 6630
3	1. 7000	0. 1314	0. 1595	0. 7906
4	2. 2000	0. 1809	0. 1692	0. 8603
5	2. 7000	0. 2463	0. 1795	0. 9305
6	3. 2000	0. 3192	0. 1887	0. 9709
7	3. 7000	0. 4005	0. 2017	0. 9899
8	4. 2000	0. 4817	0. 1989	0. 9975
9	4. 7000	0. 5695	0. 2081	0. 9970
10	5. 2000	0. 6694	0. 2059	0. 9995
11	5. 7000	0. 7431	0. 1976	0. 9990
12	6. 2000	0. 8026	0. 1767	1. 0000
13	6. 7000	0. 8445	0. 1583	0. 9995
14	7. 2000	0. 8744	0. 1313	1. 0000
15	7. 7000	0. 8891	0. 1076	0. 9995
16	8. 2000	0. 8919	0. 0822	1. 0000
17	8. 7000	0. 8944	0. 0601	1. 0000
18	9. 2000	0. 8933	0. 0574	1. 0000
19	9. 7000	0. 8873	0. 0547	1. 0000
20	10. 2000	0. 8731	0. 0698	1. 0000

PULSED-WIRE DATA FOR CASE A

X/H=8.67

NOM. UREF 12.12 M/S
FLOW TEMP : 24.81 C
ATM. PRES · 75.90 CM HG

NO. DATA PTS. : 20

PT.	Y-CM	UBAR/UREF	URMS/UREF	GAMMA
1	0.7000	0.0935	0.1242	0.8014
2	1.2000	0.1314	0.1374	0.8662
3	1.7000	0.1655	0.1443	0.9083
4	2.2000	0.2183	0.1628	0.9479
5	2.7000	0.2850	0.1832	0.9743
6	3.2000	0.3603	0.1922	0.9879
7	3.7000	0.4313	0.2044	0.9930
8	4.2000	0.5144	0.2178	0.9975
9	4.7000	0.5872	0.2086	1.0000
10	5.2000	0.6656	0.2000	1.0000
11	5.7000	0.7367	0.1901	1.0000
12	6.2000	0.7814	0.1820	1.0000
13	6.7000	0.8049	0.1579	1.0000
14	7.2000	0.8339	0.1164	1.0000
15	7.7000	0.8389	0.1055	1.0000
16	8.2000	0.8405	0.0886	1.0000
17	8.7000	0.8434	0.0834	1.0000
18	9.2000	0.8511	0.0797	1.0000
19	9.7000	0.8399	0.1036	1.0000
20	10.2000	0.8187	0.1033	1.0000

X/H=9.33

NOM. UREF : 12.13 M/S
FLOW TEMP : 26.31 C
ATM. PRES : 75.90 CM HG

NO. DATA PTS. : 20

PT.	Y-CM	UBAR/UREF	URMS/UREF	GAMMA
1	0.7000	0.1363	0.1273	0.9073
2	1.2000	0.1793	0.1381	0.9479
3	1.7000	0.2154	0.1487	0.9688
4	2.2000	0.2720	0.1703	0.9779
5	2.7000	0.3288	0.1829	0.9904
6	3.2000	0.3906	0.2000	0.9955
7	3.7000	0.4512	0.1937	0.9980
8	4.2000	0.5284	0.2047	0.9995
9	4.7000	0.5934	0.2066	0.9995
10	5.2000	0.6738	0.1954	1.0000
11	5.7000	0.7248	0.1779	0.9995
12	6.2000	0.7753	0.1598	1.0000
13	6.7000	0.8008	0.1337	1.0000
14	7.2000	0.8320	0.1066	1.0000
15	7.7000	0.8409	0.0901	1.0000
16	8.2000	0.8481	0.0701	1.0000
17	8.7000	0.8502	0.0622	1.0000
18	9.2000	0.8443	0.0747	1.0000
19	9.7000	0.8440	0.0759	1.0000
20	10.2000	0.8148	0.0888	1.0000

X/H=10

NOM. UREF : 12.24 M/S
FLOW TEMP : 25.82 C
ATM. PRES : 75.57 CM HG

NO. DATA PTS. : 20

PT.	Y-CM	UBAR/UREF	URMS/UREF	GAMMA
1	0.7000	0.1886	0.1227	0.9630
2	1.2000	0.2267	0.1334	0.9729
3	1.7000	0.2610	0.1481	0.9848
4	2.2000	0.3041	0.1539	0.9915
5	2.7000	0.3536	0.1719	0.9945
6	3.2000	0.4161	0.1771	0.9980
7	3.7000	0.4641	0.1843	0.9980
8	4.2000	0.5315	0.1854	0.9995
9	4.7000	0.5965	0.1844	1.0000
10	5.2000	0.6564	0.1776	1.0000
11	5.7000	0.7032	0.1736	1.0000
12	6.2000	0.7522	0.1570	1.0000
13	6.7000	0.7894	0.1404	1.0000
14	7.2000	0.8196	0.1165	1.0000
15	7.7000	0.8369	0.0956	1.0000
16	8.2000	0.8401	0.0883	1.0000
17	8.7000	0.8459	0.0625	1.0000
18	9.2000	0.8431	0.0613	1.0000
19	9.7000	0.8294	0.0498	1.0000
20	10.1600	0.7962	0.0579	1.0000

PULSED-WIRE DATA FOR CASE B

X/H=2.81

NOM. UREF . 12.16 M/S
FLOW TEMP : 27.11 C
ATM. PRES : 75.18 CM HG

NO. DATA PTS. : 21

PT.	Y-CM	UBAR/UREF	URMS/UREF	GAMMA
1	0.6350	-0.1591	0.0946	0.025
2	0.7596	-0.1518	0.0915	0.026
3	0.9087	-0.1550	0.0885	0.020
4	1.0870	-0.1513	0.0938	0.033
5	1.3003	-0.1442	0.0928	0.033
6	1.5554	-0.1405	0.0938	0.032
7	1.8607	-0.1240	0.0968	0.068
8	2.2258	-0.1032	0.1023	0.121
9	2.6625	-0.0714	0.1072	0.202
10	3.1850	-0.0239	0.1146	0.379
11	3.8100	0.0804	0.1346	0.697
12	4.4450	0.2381	0.1445	0.953
13	5.0800	0.4423	0.1616	0.999
14	5.7150	0.6945	0.1745	1.0
15	6.3500	0.9396	0.1372	1.0
16	6.9850	1.0660	0.0632	1.0
17	7.6200	1.0984	0.0333	1.0
18	8.2550	1.0962	0.0239	1.0
19	8.8900	1.0922	0.0216	1.0
20	9.5250	1.0902	0.0227	1.0
21	10.1600	1.0851	0.0245	1.0

X/H=4.47

NOM. UREF 12.21 M/S
FLOW TEMP : 24.97 C
ATM. PRES : 75.31 CM HG

NO. DATA PTS. : 21

PT.	Y-CM	UBAR/UREF	URMS/UREF	GAMMA
1	0.6350	-0.1950	0.1133	0.028
2	0.7596	-0.1952	0.1188	0.034
3	0.9087	-0.1806	0.1334	0.057
4	1.0870	-0.1506	0.1629	0.090
5	1.3003	-0.1491	0.1250	0.089
6	1.5554	-0.1435	0.1308	0.106
7	1.8607	-0.1084	0.1646	0.178
8	2.2258	-0.0689	0.1518	0.258
9	2.6625	-0.0163	0.1655	0.397
10	3.1850	0.0648	0.1755	0.592
11	3.8100	0.1940	0.1823	0.832
12	4.4450	0.3434	0.1777	0.966
13	5.0800	0.5107	0.1888	0.997
14	5.7150	0.6734	0.1891	1.0
15	6.3500	0.8572	0.1645	1.0
16	6.9850	0.9697	0.1164	1.0
17	7.6200	1.0198	0.0667	1.0
18	8.2550	1.0276	0.0382	1.0
19	8.8900	1.0268	0.0260	1.0
20	9.5250	1.0259	0.0267	1.0
21	10.1600	1.0188	0.0295	1.0

X/H=7.14

NOM. UREF : 12.21 M/S
FLOW TEMP : 26.13 C
ATM. PRES : 75.31 CM HG

NO. DATA PTS. : 21

PT.	Y-CM	UBAR/UREF	URMS/UREF	GAMMA
1	0.6350	-0.1047	0.1380	0.174
2	0.7596	-0.0870	0.1545	0.199
3	0.9087	-0.0806	0.1470	0.224
4	1.0870	-0.0703	0.1507	0.251
5	1.3003	-0.0538	0.1612	0.299
6	1.5554	-0.0245	0.1676	0.365
7	1.8607	0.0157	0.1917	0.449
8	2.2258	0.0478	0.1851	0.542
9	2.6625	0.1204	0.2013	0.687
10	3.1850	0.1884	0.2090	0.788
11	3.8100	0.2999	0.2141	0.912
12	4.4450	0.4157	0.2127	0.974
13	5.0800	0.5485	0.2250	0.990
14	5.7150	0.6956	0.2030	1.0
15	6.3500	0.7974	0.1878	1.0
16	6.9850	0.8928	0.1457	1.0
17	7.6200	0.9559	0.0938	1.0
18	8.2550	0.9690	0.0745	1.0
19	8.8900	0.9775	0.0526	1.0
20	9.5250	0.9784	0.0387	1.0
21	10.1600	0.9675	0.0421	1.0

PULSED-WIRE DATA FOR CASE B

X/H=8.48

NOM. UREF : 12.23 M/S
FLOW TEMP : 26.93 C
ATM. PRES : 75.18 CM HG

NO. DATA PTS. : 16

PT	Y-CM	UBAR/UREF	URMS/UREF	GAMMA
1	0.6350	0.0056	0.1413	0.415
2	1.2700	0.0503	0.1593	0.524
3	1.9050	0.1118	0.1758	0.679
4	2.5400	0.1799	0.1881	0.793
5	3.1750	0.2793	0.2021	0.905
6	3.8100	0.3692	0.2155	0.957
7	4.4450	0.4670	0.2045	0.986
8	5.0800	0.5731	0.2116	0.994
9	5.7150	0.6853	0.2028	0.999
10	6.3500	0.7635	0.1836	1.0
11	6.9850	0.8401	0.1613	1.0
12	7.6200	0.8939	0.1346	1.0
13	8.2550	0.9290	0.0926	1.0
14	8.8900	0.9484	0.0559	1.0
15	9.5250	0.9428	0.0584	1.0
16	10.1600	0.9187	0.0601	1.0

X/H=9.14

NOM. UREF : 12.18 M/S
FLOW TEMP : 26.55 C
ATM. PRES : 75.18 CM HG

NO. DATA PTS. : 21

PT.	Y-CM	UBAR/UREF	URMS/UREF	GAMMA
1	0.6350	0.0570	0.1438	0.588
2	0.7596	0.0676	0.1489	0.601
3	0.9087	0.0832	0.1527	0.639
4	1.0870	0.0959	0.1568	0.678
5	1.3003	0.1080	0.1566	0.719
6	1.5554	0.1275	0.1660	0.739
7	1.8607	0.1591	0.1756	0.783
8	2.2258	0.1895	0.1820	0.827
9	2.6625	0.2503	0.1944	0.898
10	3.1850	0.3115	0.1976	0.936
11	3.8100	0.3886	0.2077	0.973
12	4.4450	0.4853	0.2110	0.993
13	5.0800	0.5650	0.2144	0.997
14	5.7150	0.6756	0.2070	0.999
15	6.3500	0.7666	0.1816	1.0
16	6.9850	0.8317	0.1659	1.0
17	7.6200	0.8842	0.1254	1.0
18	8.2550	0.9189	0.0927	1.0
19	8.8900	0.9260	0.0811	1.0
20	9.5250	0.9270	0.0597	1.0
21	10.1600	0.8951	0.0663	1.0

X/H=9.81

NOM. UREF : 12.20 M/S
FLOW TEMP : 27.61 C
ATM. PRES : 75.18 CM HG

NO. DATA PTS. : 21

PT.	Y-CM	UBAR/UREF	URMS/UREF	GAMMA
1	0.6350	0.1159	0.1464	0.751
2	0.7596	0.1307	0.1455	0.786
3	0.9087	0.1329	0.1471	0.782
4	1.0870	0.1405	0.1511	0.812
5	1.3003	0.1579	0.1587	0.859
6	1.5554	0.1812	0.1572	0.877
7	1.8607	0.2072	0.1717	0.920
8	2.2258	0.2461	0.1726	0.934
9	2.6625	0.2816	0.1881	0.970
10	3.1850	0.3365	0.1853	0.983
11	3.8100	0.4067	0.1949	0.992
12	4.4450	0.4985	0.2094	0.998
13	5.0800	0.5771	0.2023	1.0
14	5.7150	0.6598	0.2000	1.0
15	6.3500	0.7408	0.1808	1.0
16	6.9850	0.8072	0.1571	1.0
17	7.6200	0.8534	0.1378	1.0
18	8.2550	0.8873	0.1041	1.0
19	8.8900	0.9006	0.0839	1.0
20	9.5250	0.8949	0.0611	1.0
21	10.1600	0.8570	0.0752	1.0

PULSED-WIRE DATA FOR CASE B

X/H=11.81

NOM. UREF : 12.23 M/S
FLOW TEMP : 25.81 C
ATM. PRES : 75.18 CM HG

NO. DATA PTS. : 21

PT.	Y-CM	UBAR/UREF	URMS/UREF	GAMMA
1	0.6350	0.2497	0.1378	0.982
2	0.7596	0.2592	0.1360	0.988
3	0.9087	0.2569	0.1372	0.981
4	1.0870	0.2764	0.1408	0.989
5	1.3003	0.2942	0.1467	0.990
6	1.5554	0.3007	0.1524	0.988
7	1.8607	0.3141	0.1531	0.992
8	2.2258	0.3468	0.1664	0.993
9	2.6625	0.3737	0.1694	0.993
10	3.1850	0.4121	0.1777	0.997
11	3.8100	0.4753	0.1905	0.999
12	4.4450	0.5263	0.1932	1.0
13	5.0800	0.5857	0.2019	0.999
14	5.7150	0.6566	0.1881	1.0
15	6.3500	0.7007	0.1819	1.0
16	6.9850	0.7613	0.1621	1.0
17	7.6200	0.8020	0.1412	1.0
18	8.2550	0.8266	0.1303	1.0
19	8.8900	0.8381	0.1078	1.0
20	9.5250	0.8260	0.0901	1.0
21	10.1600	0.7804	0.0935	1.0

X/H=13.81

NOM. UREF : 12.53 M/S
FLOW TEMP : 26.06 C
ATM. PRES : 75.18 CM HG

NO. DATA PTS. : 16

PT.	Y-CM	UBAR/UREF	URMS/UREF	GAMMA
1	0.6350	0.3502	0.1338	1.0
2	1.2700	0.3814	0.1438	0.999
3	1.9050	0.4082	0.1507	1.0
4	2.5400	0.4365	0.1548	1.0
5	3.1750	0.4652	0.1654	1.0
6	3.8100	0.5179	0.1685	1.0
7	4.4450	0.5560	0.1771	1.0
8	5.0800	0.6045	0.1802	1.0
9	5.7150	0.6433	0.1741	1.0
10	6.3500	0.6899	0.1735	1.0
11	6.9850	0.7287	0.1678	1.0
12	7.6200	0.7652	0.1489	1.0
13	8.2550	0.7887	0.1306	1.0
14	8.8900	0.7858	0.1188	1.0
15	9.5250	0.7655	0.1110	1.0
16	10.1600	0.7255	0.1080	1.0

X/H=15.81

NOM. UREF : 12.21 M/S
FLOW TEMP : 25.05 C
ATM. PRES : 75.18 CM HG

NO. DATA PTS. : 16

PT.	Y-CM	UBAR/UREF	URMS/UREF	GAMMA
1	0.6350	0.4026	0.1208	1.0
2	1.2700	0.4185	0.1264	1.0
3	1.9050	0.4583	0.1401	1.0
4	2.5400	0.4753	0.1387	1.0
5	3.1750	0.4999	0.1437	1.0
6	3.8100	0.5341	0.1467	1.0
7	4.4450	0.5714	0.1534	1.0
8	5.0800	0.5965	0.1572	1.0
9	5.7150	0.6286	0.1632	1.0
10	6.3500	0.6539	0.1631	1.0
11	6.9850	0.6956	0.1480	1.0
12	7.6200	0.7085	0.1450	1.0
13	8.2550	0.7223	0.1281	1.0
14	8.8900	0.7205	0.1127	1.0
15	9.5250	0.7017	0.1096	1.0
16	10.1600	0.6646	0.1113	1.0

PULSED-WIRE DATA FOR CASE C

X/H=4

NOM. UREF : 12.20 M/S
FLOW TEMP : 24.01 C
ATM. PRES : 75.80 CM HG

NO. DATA PTS. : 20

PT.	Y-CM	UBAR/UREF	URMS/UREF	GAMMA
1	0.7000	-0.1947	0.1209	0.0273
2	1.2000	-0.1551	0.1301	0.0698
3	1.7000	-0.0943	0.1422	0.2025
4	2.2000	-0.0293	0.1532	0.3649
5	2.7000	0.0749	0.1719	0.6549
6	3.2000	0.1916	0.1858	0.8689
7	3.7000	0.3320	0.1992	0.9671
8	4.2000	0.4838	0.2063	0.9965
9	4.7000	0.6417	0.2281	0.9990
10	5.2000	0.7811	0.2068	1.0000
11	5.7000	0.8659	0.1863	1.0000
12	6.2000	0.9075	0.1733	1.0000
13	6.7000	0.9276	0.1827	1.0000
14	7.2000	0.9336	0.1702	1.0000
15	7.7000	0.9468	0.1633	1.0000
16	8.2000	0.9415	0.1221	1.0000
17	8.7000	0.9355	0.0700	1.0000
18	9.2000	0.9361	0.0520	1.0000
19	9.7000	0.9387	0.0695	1.0000
20	10.2000	0.9281	0.0655	1.0000

X/H=6

NOM. UREF : 12.21 M/S
FLOW TEMP : 23.73 C
ATM. PRES : 75.80 CM HG

NO. DATA PTS. : 20

PT.	Y-CM	UBAR/UREF	URMS/UREF	GAMMA
1	0.7000	-0.0544	0.1241	0.2454
2	1.2000	-0.0077	0.1402	0.3936
3	1.7000	0.0467	0.1568	0.5748
4	2.2000	0.1256	0.1871	0.7519
5	2.7000	0.2037	0.1993	0.8577
6	3.2000	0.3178	0.2120	0.9492
7	3.7000	0.4179	0.2133	0.9844
8	4.2000	0.5229	0.2079	0.9965
9	4.7000	0.6289	0.2131	0.9990
10	5.2000	0.7114	0.1935	0.9995
11	5.7000	0.7810	0.1806	1.0000
12	6.2000	0.8224	0.1652	1.0000
13	6.7000	0.8478	0.1696	1.0000
14	7.2000	0.8728	0.1698	1.0000
15	7.7000	0.8850	0.1131	1.0000
16	8.2000	0.8868	0.0815	1.0000
17	8.7000	0.8844	0.0618	1.0000
18	9.2000	0.8840	0.0544	1.0000
19	9.7000	0.8814	0.0556	1.0000
20	10.2000	0.8736	0.0496	1.0000

X/H=6.67

NOM. UREF : 12.17 M/S
FLOW TEMP : 24.91 C
ATM. PRES : 75.80 CM HG

NO. DATA PTS. : 20

PT.	Y-CM	UBAR/UREF	URMS/UREF	GAMMA
1	0.7000	0.0199	0.1294	0.5009
2	1.2000	0.0624	0.1428	0.6385
3	1.7000	0.1163	0.1563	0.7626
4	2.2000	0.1781	0.1662	0.8678
5	2.7000	0.2580	0.1942	0.9284
6	3.2000	0.3430	0.1993	0.9766
7	3.7000	0.4251	0.2048	0.9904
8	4.2000	0.5184	0.1937	0.9990
9	4.7000	0.5828	0.1891	0.9990
10	5.2000	0.6670	0.1624	1.0000
11	5.7000	0.7174	0.1508	1.0000
12	6.2000	0.7575	0.1494	1.0000
13	6.7000	0.7873	0.1454	1.0000
14	7.2000	0.8042	0.1299	0.9995
15	7.7000	0.8126	0.1142	1.0000
16	8.2000	0.8197	0.0749	1.0000
17	8.7000	0.8200	0.0564	1.0000
18	9.2000	0.8185	0.0553	1.0000
19	9.7000	0.8160	0.0690	1.0000
20	10.2000	0.8111	0.0805	1.0000

PULSED-WIRE DATA FOR CASE C

/H=7. 33

NOM. UREF : 12. 14 M/S
FLOW TEMP : 25. 07 C
ATM. PRES : 75. 80 CM HG

NO. DATA PTS. : 20

PT.	Y-CM	UBAR/UREF	URMS/UREF	GAMMA
1	0. 7000	0. 0947	0. 1220	0. 7858
2	1. 2000	0. 1277	0. 1340	0. 8495
3	1. 7000	0. 1701	0. 1449	0. 9066
4	2. 2000	0. 2106	0. 1627	0. 9344
5	2. 7000	0. 2688	0. 1712	0. 9676
6	3. 2000	0. 3381	0. 1801	0. 9873
7	3. 7000	0. 4131	0. 1909	0. 9940
8	4. 2000	0. 4802	0. 1863	0. 9990
9	4. 7000	0. 5728	0. 1852	1. 0000
10	5. 2000	0. 6432	0. 1630	0. 9995
11	5. 7000	0. 6964	0. 1407	1. 0000
12	6. 2000	0. 7343	0. 1335	1. 0000
13	6. 7000	0. 7696	0. 1261	1. 0000
14	7. 2000	0. 7917	0. 1357	1. 0000
15	7. 7000	0. 7991	0. 1112	1. 0000
16	8. 2000	0. 8059	0. 0848	1. 0000
17	8. 7000	0. 8102	0. 0471	1. 0000
18	9. 2000	0. 8093	0. 0541	1. 0000
19	9. 7000	0. 8107	0. 0660	1. 0000
20	10. 2000	0. 7953	0. 0722	1. 0000

X/H=8

NOM UREF : 12. 15 M/S
FLOW TEMP : 24. 65 C
ATM. PRES : 75. 80 CM HG

NO. DATA PTS. : 20

PT.	Y-CM	UBAR/UREF	URMS/UREF	GAMMA
1	0. 7000	0. 1507	0 1206	0. 9342
2	1. 2000	0. 1900	0. 1348	0. 9596
3	1. 7000	0. 2265	0. 1427	0. 9731
4	2. 2000	0. 2730	0. 1530	0. 9883
5	2. 7000	0. 3230	0. 1696	0. 9939
6	3. 2000	0. 3828	0. 1779	0. 9965
7	3. 7000	0. 4510	0. 1800	0. 9990
8	4. 2000	0. 5095	0. 1872	0. 9990
9	4. 7000	0. 5744	0. 1741	0. 9995
10	5. 2000	0. 6306	0. 1630	1. 0000
11	5. 7000	0. 6803	0. 1482	1. 0000
12	6. 2000	0. 7265	0. 1269	1. 0000
13	6. 7000	0. 7563	0. 1056	1. 0000
14	7. 2000	0. 7815	0. 0837	1. 0000
15	7. 7000	0. 7949	0. 0559	1. 0000
16	8. 2000	0. 7976	0. 0538	1. 0000
17	8. 7000	0. 8019	0. 0409	1. 0000
18	9. 2000	0. 8032	0. 0466	1. 0000
19	9 7000	0. 7990	0. 0508	1. 0000
20	10. 2000	0. 7765	0. 0562	1. 0000

X/H=10

NOM. UREF : 12. 18 M/S
FLOW TEMP : 24. 70 C
ATM. PRES : 75. 80 CM HG

NO. DATA PTS. : 20

PT.	Y-CM	UBAR/UREF	URMS/UREF	GAMMA
1	0. 7000	0. 2736	0. 1170	1. 0000
2	1. 2000	0. 3019	0. 1259	0. 9990
3	1. 7000	0. 3303	0. 1324	1. 0000
4	2. 2000	0. 3543	0. 1453	1. 0000
5	2. 7000	0. 3977	0. 1492	0. 9995
6	3. 2000	0. 4334	0. 1561	1. 0000
7	3. 7000	0. 4713	0. 1638	1. 0000
8	4. 2000	0. 5202	0. 1635	1. 0000
9	4. 7000	0. 5666	0. 1656	1. 0000
10	5. 2000	0. 6130	0. 1591	1. 0000
11	5. 7000	0. 6542	0. 1552	1. 0000
12	6. 2000	0. 6952	0. 1448	1. 0000
13	6. 7000	0. 7243	0. 1337	1. 0000
14	7. 2000	0. 7466	0. 1349	1. 0000
15	7. 7000	0. 7691	0. 1101	1. 0000
16	8. 2000	0. 7743	0. 0824	1. 0000
17	8. 7000	0. 7788	0. 0781	1. 0000
18	9. 2000	0. 7801	0. 0695	1. 0000
19	9. 7000	0. 7676	0. 0794	1. 0000
20	10. 2000	0. 7307	0. 0841	1. 0000

INLET VELOCITY PROFILES

THE SUMMARY OF THESE DATA APPEARS AS TABLE 5-1

X/H=-9.75

NOM. UREF : 12.20 M/S

FOR BOUNDARY LAYER ANALYSIS UE = 11.64 M/S AT YE = 3.75 CM

PT. NO.	Y CM	UBAR M/S	Y/DEL 99	U/UE	u'/UE	Y+	U+	UTLOC M/S
1	0.000	0.00	0.000	0.000	0.000	0.0	0.0	0.000
2	0.040	6.87	0.036	0.590	0.117	19.5	12.1	0.562
3	0.053	7.35	0.047	0.631	0.110	25.4	12.9	0.570
4	0.069	7.82	0.062	0.672	0.103	33.2	13.7	0.576
5	0.090	8.18	0.081	0.703	0.096	43.5	14.4	0.575
6	0.118	8.54	0.105	0.733	0.088	56.8	15.0	0.574
7	0.154	8.84	0.138	0.759	0.083	74.3	15.5	0.570
8	0.201	9.18	0.180	0.788	0.077	97.1	16.1	0.568
9	0.263	9.56	0.235	0.821	0.071	126.8	16.8	0.569
10	0.343	9.91	0.307	0.851	0.068	165.5	17.4	0.568
11	0.449	10.26	0.401	0.881	0.064	216.2	18.0	0.566
12	0.586	10.63	0.524	0.913	0.057	282.5	18.7	0.567
13	0.766	11.02	0.684	0.947	0.050	369.0	19.3	0.568
14	1.000	11.42	0.893	0.981	0.035	481.9	20.0	0.569
15	1.250	11.64	1.117	1.000	0.021	602.3	20.4	0.565
16	1.500	11.67	1.341	1.002	0.010	723.0	20.5	0.556
17	1.750	11.68	1.564	1.004	0.006	843.5	20.5	0.547
18	2.000	11.68	1.787	1.003	0.004	964.0	20.5	0.540
19	2.250	11.65	2.011	1.001	0.003	1084.4	20.4	0.532
20	2.500	11.65	2.234	1.001	0.003	1204.9	20.4	0.527
21	2.750	11.63	2.457	0.999	0.003	1325.4	20.4	0.521
22	3.000	11.61	2.681	0.997	0.003	1446.0	20.4	0.516
23	3.250	11.60	2.904	0.997	0.003	1566.5	20.4	0.511
24	3.500	11.61	3.128	0.998	0.003	1687.0	20.4	0.508
25	3.750	11.63	3.351	0.999	0.003	1807.5	20.4	0.505
26	4.000	11.62	3.574	0.998	0.003	1927.9	20.4	0.502
27	4.250	11.59	3.798	0.996	0.003	2048.6	20.3	0.498
28	4.500	11.55	4.021	0.992	0.003	2169.1	20.3	0.494
29	4.750	11.51	4.245	0.989	0.004	2289.5	20.2	0.490
30	5.000	11.53	4.468	0.990	0.004	2410.0	20.2	0.488
31	5.080	11.51	4.539	0.989	0.004	2448.5	20.2	0.487

** INTEGRAL THICKNESS PARAMETERS **

QUANTITY	VALUE IN CM		
DELTA-99	1.119		
DISPLACEMENT THICKNESS	0.145	REDELST =	1430.
MOMENTUM THICKNESS	0.107	RETHETA =	1050.
ENERGY THICKNESS	0.0851		

SHAPE PARAMETERS : H =1.363 LAMBDA =0.130 CLAUSER G = 5.44

RESULTS OF COLES DATA ANALYSIS

COLES DELTA	1.255	CM
COLES UTAU	0.570	M/S
WAKE PARAMETER	-0.039	DIMENSIONLESS
CF BASED ON UE	0.00479	DIMENSIONLESS

PROFILE POINTS 6 THROUGH 13 USED
RESULTANT RMS ERROR FOR WALL-WAKE FIT : 0.059 M/S

TURBULENT SKIN FRICTION PROFILE CORRELATIONS

BASIS VELOCITY :	UE	UREF
CF : LOG-LAW FIT	0.00479	0.00437
CF : LUDWEIG-TILLMAN	0.00454	0.00414
CF : FRANK WHITE	0.00448	0.00408

X/H=-3

NOM. UREF : 11.72 M/S

FOR BOUNDARY LAYER ANALYSIS UE = 11.75 M/S AT YE = 3.81 CM

PT. NO.	Y CM	UBAR M/S	Y/DEL 99	U/UE	u'/UE	Y+	U+	UTLOC M/S
1	0.000	0.00	0.000	0.000	0.000	0.0	0.0	0.000
2	0.053	5.99	0.032	0.510	0.097	23.8	11.3	0.479
3	0.061	6.46	0.037	0.550	0.095	27.5	12.2	0.499
4	0.071	6.85	0.042	0.583	0.095	31.7	12.9	0.512
5	0.082	7.15	0.049	0.609	0.089	36.6	13.5	0.520
6	0.095	7.47	0.056	0.636	0.087	42.2	14.1	0.528
7	0.109	7.71	0.065	0.656	0.083	48.7	14.6	0.532
8	0.126	7.83	0.075	0.667	0.081	56.2	14.8	0.528
9	0.145	8.05	0.087	0.685	0.078	64.9	15.2	0.530
10	0.167	8.23	0.100	0.700	0.075	74.8	15.6	0.530
11	0.193	8.40	0.115	0.715	0.074	86.3	15.9	0.529
12	0.223	8.56	0.133	0.729	0.072	99.6	16.2	0.528
13	0.257	8.80	0.153	0.749	0.070	114.9	16.6	0.531
14	0.297	8.93	0.177	0.761	0.068	132.6	16.9	0.528
15	0.342	9.13	0.204	0.777	0.067	152.9	17.3	0.529
16	0.395	9.31	0.235	0.792	0.065	176.4	17.6	0.528
17	0.456	9.53	0.272	0.812	0.064	203.6	18.0	0.530
18	0.526	9.73	0.314	0.828	0.061	234.9	18.4	0.531
19	0.607	9.99	0.362	0.851	0.059	271.0	18.9	0.534
20	0.700	10.20	0.417	0.868	0.056	312.7	19.3	0.535
21	0.808	10.47	0.481	0.891	0.053	360.7	19.8	0.539
22	0.932	10.73	0.556	0.913	0.049	416.2	20.3	0.542
23	1.075	10.95	0.641	0.932	0.045	480.2	20.7	0.544
24	1.240	11.20	0.740	0.954	0.038	554.1	21.2	0.546
25	1.431	11.43	0.853	0.973	0.032	639.2	21.6	0.548
26	1.651	11.62	0.984	0.989	0.023	737.5	22.0	0.548
27	1.905	11.73	1.136	0.999	0.014	850.9	22.2	0.545
28	2.159	11.78	1.287	1.003	0.007	964.4	22.3	0.540
29	2.413	11.77	1.439	1.002	0.004	1077.8	22.3	0.534
30	2.667	11.76	1.590	1.001	0.003	1191.3	22.2	0.528
31	2.921	11.76	1.741	1.001	0.002	1304.8	22.2	0.523
32	3.175	11.74	1.893	1.000	0.002	1418.2	22.2	0.518
33	3.429	11.73	2.044	0.999	0.002	1531.7	22.2	0.514
34	3.683	11.72	2.196	0.998	0.002	1645.1	22.2	0.510
35	3.810	11.72	2.271	0.998	0.002	1701.9	22.2	0.508

** INTEGRAL THICKNESS PARAMETERS **

QUANTITY	VALUE IN CM		
DELTA-99	1.677		
DISPLACEMENT THICKNESS	0.243	REDELST =	2408.
MOMENTUM THICKNESS	0.173	RETHETA =	1712.
ENERGY THICKNESS	0.1351		

SHAPE PARAMETERS : H =1.407 LAMBDA =0.145 CLAUSER G = 6.42

RESULTS OF COLES DATA ANALYSIS

COLES DELTA	1.741 CM
COLES UTAU	0.527 M/S
WAKE PARAMETER	0.215 DIMENSIONLESS
CF BASED ON UE	0.00403 DIMENSIONLESS

PROFILE POINTS 8 THROUGH 24 USED
RESULTANT RMS ERROR FOR WALL-WAKE FIT : 0.050 M/S

TURBULENT SKIN FRICTION PROFILE CORRELATIONS

BASIS VELOCITY :	UE	UREF
CF : LOG-LAW FIT	0.00406	0.00407
CF : LUDWEIG-TILLMAN	0.00372	0.00374
CF : FRANK WHITE	0.00359	0.00361

X/H=-0.75

NOM. UREF : 11.83 M/S

FOR BOUNDARY LAYER ANALYSIS UE = 12.00 M/S AT YE = 3.81 CM

PT. NO.	Y CM	UBAR M/S	Y/DEL 99	U/UE	u'/UE	Y+	U+	UTLOC M/S
1	0.000	0.00	0.000	0.000	0.000	0.0	0.0	0.000
2	0.053	6.25	0.029	0.521	0.096	23.8	11.8	0.497
3	0.062	6.61	0.033	0.550	0.094	27.6	12.5	0.508
4	0.072	6.89	0.039	0.574	0.092	32.0	13.0	0.514
5	0.083	7.23	0.045	0.603	0.088	37.1	13.7	0.524
6	0.096	7.43	0.052	0.619	0.085	43.0	14.0	0.525
7	0.112	7.70	0.061	0.642	0.081	49.9	14.6	0.529
8	0.130	7.88	0.070	0.656	0.078	57.9	14.9	0.529
9	0.150	8.09	0.081	0.674	0.076	67.0	15.3	0.530
10	0.174	8.26	0.094	0.688	0.074	77.8	15.6	0.529
11	0.202	8.49	0.109	0.707	0.072	90.2	16.0	0.531
12	0.234	8.67	0.127	0.723	0.071	104.6	16.4	0.530
13	0.272	8.80	0.147	0.733	0.070	121.2	16.6	0.527
14	0.315	9.01	0.171	0.751	0.068	140.6	17.0	0.528
15	0.365	9.22	0.198	0.768	0.067	163.0	17.4	0.529
16	0.424	9.43	0.229	0.786	0.065	189.0	17.8	0.530
17	0.491	9.64	0.266	0.803	0.064	219.2	18.2	0.531
18	0.570	9.89	0.308	0.824	0.062	254.1	18.7	0.534
19	0.661	10.14	0.357	0.845	0.058	294.7	19.2	0.536
20	0.766	10.36	0.415	0.863	0.056	341.7	19.6	0.537
21	0.888	10.68	0.481	0.889	0.052	396.2	20.2	0.543
22	1.030	10.94	0.557	0.912	0.048	459.4	20.7	0.546
23	1.194	11.23	0.646	0.935	0.042	532.8	21.2	0.550
24	1.385	11.48	0.749	0.956	0.036	617.7	21.7	0.552
25	1.606	11.72	0.869	0.976	0.028	716.3	22.1	0.554
26	1.860	11.89	1.006	0.991	0.019	829.6	22.5	0.553
27	2.114	11.99	1.144	0.999	0.011	942.9	22.7	0.550
28	2.368	12.01	1.281	1.001	0.006	1056.2	22.7	0.544
29	2.622	12.01	1.419	1.001	0.004	1169.5	22.7	0.539
30	2.876	12.01	1.556	1.000	0.003	1282.8	22.7	0.534
31	3.130	12.01	1.694	1.000	0.002	1396.1	22.7	0.530
32	3.384	12.00	1.831	1.000	0.002	1509.4	22.7	0.525
33	3.638	12.00	1.969	1.000	0.002	1622.8	22.7	0.522
34	3.810	11.99	2.062	0.999	0.002	1699.6	22.7	0.519

** INTEGRAL THICKNESS PARAMETERS **

QUANTITY	VALUE IN CM		
DELTA-99	1.848		
DISPLACEMENT THICKNESS	0.268	REDELST =	2711.
MOMENTUM THICKNESS	0.193	RETHETA =	1956.
ENERGY THICKNESS	0.1510		

SHAPE PARAMETERS : H =1.386 LAMBDA =0.145 CLAUSER G = 6.32

RESULTS OF COLES DATA ANALYSIS

COLES DELTA	1.883 CM
COLES UTAU	0.527 M/S
WAKE PARAMETER	0.277 DIMENSIONLESS
CF BASED ON UE	0.00386 DIMENSIONLESS

PROFILE POINTS 8 THROUGH 24 USED
RESULTANT RMS ERROR FOR WALL-WAKE FIT : 0.053 M/S

TURBULENT SKIN FRICTION PROFILE CORRELATIONS

BASIS VELOCITY :	UE	UREF
CF : LOG-LAW FIT	0.00389	0.00400
CF : LUDWEIG-TILLMAN	0.00371	0.00382
CF : FRANK WHITE	0.00358	0.00368

X/H=-0.75 NOTE : CASE C ON CENTERLINE

NOM. UREF : 12.17 M/S

FOR BOUNDARY LAYER ANALYSIS UE = 12.22 M/S AT YE = 2.45 CM

PT. NO.	Y CM	UBAR M/S	Y/DEL 99	U/UE	u'/UE	Y+	U+	UTLOC M/S
1	0.000	0.00	0.000	0.000	0.000	0.0	0.0	0.000
2	0.040	7.45	0.061	0.610	0.122	21.7	11.7	0.602
3	0.054	8.22	0.081	0.673	0.112	29.0	12.9	0.625
4	0.072	8.83	0.108	0.723	0.103	38.6	13.8	0.635
5	0.096	9.30	0.144	0.761	0.095	51.5	14.6	0.636
6	0.127	9.76	0.192	0.799	0.087	68.6	15.3	0.637
7	0.170	10.23	0.256	0.838	0.079	91.5	16.0	0.639
8	0.227	10.73	0.342	0.878	0.071	122.0	16.8	0.641
9	0.302	11.25	0.455	0.921	0.060	162.5	17.6	0.645
10	0.403	11.69	0.607	0.957	0.045	216.6	18.3	0.644
11	0.537	12.00	0.808	0.982	0.032	288.6	18.8	0.637
12	0.715	12.13	1.077	0.993	0.025	384.4	19.0	0.623
13	0.952	12.17	1.434	0.996	0.024	512.0	19.1	0.606
14	1.202	12.21	1.811	0.999	0.023	646.6	19.1	0.592
15	1.452	12.22	2.187	1.000	0.021	781.0	19.1	0.581
16	1.702	12.24	2.564	1.002	0.019	915.4	19.2	0.572
17	1.952	12.22	2.940	1.000	0.016	1049.8	19.1	0.564
18	2.202	12.22	3.317	1.001	0.014	1184.2	19.1	0.557
19	2.452	12.19	3.693	0.998	0.010	1318.6	19.1	0.550
20	2.702	12.18	4.070	0.997	0.008	1453.3	19.1	0.544
21	2.952	12.14	4.446	0.994	0.007	1587.6	19.0	0.538
22	3.202	12.13	4.823	0.993	0.005	1722.0	19.0	0.533
23	3.452	12.10	5.199	0.991	0.005	1856.4	19.0	0.528
24	3.702	12.10	5.576	0.991	0.004	1990.9	19.0	0.525
25	3.952	12.09	5.953	0.990	0.004	2125.5	18.9	0.521
26	4.202	12.08	6.329	0.989	0.003	2259.9	18.9	0.518
27	4.452	12.09	6.705	0.990	0.003	2394.3	18.9	0.515
28	4.702	12.08	7.082	0.989	0.003	2528.7	18.9	0.512
29	4.952	12.06	7.458	0.987	0.004	2663.1	18.9	0.509
30	5.080	12.05	7.650	0.986	0.004	2731.6	18.9	0.507

** INTEGRAL THICKNESS PARAMETERS **

QUANTITY	VALUE IN CM		
DELTA-99	0.664		
DISPLACEMENT THICKNESS	0.085	REDELST =	871.
MOMENTUM THICKNESS	0.057	RETHETA =	591.
ENERGY THICKNESS	0.0448		

SHAPE PARAMETERS : H =1.474 LAMBDA =0.128 CLAUSER G = 6.16

RESULTS OF COLES DATA ANALYSIS

COLES DELTA	0.541 CM
COLES UTAU	0.636 M/S
WAKE PARAMETER	0.075 DIMENSIONLESS
CF BASED ON UE	0.00543 DIMENSIONLESS

PROFILE POINTS 5 THROUGH 10 USED
RESULTANT RMS ERROR FOR WALL-WAKE FIT : 0.033 M/S

TURBULENT SKIN FRICTION PROFILE CORRELATIONS

BASIS VELOCITY :	UE	UREF
CF : LOG-LAW FIT	0.00546	0.00550
CF : LUDWEIG-TILLMAN	0.00445	0.00449
CF · FRANK WHITE	0.00450	0.00453

X/H=-3 OPPOSITE WALL

NOM. UREF : 11.68 M/S

FOR BOUNDARY LAYER ANALYSIS UE = 11.72 M/S AT YE = 3.05 CM

PT. NO.	Y* CM	UBAR M/S	Y/DEL 99	U/UE	u'/UE	Y+	U+	UTLOC M/S
1	0.000	0.00	0.000	0.000	0.000	0.0	0.0	0.000
2	0.053	5.97	0.039	0.509	0.098	24.1	11.2	0.477
3	0.061	6.48	0.045	0.553	0.097	27.8	12.2	0.500
4	0.071	6.84	0.052	0.583	0.094	31.9	12.9	0.512
5	0.081	7.16	0.060	0.611	0.089	36.7	13.5	0.521
6	0.093	7.47	0.069	0.638	0.086	42.3	14.1	0.529
7	0.108	7.68	0.079	0.655	0.082	48.7	14.4	0.531
8	0.124	7.92	0.091	0.675	0.080	56.0	14.9	0.534
9	0.142	8.01	0.105	0.684	0.077	64.4	15.1	0.529
10	0.164	8.26	0.121	0.705	0.076	74.1	15.5	0.532
11	0.189	8.42	0.139	0.719	0.073	85.3	15.8	0.532
12	0.217	8.61	0.160	0.735	0.071	98.1	16.2	0.532
13	0.249	8.81	0.184	0.751	0.070	112.9	16.6	0.533
14	0.287	8.96	0.211	0.764	0.068	129.9	16.8	0.531
15	0.330	9.18	0.243	0.783	0.066	149.4	17.3	0.533
16	0.380	9.35	0.280	0.798	0.064	172.0	17.6	0.532
17	0.437	9.59	0.322	0.819	0.063	197.8	18.0	0.535
18	0.503	9.81	0.370	0.837	0.061	227.6	18.4	0.537
19	0.579	10.06	0.426	0.858	0.059	261.9	18.9	0.540
20	0.666	10.29	0.490	0.878	0.055	301.4	19.4	0.542
21	0.766	10.56	0.564	0.901	0.051	346.7	19.8	0.546
22	0.882	10.81	0.649	0.922	0.047	398.9	20.3	0.549
23	1.015	11.11	0.746	0.948	0.041	459.0	20.9	0.554
24	1.167	11.39	0.859	0.972	0.033	528.1	21.4	0.558
25	1.343	11.59	0.988	0.989	0.023	607.6	21.8	0.558
26	1.545	11.72	1.137	1.000	0.013	699.1	22.0	0.555
27	1.778	11.74	1.308	1.002	0.006	804.4	22.1	0.549
28	2.032	11.74	1.495	1.002	0.004	919.3	22.1	0.541
29	2.286	11.73	1.682	1.001	0.003	1034.2	22.1	0.534
30	2.540	11.72	1.869	1.000	0.002	1149.1	22.0	0.528
31	2.794	11.71	2.056	0.999	0.002	1264.0	22.0	0.523
32	3.048	11.69	2.242	0.997	0.002	1379.0	22.0	0.518
33	3.302	11.68	2.429	0.997	0.002	1493.9	22.0	0.513
34	3.556	11.68	2.616	0.996	0.002	1608.8	22.0	0.510
35	3.810	11.68	2.803	0.996	0.002	1723.7	22.0	0.506

** INTEGRAL THICKNESS PARAMETERS **

QUANTITY	VALUE IN CM		
DELTA-99	1.359		
DISPLACEMENT THICKNESS	0.216	REDELST =	2152.
MOMENTUM THICKNESS	0.149	RETHETA =	1484.
ENERGY THICKNESS	0.1150		

SHAPE PARAMETERS : H =1.450 LAMBDA =0.159 CLAUSER G = 6.84

RESULTS OF COLES DATA ANALYSIS

COLES DELTA 1.482 CM
COLES UTAU 0.530 M/S

WAKE PARAMETER 0.260 DIMENSIONLESS
CF BASED ON UE 0.00408 DIMENSIONLESS

PROFILE POINTS 8 THROUGH 23 USED
RESULTANT RMS ERROR FOR WALL-WAKE FIT : 0.050 M/S

TURBULENT SKIN FRICTION PROFILE CORRELATIONS

BASIS VELOCITY :	UE	UREF
CF : LOG-LAW FIT	0.00412	0.00415
CF : LUDWEIG-TILLMAN	0.00361	0.00364
CF : FRANK WHITE	0.00348	0.00351

RECOVERY PROFILES - CASES A, B, & C

A SUMMARY OF THESE DATA APPEARS AS TABLE 5-2

X/H=12 CASE A

NOM. UREF : 12.20 M/S

FOR BOUNDARY LAYER ANALYSIS UE = 9.64 M/S AT YE = 8.77 CM

PT. NO.	Y CM	UBAR M/S	Y/DEL 99	U/UE	u'/UE	Y+	U+	UTLOC M/S
1	0.000	0.00	0.000	0.000	0.000	0.0	0.0	0.000
2	0.040	1.87	0.005	0.194	0.120	7.7	8.3	0.194
3	0.062	2.27	0.008	0.236	0.134	11.9	10.1	0.209
4	0.096	2.62	0.012	0.272	0.141	18.3	11.7	0.218
5	0.147	2.91	0.019	0.302	0.150	28.2	13.0	0.222
6	0.227	3.20	0.029	0.332	0.149	43.4	14.2	0.225
7	0.349	3.44	0.044	0.357	0.156	66.8	15.3	0.225
8	0.537	3.65	0.068	0.379	0.157	102.7	16.3	0.224
9	0.825	3.90	0.104	0.405	0.163	158.0	17.4	0.225
10	1.269	4.23	0.160	0.439	0.170	242.9	18.9	0.229
11	1.768	4.61	0.223	0.478	0.179	338.6	20.5	0.238
12	2.269	5.09	0.286	0.529	0.188	434.4	22.7	0.253
13	2.769	5.51	0.349	0.572	0.196	530.1	24.5	0.266
14	3.268	5.95	0.412	0.617	0.203	625.8	26.5	0.280
15	3.769	6.49	0.475	0.674	0.204	721.6	28.9	0.298
16	4.269	6.97	0.538	0.723	0.205	817.3	31.0	0.314
17	4.768	7.44	0.601	0.773	0.198	913.0	33.2	0.330
18	5.269	7.91	0.664	0.821	0.189	1008.8	35.2	0.345
19	5.768	8.35	0.727	0.867	0.179	1104.5	37.2	0.359
20	6.269	8.72	0.790	0.905	0.160	1200.3	38.8	0.371
21	6.769	9.09	0.853	0.943	0.142	1295.9	40.5	0.382
22	7.268	9.34	0.916	0.969	0.122	1391.7	41.6	0.389
23	7.769	9.50	0.980	0.986	0.103	1487.5	42.3	0.393
24	8.269	9.61	1.043	0.998	0.084	1583.1	42.8	0.395
25	8.768	9.66	1.106	1.002	0.073	1678.8	43.0	0.394
26	9.269	9.55	1.169	0.991	0.066	1774.6	42.5	0.388
27	9.769	9.20	1.232	0.955	0.078	1870.3	41.0	0.374
28	10.120	8.86	1.276	0.919	0.088	1937.5	39.4	0.360

** INTEGRAL THICKNESS PARAMETERS **

QUANTITY	VALUE IN CM	
DELTA-99	7.931	
DISPLACEMENT THICKNESS	2.509	REDELST = 20619.
MOMENTUM THICKNESS	1.363	RETHETA = 11197.
ENERGY THICKNESS	0.8162	

SHAPE PARAMETERS : H =1.842 LAMBDA =0.316 CLAUSER G =19.61

RESULTS OF COLES DATA ANALYSIS

COLES DELTA	8.545 CM
COLES UTAU	0.219 M/S
WAKE PARAMETER	4.292 DIMENSIONLESS
CF BASED ON UE	0.00104 DIMENSIONLESS

PROFILE POINTS 7 THROUGH 20 USED
RESULTANT RMS ERROR FOR WALL-WAKE FIT : 0.164 M/S

TURBULENT SKIN FRICTION PROFILE CORRELATIONS

BASIS VELOCITY :	UE	UREF
CF : LOG-LAW FIT	0.00109	0.00068
CF : LUDWEIG-TILLMAN	0.00114	0.00071
CF : FRANK WHITE	0.00102	0.00064

X/H=14 CASE A

NOM. UREF : 12.26 M/S

FOR BOUNDARY LAYER ANALYSIS UE = 9.73 M/S AT YE = 8.50 CM

PT. NO.	Y CM	UBAR M/S	Y/DEL 99	U/UE	u'/UE	Y+	U+	UTLOC M/S
1	0.000	0.00	0.000	0.000	0.000	0.0	0.0	0.000
2	0.040	2.35	0.005	0.242	0.117	9.3	8.3	0.236
3	0.060	2.99	0.008	0.307	0.129	13.8	10.6	0.266
4	0.090	3.40	0.011	0.349	0.136	20.7	12.0	0.275
5	0.135	3.76	0.017	0.386	0.141	31.0	13.3	0.281
6	0.202	4.09	0.025	0.420	0.144	46.2	14.5	0.284
7	0.302	4.33	0.038	0.445	0.143	69.1	15.3	0.283
8	0.450	4.61	0.057	0.474	0.146	103.2	16.3	0.283
9	0.673	4.82	0.085	0.496	0.153	154.1	17.1	0.279
10	1.005	5.09	0.127	0.523	0.151	230.2	18.0	0.279
11	1.501	5.44	0.190	0.559	0.161	343.9	19.3	0.283
12	2.001	5.78	0.253	0.594	0.168	458.4	20.4	0.289
13	2.501	6.16	0.316	0.633	0.172	572.9	21.8	0.298
14	3.001	6.42	0.379	0.660	0.183	687.6	22.7	0.304
15	3.501	6.77	0.442	0.696	0.183	802.1	24.0	0.314
16	4.000	7.13	0.505	0.732	0.185	916.6	25.2	0.324
17	4.501	7.52	0.569	0.773	0.187	1031.3	26.6	0.336
18	5.001	7.91	0.632	0.813	0.182	1145.8	28.0	0.348
19	5.501	8.37	0.695	0.860	0.172	1260.4	29.6	0.363
20	6.001	8.70	0.758	0.894	0.163	1374.9	30.8	0.373
21	6.501	8.93	0.821	0.918	0.162	1489.5	31.6	0.379
22	7.001	9.32	0.884	0.957	0.139	1604.1	33.0	0.391
23	7.501	9.53	0.948	0.979	0.127	1718.6	33.7	0.397
24	8.000	9.65	1.011	0.992	0.108	1833.1	34.2	0.399
25	8.501	9.73	1.074	1.000	0.092	1947.8	34.4	0.400
26	9.001	9.56	1.137	0.983	0.088	2062.3	33.8	0.392
27	9.500	9.27	1.200	0.953	0.090	2176.8	32.8	0.379
28	10.001	8.75	1.263	0.899	0.102	2291.5	31.0	0.358
29	10.159	8.59	1.284	0.883	0.104	2327.8	30.4	0.351

** INTEGRAL THICKNESS PARAMETERS **

QUANTITY	VALUE IN CM	
DELTA-99	7.915	
DISPLACEMENT THICKNESS	2.137	REDELST = 16851.
MOMENTUM THICKNESS	1.322	RETHETA = 10429.
ENERGY THICKNESS	0.8689	

SHAPE PARAMETERS : H =1.616 LAMBDA =0.270 CLAUSER G =13.12

RESULTS OF COLES DATA ANALYSIS

COLES DELTA	9.162 CM
COLES UTAU	0.275 M/S
WAKE PARAMETER	2.424 DIMENSIONLESS
CF BASED ON UE	0.00160 DIMENSIONLESS

PROFILE POINTS 7 THROUGH 21 USED
RESULTANT RMS ERROR FOR WALL-WAKE FIT : 0.301 M/S

TURBULENT SKIN FRICTION PROFILE CORRELATIONS

BASIS VELOCITY :	UE	UREF
CF : LOG-LAW FIT	0.00169	0.00106
CF : LUDWEIG-TILLMAN	0.00165	0.00104
CF : FRANK WHITE	0.00155	0.00098

X/H=16 CASE A

NOM. UREF : 12.25 M/S

FOR BOUNDARY LAYER ANALYSIS UE = 9.27 M/S AT YE = 8.00 CM

PT. NO.	Y CM	UBAR M/S	Y/DEL 99	U/UE	u'/UE	Y+	U+	UTLOC M/S
1	0.000	0.00	0.000	0.000	0.000	0.0	0.0	0.000
2	0.040	2.42	0.005	0.261	0.114	10.1	7.8	0.241
3	0.060	3.19	0.008	0.344	0.131	15.1	10.3	0.280
4	0.090	3.74	0.012	0.404	0.135	22.6	12.1	0.299
5	0.135	4.20	0.018	0.453	0.141	33.8	13.6	0.309
6	0.202	4.53	0.027	0.489	0.139	50.4	14.6	0.311
7	0.302	4.81	0.040	0.518	0.142	75.4	15.5	0.309
8	0.450	5.10	0.060	0.550	0.144	112.5	16.5	0.309
9	0.673	5.32	0.089	0.573	0.146	168.0	17.2	0.304
10	1.005	5.57	0.133	0.601	0.152	251.0	18.0	0.303
11	1.501	5.87	0.199	0.633	0.153	375.0	18.9	0.302
12	2.001	6.07	0.266	0.655	0.163	499.9	19.6	0.302
13	2.501	6.45	0.332	0.696	0.169	624.8	20.8	0.311
14	3.001	6.62	0.399	0.714	0.172	749.8	21.4	0.312
15	3.501	6.92	0.465	0.746	0.177	874.7	22.3	0.320
16	4.000	7.22	0.531	0.779	0.177	999.5	23.3	0.328
17	4.501	7.53	0.598	0.813	0.179	1124.5	24.3	0.337
18	5.001	7.78	0.664	0.839	0.178	1249.4	25.1	0.343
19	5.501	8.15	0.731	0.878	0.174	1374.4	26.3	0.355
20	6.001	8.44	0.797	0.910	0.170	1499.3	27.3	0.363
21	6.501	8.77	0.864	0.946	0.163	1624.2	28.3	0.373
22	7.001	9.00	0.930	0.971	0.150	1749.2	29.1	0.380
23	7.501	9.17	0.996	0.989	0.136	1874.1	29.6	0.384
24	8.000	9.27	1.063	1.000	0.124	1998.9	29.9	0.385
25	8.501	9.22	1.129	0.994	0.110	2123.9	29.8	0.381
26	9.001	9.06	1.196	0.977	0.106	2248.8	29.2	0.373
27	9.500	8.72	1.262	0.941	0.110	2373.7	28.2	0.359
28	10.001	8.35	1.329	0.900	0.119	2498.7	27.0	0.343
29	10.159	8.15	1.350	0.880	0.120	2538.4	26.3	0.335

** INTEGRAL THICKNESS PARAMETERS **

QUANTITY	VALUE IN CM	
DELTA-99	7.528	
DISPLACEMENT THICKNESS	1.793	REDELST = 13415.
MOMENTUM THICKNESS	1.200	RETHETA = 8981.
ENERGY THICKNESS	0.8413	

SHAPE PARAMETERS : H =1.494 LAMBDA =0.238 CLAUSER Q = 9.90

RESULTS OF COLES DATA ANALYSIS

COLES DELTA	9.354 CM
COLES UTAU	0.298 M/S
WAKE PARAMETER	1.491 DIMENSIONLESS
CF BASED ON UE	0.00207 DIMENSIONLESS

PROFILE POINTS 7 THROUGH 21 USED
RESULTANT RMS ERROR FOR WALL-WAKE FIT : 0.423 M/S

TURBULENT SKIN FRICTION PROFILE CORRELATIONS

BASIS VELOCITY :	UE	UREF
CF : LOG-LAW FIT	0.00223	0.00128
CF : LUDWEIG-TILLMAN	0.00208	0.00119
CF : FRANK WHITE	0.00199	0.00114

X/H=18 CASE A

NOM. UREF : 12.17 M/S

FOR BOUNDARY LAYER ANALYSIS UE = 8.73 M/S AT YE = 8.27 CM

PT. NO.	Y CM	UBAR M/S	Y/DEL 99	U/UE	u'/UE	Y+	U+	UTLOC M/S
1	0.000	0.00	0.000	0.000	0.000	0.0	0.0	0.000
2	0.040	3.03	0.006	0.347	0.130	11.5	9.1	0.286
3	0.062	3.81	0.009	0.436	0.137	17.6	11.5	0.320
4	0.096	4.31	0.013	0.494	0.140	27.2	13.0	0.331
5	0.147	4.77	0.020	0.547	0.140	41.8	14.4	0.337
6	0.227	5.10	0.031	0.584	0.138	64.4	15.4	0.336
7	0.349	5.40	0.048	0.618	0.138	99.0	16.3	0.333
8	0.537	5.62	0.074	0.644	0.140	152.3	16.9	0.326
9	0.825	5.92	0.114	0.678	0.145	234.1	17.9	0.324
10	1.269	6.11	0.175	0.699	0.147	360.0	18.4	0.317
11	1.768	6.34	0.244	0.726	0.151	501.9	19.1	0.316
12	2.269	6.51	0.312	0.745	0.157	643.8	19.6	0.315
13	2.769	6.70	0.381	0.767	0.157	785.7	20.2	0.317
14	3.268	6.96	0.450	0.796	0.160	927.5	21.0	0.322
15	3.769	7.13	0.519	0.817	0.162	1069.5	21.5	0.325
16	4.269	7.36	0.588	0.843	0.165	1211.3	22.2	0.330
17	4.768	7.62	0.657	0.873	0.166	1353.2	23.0	0.337
18	5.269	7.86	0.726	0.900	0.167	1495.2	23.7	0.343
19	5.768	8.13	0.794	0.931	0.163	1637.0	24.5	0.350
20	6.269	8.30	0.863	0.950	0.160	1779.0	25.0	0.354
21	6.769	8.53	0.932	0.977	0.152	1920.8	25.7	0.361
22	7.268	8.65	1.001	0.990	0.145	2062.7	26.1	0.363
23	7.769	8.74	1.070	1.001	0.132	2204.6	26.4	0.364
24	8.269	8.72	1.139	0.999	0.123	2346.5	26.3	0.361
25	8.768	8.63	1.207	0.988	0.117	2488.3	26.0	0.356
26	9.269	8.41	1.276	0.963	0.115	2630.3	25.3	0.346
27	9.769	8.13	1.345	0.931	0.119	2772.1	24.5	0.334
28	10.159	7.81	1.399	0.895	0.125	2883.1	23.6	0.321

** INTEGRAL THICKNESS PARAMETERS **

QUANTITY	VALUE IN CM	
DELTA-99	7.262	
DISPLACEMENT THICKNESS	1.390	REDELST = 10389.
MOMENTUM THICKNESS	1.014	RETHETA = 7575.
ENERGY THICKNESS	0.7648	

SHAPE PARAMETERS : H =1.371 LAMBDA =0.191 CLAUSER G = 7.13

RESULTS OF COLES DATA ANALYSIS

COLES DELTA	9.390 CM
COLES UTAU	0.318 M/S
WAKE PARAMETER	0.687 DIMENSIONLESS
CF BASED ON UE	0.00265 DIMENSIONLESS

PROFILE POINTS 6 THROUGH 21 USED
RESULTANT RMS ERROR FOR WALL-WAKE FIT : 0.574 M/S

TURBULENT SKIN FRICTION PROFILE CORRELATIONS

BASIS VELOCITY :	UE	UREF
CF : LOG-LAW FIT	0.00289	0.00149
CF : LUDWEIG-TILLMAN	0.00264	0.00136
CF : FRANK WHITE	0.00257	0.00132

X/H=20 CASE A

NOM. UREF : 12.19 M/S

FOR BOUNDARY LAYER ANALYSIS UE = 8.42 M/S AT YE = 8.27 CM

PT. NO.	Y CM	UBAR M/S	Y/DEL 99	U/UE	u'/UE	Y+	U+	UTLOC M/S
1	0.000	0.00	0.000	0.000	0.000	0.0	0.0	0.000
2	0.040	3.22	0.006	0.382	0.132	12.0	9.3	0.300
3	0.062	3.97	0.009	0.471	0.139	18.4	11.4	0.331
4	0.096	4.53	0.014	0.538	0.140	28.4	13.1	0.345
5	0.147	5.01	0.021	0.594	0.136	43.7	14.4	0.351
6	0.227	5.37	0.033	0.637	0.138	67.3	15.5	0.351
7	0.349	5.60	0.051	0.665	0.136	103.5	16.1	0.344
8	0.537	5.93	0.078	0.704	0.138	159.2	17.1	0.342
9	0.825	6.15	0.120	0.730	0.138	244.7	17.7	0.335
10	1.269	6.41	0.184	0.761	0.141	376.3	18.5	0.331
11	1.768	6.59	0.257	0.782	0.144	524.5	19.0	0.327
12	2.269	6.79	0.330	0.806	0.149	672.9	19.5	0.327
13	2.769	6.98	0.402	0.829	0.153	821.2	20.1	0.329
14	3.268	7.07	0.475	0.839	0.155	969.4	20.4	0.327
15	3.769	7.24	0.547	0.860	0.155	1117.8	20.9	0.329
16	4.269	7.44	0.620	0.884	0.159	1266.1	21.4	0.333
17	4.768	7.59	0.693	0.900	0.163	1414.3	21.8	0.335
18	5 269	7.77	0.765	0.922	0.160	1562.7	22.4	0.339
19	5.768	8.00	0.838	0.949	0.156	1711.0	23.0	0.345
20	6.269	8.14	0.911	0.967	0.154	1859.4	23.5	0.348
21	6.769	8.32	0.983	0.987	0.149	2007.6	23.9	0.352
22	7.268	8.42	1.056	0.999	0.137	2155.9	24.2	0.354
23	7.769	8.42	1.128	1.000	0.134	2304.3	24.3	0.352
24	8.269	8.43	1.201	1.001	0.127	2452.5	24.3	0.350
25	8.768	8.33	1.274	0.988	0.124	2600.7	24.0	0.344
26	9.269	8.16	1.346	0.968	0.123	2749.1	23.5	0.336
27	9.769	7.89	1.419	0.936	0.127	2897.4	22.7	0.325
28	10.159	7.63	1.476	0.906	0.132	3013.4	22.0	0.314

** INTEGRAL THICKNESS PARAMETERS **

QUANTITY	VALUE IN CM		
DELTA-99	6.885		
DISPLACEMENT THICKNESS	1.105	REDELST =	7948.
MOMENTUM THICKNESS	0.850	RETHETA =	6112.
ENERGY THICKNESS	0.6708		

SHAPE PARAMETERS : H =1.300 LAMBDA =0.160 CLAUSER G = 5.60

RESULTS OF COLES DATA ANALYSIS

COLES DELTA	119.723 CM
COLES UTAU	0.339 M/S
WAKE PARAMETER	-1.155 DIMENSIONLESS
CF BASED ON UE	0.00324 DIMENSIONLESS

PROFILE POINTS 6 THROUGH 28 USED
RESULTANT RMS ERROR FOR WALL-WAKE FIT : 0.790 M/S

TURBULENT SKIN FRICTION PROFILE CORRELATIONS

BASIS VELOCITY :	UE	UREF
CF : LOG-LAW FIT	0.00340	0.00162
CF : LUDWEIG-TILLMAN	0.00312	0.00149
CF : FRANK WHITE	0.00307	0.00147

X/H=11.8 CASE B

NOM. UREF : 12.17 M/S

FOR BOUNDARY LAYER ANALYSIS UE = 10.28 M/S AT YE = 9.03 CM

PT. NO.	Y CM	UBAR M/S	Y/DEL 99	U/UE	u'/UE	Y+	U+	UTLOC M/S
1	0.000	0.00	0.000	0.000	0.000	0.0	0.0	0.000
2	0.053	1.57	0.006	0.153	0.098	8.6	8.0	0.161
3	0.072	1.83	0.009	0.178	0.112	11.6	9.4	0.172
4	0.098	2.17	0.012	0.211	0.123	15.7	11.1	0.187
5	0.133	2.31	0.016	0.225	0.127	21.3	11.8	0.187
6	0.180	2.54	0.022	0.247	0.138	28.8	13.0	0.193
7	0.244	2.71	0.029	0.263	0.140	39.1	13.9	0.194
8	0.330	2.83	0.039	0.276	0.141	53.0	14.5	0.193
9	0.447	2.97	0.053	0.289	0.144	71.7	15.2	0.193
10	0.606	3.20	0.072	0.311	0.152	97.2	16.4	0.197
11	0.821	3.36	0.098	0.327	0.154	131.7	17.2	0.198
12	1.112	3.68	0.133	0.358	0.163	178.5	18.8	0.207
13	1.507	3.97	0.180	0.386	0.174	241.8	20.3	0.213
14	2.042	4.33	0.244	0.421	0.187	327.6	22.1	0.222
15	2.677	4.87	0.320	0.474	0.197	429.5	24.9	0.240
16	3.312	5.47	0.396	0.533	0.210	531.4	28.0	0.260
17	3.947	6.07	0.472	0.590	0.215	633.3	31.0	0.281
18	4.582	6.74	0.548	0.656	0.221	735.1	34.5	0.304
19	5.217	7.53	0.624	0.732	0.218	837.0	38.5	0.331
20	5.852	8.01	0.700	0.779	0.216	938.9	41.0	0.347
21	6.487	8.83	0.776	0.859	0.196	1040.7	45.2	0.375
22	7.122	9.34	0.852	0.909	0.184	1142.6	47.8	0.391
23	7.757	9.86	0.928	0.959	0.155	1244.5	50.4	0.407
24	8.392	10.19	1.004	0.992	0.127	1346.4	52.2	0.417
25	9.027	10.28	1.080	1.000	0.114	1448.2	52.6	0.418
26	9.662	10.17	1.156	0.990	0.096	1550.1	52.0	0.411
27	10.297	9.76	1.232	0.950	0.099	1652.0	49.9	0.394
28	10.795	9.07	1.291	0.882	0.113	1731.8	46.4	0.367

** INTEGRAL THICKNESS PARAMETERS **

QUANTITY	VALUE IN CM	
DELTA-99	8.359	
DISPLACEMENT THICKNESS	3.139	REDELST = 26480.
MOMENTUM THICKNESS	1.529	RETHETA = 12903.
ENERGY THICKNESS	0.8496	

SHAPE PARAMETERS : H =2.052 LAMBDA =0.375 CLAUSER G =26.96

RESULTS OF COLES DATA ANALYSIS

COLES DELTA	9.559 CM
COLES UTAU	0.193 M/S
WAKE PARAMETER	6.206 DIMENSIONLESS
CF BASED ON UE	0.00071 DIMENSIONLESS

PROFILE POINTS 8 THROUGH 22 USED
RESULTANT RMS ERROR FOR WALL-WAKE FIT : 0.327 M/S

TURBULENT SKIN FRICTION PROFILE CORRELATIONS

BASIS VELOCITY :	UE	UREF
CF : LOG-LAW FIT	0.00072	0.00052
CF : LUDWEIG-TILLMAN	0.00079	0.00056
CF : FRANK WHITE	0.00068	0.00049

X/H=13.8 CASE B

NOM. UREF : 12.12 M/S

FOR BOUNDARY LAYER ANALYSIS UE = 9.55 M/S AT YE = 9.03 CM

PT. NO.	Y CM	UBAR M/S	Y/DEL 99	U/UE	u'/UE	Y+	U+	UTLOC M/S
1	0.000	0.00	0.000	0.000	0.000	0.0	0.0	0.000
2	0.053	2.08	0.007	0.217	0.116	10.9	8.4	0.201
3	0.072	2.55	0.009	0.267	0.131	14.7	10.3	0.225
4	0.098	2.92	0.012	0.306	0.141	19.9	11.8	0.239
5	0.133	3.13	0.016	0.327	0.148	27.0	12.6	0.241
6	0.180	3.42	0.022	0.358	0.149	36.6	13.8	0.248
7	0.244	3.65	0.030	0.382	0.153	49.6	14.7	0.251
8	0.330	3.78	0.040	0.396	0.159	67.2	15.2	0.248
9	0.447	3.95	0.055	0.413	0.163	91.1	15.9	0.247
10	0.606	4.16	0.074	0.435	0.161	123.4	16.7	0.248
11	0.821	4.41	0.100	0.462	0.165	167.2	17.8	0.252
12	1.112	4.55	0.136	0.476	0.170	226.6	18.3	0.249
13	1.507	4.79	0.184	0.502	0.177	307.0	19.3	0.252
14	2.042	5.17	0.250	0.542	0.184	415.9	20.8	0.261
15	2.677	5.47	0.328	0.573	0.193	545.3	22.0	0.266
16	3.312	5.96	0.405	0.624	0.209	674.6	24.0	0.281
17	3.947	6.41	0.483	0.671	0.206	803.9	25.8	0.295
18	4.582	6.96	0.561	0.729	0.210	933.2	28.0	0.313
19	5.217	7.45	0.639	0.781	0.207	1062.6	30.0	0.328
20	5.852	7.92	0.716	0.830	0.212	1191.9	31.9	0.343
21	6.487	8.45	0.794	0.885	0.202	1321.2	34.0	0.360
22	7.122	8.93	0.872	0.935	0.191	1450.6	36.0	0.376
23	7.757	9.29	0.949	0.973	0.171	1579.9	37.4	0.386
24	8.392	9.54	1.027	0.999	0.146	1709.2	38.4	0.393
25	9.027	9.56	1.105	1.001	0.127	1838.5	38.5	0.391
26	9.662	9.30	1.183	0.974	0.121	1967.9	37.5	0.379
27	10.297	8.81	1.260	0.922	0.126	2097.2	35.5	0.359
28	10.795	8.21	1.321	0.859	0.138	2198.6	33.0	0.335

** INTEGRAL THICKNESS PARAMETERS **

QUANTITY	VALUE IN CM	
DELTA-99	8.170	
DISPLACEMENT THICKNESS	2.532	REDELST = 19822.
MOMENTUM THICKNESS	1.459	RETHETA = 11424.
ENERGY THICKNESS	0.9054	

SHAPE PARAMETERS : H =1.735 LAMBDA =0.310 CLAUSER G =16.29

RESULTS OF COLES DATA ANALYSIS

COLES DELTA	9.688 CM
COLES UTAU	0.243 M/S
WAKE PARAMETER	3.258 DIMENSIONLESS
CF BASED ON UE	0.00129 DIMENSIONLESS

PROFILE POINTS 8 THROUGH 22 USED
RESULTANT RMS ERROR FOR WALL-WAKE FIT : 0.378 M/S

TURBULENT SKIN FRICTION PROFILE CORRELATIONS

BASIS VELOCITY :	UE	UREF
CF : LOG-LAW FIT	0.00135	0.00084
CF : LUDWEIG-TILLMAN	0.00134	0.00083
CF : FRANK WHITE	0.00123	0.00076

X/H=15.8 CASE B

NOM. UREF : 12.13 M/S

FOR BOUNDARY LAYER ANALYSIS UE = 8.84 M/S AT YE = 9.03 CM

PT. NO.	Y CM	UBAR M/S	Y/DEL 99	U/UE	u'/UE	Y+	U+	UTLOC M/S
1	0.000	0.00	0.000	0.000	0.000	0.0	0.0	0.000
2	0.053	2.31	0.007	0.262	0.116	12.4	8.2	0.220
3	0.072	2.94	0.009	0.333	0.134	16.8	10.4	0.253
4	0.098	3.45	0.013	0.390	0.148	22.8	12.2	0.274
5	0.133	3.71	0.017	0.420	0.149	30.9	13.1	0.278
6	0.180	3.97	0.023	0.449	0.153	41.9	14.0	0.281
7	0.244	4.22	0.032	0.477	0.157	56.7	14.9	0.284
8	0.330	4.44	0.043	0.502	0.157	76.9	15.7	0.284
9	0.447	4.62	0.058	0.523	0.162	104.2	16.3	0.283
10	0.606	4.79	0.079	0.541	0.168	141.1	16.9	0.280
11	0.821	4.98	0.107	0.564	0.165	191.2	17.6	0.280
12	1.112	5.18	0.145	0.585	0.172	259.1	18.3	0.279
13	1.507	5.36	0.197	0.606	0.175	351.1	18.9	0.278
14	2.042	5.74	0.266	0.649	0.182	475.7	20.3	0.286
15	2.677	5.90	0.349	0.667	0.193	623.6	20.9	0.285
16	3.312	6.29	0.432	0.712	0.201	771.5	22.3	0.295
17	3.947	6.55	0.515	0.740	0.208	919.4	23.2	0.300
18	4.582	6.97	0.598	0.788	0.208	1067.4	24.6	0.313
19	5.217	7.39	0.681	0.836	0.214	1215.3	26.1	0.326
20	5.852	7.77	0.764	0.879	0.210	1363.2	27.5	0.337
21	6.487	8.24	0.846	0.932	0.204	1511.1	29.1	0.352
22	7.122	8.51	0.929	0.963	0.189	1659.0	30.1	0.359
23	7.757	8.80	1.012	0.995	0.178	1806.9	31.1	0.367
24	8.392	8.84	1.095	1.000	0.165	1954.8	31.3	0.367
25	9.027	8.84	1.178	1.000	0.150	2102.7	31.3	0.364
26	9.662	8.60	1.261	0.972	0.141	2250.7	30.4	0.353
27	10.297	8.13	1.343	0.919	0.146	2398.6	28.7	0.333
28	10.932	7.45	1.426	0.843	0.152	2546.5	26.3	0.306
29	11.430	6.97	1.491	0.788	0.154	2662.4	24.6	0.287

** INTEGRAL THICKNESS PARAMETERS **

QUANTITY	VALUE IN CM	
DELTA-99	7.665	
DISPLACEMENT THICKNESS	1.965	REDELST = 14312.
MOMENTUM THICKNESS	1.278	RETHETA = 9307.
ENERGY THICKNESS	0.8742	

SHAPE PARAMETERS : H =1.538 LAMBDA =0.256 CLAUSER G =10.94

RESULTS OF COLES DATA ANALYSIS

COLES DELTA	9.595 CM
COLES UTAU	0.275 M/S
WAKE PARAMETER	1.713 DIMENSIONLESS
CF BASED ON UE	0.00194 DIMENSIONLESS

PROFILE POINTS 7 THROUGH 22 USED
RESULTANT RMS ERROR FOR WALL-WAKE FIT : 0.504 M/S

TURBULENT SKIN FRICTION PROFILE CORRELATIONS

BASIS VELOCITY :	UE	UREF
CF : LOG-LAW FIT	0.00205	0.00109
CF : LUDWEIG-TILLMAN	0.00193	0.00102
CF : FRANK WHITE	0.00183	0.00097

X/H=17.8 CASE B

NOM. UREF : 12.20 M/S

FOR BOUNDARY LAYER ANALYSIS UE = 8.75 M/S AT YE = 8.38 CM

PT. NO.	Y CM	UBAR M/S	Y/DEL 99	U/UE	u'/UE	Y+	U+	UTLOC M/S
1	0.000	0.00	0.000	0.000	0.000	0.0	0.0	0.000
2	0.053	2.72	0.007	0.311	0.117	14.5	8.3	0.250
3	0.074	3.54	0.010	0.404	0.135	20.2	10.8	0.293
4	0.103	4.14	0.013	0.474	0.146	28.1	12.7	0.317
5	0.144	4.57	0.019	0.522	0.146	39.0	14.0	0.328
6	0.200	4.85	0.026	0.554	0.148	54.3	14.9	0.328
7	0.279	5.10	0.036	0.583	0.150	75.6	15.6	0.328
8	0.388	5.35	0.050	0.612	0.152	105.3	16.4	0.327
9	0.540	5.52	0.070	0.631	0.152	146.6	16.9	0.322
10	0.752	5.69	0.097	0.651	0.158	204.1	17.4	0.318
11	1.047	5.90	0.135	0.674	0.159	284.1	18.1	0.315
12	1.458	6.11	0.188	0.698	0.163	395.5	18.7	0.313
13	2.029	6.44	0.262	0.736	0.174	550.6	19.7	0.317
14	2.664	6.63	0.344	0.758	0.176	722.8	20.3	0.316
15	3.299	6.85	0.426	0.783	0.179	895.1	21.0	0.318
16	3.934	7.12	0.508	0.813	0.186	1067.4	21.8	0.323
17	4.569	7.42	0.590	0.848	0.191	1239.7	22.7	0.331
18	5.204	7.73	0.672	0.883	0.191	1412.0	23.7	0.339
19	5.839	8.04	0.754	0.918	0.189	1584.3	24.6	0.347
20	6.474	8.32	0.836	0.951	0.189	1756.6	25.5	0.355
21	7.109	8.58	0.918	0.981	0.182	1928.8	26.3	0.362
22	7.744	8.66	1.000	0.990	0.170	2101.1	26.5	0.362
23	8.379	8.75	1.082	1.000	0.156	2273.4	26.8	0.363
24	9.014	8.68	1.164	0.992	0.145	2445.7	26.6	0.358
25	9.649	8.46	1.246	0.966	0.142	2618.0	25.9	0.347
26	10.284	8.06	1.328	0.921	0.151	2790.3	24.7	0.330
27	10.795	7.72	1.394	0.882	0.151	2928.9	23.6	0.316

** INTEGRAL THICKNESS PARAMETERS **

QUANTITY	VALUE IN CM	
DELTA-99	7.747	
DISPLACEMENT THICKNESS	1.486	REDELST = 10813.
MOMENTUM THICKNESS	1.068	RETHETA = 7767.
ENERGY THICKNESS	0.8001	

SHAPE PARAMETERS : H =1.392 LAMBDA =0.192 CLAUSER Q = 7.55

RESULTS OF COLES DATA ANALYSIS

COLES DELTA	9.656 CM
COLES UTAU	0.316 M/S
WAKE PARAMETER	0.738 DIMENSIONLESS
CF BASED ON UE	0.00260 DIMENSIONLESS

PROFILE POINTS 6 THROUGH 21 USED
RESULTANT RMS ERROR FOR WALL-WAKE FIT : 0.517 M/S

TURBULENT SKIN FRICTION PROFILE CORRELATIONS

BASIS VELOCITY :	UE	UREF
CF : LOG-LAW FIT	0.00278	0.00143
CF : LUDWEIG-TILLMAN	0.00254	0.00131
CF : FRANK WHITE	0.00247	0.00127

X/H=19.8 CASE B

NOM. UREF : 12.13 M/S

FOR BOUNDARY LAYER ANALYSIS UE = 8.01 M/S AT YE = 8.38 CM

PT. NO.	Y CM	UBAR M/S	Y/DEL 99	U/UE	u'/UE	Y+	U+	UTLOC M/S
1	0.000	0.00	0.000	0.000	0.000	0.0	0.0	0.000
2	0.053	2.95	0.008	0.368	0.129	14.4	9.0	0.267
3	0.074	3.67	0.010	0.458	0.145	20.1	11.2	0.302
4	0.103	4.22	0.015	0.527	0.148	27.9	12.9	0.322
5	0.144	4.52	0.020	0.564	0.150	38.9	13.8	0.325
6	0.200	4.87	0.028	0.609	0.154	54.1	14.9	0.330
7	0.279	5.11	0.039	0.638	0.154	75.3	15.6	0.329
8	0.388	5.38	0.055	0.672	0.157	104.8	16.4	0.329
9	0.540	5.51	0.076	0.688	0.157	146.0	16.8	0.322
10	0.752	5.72	0.106	0.714	0.160	203.2	17.5	0.319
11	1.047	5.96	0.147	0.744	0.162	282.8	18.2	0.319
12	1.458	6.10	0.205	0.762	0.166	393.7	18.6	0.313
13	2.029	6.24	0.286	0.779	0.172	548.1	19.1	0.308
14	2.664	6.58	0.375	0.821	0.179	719.6	20.1	0.314
15	3.299	6.69	0.464	0.835	0.184	891.1	20.4	0.312
16	3.934	6.91	0.554	0.863	0.183	1062.6	21.1	0.315
17	4.569	7.13	0.643	0.891	0.192	1234.1	21.8	0.320
18	5.204	7.33	0.732	0.916	0.189	1405.6	22.4	0.324
19	5.839	7.53	0.822	0.941	0.184	1577.1	23.0	0.328
20	6.474	7.74	0.911	0.967	0.188	1748.6	23.7	0.333
21	7.109	7.93	1.001	0.990	0.181	1920.1	24.2	0.337
22	7.744	7.96	1.090	0.994	0.174	2091.6	24.3	0.336
23	8.379	8.01	1.179	1.000	0.160	2263.1	24.5	0.335
24	9.014	7.96	1.269	0.994	0.159	2434.6	24.3	0.331
25	9.649	7.79	1.358	0.973	0.153	2606.1	23.8	0.322
26	10.284	7.46	1.447	0.931	0.155	2777.6	22.8	0.308
27	10.795	7.17	1.519	0.895	0.158	2915.5	21.9	0.296

** INTEGRAL THICKNESS PARAMETERS **

QUANTITY	VALUE IN CM	
DELTA-99	7.105	
DISPLACEMENT THICKNESS	1.168	REDELST = 7717.
MOMENTUM THICKNESS	0.886	RETHETA = 5856.
ENERGY THICKNESS	0.6997	

SHAPE PARAMETERS : H =1.318 LAMBDA =0.164 CLAUSER G = 5.90

RESULTS OF COLES DATA ANALYSIS

COLES DELTA	9.322 CM
COLES UTAU	0.317 M/S
WAKE PARAMETER	0.258 DIMENSIONLESS
CF BASED ON UE	0.00313 DIMENSIONLESS

PROFILE POINTS 6 THROUGH 22 USED
RESULTANT RMS ERROR FOR WALL-WAKE FIT : 0.493 M/S

TURBULENT SKIN FRICTION PROFILE CORRELATIONS

BASIS VELOCITY :	UE	UREF
CF : LOG-LAW FIT	0.00334	0.00146
CF : LUDWEIG-TILLMAN	0.00307	0.00134
CF : FRANK WHITE	0.00301	0.00131

X/H=12 CASE C

NOM. UREF : 12.23 M/S

FOR BOUNDARY LAYER ANALYSIS UE = 9.54 M/S AT YE = 8.77 CM

PT. NO.	Y CM	UBAR M/S	Y/DEL 99	U/UE	u''/UE	Y+	U+	UTLOC M/S
1	0.000	0.00	0.000	0.000	0.000	0.0	0.0	0.000
2	0.040	2.24	0.005	0.235	0.110	8.6	8.9	0.225
3	0.062	2.69	0.008	0.282	0.119	13.2	10.7	0.240
4	0.096	3.12	0.012	0.328	0.122	20.4	12.4	0.253
5	0.147	3.42	0.018	0.359	0.128	31.4	13.6	0.255
6	0.227	3.69	0.028	0.387	0.129	48.2	14.6	0.255
7	0.349	3.90	0.044	0.409	0.128	74.2	15.5	0.251
8	0.537	4.19	0.067	0.439	0.135	114.1	16.6	0.253
9	0.825	4.36	0.103	0.457	0.139	175.5	17.3	0.248
10	1.269	4.68	0.159	0.490	0.148	269.8	18.5	0.251
11	1.768	4.94	0.221	0.518	0.152	376.1	19.6	0.253
12	2.269	5.29	0.284	0.555	0.159	482.6	21.0	0.262
13	2.769	5.50	0.346	0.576	0.165	588.9	21.8	0.266
14	3.268	5.87	0.409	0.615	0.168	695.2	23.3	0.277
15	3.769	6.23	0.471	0.653	0.179	801.6	24.7	0.288
16	4.269	6.67	0.534	0.699	0.177	907.9	26.5	0.302
17	4.768	7.06	0.596	0.740	0.181	1014.2	28.0	0.315
18	5.269	7.61	0.659	0.798	0.173	1120.6	30.2	0.333
19	5.768	7.89	0.721	0.827	0.179	1226.9	31.3	0.341
20	6.269	8.43	0.784	0.884	0.162	1333.3	33.5	0.360
21	6.769	8.79	0.846	0.922	0.151	1439.6	34.9	0.371
22	7.268	9.11	0.909	0.955	0.134	1545.9	36.1	0.381
23	7.769	9.38	0.971	0.983	0.111	1652.3	37.2	0.389
24	8.269	9.52	1.034	0.998	0.091	1758.6	37.8	0.392
25	8.768	9.56	1.096	1.002	0.075	1864.9	37.9	0.391
26	9.269	9.40	1.159	0.986	0.072	1971.4	37.3	0.383
27	9.769	9.07	1.222	0.950	0.077	2077.7	36.0	0.369
28	10.200	8.59	1.275	0.901	0.089	2169.4	34.1	0.350

** INTEGRAL THICKNESS PARAMETERS **

QUANTITY	VALUE IN CM	
DELTA-99	7.997	
DISPLACEMENT THICKNESS	2.496	REDELST = 20088.
MOMENTUM THICKNESS	1.439	RETHETA = 11583.
ENERGY THICKNESS	0.8878	

SHAPE PARAMETERS : H =1.734 LAMBDA =0.312 CLAUSER G =16.02

RESULTS OF COLES DATA ANALYSIS

COLES DELTA	9.588 CM
COLES UTAU	0.241 M/S
WAKE PARAMETER	3.304 DIMENSIONLESS
CF BASED ON UE	0.00128 DIMENSIONLESS

PROFILE POINTS 7 THROUGH 21 USED
RESULTANT RMS ERROR FOR WALL-WAKE FIT : 0.571 M/S

TURBULENT SKIN FRICTION PROFILE CORRELATIONS

BASIS VELOCITY :	UE	UREF
CF : LOG-LAW FIT	0.00140	0.00085
CF : LUDWEIG-TILLMAN	0.00134	0.00081
CF : FRANK WHITE	0.00123	0.00075

X/H=14 CASE C

NOM. UREF : 12.18 M/S

FOR BOUNDARY LAYER ANALYSIS UE = 9.26 M/S AT YE = 8.77 CM

PT. NO.	Y CM	UBAR M/S	Y/DEL 99	U/UE	u'/UE	Y+	U+	UTLOC M/S
1	0.000	0.00	0.000	0.000	0.000	0.0	0.0	0.000
2	0.040	2.48	0.005	0.268	0.105	9.5	8.9	0.244
3	0.062	3.11	0.008	0.336	0.118	14.6	11.1	0.271
4	0.096	3.48	0.012	0.376	0.123	22.4	12.5	0.277
5	0.147	3.88	0.019	0.419	0.124	34.6	13.9	0.283
6	0.227	4.13	0.028	0.446	0.121	53.2	14.8	0.281
7	0.349	4.42	0.044	0.478	0.129	81.8	15.8	0.281
8	0.537	4.63	0.067	0.500	0.129	125.9	16.6	0.276
9	0.825	4.85	0.104	0.524	0.135	193.5	17.4	0.273
10	1.269	5.13	0.159	0.554	0.135	297.6	18.4	0.272
11	1.768	5.43	0.222	0.586	0.145	414.8	19.5	0.276
12	2.269	5.66	0.285	0.611	0.150	532.2	20.3	0.278
13	2.769	5.93	0.348	0.640	0.155	649.4	21.2	0.284
14	3.268	6.29	0.410	0.679	0.157	766.7	22.5	0.295
15	3.769	6.48	0.473	0.700	0.166	884.0	23.2	0.298
16	4.269	6.90	0.536	0.745	0.172	1001.3	24.7	0.312
17	4.768	7.20	0.599	0.778	0.170	1118.5	25.8	0.321
18	5.269	7.57	0.661	0.817	0.172	1235.9	27.1	0.332
19	5.768	7.97	0.724	0.861	0.167	1353.1	28.6	0.345
20	6.269	8.25	0.787	0.891	0.165	1470.5	29.5	0.353
21	6.769	8.61	0.850	0.930	0.154	1587.7	30.9	0.364
22	7.268	8.93	0.912	0.964	0.137	1705.0	32.0	0.374
23	7.769	9.10	0.975	0.983	0.124	1822.3	32.6	0.378
24	8.269	9.27	1.038	1.001	0.100	1939.6	33.2	0.382
25	8.768	9.25	1.101	0.999	0.092	2056.8	33.1	0.379
26	9.269	8.99	1.163	0.971	0.091	2174.2	32.2	0.368
27	9 769	8.60	1.226	0.929	0.096	2291.4	30.8	0.352
28	10.200	8.19	1.280	0.885	0.104	2392.6	29.4	0.335

** INTEGRAL THICKNESS PARAMETERS **

QUANTITY	VALUE IN CM	
DELTA-99	7.967	
DISPLACEMENT THICKNESS	2.170	REDELST = 16886.
MOMENTUM THICKNESS	1.362	RETHETA = 10595.
ENERGY THICKNESS	0.8995	

SHAPE PARAMETERS : H =1.594 LAMBDA =0.272 CLAUSER G =12.36

RESULTS OF COLES DATA ANALYSIS

COLES DELTA	9.786 CM
COLES UTAU	0.268 M/S
WAKE PARAMETER	2.203 DIMENSIONLESS
CF BASED ON UE	0.00168 DIMENSIONLESS

PROFILE POINTS 6 THROUGH 21 USED
RESULTANT RMS ERROR FOR WALL-WAKE FIT : 0.504 M/S

TURBULENT SKIN FRICTION PROFILE CORRELATIONS

BASIS VELOCITY :	UE	UREF
CF : LOG-LAW FIT	0.00182	0.00105
CF : LUDWEIG-TILLMAN	0.00170	0.00099
CF : FRANK WHITE	0.00160	0.00093

X/H=16 CASE C

NOM. UREF : 12.17 M/S

FOR BOUNDARY LAYER ANALYSIS UE = 9.01 M/S AT YE = 8.27 CM

PT. NO.	Y CM	UBAR M/S	Y/DEL 99	U/UE	u'/UE	Y+	U+	UTLOC M/S
1	0.000	0.00	0.000	0.000	0.000	0.0	0.0	0.000
2	0.040	2.53	0.005	0.281	0.105	10.2	8.4	0.248
3	0.062	3.19	0.008	0.354	0.117	15.6	10.6	0.277
4	0.096	3.75	0.012	0.417	0.117	24.1	12.5	0.295
5	0.147	4.24	0.019	0.471	0.121	37.1	14.1	0.306
6	0.227	4.50	0.029	0.499	0.120	57.1	14.9	0.302
7	0.349	4.77	0.044	0.529	0.122	87.9	15.8	0.300
8	0.537	5.13	0.068	0.570	0.127	135.2	17.0	0.302
9	0.825	5.26	0.105	0.584	0.129	207.9	17.4	0.293
10	1.269	5.60	0.161	0.621	0.131	319.6	18.6	0.294
11	1.768	5.72	0.224	0.635	0.138	445.6	19.0	0.289
12	2.269	6.05	0.288	0.672	0.145	571.7	20.1	0.296
13	2.769	6.27	0.351	0.697	0.148	697.6	20.8	0.299
14	3.268	6.50	0.414	0.722	0.152	823.5	21.6	0.304
15	3.769	6.88	0.478	0.764	0.157	949.6	22.8	0.315
16	4.269	7.03	0.541	0.780	0.161	1075.6	23.3	0.317
17	4.768	7.33	0.605	0.814	0.163	1201.5	24.3	0.326
18	5.269	7.63	0.668	0.847	0.163	1327.6	25.3	0.335
19	5.768	7.91	0.731	0.879	0.161	1453.5	26.3	0.343
20	6.269	8.20	0.795	0.911	0.159	1579.5	27.2	0.351
21	6.769	8.47	0.858	0.940	0.155	1705.5	28.1	0.359
22	7.268	8.72	0.922	0.968	0.145	1831.4	28.9	0.366
23	7.769	8.89	0.985	0.987	0.131	1957.5	29.5	0.370
24	8.269	9.01	1.048	1.000	0.114	2083.4	29.9	0.373
25	8.768	8.89	1.112	0.987	0.108	2209.4	29.5	0.366
26	9.269	8.67	1.175	0.963	0.106	2335.4	28.8	0.356
27	9.769	8.34	1.239	0.926	0.108	2461.4	27.7	0.342
28	10.200	8.00	1.293	0.888	0.113	2570.1	26.5	0.328

** INTEGRAL THICKNESS PARAMETERS **

QUANTITY	VALUE IN CM	
DELTA-99	7.887	
DISPLACEMENT THICKNESS	1.866	REDELST = 14051.
MOMENTUM THICKNESS	1.255	RETHETA = 9451.
ENERGY THICKNESS	0.8825	

SHAPE PARAMETERS : H =1.487 LAMBDA =0.237 CLAUSER G = 9.79

RESULTS OF COLES DATA ANALYSIS

COLES DELTA	9.697 CM
COLES UTAU	0.289 M/S
WAKE PARAMETER	1.479 DIMENSIONLESS
CF BASED ON UE	0.00206 DIMENSIONLESS

PROFILE POINTS 6 THROUGH 22 USED
RESULTANT RMS ERROR FOR WALL-WAKE FIT : 0.503 M/S

TURBULENT SKIN FRICTION PROFILE CORRELATIONS

BASIS VELOCITY :	UE	UREF
CF : LOG-LAW FIT	0.00224	0.00123
CF : LUDWEIG-TILLMAN	0.00208	0.00114
CF : FRANK WHITE	0.00199	0.00109

X/H=18 CASE C

NOM. UREF : 12.15 M/S

FOR BOUNDARY LAYER ANALYSIS UE = 8.69 M/S AT YE = 8.27 CM

PT. NO.	Y CM	UBAR M/S	Y/DEL 99	U/UE	u'/UE	Y+	U+	UTLOC M/S
1	0.000	0.00	0.000	0.000	0.000	0.0	0.0	0.000
2	0.040	2.71	0.005	0.312	0.112	10.5	8.7	0.263
3	0.062	3.45	0.008	0.397	0.121	16.2	11.0	0.296
4	0.096	4.01	0.012	0.462	0.122	25.0	12.8	0.312
5	0.147	4.37	0.019	0.503	0.121	38.4	14.0	0.314
6	0.227	4.71	0.029	0.542	0.118	59.1	15.0	0.314
7	0.349	5.03	0.045	0.579	0.123	91.0	16.1	0.314
8	0.537	5.29	0.068	0.609	0.123	139.9	16.9	0.310
9	0.825	5.51	0.105	0.634	0.124	215.1	17.6	0.305
10	1.269	5.82	0.162	0.670	0.130	330.8	18.6	0.305
11	1.768	6.07	0.226	0.698	0.135	461.2	19.4	0.305
12	2.269	6.27	0.289	0.721	0.138	591.6	20.0	0.305
13	2.769	6.32	0.353	0.727	0.147	722.0	20.2	0.301
14	3.268	6.72	0.417	0.773	0.150	852.3	21.5	0.313
15	3.769	6.89	0.481	0.793	0.153	982.7	22.0	0.316
16	4.269	7.15	0.545	0.823	0.156	1113.1	22.8	0.322
17	4.768	7.30	0.608	0.840	0.158	1243.4	23.3	0.325
18	5.269	7.51	0.672	0.864	0.161	1373.9	24.0	0.330
19	5.768	7.82	0.736	0.901	0.156	1504.2	25.0	0.339
20	6.269	8.06	0.800	0.928	0.155	1634.7	25.8	0.346
21	6.769	8.26	0.864	0.951	0.150	1765.0	26.4	0.351
22	7.268	8.54	0.927	0.983	0.139	1895.4	27.3	0.360
23	7.769	8.59	0.991	0.988	0.130	2025.8	27.4	0.359
24	8.269	8.69	1.055	1.000	0.118	2156.2	27.8	0.361
25	8.768	8.59	1.119	0.989	0.113	2286.5	27.5	0.355
26	9.269	8.38	1.183	0.965	0.115	2417.0	26.8	0.346
27	9.769	8.08	1.246	0.931	0.115	2547.3	25.8	0.333
28	10.200	7.74	1.301	0.890	0.122	2659.8	24.7	0.318

** INTEGRAL THICKNESS PARAMETERS **

QUANTITY	VALUE IN CM	
DELTA-99	7.838	
DISPLACEMENT THICKNESS	1.608	REDELST = 11645.
MOMENTUM THICKNESS	1.139	RETHETA = 8244.
ENERGY THICKNESS	0.8370	

SHAPE PARAMETERS : H =1.413 LAMBDA =0.205 CLAUSER G = 8.11

RESULTS OF COLES DATA ANALYSIS

COLES DELTA	9.970 CM
COLES UTAU	0.302 M/S
WAKE PARAMETER	0.948 DIMENSIONLESS
CF BASED ON UE	0.00242 DIMENSIONLESS

PROFILE POINTS 6 THROUGH 21 USED
RESULTANT RMS ERROR FOR WALL-WAKE FIT : 0.450 M/S

TURBULENT SKIN FRICTION PROFILE CORRELATIONS

BASIS VELOCITY :	UE	UREF
CF : LOG-LAW FIT	0.00259	0.00133
CF : LUDWEIG-TILLMAN	0.00242	0.00124
CF : FRANK WHITE	0.00234	0.00120

X/H=20 CASE C

NOM. UREF : 12.12 M/S

FOR BOUNDARY LAYER ANALYSIS UE = 8.32 M/S AT YE = 8.27 CM

PT. NO.	Y CM	UBAR M/S	Y/DEL 99	U/UE	u'/UE	Y+	U+	UTLOC M/S
1	0.000	0.00	0.000	0.000	0.000	0.0	0.0	0.000
2	0.040	2.99	0.005	0.360	0.122	10.9	9.3	0.285
3	0.062	3.70	0.008	0.445	0.126	16.7	11.4	0.314
4	0.096	4.28	0.013	0.515	0.130	25.8	13.2	0.330
5	0.147	4.58	0.020	0.551	0.124	39.7	14.2	0.327
6	0.227	4.91	0.031	0.590	0.121	61.0	15.2	0.326
7	0.349	5.22	0.047	0.627	0.123	93.9	16.1	0.324
8	0.537	5.48	0.073	0.658	0.125	144.4	16.9	0.320
9	0.825	5.73	0.112	0.688	0.129	222.0	17.7	0.316
10	1.269	6.04	0.172	0.726	0.130	341.4	18.7	0.315
11	1.768	6.22	0.239	0.747	0.131	475.9	19.2	0.312
12	2.269	6.41	0.307	0.770	0.136	610.5	19.8	0.312
13	2.769	6.62	0.375	0.795	0.145	745.0	20.4	0.314
14	3.268	6.75	0.442	0.811	0.146	879.5	20.8	0.314
15	3.769	7.00	0.510	0.841	0.151	1014.1	21.6	0.320
16	4.269	7.13	0.578	0.857	0.149	1148.6	22.0	0.322
17	4.768	7.41	0.645	0.891	0.154	1283.1	22.9	0.329
18	5.269	7.49	0.713	0.900	0.156	1417.7	23.1	0.329
19	5.768	7.77	0.781	0.934	0.159	1552.2	24.0	0.337
20	6.269	7.95	0.848	0.955	0.151	1686.9	24.6	0.342
21	6.769	8.14	0.916	0.979	0.148	1821.3	25.2	0.347
22	7.268	8.21	0.983	0.986	0.146	1955.9	25.4	0.347
23	7.769	8.33	1.051	1.002	0.134	2090.5	25.8	0.350
24	8.269	8.31	1.119	0.998	0.127	2225.0	25.7	0.346
25	8.768	8.28	1.186	0.995	0.122	2359.5	25.6	0.343
26	9.269	8.12	1.254	0.976	0.120	2494.1	25.1	0.336
27	9.769	7.85	1.322	0.944	0.127	2628.6	24.3	0.324
28	10.200	7.63	1.380	0.917	0.129	2744.7	23.6	0.315

** INTEGRAL THICKNESS PARAMETERS **

QUANTITY	VALUE IN CM		
DELTA-99	7.390		
DISPLACEMENT THICKNESS	1.292	REDELST =	8937
MOMENTUM THICKNESS	0.960	RETHETA =	6643.
ENERGY THICKNESS	0.7387		

SHAPE PARAMETERS : H =1.345 LAMBDA =0.175 CLAUSER G = 6.60

RESULTS OF COLES DATA ANALYSIS

COLES DELTA	9.341 CM
COLES UTAU	0.313 M/S
WAKE PARAMETER	0.525 DIMENSIONLESS
CF BASED ON UE	0.00283 DIMENSIONLESS

PROFILE POINTS 6 THROUGH 21 USED
RESULTANT RMS ERROR FOR WALL-WAKE FIT : 0.438 M/S

TURBULENT SKIN FRICTION PROFILE CORRELATIONS

BASIS VELOCITY :	UE	UREF
CF : LOG-LAW FIT	0.00303	0.00143
CF : LUDWEIG-TILLMAN	0.00285	0.00134
CF : FRANK WHITE	0.00278	0.00131

OPPOSITE WALL BOUNDARY LAYER PROFILES

A SUMMARY OF THESE DATA APPEARS AS TABLE 5-3

X/H=2 CASE A OPPOSITE WALL

NOM. UREF : 12.12 M/S

FOR BOUNDARY LAYER ANALYSIS UE = 12.11 M/S AT YE = 5.00 CM

PT. NO.	Y* CM	UBAR M/S	Y/DEL 99	U/UE	u'/UE	Y+	U+	UTLOC M/S
1	0.000	0.00	0.000	0.000	0.000	0.0	0.0	0.000
2	0.040	5.49	0.024	0.454	0.110	18.1	10.3	0.467
3	0.055	6.41	0.033	0.530	0.105	24.8	12.1	0.504
4	0.076	7.14	0.045	0.590	0.099	34.2	13.5	0.525
5	0.104	7.61	0.062	0.628	0.090	46.8	14.3	0.529
6	0.143	8.05	0.085	0.665	0.083	64.3	15.2	0.531
7	0.197	8.48	0.116	0.700	0.077	88.3	16.0	0.532
8	0.270	8.86	0.160	0.732	0.073	121.2	16.7	0.530
9	0.371	9.27	0.219	0.766	0.071	166.2	17.5	0.531
10	0.508	9.78	0.300	0.808	0.068	228.1	18.4	0.535
11	0.697	10.30	0.412	0.851	0.061	312.7	19.4	0.540
12	0.957	10.94	0.565	0.904	0.052	429.1	20.6	0.550
13	1.312	11.60	0.775	0.958	0.039	588.6	21.8	0.560
14	1.800	12.09	1.063	0.999	0.016	807.3	22.8	0.563
15	2.300	12.14	1.358	1.003	0.007	1031.5	22.9	0.551
16	2.800	12.13	1.654	1.002	0.005	1256.0	22.8	0.540
17	3.300	12.11	1.949	1.000	0.005	1480.2	22.8	0.531
18	3.800	12.10	2.245	0.999	0.005	1704.4	22.8	0.523
19	4.300	12.08	2.540	0.998	0.006	1928.8	22.8	0.516
20	4.800	12.09	2.835	0.999	0.007	2153.0	22.8	0.511
21	5.000	12.10	2.953	1.000	0.008	2242.7	22.8	0.510

** INTEGRAL THICKNESS PARAMETERS **

QUANTITY	VALUE IN CM		
DELTA-99	1.693		
DISPLACEMENT THICKNESS	0.258	REDELST =	2643.
MOMENTUM THICKNESS	0.184	RETHETA =	1879.
ENERGY THICKNESS	0.1416		

SHAPE PARAMETERS : H =1.407 LAMBDA =0.153 CLAUSER G = 6.59

RESULTS OF COLES DATA ANALYSIS

COLES DELTA	1.771 CM
COLES UTAU	0.528 M/S
WAKE PARAMETER	0.337 DIMENSIONLESS
CF BASED ON UE	0.00381 DIMENSIONLESS

PROFILE POINTS 6 THROUGH 13 USED
RESULTANT RMS ERROR FOR WALL-WAKE FIT : 0.052 M/S

TURBULENT SKIN FRICTION PROFILE CORRELATIONS

BASIS VELOCITY :	UE	UREF
CF : LOG-LAW FIT	0.00385	0.00384
CF : LUDWEIG-TILLMAN	0.00363	0.00362
CF : FRANK WHITE	0.00350	0.00349

X/H=4 CASE A OPPOSITE WALL

NOM. UREF : 12.16 M/S

FOR BOUNDARY LAYER ANALYSIS UE = 12.18 M/S AT YE = 5.00 CM

PT. NO.	Y* CM	UBAR M/S	Y/DEL 99	U/UE	u'/UE	Y+	U+	UTLOC M/S
1	0.000	0.00	0.000	0.000	0.000	0.0	0.0	0.000
2	0.040	5.41	0.021	0.444	0.110	17.6	10.5	0.461
3	0.056	6.24	0.029	0.512	0.105	24.3	12.1	0.492
4	0.078	6.91	0.041	0.567	0.101	33.8	13.4	0.509
5	0.108	7.41	0.057	0.608	0.092	46.8	14.4	0.515
6	0 149	7.78	0.079	0.639	0.085	64.8	15.1	0.513
7	0.206	8.21	0.109	0.674	0.081	89.7	16.0	0.514
8	0 285	8.65	0.150	0.710	0.077	124.1	16.8	0.516
9	0.394	9.12	0.208	0.748	0.074	171.7	17.7	0.519
10	0.545	9.62	0.288	0.789	0.069	237.5	18.7	0.523
11	0.755	10.17	0.398	0.835	0.065	328.8	19.8	0.529
12	1.045	10.87	0.551	0.892	0.056	455.1	21.1	0.542
13	1.445	11.58	0.763	0.950	0.041	629.5	22.5	0.554
14	1.945	12.12	1.027	0.994	0.019	847.5	23.6	0.559
15	2.445	12.16	1.291	0.998	0.009	1065.2	23.7	0.548
16	2.945	12.18	1.555	1.000	0.009	1282.9	23.7	0.539
17	3.445	12.15	1.819	0.997	0.010	1500.9	23.6	0.530
18	3.945	12.16	2.083	0.998	0.012	1718.7	23.6	0.523
19	4.445	12.19	2.346	1.000	0.015	1936.4	23.7	0.519
20	4.945	12.20	2.610	1.002	0.018	2154.3	23.7	0.514
21	5.000	12.22	2.639	1.003	0.020	2178.0	23.8	0.514

** INTEGRAL THICKNESS PARAMETERS **

QUANTITY	VALUE IN CM		
DELTA-99	1.894		
DISPLACEMENT THICKNESS	0.309	REDELST =	3190.
MOMENTUM THICKNESS	0.221	RETHETA =	2281.
ENERGY THICKNESS	0.1701		

SHAPE PARAMETERS : H =1.399 LAMBDA =0.163 CLAUSER G = 6.75

RESULTS OF COLES DATA ANALYSIS

COLES DELTA	1.977 CM
COLES UTAU	0.513 M/S
WAKE PARAMETER	0.467 DIMENSIONLESS
CF BASED ON UE	0.00354 DIMENSIONLESS

PROFILE POINTS 6 THROUGH 13 USED
RESULTANT RMS ERROR FOR WALL-WAKE FIT : 0.024 M/S

TURBULENT SKIN FRICTION PROFILE CORRELATIONS

BASIS VELOCITY :	UE	UREF
CF : LOG-LAW FIT	0.00356	0.00357
CF : LUDWEIG-TILLMAN	0.00349	0.00350
CF : FRANK WHITE	0.00336	0.00337

X/H=6 CASE A OPPOSITE WALL

NOM. UREF : 12.18 M/S

FOR BOUNDARY LAYER ANALYSIS UE = 11.55 M/S AT YE = 4.95 CM

PT. NO.	Y* CM	UBAR M/S	Y/DEL 99	U/UE	u'/UE	Y+	U+	UTLOC M/S
1	0.000	0.00	0.000	0.000	0.000	0.0	0.0	0.000
2	0.040	4.45	0.018	0.385	0.111	15.7	9.8	0.392
3	0.056	5.31	0.025	0.459	0.106	21.6	11.7	0.429
4	0.078	5.82	0.035	0.504	0.102	30.1	12.8	0.440
5	0.108	6.36	0.048	0.551	0.095	41.7	14.0	0.452
6	0.149	6.74	0.067	0.584	0.091	57.7	14.8	0.453
7	0.206	7.14	0.092	0.618	0.088	79.8	15.7	0.455
8	0.285	7.53	0.127	0.652	0.085	110.4	16.6	0.456
9	0.394	7.98	0.176	0.691	0.084	152.8	17.6	0.461
10	0.545	8.54	0.244	0.740	0.081	211.4	18.8	0.471
11	0.755	9.12	0.338	0.790	0.075	292.6	20.1	0.480
12	1.045	9.83	0.468	0.851	0.066	405.0	21.6	0.495
13	1.445	10.58	0.647	0.916	0.054	560.3	23.3	0.510
14	1.945	11.26	0.871	0.975	0.036	754.2	24.8	0.524
15	2.445	11.56	1.094	1.001	0.018	948.0	25.4	0.524
16	2.945	11.56	1.318	1.001	0.015	1141.8	25.4	0.514
17	3.445	11.54	1.542	0.999	0.018	1335.7	25.4	0.506
18	3.945	11.56	1.766	1.001	0.023	1529.5	25.4	0.500
19	4.445	11.55	1.990	1.000	0.027	1723.3	25.4	0.494
20	4.945	11.53	2.213	0.998	0.038	1917.3	25.4	0.488
21	5.445	11.43	2.437	0.990	0.058	2111.1	25.1	0.480
22	5.945	11.07	2.661	0.958	0.096	2304.9	24.3	0.462
23	6.445	10.51	2.885	0.910	0.120	2498.8	23.1	0.438
24	6.945	9.28	3.109	0.804	0.167	2692.6	20.4	0.388
25	7.445	8.12	3.332	0.703	0.180	2886.6	17.9	0.342
26	7.945	6.58	3.556	0.569	0.190	3080.3	14.5	0.281
27	8.000	6.59	3.581	0.571	0.190	3101.4	14.5	0.281

** INTEGRAL THICKNESS PARAMETERS **

QUANTITY	VALUE IN CM		
DELTA-99	2.234		
DISPLACEMENT THICKNESS	0.391	REDELST =	3849.
MOMENTUM THICKNESS	0.269	RETHETA =	2647.
ENERGY THICKNESS	0.1998		

SHAPE PARAMETERS : H =1.454 LAMBDA =0.175 CLAUSER G = 7.93

RESULTS OF COLES DATA ANALYSIS

COLES DELTA	2.165 CM
COLES UTAU	0.454 M/S
WAKE PARAMETER	0.818 DIMENSIONLESS
CF BASED ON UE	0.00310 DIMENSIONLESS

PROFILE POINTS 6 THROUGH 13 USED
RESULTANT RMS ERROR FOR WALL-WAKE FIT : 0.107 M/S

TURBULENT SKIN FRICTION PROFILE CORRELATIONS

BASIS VELOCITY :	UE	UREF
CF : LOG-LAW FIT	0.00310	0.00279
CF : LUDWEIG-TILLMAN	0.00308	0.00276
CF : FRANK WHITE	0.00293	0.00263

X/H=8 CASE A OPPOSITE WALL

NOM. UREF : 12.18 M/S

FOR BOUNDARY LAYER ANALYSIS UE = 10.87 M/S AT YE = 4.14 CM

PT. NO.	Y* CM	UBAR M/S	Y/DEL 99	U/UE	u'/UE	Y+	U+	UTLOC M/S
1	0.000	0.00	0.000	0.000	0.000	0.0	0.0	0.000
2	0.040	3.69	0.015	0.339	0.105	13.3	9.5	0.336
3	0.057	4.31	0.022	0.397	0.105	18.7	11.1	0.360
4	0.079	4.79	0.030	0.440	0.104	26.1	12.4	0.372
5	0.111	5.26	0.042	0.484	0.100	36.6	13.6	0.383
6	0.156	5.56	0.059	0.511	0.097	51.2	14.4	0.382
7	0.218	5.94	0.083	0.546	0.096	71.8	15.3	0.385
8	0.305	6.31	0.116	0.580	0.096	100.5	16.3	0.388
9	0.428	6.73	0.163	0.619	0.096	140.7	17.4	0.393
10	0.599	7.28	0.228	0.670	0.094	197.0	18.8	0.405
11	0.838	7.93	0.319	0.729	0.089	275.8	20.5	0.419
12	1.173	8.80	0.447	0.809	0.082	386.1	22.7	0.443
13	1.643	9.65	0.625	0.887	0.070	540.6	24.9	0.464
14	2.143	10.36	0.815	0.953	0.052	705.1	26.8	0.481
15	2.643	10.78	1.006	0.991	0.034	869.7	27.9	0.488
16	3.143	10.89	1.196	1.002	0.026	1034.1	28.2	0.484
17	3.643	10.89	1.386	1.001	0.031	1198.6	28.1	0.477
18	4.143	10.84	1.577	0.997	0.037	1363.2	28.0	0.470
19	4.643	10.80	1.767	0.993	0.049	1527.7	27.9	0.463
20	5.143	10.69	1.957	0.983	0.069	1692.2	27.6	0.454
21	5.643	10.51	2.148	0.967	0.088	1856.8	27.2	0.444
22	6.143	10.14	2.338	0.933	0.123	2021.2	26.2	0.426
23	6.643	9.55	2.528	0.878	0.155	2185.7	24.7	0.400
24	7.143	8.70	2.718	0.800	0.177	2350.3	22.5	0.365
25	7.643	7.72	2.909	0.710	0.198	2514.8	19.9	0.326
26	8.000	7.05	3.044	0.649	0.202	2632.3	18.2	0.299

** INTEGRAL THICKNESS PARAMETERS **

QUANTITY	VALUE IN CM		
DELTA-99	2.628		
DISPLACEMENT THICKNESS	0.544	REDELST =	5029.
MOMENTUM THICKNESS	0.357	RETHETA =	3305.
ENERGY THICKNESS	0.2539		

SHAPE PARAMETERS : H =1.521 LAMBDA =0.207 CLAUSER G = 9.63

RESULTS OF COLES DATA ANALYSIS

COLES DELTA	2.513 CM
COLES UTAU	0.385 M/S
WAKE PARAMETER	1.415 DIMENSIONLESS
CF BASED ON UE	0.00250 DIMENSIONLESS

PROFILE POINTS 6 THROUGH 13 USED
RESULTANT RMS ERROR FOR WALL-WAKE FIT : 0.186 M/S

TURBULENT SKIN FRICTION PROFILE CORRELATIONS

BASIS VELOCITY :	UE	UREF
CF : LOG-LAW FIT	0.00253	0.00202
CF : LUDWEIG-TILLMAN	0.00261	0.00208
CF : FRANK WHITE	0.00245	0.00196

X/H=10 CASE A OPPOSITE WALL

NOM. UREF : 12.16 M/S

FOR BOUNDARY LAYER ANALYSIS UE = 10.27 M/S AT YE = 3.76 CM

PT. NO.	Y* CM	UBAR M/S	Y/DEL 99	U/UE	u'/UE	Y+	U+	UTLOC M/S
1	0.000	0.00	0.000	0.000	0.000	0.0	0.0	0.000
2	0.040	3.11	0.013	0.303	0.105	11.5	9.3	0.293
3	0.057	3.67	0.018	0.357	0.105	16.3	10.9	0.315
4	0.080	4.08	0.026	0.397	0.104	22.9	12.1	0.325
5	0.113	4.43	0.036	0.432	0.101	32.3	13.2	0.330
6	0.160	4.74	0.051	0.461	0.102	45.6	14.1	0.331
7	0.226	5.04	0.072	0.491	0.100	64.4	15.0	0.333
8	0.318	5.36	0.102	0.522	0.102	90.8	15.9	0.335
9	0.449	5.75	0.144	0.560	0.103	128.0	17.1	0.341
10	0.633	6.22	0.203	0.605	0.105	180.4	18.5	0.350
11	0.892	6.86	0.286	0.668	0.105	254.4	20.4	0.366
12	1.258	7.67	0.404	0.747	0.100	358.6	22.8	0.389
13	1.758	8.68	0.564	0.845	0.088	501.2	25.8	0.419
14	2.258	9.44	0.724	0.919	0.074	643.7	28.1	0.440
15	2.758	9.97	0.885	0.971	0.055	786.2	29.6	0.453
16	3.258	10.24	1.045	0.998	0.043	928.8	30.5	0.457
17	3.758	10.29	1.206	1.002	0.044	1071.3	30.6	0.452
18	4.258	10.24	1.366	0.997	0.059	1213.8	30.5	0.445
19	4.758	10.16	1.527	0.990	0.069	1356.5	30.2	0.437
20	5.258	10.00	1.687	0.974	0.092	1499.0	29.8	0.427
21	5.758	9.69	1.847	0.944	0.120	1641.4	28.8	0.411
22	6.258	9.37	2.008	0.913	0.141	1784.1	27.9	0.396
23	6.758	8.90	2.168	0.867	0.165	1926.6	26.5	0.375
24	7.258	8.28	2.329	0.807	0.185	2069.2	24.6	0.349
25	7.758	7.59	2.489	0.739	0.200	2211.7	22.6	0.320
26	8.000	7.19	2.567	0.700	0.204	2280.6	21.4	0.304

** INTEGRAL THICKNESS PARAMETERS **

QUANTITY	VALUE IN CM		
DELTA-99	3.117		
DISPLACEMENT THICKNESS	0.714	REDELST =	6216.
MOMENTUM THICKNESS	0.449	RETHETA =	3908.
ENERGY THICKNESS	0.3059		

SHAPE PARAMETERS : H =1.590 LAMBDA =0.229 CLAUSER G =11.34

RESULTS OF COLES DATA ANALYSIS

COLES DELTA	3.041 CM
COLES UTAU	0.334 M/S
WAKE PARAMETER	1.905 DIMENSIONLESS
CF BASED ON UE	0.00211 DIMENSIONLESS

PROFILE POINTS 7 THROUGH 14 USED
RESULTANT RMS ERROR FOR WALL-WAKE FIT : 0.187 M/S

TURBULENT SKIN FRICTION PROFILE CORRELATIONS

BASIS VELOCITY :	UE	UREF
CF : LOG-LAW FIT	0.00214	0.00153
CF : LUDWEIG-TILLMAN	0.00224	0.00160
CF : FRANK WHITE	0.00208	0.00148

X/H=12 CASE A OPPOSITE WALL

NOM. UREF : 12.15 M/S

FOR BOUNDARY LAYER ANALYSIS UE = 9.78 M/S AT YE = 4.54 CM

PT. NO.	Y* CM	UBAR M/S	Y/DEL 99	U/UE	u'/UE	Y+	U+	UTLOC M/S
1	0.000	0.00	0.000	0.000	0.000	0.0	0.0	0.000
2	0.040	2.73	0.012	0.279	0.107	10.7	8.8	0.263
3	0.053	3.16	0.016	0.323	0.109	14.2	10.2	0.281
4	0.071	3.55	0.021	0.363	0.110	18.8	11.4	0.295
5	0.094	3.87	0.028	0.396	0.108	24.9	12.5	0.303
6	0.124	4.14	0.037	0.423	0.109	33.0	13.3	0.307
7	0.164	4.39	0.048	0.449	0.110	43.5	14.1	0.309
8	0.217	4.58	0.064	0.469	0.106	57.6	14.8	0.308
9	0.288	4.82	0.085	0.492	0.108	76.3	15.5	0.309
10	0.380	5.06	0.112	0.517	0.109	100.9	16.3	0.311
11	0.504	5.33	0.148	0.545	0.113	133.5	17.2	0.314
12	0.666	5.68	0.196	0.581	0.115	176.7	18.3	0.321
13	0 881	6.16	0.260	0.630	0.117	233.7	19.8	0.333
14	1.166	6.70	0.344	0.685	0.116	309.2	21.6	0.348
15	1.543	7.42	0.454	0.759	0.112	409.0	23.9	0.369
16	2.041	8.27	0.601	0.846	0.101	541.0	26.6	0.395
17	2.541	8.97	0.749	0.917	0.087	673.7	28.9	0.415
18	3.041	9.47	0.896	0.968	0.071	806.2	30.5	0.428
19	3.541	9.77	1.043	0.999	0.064	938.7	31.5	0.434
20	4.041	9.81	1.190	1.003	0.070	1071.4	31.6	0.430
21	4.541	9.76	1.338	0.998	0.085	1203.9	31.4	0.423
22	5.040	9.58	1.485	0.979	0.108	1336.4	30.8	0.412
23	5.541	9.36	1.632	0.957	0.127	1469.1	30.1	0.400
24	6 041	9.02	1.779	0.923	0.145	1601.6	29.1	0.384
25	6 541	8.70	1.927	0.890	0.162	1734.3	28.0	0.368
26	7.041	8.19	2.074	0.838	0.179	1866.8	26.4	0.346
27	7.541	7.73	2.221	0.790	0.188	1999.3	24.9	0.327
28	8.000	7.33	2.357	0.749	0.195	2121.0	23.6	0.309

** INTEGRAL THICKNESS PARAMETERS **

QUANTITY	VALUE IN CM		
DELTA-99	3.395		
DISPLACEMENT THICKNESS	0.826	REDELST =	6892.
MOMENTUM THICKNESS	0.511	RETHETA =	4266.
ENERGY THICKNESS	0.3428		

SHAPE PARAMETERS : H =1.616 LAMBDA =0.243 CLAUSER G =12.00

RESULTS OF COLES DATA ANALYSIS

COLES DELTA	3.443 CM
COLES UTAU	0 308 M/S
WAKE PARAMETER	2.086 DIMENSIONLESS
CF BASED ON UE	0.00198 DIMENSIONLESS

PROFILE POINTS 8 THROUGH 17 USED
RESULTANT RMS ERROR FOR WALL-WAKE FIT : 0.151 M/S

TURBULENT SKIN FRICTION PROFILE CORRELATIONS

BASIS VELOCITY :	UE	UREF
CF : LOG-LAW FIT	0.00202	0.00131
CF : LUDWEIG-TILLMAN	0.00210	0.00136
CF : FRANK WHITE	0.00195	0.00126

X/H=14 CASE A OPPOSITE WALL

NOM. UREF : 12.17 M/S

FOR BOUNDARY LAYER ANALYSIS UE = 9.53 M/S AT YE = 4.69 CM

PT. NO.	Y* CM	UBAR M/S	Y/DEL 99	U/UE	u'/UE	Y+	U+	UTLOC M/S
1	0.000	0.00	0.000	0.000	0.000	0.0	0.0	0.000
2	0.040	2.46	0.011	0.258	0.103	10.8	7.8	0.242
3	0.054	3.03	0.015	0.318	0.110	14.5	9.6	0.271
4	0.072	3.48	0.020	0.365	0.113	19.2	11.1	0.290
5	0.096	3.87	0.026	0.406	0.113	25.6	12.3	0.302
6	0.127	4.20	0.035	0.440	0.112	34.1	13.4	0.309
7	0.170	4.47	0.046	0.469	0.111	45.5	14.2	0.312
8	0.227	4.73	0.062	0.496	0.110	60.7	15.1	0.315
9	0.302	4.92	0.082	0.516	0.112	80.8	15.7	0.313
10	0.403	5.16	0.110	0.541	0.115	107.8	16.4	0.314
11	0.537	5.39	0.146	0.565	0.119	143.6	17.1	0.315
12	0.715	5.75	0.195	0.603	0.121	191.3	18.3	0.322
13	0.952	6.15	0.260	0.645	0.123	254.8	19.6	0.330
14	1.269	6.71	0.346	0.704	0.125	339.5	21.4	0.345
15	1.690	7.38	0.461	0.775	0.121	452.3	23.5	0.364
16	2.190	8.07	0.597	0.847	0.114	586.1	25.7	0.384
17	2.690	8.68	0.734	0.911	0.099	719.9	27.6	0.401
18	3.190	9.16	0.870	0.961	0.089	853.7	29.1	0.414
19	3.690	9.45	1.006	0.991	0.086	987.5	30.1	0.419
20	4.190	9.55	1.143	1.002	0.094	1121.3	30.4	0.418
21	4.690	9.52	1.279	0.998	0.108	1255.0	30.3	0.412
22	5.190	9.33	1.416	0.978	0.126	1388.9	29.7	0.401
23	5.690	9.13	1.552	0.958	0.139	1522.7	29.1	0.390
24	6.190	8.71	1.688	0.913	0.158	1656.6	27.7	0.371
25	6.690	8.42	1.825	0.883	0.167	1790.3	26.8	0.357
26	7.190	8.08	1.961	0.847	0.174	1924.1	25.7	0.341
27	7.690	7.68	2.097	0.806	0.179	2058.0	24.4	0.324
28	8.000	7.52	2.182	0.789	0.177	2140.7	23.9	0.317

** INTEGRAL THICKNESS PARAMETERS **

QUANTITY	VALUE IN CM	
DELTA-99	3 667	
DISPLACEMENT THICKNESS	0.859	REDELST = 6971.
MOMENTUM THICKNESS	0.545	RETHETA = 4424.
ENERGY THICKNESS	0.3739	

SHAPE PARAMETERS : H =1.576 LAMBDA =0.234 CLAUSER G =11.08

RESULTS OF COLES DATA ANALYSIS

COLES DELTA	3.797 CM
COLES UTAU	0.311 M/S
WAKE PARAMETER	1.795 DIMENSIONLESS
CF BASED ON UE	0.00213 DIMENSIONLESS

PROFILE POINTS 8 THROUGH 17 USED
RESULTANT RMS ERROR FOR WALL-WAKE FIT : 0.131 M/S

TURBULENT SKIN FRICTION PROFILE CORRELATIONS

BASIS VELOCITY :	UE	UREF
CF : LOG-LAW FIT	0.00217	0.00133
CF : LUDWEIG-TILLMAN	0.00222	0.00136
CF : FRANK WHITE	0.00207	0.00127

X/H=16 CASE A OPPOSITE WALL

NOM. UREF : 12.19 M/S

FOR BOUNDARY LAYER ANALYSIS UE = 9.11 M/S AT YE = 4.79 CM

PT. NO.	Y* CM	UBAR M/S	Y/DEL 99	U/UE	u'/UE	Y+	U+	UTLOC M/S
1	0.000	0.00	0.000	0.000	0.000	0.0	0.0	0.000
2	0.040	2.59	0.011	0.284	0.109	11.0	8.1	0.252
3	0.054	3.21	0.014	0.352	0.117	14.7	10.1	0.284
4	0.073	3.70	0.019	0.406	0.120	19.7	11.6	0.304
5	0.097	4.05	0.025	0.445	0.120	26.4	12.7	0.313
6	0.130	4.34	0.034	0.477	0.117	35.3	13.6	0.317
7	0.174	4.65	0.045	0.510	0.119	47.2	14.6	0.322
8	0.233	4.84	0.061	0.531	0.118	63.3	15.2	0.320
9	0.312	5.03	0.081	0.553	0.119	84.7	15.8	0.318
10	0.417	5.25	0.109	0.576	0.122	113.3	16.5	0.317
11	0.557	5.52	0.146	0.606	0.127	151.5	17.3	0.320
12	0.746	5.82	0.195	0.639	0.131	202.8	18.3	0.323
13	0.998	6.18	0.261	0.679	0.134	271.4	19.4	0.330
14	1.336	6.72	0.349	0.738	0.132	363.1	21.1	0.343
15	1.788	7.26	0.467	0.798	0.129	485.9	22.8	0.356
16	2.287	7.85	0.598	0.862	0.123	621.8	24.7	0.372
17	2.787	8.34	0.728	0.916	0.115	757.7	26.2	0.385
18	3.287	8.73	0.859	0.958	0.105	893.7	27.4	0.395
19	3.787	9.00	0.989	0.989	0.105	1029.6	28.3	0.400
20	4.287	9.12	1.120	1.002	0.110	1165.5	28.7	0.400
21	4.787	9.09	1.251	0.998	0.128	1301.5	28.5	0.395
22	5.287	8.97	1.381	0.985	0.141	1437.4	28.2	0.386
23	5.788	8.75	1.512	0.961	0.151	1573.4	27.5	0.375
24	6.287	8.48	1.643	0.932	0.158	1709.2	26.7	0.361
25	6.787	8.17	1.773	0.897	0.166	1845.1	25.7	0.347
26	7.288	7.84	1.904	0.861	0.170	1981.1	24.6	0.332
27	7.787	7.61	2.035	0.836	0.173	2117.0	23.9	0.321
28	8.000	7.42	2.090	0.814	0.174	2174.7	23.3	0.313

** INTEGRAL THICKNESS PARAMETERS **

QUANTITY	VALUE IN CM		
DELTA-99	3.828		
DISPLACEMENT THICKNESS	0.821	REDELST =	6380.
MOMENTUM THICKNESS	0.543	RETHETA =	4224.
ENERGY THICKNESS	0.3855		

SHAPE PARAMETERS : H =1.511 LAMBDA =0.214 CLAUSER G = 9.67

RESULTS OF COLES DATA ANALYSIS

COLES DELTA	3.999 CM
COLES UTAU	0.316 M/S
WAKE PARAMETER	1.387 DIMENSIONLESS
CF BASED ON UE	0.00241 DIMENSIONLESS

PROFILE POINTS 8 THROUGH 17 USED
RESULTANT RMS ERROR FOR WALL-WAKE FIT : 0.108 M/S

TURBULENT SKIN FRICTION PROFILE CORRELATIONS

BASIS VELOCITY :	UE	UREF
CF : LOG-LAW FIT	0.00244	0.00136
CF : LUDWEIG-TILLMAN	0.00248	0.00139
CF : FRANK WHITE	0.00234	0.00131

X/H=18 CASE A OPPOSITE WALL

NOM. UREF : 12.15 M/S

FOR BOUNDARY LAYER ANALYSIS UE = 8.78 M/S AT YE = 5.07 CM

PT. NO.	Y* CM	UBAR M/S	Y/DEL 99	U/UE	u'/UE	Y+	U+	UTLOC M/S
1	0.000	0.00	0.000	0.000	0.000	0.0	0.0	0.000
2	0.040	2.68	0.010	0.305	0.117	11.2	8.2	0.259
3	0.053	3.22	0.014	0.367	0.125	14.6	9.9	0.287
4	0.069	3.69	0.018	0.420	0.128	19.0	11.3	0.306
5	0.089	4.05	0.023	0.461	0.127	24.7	12.4	0.317
6	0.116	4.34	0.030	0.494	0.124	32.2	13.3	0.323
7	0.151	4.63	0.039	0.527	0.121	41.9	14.2	0.328
8	0.195	4.82	0.051	0.549	0.125	54.4	14.8	0.327
9	0.254	5.00	0.066	0.570	0.125	70.6	15.4	0.325
10	0.330	5.22	0.085	0.595	0.126	91.8	16.0	0.326
11	0.429	5.41	0.111	0.616	0.127	119.4	16.6	0.324
12	0.558	5.66	0.145	0.645	0.129	155.2	17.4	0.327
13	0.726	5.90	0.188	0.672	0.135	201.8	18.1	0.328
14	0.943	6.19	0.244	0.705	0.136	262.3	19.0	0.332
15	1.226	6.55	0.317	0.746	0.139	340.9	20.1	0.339
16	1.594	7.00	0.413	0.797	0.137	443.2	21.5	0.349
17	2.072	7.49	0.536	0.853	0.135	576.0	23.0	0.361
18	2.572	7.92	0.666	0.902	0.126	715.1	24.3	0.371
19	3.072	8.33	0.795	0.949	0.119	854.1	25.6	0.381
20	3.571	8.60	0.924	0.980	0.117	993.0	26.4	0.386
21	4.072	8.76	1.054	0.997	0.117	1132.1	26.9	0.388
22	4.572	8.79	1.183	1.001	0.126	1271.1	27.0	0.385
23	5.072	8.80	1.313	1.002	0.133	1410.2	27.0	0.381
24	5.572	8.63	1.442	0.783	0.147	1549.2	26.5	0.371
25	6.072	8.44	1.572	0.961	0.155	1688.2	25.9	0.361
26	6.572	8.23	1.701	0.937	0.162	1827.3	25.3	0.350
27	7.072	7.94	1.831	0.904	0.166	1966.3	24.4	0.336
28	7.571	7.68	1.960	0.874	0.164	2105.3	23.6	0.324
29	8.000	7.43	2.071	0.846	0.167	2224.3	22.8	0.313

** INTEGRAL THICKNESS PARAMETERS **

QUANTITY	VALUE IN CM		
DELTA-99	3.863		
DISPLACEMENT THICKNESS	0.748	REDELST =	5609
MOMENTUM THICKNESS	0.512	RETHETA =	3840.
ENERGY THICKNESS	0.3740		

SHAPE PARAMETERS : H =1.461 LAMBDA =0.194 CLAUSER G = 8.51

RESULTS OF COLES DATA ANALYSIS

COLES DELTA	4.058 CM
COLES UTAU	0.324 M/S
WAKE PARAMETER	1.025 DIMENSIONLESS
CF BASED ON UE	0.00272 DIMENSIONLESS

PROFILE POINTS 8 THROUGH 18 USED
RESULTANT RMS ERROR FOR WALL-WAKE FIT : 0.078 M/S

TURBULENT SKIN FRICTION PROFILE CORRELATIONS

BASIS VELOCITY :	UE	UREF
CF : LOG-LAW FIT	0.00275	0.00144
CF : LUDWEIG-TILLMAN	0.00275	0.00144
CF : FRANK WHITE	0.00262	0.00137

X/H=5 CASE B OPPOSITE WALL

NOM. UREF : 12.24 M/S

FOR BOUNDARY LAYER ANALYSIS UE = 12.89 M/S AT YE = 4.57 CM

PT. NO.	Y* CM	UBAR M/S	Y/DEL 99	U/UE	u'/UE	Y+	U+	UTLOC M/S
1	0.000	0.00	0.000	0.000	0.000	0.0	0.0	0.000
2	0.053	6.75	0.027	0.524	0.111	25.0	11.9	0.532
3	0.072	7.51	0.037	0.583	0.105	33.9	13.2	0.555
4	0.098	8.11	0.050	0.629	0.096	45.9	14.3	0.566
5	0.132	8.55	0.068	0.663	0.090	62.2	15.0	0.567
6	0.179	8.97	0.092	0.696	0.087	84.3	15.8	0.567
7	0.243	9.49	0.125	0.736	0.083	114.2	16.7	0.573
8	0.329	9.92	0.169	0.769	0.081	154.6	17.4	0.573
9	0.446	10.38	0.229	0.805	0.075	209.4	18.2	0.575
10	0.604	10.82	0.311	0.839	0.068	283.6	19.0	0.575
11	0.818	11.28	0.421	0.875	0.062	384.1	19.8	0.577
12	1.108	11.79	0.570	0.914	0.056	520.2	20.7	0.580
13	1.500	12.36	0.772	0.958	0.046	704.5	21.7	0.586
14	2.032	12.85	1.045	0.996	0.025	954.1	22.6	0.589
15	2.667	12.90	1.372	1.000	0.017	1252.3	22.7	0.575
16	3.302	12.92	1.698	1.002	0.021	1550.5	22.7	0.564
17	3.937	12.89	2.025	0.999	0.027	1848.7	22.6	0.553
18	4.572	12.87	2.352	0.998	0.043	2146.8	22.6	0.545
19	5.207	12.55	2.678	0.973	0.075	2445.0	22.1	0.526
20	5.842	11.34	3.005	0.879	0.128	2743.2	19.9	0.475
21	6.477	9.52	3.331	0.738	0.160	3041.3	16.7	0.401
22	7.112	7.45	3.658	0.578	0.179	3339.5	13.1	0.319
23	7.747	5.51	3.985	0.427	0.175	3637.7	9.7	0.241
24	8.382	4.14	4.311	0.321	0.156	3935.9	7.3	0.184
25	8.890	3.14	4.572	0.243	0.132	4174.4	5.5	0.143

** INTEGRAL THICKNESS PARAMETERS **

QUANTITY	VALUE IN CM		
DELTA-99	1.944		
DISPLACEMENT THICKNESS	0.269	REDELST =	2864.
MOMENTUM THICKNESS	0.197	RETHETA =	2091.
ENERGY THICKNESS	0.1552		

SHAPE PARAMETERS : H =1.370 LAMBDA =0.138 CLAUSER G = 6.12

RESULTS OF COLES DATA ANALYSIS

COLES DELTA	2.083 CM
COLES UTAU	0.570 M/S
WAKE PARAMETER	0.167 DIMENSIONLESS
CF BASED ON UE	0.00391 DIMENSIONLESS

PROFILE POINTS 5 THROUGH 13 USED
RESULTANT RMS ERROR FOR WALL-WAKE FIT : 0.062 M/S

TURBULENT SKIN FRICTION PROFILE CORRELATIONS

BASIS VELOCITY :	UE	UREF
CF : LOG-LAW FIT	0.00389	0.00432
CF : LUDWEIG-TILLMAN	0.00373	0.00414
CF : FRANK WHITE	0.00361	0.00401

X/H=7 CASE B OPPOSITE WALL

NOM. UREF : 12.00 M/S

FOR BOUNDARY LAYER ANALYSIS UE = 12.04 M/S AT YE = 3.56 CM

PT. NO.	Y* CM	UBAR M/S	Y/DEL 99	U/UE	u'/UE	Y+	U+	UTLOC M/S
1	0.000	0.00	0.000	0.000	0.000	0.0	0.0	0.000
2	0.053	5.60	0.023	0.465	0.110	21.6	11.4	0.455
3	0.073	6.23	0.031	0.517	0.106	29.6	12.7	0.473
4	0.100	6.76	0.042	0.561	0.103	40.4	13.8	0.483
5	0.136	7.18	0.058	0.596	0.096	55.3	14.6	0.486
6	0.187	7.61	0.079	0.632	0.095	75.6	15.5	0.490
7	0.255	8.05	0.108	0.669	0.095	103.4	16.4	0.493
8	0.349	8.51	0.148	0.707	0.091	141.4	17.3	0.497
9	0.478	9.02	0.202	0.749	0.088	193.4	18.4	0.504
10	0.653	9.55	0.276	0.793	0.084	264.5	19.4	0.511
11	0.894	10.14	0.378	0.842	0.075	361.8	20.6	0.520
12	1.222	10.74	0.517	0.892	0.066	494.8	21.8	0.528
13	1.671	11.37	0.707	0.945	0.056	676.7	23.1	0.538
14	2.286	11.90	0.967	0.989	0.039	925.5	24.2	0.543
15	2.921	12.04	1.236	1.000	0.032	1182.6	24.5	0.535
16	3.556	12.04	1.505	1.000	0.039	1439.7	24.5	0.526
17	4.191	11.94	1.773	0.992	0.062	1696.8	24.3	0.513
18	4.826	11.73	2.042	0.974	0.092	1953.9	23.9	0.498
19	5.461	11.05	2.311	0.917	0.134	2211.0	22.5	0.467
20	6.096	9.95	2.579	0.826	0.171	2468.1	20.2	0.420
21	6.731	8.57	2.848	0.712	0.191	2725.2	17.4	0.364
22	7.366	7.05	3.117	0.586	0.201	2982.3	14.3	0.302
23	8.001	5.69	3.385	0.473	0.200	3239.4	11.6	0.247
24	8.636	4.50	3.654	0.374	0.183	3496.5	9.2	0.198
25	8.890	4.14	3.761	0.344	0.176	3599.3	8.4	0.183

** INTEGRAL THICKNESS PARAMETERS **

QUANTITY	VALUE IN CM		
DELTA-99	2.364		
DISPLACEMENT THICKNESS	0.367	REDELST =	3636.
MOMENTUM THICKNESS	0.260	RETHETA =	2583.
ENERGY THICKNESS	0.1994		

SHAPE PARAMETERS : H =1.408 LAMBDA =0.155 CLAUSER G = 7.10

RESULTS OF COLES DATA ANALYSIS

COLES DELTA	2.230 CM
COLES UTAU	0.493 M/S
WAKE PARAMETER	0.577 DIMENSIONLESS
CF BASED ON UE	0.00335 DIMENSIONLESS

PROFILE POINTS 5 THROUGH 13 USED
RESULTANT RMS ERROR FOR WALL-WAKE FIT : 0.172 M/S

TURBULENT SKIN FRICTION PROFILE CORRELATIONS

BASIS VELOCITY :	UE	UREF
CF : LOG-LAW FIT	0.00333	0.00336
CF : LUDWEIG-TILLMAN	0.00333	0.00335
CF : FRANK WHITE	0.00319	0.00321

X/H=9 CASE B OPPOSITE WALL

NOM. UREF : 12.12 M/S

FOR BOUNDARY LAYER ANALYSIS UE = 11.33 M/S AT YE = 3.63 CM

PT. NO.	Y* CM	UBAR M/S	Y/DEL 99	U/UE	u'/UE	Y+	U+	UTLOC M/S
1	0.000	0.00	0.000	0.000	0.000	0.0	0.0	0.000
2	0.053	4.53	0.019	0.399	0.111	18.6	10.8	0.380
3	0.079	5.20	0.029	0.459	0.112	27.3	12.4	0.401
4	0.116	5.71	0.042	0.504	0.109	40.2	13.7	0.409
5	0.170	6.19	0.062	0.547	0.109	59.2	14.8	0.415
6	0.250	6.63	0.091	0.585	0.107	87.1	15.8	0.417
7	0.368	7.14	0.134	0.630	0.110	128.2	17.1	0.423
8	0.542	7.74	0.197	0.683	0.110	188.6	18.5	0.433
9	0.797	8.52	0.290	0.752	0.107	277.5	20.4	0.450
10	1.173	9.44	0.427	0.833	0.094	408.4	22.6	0.473
11	1.726	10.34	0.628	0.913	0.082	601.0	24.7	0.492
12	2.361	11.05	0.859	0.975	0.065	822.0	26.4	0.506
13	2.996	11.33	1.090	0.999	0.054	1043.1	27.1	0.505
14	3.631	11.34	1.321	1.001	0.065	1264.2	27.1	0.496
15	4.266	11.14	1.552	0.983	0.093	1485.3	26.6	0.481
16	4.901	10.78	1.782	0.951	0.127	1706.3	25.8	0.461
17	5.536	10.12	2.013	0.893	0.162	1927.4	24.2	0.430
18	6.171	9.35	2.244	0.825	0.189	2148.5	22.4	0.376
19	6.806	8.35	2.475	0.737	0.209	2369.6	20.0	0.355
20	7.441	7.12	2.706	0.628	0.217	2590.7	17.0	0.304
21	8.076	6.20	2.937	0.547	0.217	2811.7	14.8	0.266
22	8.711	5.10	3.168	0.450	0.203	3032.8	12.2	0.221
23	9.346	4.36	3.399	0.385	0.193	3253.9	10.4	0.191
24	9.981	3.65	3.630	0.322	0.176	3475.0	8.7	0.162
25	10.160	3.47	3.695	0.306	0.168	3537.3	8.3	0.154

** INTEGRAL THICKNESS PARAMETERS **

QUANTITY	VALUE IN CM		
DELTA-99	2.750		
DISPLACEMENT THICKNESS	0.498	REDELST =	4693.
MOMENTUM THICKNESS	0.335	RETHETA =	3158.
ENERGY THICKNESS	0.2437		

SHAPE PARAMETERS : H =1.486 LAMBDA =0.181 CLAUSER G = 8.86

RESULTS OF COLES DATA ANALYSIS

COLES DELTA	2.461 CM
COLES UTAU	0.418 M/S
WAKE PARAMETER	1.153 DIMENSIONLESS
CF BASED ON UE	0.00272 DIMENSIONLESS

PROFILE POINTS 5 THROUGH 11 USED
RESULTANT RMS ERROR FOR WALL-WAKE FIT : 0.237 M/S

TURBULENT SKIN FRICTION PROFILE CORRELATIONS

BASIS VELOCITY :	UE	UREF
CF : LOG-LAW FIT	0.00272	0.00238
CF : LUDWEIG-TILLMAN	0.00279	0.00244
CF : FRANK WHITE	0.00264	0.00231

X/H=11 CASE B OPPOSITE WALL

NOM. UREF : 12.13 M/S

FOR BOUNDARY LAYER ANALYSIS UE = 10.52 M/S AT YE = 3.45 CM

PT. NO.	Y* CM	UBAR M/S	Y/DEL 99	U/UE	u'/UE	Y+	U+	UTLOC M/S
1	0.000	0.00	0.000	0.000	0.000	0.0	0.0	0.000
2	0.053	3.70	0.017	0.352	0.114	16.3	10.0	0.322
3	0.075	4.37	0.024	0.415	0.120	22.9	11.8	0.349
4	0.105	4.81	0.034	0.457	0.119	32.1	13.0	0.359
5	0.147	5.21	0.047	0.495	0.118	44.9	14.1	0.365
6	0.205	5.56	0.066	0.529	0.119	63.0	15.0	0.368
7	0.288	5.89	0.093	0.560	0.120	88.2	15.9	0.370
8	0.403	6.26	0.130	0.595	0.124	123.5	16.9	0.373
9	0.565	6.73	0.183	0.640	0.127	173.1	18.2	0.381
10	0.791	7.27	0.256	0.691	0.126	242.4	19.6	0.392
11	1.109	8.05	0.358	0.765	0.124	339.6	21.7	0.413
12	1.553	8.88	0.502	0.844	0.113	475.8	24.0	0.434
13	2.176	9.76	0.703	0.928	0.098	666.6	26.3	0.457
14	2.811	10.33	0.909	0.982	0.084	861.1	27.9	0.468
15	3.446	10.52	1.114	1.000	0.091	1055.7	28.4	0.466
16	4.081	10.42	1.319	0.991	0.111	1250.2	28.1	0.455
17	4.716	10.14	1.525	0.964	0.134	1444.7	27.4	0.438
18	5.351	9.69	1.730	0.922	0.162	1639.3	26.2	0.415
19	5.986	8.99	1.935	0.855	0.189	1833.8	24.3	0.384
20	6.621	8.27	2.141	0.786	0.206	2028.4	22.3	0.352
21	7.256	7.55	2.346	0.717	0.216	2222.9	20.4	0.322
22	7.891	6.84	2.551	0.650	0.215	2417.5	18.5	0.292
23	8.526	6.01	2.757	0.572	0.217	2612.0	16.2	0.258
24	9.161	5.28	2.962	0.502	0.213	2806.5	14.3	0.228
25	9.796	4.56	3.167	0.434	0.194	3001.1	12.3	0.198
26	10.160	4.32	3.285	0.411	0.186	3112.7	11.7	0.188

** INTEGRAL THICKNESS PARAMETERS **

QUANTITY	VALUE IN CM		
DELTA-99	3.093		
DISPLACEMENT THICKNESS	0.619	REDELST =	5382.
MOMENTUM THICKNESS	0.405	RETHETA =	3524.
ENERGY THICKNESS	0.2876		

SHAPE PARAMETERS : H =1.528 LAMBDA =0.200 CLAUSER G = 9.81

RESULTS OF COLES DATA ANALYSIS

COLES DELTA	2.764 CM
COLES UTAU	0.367 M/S
WAKE PARAMETER	1.475 DIMENSIONLESS
CF BASED ON UE	0.00244 DIMENSIONLESS

PROFILE POINTS 6 THROUGH 12 USED
RESULTANT RMS ERROR FOR WALL-WAKE FIT : 0.107 M/S

TURBULENT SKIN FRICTION PROFILE CORRELATIONS

BASIS VELOCITY :	UE	UREF
CF : LOG-LAW FIT	0.00248	0.00187
CF : LUDWEIG-TILLMAN	0.00254	0.00191
CF : FRANK WHITE	0.00239	0.00179

X/H=13 CASE 8 OPPOSITE WALL

NOM. UREF : 12.14 M/S

FOR BOUNDARY LAYER ANALYSIS UE = 9.79 M/S AT YE = 3.94 CM

PT. NO.	Y* CM	UBAR M/S	Y/DEL 99	U/UE	u'/UE	Y+	U+	UTLOC M/S
1	0.000	0.00	0.000	0.000	0.000	0.0	0.0	0.000
2	0.053	2.84	0.017	0.290	0.109	15.1	8.2	0.260
3	0.071	3.58	0.022	0.366	0.121	20.0	10.3	0.300
4	0.093	4.19	0.029	0.428	0.124	26.4	12.0	0.326
5	0.124	4.64	0.039	0.474	0.130	35.0	13.3	0.340
6	0.163	4.93	0.051	0.503	0.128	46.3	14.2	0.344
7	0.216	5.21	0.068	0.532	0.131	61.2	15.0	0.347
8	0.286	5.45	0.090	0.556	0.130	81.0	15.7	0.347
9	0.379	5.70	0.119	0.582	0.133	107.2	16.4	0.348
10	0.501	6.00	0.158	0.612	0.135	141.8	17.2	0.350
11	0.663	6.32	0.209	0.645	0.146	187.6	18.2	0.355
12	0.877	6.77	0.276	0.691	0.140	248.3	19.5	0.364
13	1.160	7.35	0.365	0.750	0.140	328.5	21.1	0.380
14	1.535	7.94	0.483	0.811	0.139	434.6	22.8	0.394
15	2.031	8.68	0.639	0.886	0.127	575.1	25.0	0.415
16	2.666	9.35	0.839	0.955	0.118	754.8	26.9	0.431
17	3.301	9.78	1.039	0.999	0.114	934.6	28.1	0.439
18	3.936	9.81	1.238	1.001	0.130	1114.4	28.2	0.433
19	4.571	9.65	1.438	0.985	0.152	1294.1	27.7	0.420
20	5.206	9.26	1.638	0.945	0.174	1473.9	26.6	0.400
21	5.841	8.72	1.838	0.891	0.192	1653.7	25.1	0.375
22	6.476	8.21	2.038	0.838	0.203	1833.4	23.6	0.351
23	7.111	7.65	2.237	0.781	0.209	2013.2	22.0	0.327
24	7.746	7.02	2.437	0.717	0.212	2193.0	20.2	0.300
25	8.381	6.47	2.637	0.661	0.209	2372.7	18.6	0.277
26	9.016	5.99	2.837	0.612	0.204	2552.5	17.2	0.256
27	9.651	5.43	3.036	0.554	0.199	2732.3	15.6	0.233
28	10.286	4.97	3.236	0.507	0.192	2912.0	14.3	0.213
29	10.795	4.63	3.396	0.473	0.180	3056.1	13.3	0.199

** INTEGRAL THICKNESS PARAMETERS **

QUANTITY	VALUE IN CM		
DELTA-99	3.178		
DISPLACEMENT THICKNESS	0.681	REDELST =	5428.
MOMENTUM THICKNESS	0.441	RETHETA =	3512.
ENERGY THICKNESS	0.3114		

SHAPE PARAMETERS : H =1.545 LAMBDA =0.214 CLAUSER G = 9.93

RESULTS OF COLES DATA ANALYSIS

COLES DELTA	3.191 CM
COLES UTAU	0.344 M/S
WAKE PARAMETER	1.406 DIMENSIONLESS
CF BASED ON UE	0.00247 DIMENSIONLESS

PROFILE POINTS 7 THROUGH 15 USED
RESULTANT RMS ERROR FOR WALL-WAKE FIT : 0.097 M/S

TURBULENT SKIN FRICTION PROFILE CORRELATIONS

BASIS VELOCITY :	UE	UREF
CF : LOG-LAW FIT	0.00252	0.00164
CF : LUDWEIG-TILLMAN	0.00247	0.00161
CF : FRANK WHITE	0.00232	0.00151

X/H=15 CASE B OPPOSITE WALL

NOM. UREF : 12.13 M/S

FOR BOUNDARY LAYER ANALYSIS UE = 9.15 M/S AT YE = 4.06 CM

PT. NO.	Y* CM	UBAR M/S	Y/DEL 99	U/UE	u'/UE	Y+	U+	UTLOC M/S
1	0.000	0.00	0.000	0.000	0.000	0.0	0.0	0.000
2	0.053	2.69	0.014	0.294	0.114	14.7	8.0	0.249
3	0.071	3.46	0.019	0.378	0.129	19.6	10.3	0.291
4	0.094	4.00	0.025	0.437	0.132	26.0	11.8	0.313
5	0.125	4.51	0.033	0.493	0.138	34.6	13.4	0.332
6	0.166	4.83	0.044	0.528	0.135	46.0	14.3	0.337
7	0.221	5.07	0.059	0.554	0.140	61.1	15.0	0.337
8	0.294	5.30	0.079	0.579	0.143	81.2	15.7	0.337
9	0.391	5.53	0.104	0.605	0.144	108.0	16.4	0.337
10	0.520	5.82	0.139	0.636	0.150	143.5	17.2	0.340
11	0.691	6.13	0.185	0.670	0.150	190.8	18.2	0.343
12	0.918	6.50	0.245	0.711	0.155	253.6	19.3	0.350
13	1.221	6.96	0.326	0.761	0.150	337.1	20.6	0.360
14	1.622	7.56	0.433	0.826	0.148	448.0	22.4	0.375
15	2.156	8.13	0.576	0.888	0.144	595.5	24.1	0.388
16	2.791	8.68	0.746	0.948	0.129	770.9	25.7	0.401
17	3.427	8.97	0.915	0.980	0.137	946.2	26.6	0.405
18	4.061	9.15	1.085	1.000	0.145	1121.6	27.1	0.405
19	4.697	8.95	1.254	0.977	0.164	1297.0	26.5	0.391
20	5.332	8.73	1.424	0.954	0.182	1472.3	25.9	0.378
21	5.967	8.28	1.594	0.905	0.196	1647.7	24.5	0.357
22	6.602	7.85	1.763	0.858	0.201	1823.0	23.2	0.337
23	7.237	7.37	1.933	0.805	0.203	1998.4	21.8	0.315
24	7.872	7.01	2.102	0.766	0.206	2173.8	20.8	0.299
25	8.506	6.58	2.272	0.719	0.202	2349.1	19.5	0.280
26	9.141	6.12	2.442	0.669	0.191	2524.5	18.1	0.261
27	9.776	5.78	2.611	0.632	0.196	2699.8	17.1	0.246
28	10.411	5.44	2.781	0.594	0.182	2875.2	16.1	0.231
29	10.795	5.27	2.883	0.576	0.175	2981.1	15.6	0.224

** INTEGRAL THICKNESS PARAMETERS **

QUANTITY	VALUE IN CM		
DELTA-99	3.744		
DISPLACEMENT THICKNESS	0.698	REDELST =	5222.
MOMENTUM THICKNESS	0.467	RETHETA =	3497.
ENERGY THICKNESS	0.3408		

SHAPE PARAMETERS : H =1.493 LAMBDA =0.186 CLAUSER G = 8.95

RESULTS OF COLES DATA ANALYSIS

COLES DELTA	3.469 CM
COLES UTAU	0.335 M/S
WAKE PARAMETER	1.141 DIMENSIONLESS
CF BASED ON UE	0.00269 DIMENSIONLESS

PROFILE POINTS 7 THROUGH 15 USED
RESULTANT RMS ERROR FOR WALL-WAKE FIT : 0.084 M/S

TURBULENT SKIN FRICTION PROFILE CORRELATIONS

BASIS VELOCITY :	UE	UREF
CF : LOG-LAW FIT	0.00272	0.00155
CF : LUDWEIG-TILLMAN	0.00268	0.00153
CF : FRANK WHITE	0.00254	0.00144

X/H=17 CASE B OPPOSITE WALL

NOM. UREF : 12.14 M/S

FOR BOUNDARY LAYER ANALYSIS UE = 8.80 M/S AT YE = 4.31 CM

PT. NO.	Y* CM	UBAR M/S	Y/DEL 99	U/UE	u'/UE	Y+	U+	UTLOC M/S
1	0.000	0.00	0.000	0.000	0.000	0.0	0.0	0.000
2	0.053	2.95	0.014	0.335	0.120	15.0	8.6	0.268
3	0.071	3.71	0.019	0.422	0.135	20.2	10.8	0.308
4	0.096	4.16	0.025	0.473	0.152	27.0	12.1	0.323
5	0.128	4.68	0.033	0.532	0.139	36.2	13.6	0.340
6	0.172	5.01	0.045	0.569	0.144	48.6	14.5	0.346
7	0.231	5.21	0.060	0.592	0.143	65.1	15.1	0.343
8	0.309	5.50	0.080	0.625	0.145	87.3	16.0	0.345
9	0.415	5.73	0.107	0.652	0.150	117.0	16.6	0.345
10	0.556	6.01	0.144	0.683	0.152	156.8	17.4	0.346
11	0.745	6.31	0.193	0.717	0.155	210.2	18.3	0.349
12	0.998	6.66	0.259	0.758	0.160	281.7	19.3	0.354
13	1.338	7.07	0.347	0.804	0.157	377.6	20.5	0.361
14	1.793	7.56	0.465	0.860	0.153	506.1	22.0	0.371
15	2.404	8.08	0.623	0.918	0.150	678.3	23.5	0.382
16	3.038	8.49	0.788	0.965	0.148	857.5	24.6	0.390
17	3.674	8.67	0.952	0.986	0.152	1036.7	25.2	0.390
18	4.308	8.80	1.117	1.000	0.159	1215.9	25.5	0.389
19	4.944	8.70	1.282	0.989	0.171	1395.2	25.3	0.380
20	5.579	8.42	1.446	0.957	0.187	1574.4	24.5	0.365
21	6.214	8.13	1.611	0.924	0.190	1753.6	23.6	0.349
22	6.849	7.77	1.775	0.884	0.196	1932.8	22.6	0.332
23	7.484	7.37	1.940	0.838	0.198	2112.0	21.4	0.314
24	8.119	7.06	2.105	0.802	0.196	2291.2	20.5	0.300
25	8.754	6.72	2.269	0.764	0.193	2470.4	19.5	0.285
26	9.389	6.46	2.434	0.734	0.184	2649.6	18.8	0.273
27	10.024	6.20	2.599	0.705	0.177	2828.8	18.0	0.261
28	10.659	5.92	2.763	0.673	0.173	3008.0	17.2	0.249
29	10.795	5.91	2.799	0.672	0.171	3046.6	17.2	0.249

** INTEGRAL THICKNESS PARAMETERS **

QUANTITY	VALUE IN CM		
DELTA-99	3.857		
DISPLACEMENT THICKNESS	0.640	REDELST =	4614.
MOMENTUM THICKNESS	0.446	RETHETA =	3216.
ENERGY THICKNESS	0.3363		

SHAPE PARAMETERS : H =1.435 LAMBDA =0.166 CLAUSER G = 7.74

RESULTS OF COLES DATA ANALYSIS

COLES DELTA	3.674 CM
COLES UTAU	0.343 M/S
WAKE PARAMETER	0.757 DIMENSIONLESS
CF BASED ON UE	0.00305 DIMENSIONLESS

PROFILE POINTS 7 THROUGH 15 USED
RESULTANT RMS ERROR FOR WALL-WAKE FIT : 0.046 M/S

TURBULENT SKIN FRICTION PROFILE CORRELATIONS

BASIS VELOCITY :	UE	UREF
CF : LOG-LAW FIT	0.00307	0.00161
CF : LUDWEIG-TILLMAN	0.00301	0.00158
CF : FRANK WHITE	0.00287	0.00151

X/H=16 CASE C OPPOSITE WALL

NOM. UREF : 12.16 M/S

FOR BOUNDARY LAYER ANALYSIS UE = 8.90 M/S AT YE = 4.51 CM

PT. NO.	Y* CM	UBAR M/S	Y/DEL 99	U/UE	u'/UE	Y+	U+	UTLOC M/S
1	0.000	0.00	0.000	0.000	0.000	0.0	0.0	0.000
2	0.040	3.09	0.011	0.347	0.114	11.1	9.4	0.292
3	0.064	3.80	0.017	0.427	0.119	17.7	11.6	0.318
4	0.102	4.33	0.027	0.487	0.116	28.0	13.2	0.330
5	0.161	4.72	0.043	0.530	0.112	44.3	14.4	0.331
6	0.254	5.07	0.068	0.570	0.113	70.2	15.4	0.329
7	0.403	5.40	0.108	0.607	0.115	111.2	16.4	0.328
8	0.638	5.75	0.171	0.647	0.122	176.0	17.5	0.327
9	1.009	6.27	0.270	0.705	0.128	278.5	19.1	0.334
10	1.509	6.93	0.404	0.779	0.128	416.4	21.1	0.349
11	2.009	7.55	0.538	0.849	0.122	554.4	23.0	0.365
12	2.509	8.00	0.672	0.900	0.114	692.5	24.4	0.376
13	3.009	8.47	0.806	0.952	0.103	830.4	25.8	0.388
14	3.509	8.72	0.940	0.980	0.104	968.3	26.6	0.393
15	4.009	8.91	1.074	1.002	0.101	1106.4	27.1	0.395
16	4.509	8.88	1.207	0.998	0.120	1244.4	27.0	0.389
17	5.009	8.79	1.341	0.989	0.132	1382.4	26.8	0.382
18	5.509	8.60	1.475	0.967	0.146	1520.4	26.2	0.371
19	6.009	8.32	1.609	0.935	0.151	1658.3	25.3	0.357
20	6.509	8.06	1.743	0.906	0.158	1796.4	24.5	0.344
21	7.009	7.65	1.877	0.860	0.162	1934.3	23.3	0.326
22	7.509	7.43	2.011	0.835	0.158	2072.3	22.6	0.316
23	7.620	7.22	2.040	0.812	0.163	2102.8	22.0	0.307

** INTEGRAL THICKNESS PARAMETERS **

QUANTITY	VALUE IN CM		
DELTA-99	3.734		
DISPLACEMENT THICKNESS	0.746	REDELST =	5576.
MOMENTUM THICKNESS	0.509	RETHETA =	3801.
ENERGY THICKNESS	0.3676		

SHAPE PARAMETERS : H =1.467 LAMBDA =0.200 CLAUSER G = 8.62

RESULTS OF COLES DATA ANALYSIS

COLES DELTA	3.958 CM
COLES UTAU	0.324 M/S
WAKE PARAMETER	1.108 DIMENSIONLESS
CF BASED ON UE	0.00266 DIMENSIONLESS

PROFILE POINTS 6 THROUGH 12 USED
RESULTANT RMS ERROR FOR WALL-WAKE FIT : 0.146 M/S

TURBULENT SKIN FRICTION PROFILE CORRELATIONS

BASIS VELOCITY :	UE	UREF
CF : LOG-LAW FIT	0.00273	0.00146
CF : LUDWEIG-TILLMAN	0.00273	0.00146
CF : FRANK WHITE	0.00260	0.00139

1. Report No.	2. Government Accession No.	3. Recipient's Catalog No.
NASA CR-3765		

4. Title and Subtitle EXPERIMENTAL STUDY OF FLOW REATTACHMENT IN A SINGLE-SIDED SUDDEN EXPANSION	5. Report Date January 1984
	6. Performing Organization Code
7. Author(s) R. V. Westphal, J. P. Johnston, and J. K. Eaton	8. Performing Organization Report No.
	10. Work Unit No.
9. Performing Organization Name and Address Mechanical Engineering Department Stanford University Stanford, CA 94305	11. Contract or Grant No. NAG2-42
	13. Type of Report and Period Covered Contractor report
12. Sponsoring Agency Name and Address National Aeronautics and Space Administration Washington, D. C. 20546	14. Sponsoring Agency Code 505-21-21

15. Supplementary Notes

Point of contact: Technical Monitor, Dennis A. Johnson
Ames Research Center, Moffett Field, CA
(415) 965-5655 or FTS 448-5655

16. Abstract

The reattachment of a fully turbulent, two-dimensional, separated shear layer downstream of a single-sided sudden expansion in a planar duct flow has been examined experimentally. The specific objective of this study was to examine the importance of changing the structure of the separated shear layer on the reattachment process itself. For all cases, the Reynolds number based on step height was greater than 20,000, the expansion ratio was 5/3, and the inlet boundary layer was less than one-half step height in thickness. A crucially important phase of the work was the development of a new "pulsed wall probe" for measurement of skin friction in the reattachment region, thus providing an unambiguous definition of the reattachment length. Quantitative features of reattachment - including streamwise development of the mean and fluctuating velocity field, pressure rise, and skin friction - were found to be similar for all cases studied when scaled by the reattachment length. A definition of the reattachment zone is proposed.

17. Key Words (Suggested by Author(s))	18. Distribution Statement
Reattachment, separation turbulent, shear layer sudden expansion	Unclassified - Unlimited STAR category 34

19. Security Classif. (of this report)	20. Security Classif. (of this page)	21. No. of Pages	22. Price*
Unclassified	Unclassified	283	A13

*For sale by the National Technical Information Service, Springfield, Virginia 22161

☆U.S. GOVERNMENT PRINTING OFFICE:1984 -739-010/ 54 REGION NO. 4